Adaptability of the distal convoluted tubule in magnesium homeostasis

Annelies van Angelen

The research described in this thesis was performed at the department of Physiology, Radboud university medical center, the Netherlands and financially supported by the department of Physiology and the European Science Foundation (EURYI 044.036.001).

ISBN: 978-90-9028139-1

Cover and page design: Annelies van Angelen
Printed by: proefschriftmaken.nl, Uitgeverij BOXPress

Adaptability of the distal convoluted tubule in magnesium homeostasis

Proefschrift

ter verkrijging van de graad van doctor
aan de Radboud Universiteit Nijmegen
op gezag van de rector magnificus prof. mr. S.C.J.J. Kortmann,
volgens besluit van het college van decanen
in het openbaar te verdedigen op dinsdag 27 mei 2014
om 12.30 uur precies

door

Annelies Arachne van Angelen
geboren op 27 oktober 1981
te Utrecht

Promotoren:
Prof. dr. R.J.M. Bindels
Prof. dr. J.G.J. Hoenderop

Manuscriptcommissie:
Prof. dr. F.G.M Russel (voorzitter)
Prof. dr. W.F.J. Feitz
Dr. J.A. Joles (UMC Utrecht)

Het is onmogelijk om te voorspellen wat we gaan ontdekken, en wanneer.
(Hans Clevers)

Table of Contents

Chapter 1

General Introduction

Magnesium: from metal to ion

Magnesium (Mg) is a chemical element with atomic number 12, derived from Magnesia, a district of Eastern Thessaly in Greece (**Figure 1A**). Mg is the seventh most abundant element in the Earth's crust. It is found in large deposits of magnesite, dolomite, and other minerals. The atom preferentially loses its two exterior electrons, to form the divalent ion (Mg^{2+}) (**Figure 1B**). An example is magnesium sulfate ($MgSO_4$) in mineral waters, where Mg^{2+} is soluble (1). In 1755 the Scottish Joseph Black found out that Mg is an element itself. The British chemist Sir Humphrey Davy is seen as 'the discoverer' since he unraveled in 1808 how to isolate Mg from wet $MgSO_4$ by electrolysis. In 1828, the French chemist Antoine Bussy prepared the metal in an almost pure state. In 1833, Michael Faraday, was the fist to obtain pure metallic Mg (2, 3). Mg is a relatively solid and flammable silvery-white metal. It is commonly used, among others because it is the lightest structural metal. Mg is strong enough to be used in alloys to build bridges, automobiles (especially wheels), airplanes and electronic devices (**Figure 1C**) (4).

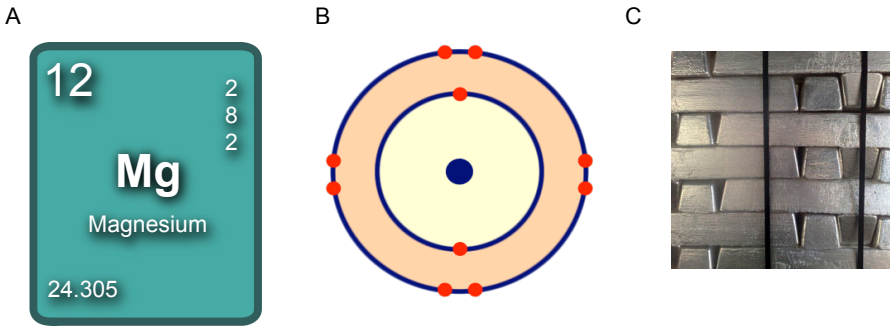

Figure 1. Magnesium (Mg/Mg^{2+}) visualized. (**A**) Mg in the periodic table of elements. (**B**) Mg^{2+}: the two outermost electrons are removed resulting in the ionic state with 10 electrons (red dots) left, surrounding the nucleus (blue dot), which contains the protons and neutrons). (**C**) Mg as alloy.

Mg^{2+} is also an essential biological component of the human body. It is the most prevalent intracellular divalent cation (5). Around 60% of the Mg^{2+} is stored in bone, and the other part is mainly localized in skeletal muscle and soft tissues (**Figure 2**). In the cytosol, Mg^{2+} chiefly forms complexes with adenosine 5'-triphosphate (ATP) and, to a lesser extent, with nucleotides and enzymes. The total Mg^{2+} content in tissues is estimated around 10 µmol/g wet weight, whereas not more than ~10% of the total amount of intracellular Mg^{2+} exists in the free ionized form, resulting in a concentration of 0.5-1.0 mmol/L (6, 7). In addition, only 1% of body Mg^{2+} resides in the extracellular compartment, corresponding with a serum concentration of 0.7-1.1 mmol/L (1.7-2.2 mg/dL or 1.5-1.9 mEq/L) (8, 9). This suggests that the free Mg^{2+} concentration is relatively constant between these different fluids, while surrounded by higher concentrations of bound Mg^{2+} (7). In plasma, Mg^{2+} is present in three different states: *i*) 60% exists in its ionized form; *ii*) 30% is protein bound (the majority to albumin) and; *iii*) around 10% forms complexes with anions (10, 11). Mg^{2+}

is involved, only in its physiologically active ionized form, in many enzymatic reactions, deoxyribonucleic acid (DNA) and protein synthesis and has a pivotal role especially in neurons and muscular cells (12, 13). The daily recommended dietary allowance (RDA) of Mg^{2+} intake for an adult is approximately 350 mg. Seeds, grains, green leafy vegetables, legumes and nuts are the richest dietary sources of Mg^{2+}, however, only in an unprocessed state (14).

Mg^{2+} homeostasis

The plasma Mg^{2+} level is maintained within a narrow range by the concerted action of intestinal absorption, renal excretion and exchange with bone, and disturbances in one of these processes can have serious consequences. First, the situation in healthy individuals will be discussed. Secondly, hypermagnesemia and hypomagnesemia and the factors causing these disturbances of the Mg^{2+} balance will be described in more detail.

Mg^{2+} absorption by the intestine

The entire bowel, including the colon, is capable of absorbing Mg^{2+} from nutrients and in minor amounts from drinks (15, 16). The amount of Mg^{2+} absorption is dependent on the dietary intake and the Mg^{2+} requirement of the body at the particular moment. Typically, around 30-50% of Mg^{2+} intake is absorbed by the intestine, although this percentage can be markedly reduced during enriched dietary Mg^{2+} intake. The remainder is eliminated in the faeces (**Figure 2**) (17). Under physiological conditions, approximately 90% of the Mg^{2+} ingested, is absorbed in a passive manner, probably depending on the lumen-positive electrical voltage and the transepithelial concentration gradient of Mg^{2+} (18). The rest is absorbed via a saturable transcellular way, in which the epithelial Mg^{2+} channel, baptized transient receptor potential subfamily M, member 6 (TRPM6), is involved (18). This active transport is especially assigned to the colon, since TRPM6 is most abundantly expressed along the luminal membrane of these epithelial cells (19-21).

Storage of Mg^{2+} in bone

Mg^{2+} is a normal constituent of bone and divided in at least two distinct pools. ~70% is incorporated in the complex of hydroxyapatite crystal deposition and not exchangeable. The other ~30% is rapidly exchangeable and elutable (**Figure 2**). This Mg^{2+} reservoir in bone serves as a buffer from which Mg^{2+} can be released or stored, as required (22).
Importantly, the Mg^{2+} concentration is essential for bone function. It influences both mineral and matrix metabolism; directly and by affecting the release and activity of hormones, like parathyroid hormone (PTH) and the active form of vitamin D ($1,25(OH)_2D_3$), which regulate skeletal and mineral metabolism (23, 24). This key role is highlighted by the existence of osteoporosis during a Mg^{2+}-deficient status (25).

Mg^{2+} reabsorption by the kidneys

The kidney is the most important organ for the regulation of the Mg^{2+} balance. It accurately maintains the Mg^{2+} excretion via the urine and consequently the plasma Mg^{2+} level in response to changes in intestinal Mg^{2+} absorption and shifts in bone absorption and release (**Figure 2**) (26). Approximately 80% of total plasma Mg^{2+} is filtered by the

glomeruli, since the remaining part is bound to protein (27, 28). This filtered fraction is called pro-urine. Useful components and most water (H_2O) will be reabsorbed from the pro-urine to the blood compartment and waste products are secreted, finally producing the urine. The majority of the filtered Mg^{2+} is reabsorbed along the nephron, the functional unit of the kidney, of which each kidney contains about one million structures. Only about 3-5% of filtered Mg^{2+} is normally excreted in the urine. However, when dietary Mg^{2+} is restricted, the kidney is capable of reabsorbing almost all filtered Mg^{2+}. Mg^{2+} reabsorption takes place in the proximal tubule (PT), the thick ascending limb of Henle's loop (TAL) and the distal convoluted tubule (DCT) (**Figure 3**), these successive nephron segments will be discussed in the next paragraphs.

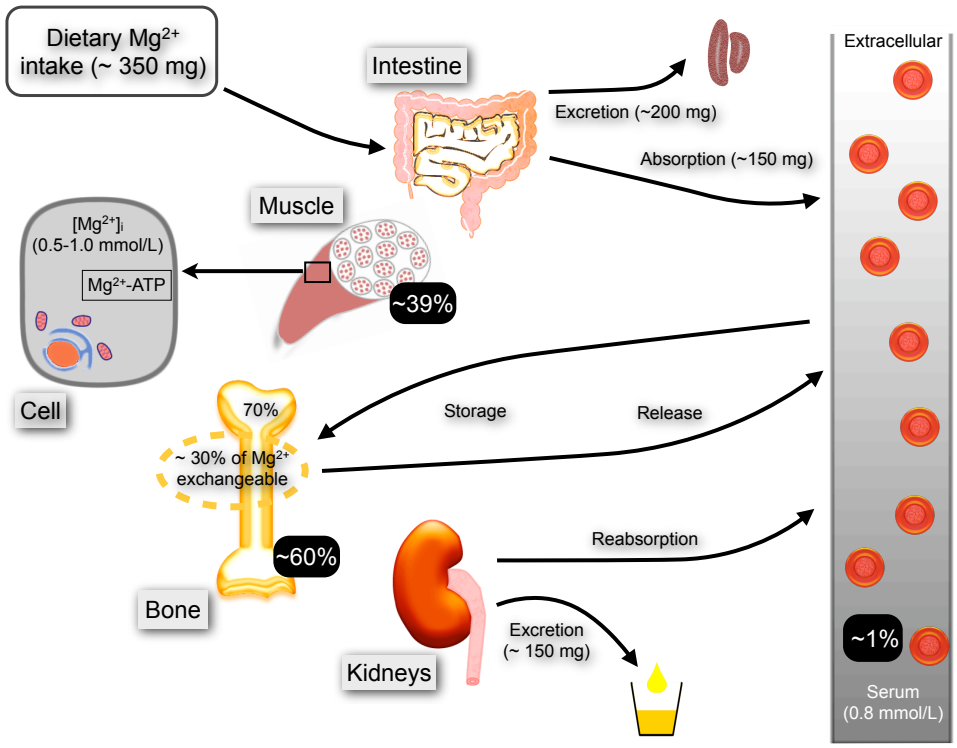

Figure 2. **Overview of Mg^{2+} homeostasis.** Schematic model of the regulation of Mg^{2+} balance by the concerted action of intestinal absorption, renal excretion and storage in bone. In addition, this figure shows the distribution of Mg^{2+} over the different organs of the human body.

The epithelial cells lining the tubular system are characterized by their highly polarized appearance. The proteins are asymmetrically divided over two distinct membrane areas; the apical side, facing the pro-urine and the basolateral side, facing the extracellular matrix and blood vessels (**Figure 3**). These membrane domains, separated by tight junctions, have distinct and clearly defined tasks for transport of Mg^{2+} (29, 30). For the

preservation, protein sorting via vesicles from the Golgi network, the subsequent selective retention in the specific membrane compartment and cell adhesion to the extracellular matrix, are major issues (29, 31).

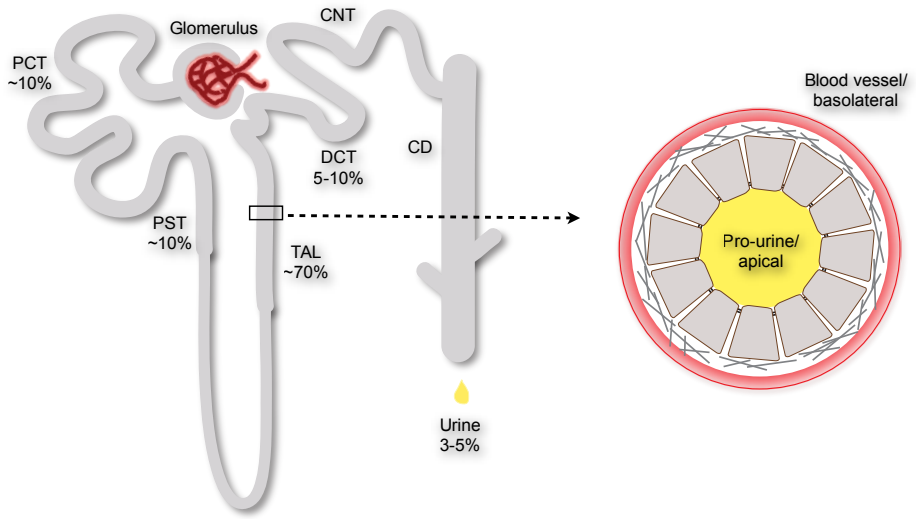

Figure 3. Schematic overview of Mg^{2+} reabsorption along the nephron. The relative percentages of Mg^{2+} reabsorption, as fraction of the total amount of Mg^{2+} filtrated by the glomerulus, are indicated per segment. On the right side, a magnified cross-section of the tubulus is depicted with individual polarized epithelial cells and the surrounding blood and urine compartments. Nephron segments: PCT, proximal convoluted tubule; PST, proximal straight tubule; TAL, thick ascending limb of Henle's loop; DCT, distal convoluted tubule; CNT, connecting tubule; CD, collecting duct.

Paracellular Mg^{2+} reabsorption

Most reabsorption of Mg^{2+} occurs in a passive, paracellular manner. In the PT and TAL Mg^{2+} flows through the tight junctions between the epithelial cells from the pro-urine to the interstitium and subsequently the blood compartment (32). The PT is characterized by the prominent brush border and consists of the proximal convoluted tubule (PCT) which is connected to the Bowmans capsule, with adjacent the proximal straight tubule (PST) (33). Interestingly, the PCT has a high permeability to H_2O, sodium (Na^+) and calcium (Ca^{2+}). During basal conditions only ~10% of the Mg^{2+} reabsorption takes place in this segment.

A similar amount of Mg^{2+} is reabsorbed in the PST (34-36). The molecular mechanism of this paracellular process is not well understood. Mg^{2+} reabsorption is thought to be dependent on the filtered load and Na^+-driven H_2O transport (37, 38), executed by the Na^+, H^+ exchanger 3 (NHE3) (39) and the H_2O channel aquaporin 1 (AQP1) (**Figure 4**) (40, 41).

The majority, ~70% of the Mg^{2+} filtered by the glomerulus, is reabsorbed in TAL (34, 42). This paracellular reabsorption is driven by the lumen-positive transepithelial potential, which is mainly generated by the apical Na^+ and Cl^- transport via the Na^+, K^+, $2Cl^-$ cotransporter (NKCC2). The generation of the driving force for apical Na^+ transport and

consequently Mg^{2+} reabsorption down the electrochemical gradient, is provided by three other transporters. Exchange of three Na^+ ions for two K^+ ions mediated by the Na^+, K^+-ATPase, the apical recycling of potassium (K^+) by the renal outer medullary K^+ channel (ROMK) and the extrusion of chloride (Cl^-) over the basolateral membrane via the Cl^- channel, subunit b (CLC-Kb), are essential for paracellular Mg^{2+} reabsorption in this nephron segment (42-44). Moreover, tight junction proteins including claudin-16 (CLDN16) and claudin-19 (CLDN19) and in particular their interaction, are of importance for Mg^{2+} diffusion through these complexes towards the blood compartment in TAL (45-47). Finally, the Ca^{2+}-sensing receptor (CaSR) located in the basolateral membrane probably regulates the paracellular permeability of Ca^{2+} and Mg^{2+} in response to the sensed extracellular Ca^{2+} and Mg^{2+} concentration (**Figure 4**) (48, 49).

Transcellular Mg^{2+} transport

The fine-tuning of Mg^{2+} reabsorption takes place in the DCT, as there is no significant Mg^{2+} reabsorption beyond this segment. About 5-10% of the filtered load of Mg^{2+} is reabsorbed via an active transport process in the DCT. Noteworthy, micropuncture and microperfusion studies taught us that the capacity for Mg^{2+} transport in DCT is enormous when needed (26). The high mitochondrial density is of interest, probably representing the massive hydrolysis of ATP, necessary for accomplishment of the active transport in this segment (50, 51). In addition, it has been shown that a defect in the function of mitochondria results in several metabolic disorders including hypomagnesemia (52).

The expression profile of Ca^{2+} and Na^+ transport proteins indicates that the DCT consists of two different parts including the early DCT (DCT1) and the late DCT (DCT2) segment (53). DCT1 is primarily responsible for Mg^{2+} transport, mainly indicated by the predominant expression of TRPM6 in this compartment (19). TRPM6 forms the apical entry for Mg^{2+}, driven by a favourable transmembrane potential (26). The transport of Mg^{2+} to the basolateral side of the DCT cell and its extrusion against the electrochemical gradient to the blood side are not completely resolved. It has been proposed that Mg^{2+} crosses the cytosol via diffusion. Possibly, the cytosolic protein parvalbumin (PV) plays a role of significance and could act as a Mg^{2+} buffer. PV originally belongs to the Ca^{2+}-binding proteins (54), however, depending on the physiological conditions, it can bind Mg^{2+} as well (55-57). PV contains two equivalent Ca^{2+}/Mg^{2+} EF-hand binding sites. At a temperature of 35 °C and pH 7.2, PV has a dissociation constant (K_d) of 11.0 nM for Ca^{2+} and 41.0 μM for Mg^{2+} (57). Considering the exclusive renal expression in of this protein in DCT1 (58) makes PV a possible candidate. Most likely, Mg^{2+} is translocated over the basolateral membrane via a Na^+-dependent exchanger or an ATP-dependent Mg^{2+} pump (**Figure 4**) (26, 59).

For Mg^{2+} transport via TRPM6, it is important that other proteins in DCT cells generate the electrochemical driving force for Mg^{2+} influx. Similar as for the TAL, the Na^+, K^+-ATPase located in the basolateral membrane is responsible for establishing a negative intracellular membrane potential and Na^+ gradient by extruding three Na^+ ions out of the cell against the uptake of two K^+ into the cytoplasm. The realized Na^+ gradient facilitates the apical entry of Na^+ via the thiazide-sensitive Na^+, Cl^- cotransporter (NCC) together with the uptake of Cl^- from the pro-urine (60). Recently, it was proposed that the voltage-gated K^+ channel 1.1 (Kv1.1) contributes to a favourable membrane potential by secreting K^+ in the luminal compartment (**Figure 4**) (61). At the basolateral side Cl^- and K^+ are translocated

into the interstitium via CLC-Kb (62, 63) and the inward rectifier K^+-channel 4.1 (Kir4.1), probably in complex with Kir5.1 (64), respectively. Possibly, cyclin M2 (CNNM2) is involved in Mg^{2+} transport across the basolateral membrane in DCT (65). It is hypothesized that CNNM2 senses the intracellular Mg^{2+} concentration ($[Mg^{2+}]_i$) and triggers other proteins to react accordingly (66). Finally, it has been shown that *FXYD2* gene, encoding the γ-subunit of the Na^+, K^+-ATPase, and its regulation by the transcription factor hepatocyte nuclear factor 1 homeobox B (HNF1B) are essential players relating to Mg^{2+} reabsorption in the DCT (67).

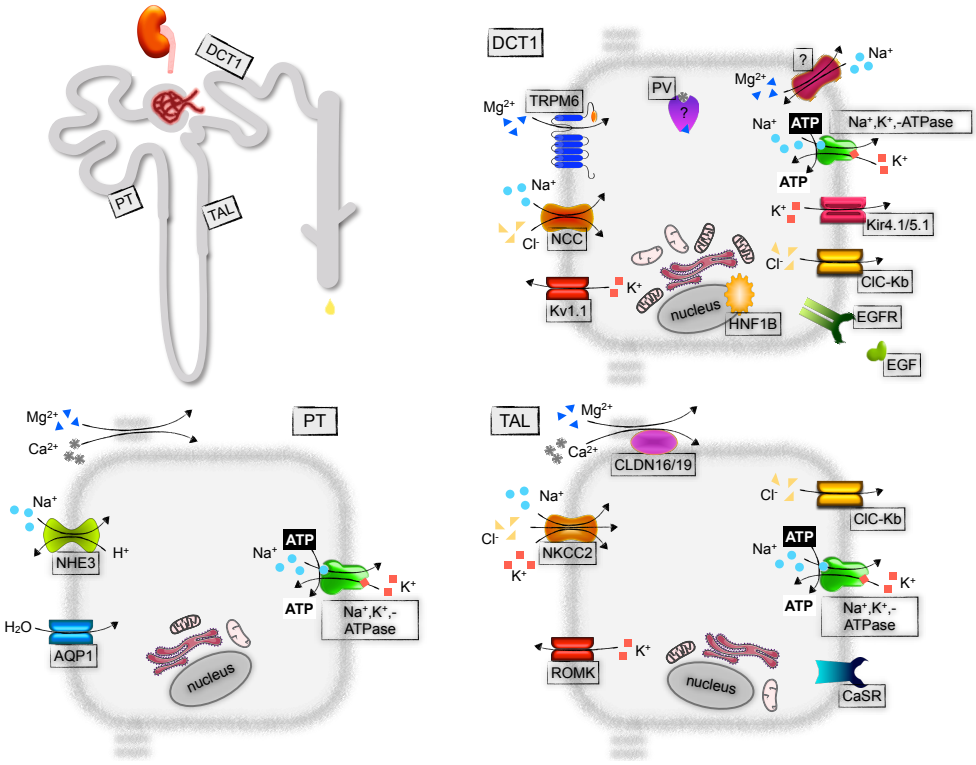

Figure 4. Schematic overview of proteins associated with electrolyte movement in PT, TAL and DCT of the nephron, with the emphasis on Mg^{2+} transport. Mg^{2+} reabsorption in the proximal tubule (PT) and the thick ascending limb of Henle's loop (TAL) is paracellular, closely related to calcium (Ca^{2+}) reabsorption and secondary to sodium (Na^+) and water (H_2O) transport. In the distal convoluted tubule (DCT) Mg^{2+} is transported by TRPM6. See body text for details and explanation.

TRPM6

TRPM6 is composed of six transmembrane (TM) spanning domains, a pore-forming region between domains TM 5 and 6, and large intracellular tails (68) (**Figure 5**). *In vitro*, TRPM6 can form homotetramers and heterotetramers with the epithelial Mg^{2+} channel transient receptor potential subfamily M, member 7 (TRPM7). TRPM7 is more ubiquitously

expressed and crucial for cellular Mg^{2+} homeostasis. Previous studies have shown that TRPM7 is important for trafficking of TRPM6 to the plasma membrane (69-71). However, the exact composition of the multimeric TRPM6 channels in mammals has not yet been unraveled. TRPM6 is tightly regulated by $[Mg^{2+}]_i$ (26) and by the dietary intake of Mg^{2+} (21). Moreover, it has been shown that phosphatidylinositol 4,5-bisphosphate (PIP_2) is important for TRPM6 activation (72). In addition, this ion-channel is modulated by the intracellular pH (73).

Interestingly, the carboxyl-termini of TRPM6 and TRPM7 contain a special serine/threonine protein kinase domain, known as the α-kinase (74). It is the combination of the channel and this enzyme domain, which makes these "chanzyme" proteins unique among ion channels. Although the kinase domain is not necessary for channel activity, an important role as modulator of TRPM6 has been reported (75). However, the detailed function of the kinase domain remains poorly understood. In recent years, the direct interacting proteins, receptor for activated C-kinase (RACK1), repressor of estrogen receptor activity (REA) and methionine sulfoxide reductase B1 (MsrB1) were identified as potential regulators of the channel via the α-kinase domain of TRPM6 (76-78). RACK1 probably maintains a control function in Mg^{2+} influx in DCT by inhibition of TRPM6 channel activity (76). Similarly, REA is supposed to play a role in providing negative feedback in response to Mg^{2+} transport by TRPM6 (77). Finally, MsrB1 recovers TRPM6 activity during oxidative stress by affecting the effect of hydrogen peroxide (H_2O_2) on TRPM6 (78).

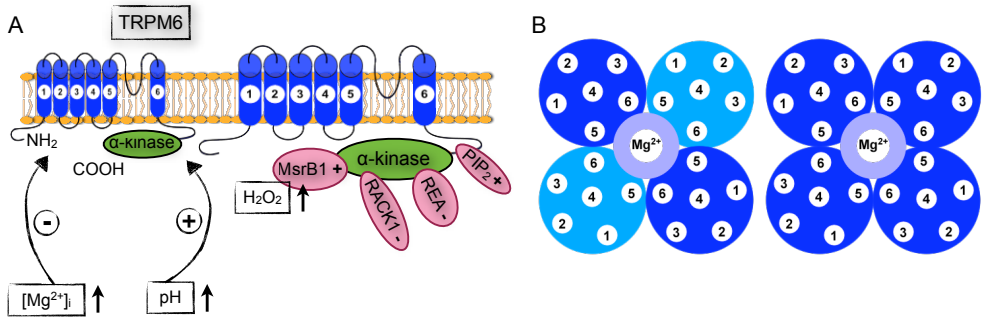

Figure 5. Structural organization of TRPM6. (**A**) TRPM6 consists of six transmembrane domains, one putative pore-forming region between the fifth and sixth domain, an atypical α-kinase domain and large cytosolic amino (NH_2) and carboxyl (COOH) termini. The six transmembrane domains are presumed to form a function channel with a central pore to reabsorb Mg^{2+}. The TRPM6 interacting proteins and regulating factors, as described in the body text, are depicted in this figure. (**B**) Four monomers assemble, probably by heteromeric formation with TRPM7 (light blue), alternatively, four TRPM6 subunits (dark blue) form a homotetramer. The numbers 1-6 represent the corresponding transmembrane units.

The TRPM6 knockout mouse model is embryonic lethal (79, 80). This was explained by the crucial role that TRPM6 exerts during embryogenesis (79). In addition, TRPM6 expression is not restricted to kidney and colon, but also found in lung (21). Despite the interesting observation that Mg^{2+} supplementation ameliorates asthma (81), the physiological function of TRPM6 in lung remains to be elucidated.

Regulation of the Mg^{2+} balance

The Mg^{2+} concentration in body fluids is regulated in many ways. Different hormones have been reported to play a role in the regulation of the Mg^{2+} balance including PTH, $1,25(OH)_2D_3$, calcitonin and glucagon (8, 32, 82-84). These compounds, probably act in an indirect manner, via changes in extracellular volume, acid-base status or Ca^{2+} concentration (85, 86). Interestingly, estrogen and insulin have been shown to exert an direct effect on TRPM6 (21, 87). Furthermore, our group showed that epidermal growth factor (EGF), which is mainly known for its role in cell growth, proliferation and differentiation, can activate TRPM6 (88). Phosphorylation of the EGF receptor (EGFR), in the basolateral membrane of the DCT, triggers an intracellular cascade, in which the sarcoma (Src) family of tyrosine kinases and the down-stream small Rho GTPase Rac1, are involved. This promotes the trafficking of TRPM6 to the membrane, resulting in increased capacity for Mg^{2+} influx (89). In addition, activation of the EGFR by EGF might increase the expression of TRPM6 via phosphorylation of extracellular signal-regulated kinases (90). Finally, Mg^{2+} reabsorption is dependent on the circadian rhythm with increased urinary Mg^{2+} excretion during the night (91).

Mg^{2+}-related diseases

Dietary intake, absorption, storage and excretion of Mg^{2+} all need to be carefully tuned, to control a healthy Mg^{2+} status. A surplus of Mg^{2+} can result in hypermagnesemia, whereas a deficiency can cause hypomagnesemia. The symptoms associated with these medical conditions will be discussed. The central focus will be on hypomagnesemia, by considering its different causes and appearances, since it is associated with of a serious burden of disease. In general, it is important that people at risk for developing Mg^{2+} disturbances, are regularly monitored.

Hypermagnesemia

Hypermagnesemia (serum Mg^{2+} > 1.2 mmol/L) is rare in the general population, however, the prevalence can increase up to 10% in seriously ill patients (92, 93). Usually symptoms are not declared (94). Nevertheless, markedly increased plasma Mg^{2+} levels result in a block of ion channels gated by other cations and executing essential functions in brain or heart tissue. This might result in cardiac arrhythmias, apnea and even coma (**Table 1**) (95). Hypermagnesemia is in most patients the consequence of a defect in excretion of Mg^{2+} by the kidney, caused by progressed chronic kidney disease (CKD) (96). Also treatment with lithium and hypothyroidism can result in hypermagnesemia via unknown mechanisms (95). Finally, in rare cases, an overdose of Mg^{2+} intake via infusion, oral-ingestion of Mg^{2+} or treatment with Mg^{2+}-containing cathartics or antacids, resulted in a serious rise of plasma Mg^{2+} level (95, 97). Metabolic disturbances like for Ca^{2+} and K^+ are not regularly recognized. Especially, due to the ability of the kidneys to adapt to increased Mg^{2+} intake and to excrete almost all Mg^{2+} filtered by the glomerulus, hypermagnesemia is not often diagnosed in healthy individuals (95).

Hypomagnesemia

Hypomagnesemia (serum Mg^{2+} < 0.7 mmol/L) is mostly asymptomatic, like for

hypermagnesemia, although the clinical picture may comprise neuromuscular, cardiovascular and metabolic disturbances like tremor, convolutions and cardiac arrhythmias (**Table 1**) (95, 98). Hypomagnesemia is diagnosed in approximately 10% of the hospitalized patients and can be as high as 65% in intensive care patients (92, 99, 100). Interestingly, hypomagnesemia is often observed in patients with chronic diseases like, diabetes mellitus type 2 (DM2), heart and vascular diseases, osteoporosis, depression and asthma (25, 101). The affection of blood pressure and induction of hypertension due to Mg^{2+} deficiency is probable a key initiator in causing the final morbidity (102). In the next paragraphs the different causes of hypomagnesemia will be discussed in more detail.

Table 1. Clinical symptoms of hypermagnesemia and hypomagnesemia

Hypermagnesemia (95)	***Hypomagnesemia (95, 98)***
Neuromuscular: diminished reflexes, somnolence, paralysis, apnea	Neuromuscular: muscle weakness, nystagmus, tetany, seizures
Cardiovascular: bradycardia, hypotension, arrhythmias and even cardiac arrest	Cardiovascular: arrhythmias, heart arrest
Hyperkalemia	Hypokalemia
Hypocalcemia	Hypocalcemia
Nausea	Bone instability

Short overview of different forms of primary inherited hypomagnesemia

In recent years, genetic investigations of patients with hereditary forms of hypomagnesemia unraveled many details of Mg^{2+} homeostasis, especially contributing to our knowledge of the DCT. Interestingly, besides hypomagnesemia the phenotypes of these patients are quite diverse (**Table 2**). This is dependent on the affected gene involved. Two factors are essential for the severity of the disease: *i*) the expression profile of the gene and; *ii*) the importance of the gene during different developmental stages and during maturity. These factors determine the extensiveness and the onset of the disease. Finally, the quality of individual diagnoses is crucial in order to obtain the complete picture. Two independent groups identified mutations in *TRPM6* as underlying cause of the disease hypomagnesemia with secondary hypocalcemia (HSH). Patients affected by this autosomal-recessive disease, were diagnosed early after birth with seizures and tetany (103, 104). The elucidation of the genetic basis of isolated dominant hypomagnesemia (IDH) pointed to the *FXYD2* gene (105). Whereas, mutations in its regulating factor *HNF1B* are associated with hypomagnesemia combined with renal malformations, including cysts (67). Moreover, DNA screening of patients suffering from dominant hypomagnesemia revealed mutations in *CNNM2* (65). In addition, two groups independently revealed a new syndrome, in which hypomagnesemia is one of the symptoms. A mutation in the *KCNJ10* gene, which encodes Kir4.1, was the underlying cause (106, 107). Besides, EGF was identified as a magnesiotropic hormone, since a mutation in this gene resulted in isolated autosomal recessive renal hypomagnesemia

(IRH) (88). EGF is the end product of a cleavage process of its large membrane anchored precursor, called pro-EGF (108). Groenestege *et al*. showed that supernatant collected from the basolateral side of Madin-Darby canine kidney (MDCK) cells, stably transfected with mutant pro-EGF, fails to stimulate the TRPM6 current in TRPM6-transfected human embryonic kidney 293 (HEK293) cells. In contrast, the apical supernatant of this mutant pro-EGF-transfected cells showed a similar stimulatory effect as wild type pro-EGF. Therefore, the authors hypothesized that the mutation causes impaired basolateral sorting or cleavage of pro-EGF, resulting in defective stimulation of TRPM6 and consequently Mg^{2+} loss via the urine (88). Finally, our group has shown that autosomal-dominant hypomagnesemia in a large Brazilian family is caused by a mutation in the *KCNA1* gene, encoding Kv1.1 (61).

Also mutations in proteins involved in paracellular transport in TAL were linked to disturbances of Mg^{2+} homeostasis. Patients with the renal disorder familial hypomagnesemia with hypercalciuria and nephrocalcinosis (FHHNC), develop hypomagnesemia due to progressive renal Mg^{2+} wasting. The underlying causes are mutations in CLDN16 (45) and CLDN19 (**Table 2**) (46).

Secondary inherited hypomagnesemia: Bartter and Gitelman syndromes

Several inherited disorders exist which cause hypomagnesemia as additional effect. Bartter and Gitelman syndromes are classical examples. These syndromes are characterized amongst the salt-losing tubulopathies with secondary hyperaldosteronism, indicating the activation of the renin-aldosterone-angiotensin system (RAAS) due to H_2O loss initiated by the salt wastage (109). Bartter syndrome consists of five subtypes (type I-V), correlating with five different genes, which are all expressed in TAL and some in DCT as well, that can be affected. These genes code for: NKCC2, ROMK, CLC-Kb, and its essential β-subunit Barttin, and the CaSR. The subtypes cause different phenotypes, however, all of them already *in utero* or in the first years of life (110). All five types of Bartter syndrome are characterized by severe Na^+ and Cl^- wasting, resulting in polyuria and hypokalemic metabolic alkalosis (111). Interestingly, hypomagnesemia is only sporadically observed in antenatal Bartter syndrome (Bartter types I and II) and type IV (**Table 2**), whereas patients with classical Bartter syndrome (subtype III) or type V are regularly diagnosed with aberrations in Mg^{2+} homeostasis (112-114). Probably, the degree of Na^+ loss is a determinant for whether or not Mg^{2+} reabsorption in TAL is disturbed. However, the detailed mechanism causing these different phenotypes, concerning Mg^{2+} status, is not yet resolved (115). Gitelman syndrome manifests at a later age and has a milder phenotype compared to Bartter syndrome. This disease is caused by mutations in NCC present in DCT and is characterized by hypokalemic metabolic alkalosis, hypomagnesemia and hypocalciuria (116).

Table 2. Overview of factors causing hypomagnesemia

Primary inherited hypomagnesemia		
Disorder	***Gene (Protein)***	***Ref.***
Hypomagnesemia with Secondary Hypocalcemia (HSH)	*TRPM6* (TRPM6)	(103, 104)
Isolated Dominant Hypomagnesemia (IDH)	*FXYD2* (Na^+, K^+-ATPase γ-subunit)	(105)
Abnormal renal development and hypomagnesemia	*HNF1B* (HNF1B)	(67)
Dominant hypomagnesemia	*CNNM2* (CNNM2)	(65)
Epilepsy, Ataxia, Sensorineural deafness and Tubulopathy (EAST syndrome) or Seizures, Sensorineural deafness, Ataxia, Mental retardation and Electrolyte imbalance (SeSAME syndrome)	*KCNJ10* (Kir4.1)	(106, 107)
Isolated autosomal Recessive renal Hypomagnesemia (IRH)	*EGF* (EGF)	(88)
Autosomal dominant hypomagnesemia	*KCNA1* (Kv1.1)	(61)
Familial Hypomagnesemia with Hypercalciuria and Nephro Calcinosis (FHHNC)	*CLDN16* (claudin-16) or *CLDN19* (claudin-19)	(45, 46)
Secondary inherited hypomagnesemia		
Disorder	***Gene (Protein)***	***Ref.***
Bartter syndrome	*CLCNKB* (CLC-Kb) or *CASR* (CaSR)	(62, 114, 117)
Gitelman syndrome	*SLC12A3* (NCC)	(116)
Acquired hypomagnesemia (factors might coincide)		
Causative factor	***Examples***	***Ref.***
Drug-induced	Thiazide and loop diuretics, cisplatin, erlotinib, cyclosporine A, rapamycin	(118-122)
Insufficient dietary Mg^{2+} intake	Malnutrition	(123)
Malabsorption of Mg^{2+}	Diarrhea, vomiting	(124)

Acquired hypomagnesemia

Drug use and malnutrition are the most important causes of acquired hypomagnesemia and will be discussed in this paragraph in more detail. Unlike the inherited forms of hypomagnesemia, this electrolyte disturbance can be obtained during life.

Hypomagnesemia as side effect of medication

Diuretics are drugs that induce Na^+ wastage and secondary H_2O loss. They are generally prescribed in the treatment of hypertension and edema. A well-known adverse effect of diuretics is the development of hypomagnesemia. Loop diuretics inhibit the reabsorption activities of the TAL. For example, furosemide-treatment might result in a similar phenotype as antenatal Bartter syndrome, caused by blocking NKCC2 (119). Within the first hours after a single dose of furosemide, urinary Mg^{2+} excretion is significantly increased (125, 126). However, like for antenatal Bartter syndrome, hypomagnesemia is not regularly diagnosed in patients chronically treated with furosemide; the Mg^{2+} status seems to depend mainly on the general state of health of these patients (127-130). Thiazide diuretics act on NCC, causing equivalent symptoms as observed for Gitelman syndrome (120). The anticancer drug cis-diamminedichloroplatinum(II) (cisplatin) is a potent agent for the treatment of solid tumors. This compound induces hypomagnesemia in about 50% of the patients treated, depending on dosage, amount of cycles and combination of the chemotherapy (121, 122). Although, nephrotoxicity and damage to DCT cells plays a role in the development of hypomagnesemia due to cisplatin treatment, the detailed mechanism is still unknown. Another group of chemotherapeutics, which act on the EGFR (Erlotinib and Cetuximab), regularly cause hypomagnesemia, by obstructing ligand binding to this receptor and consequently prevent the stimulation of TRPM6 in DCT (131). In addition, the calcineurin inhibitors (cyclosporin A and tacrolimus) form a group of immunosuppressive agents with nephrotoxicity and hypomagnesemia as iterative side effects. Moreover, antimicrobials, with gentamycin, rapamycin and pentamidine as most prominent examples can affect Mg^{2+} homeostasis as well (**Table 2**) (118). In contrast to the above described drugs which all have a renal effect, proton pump inhibitors induce hypomagnesemia possibly by affecting the intestine (132). These compounds, prescribed for their reduction of acid secretion, probably affect the absorption of Mg^{2+} (118).

Hypomagnesemia due to insufficient dietary Mg^{2+} intake, malabsorption and co-morbidity

Consuming a healthy diverse diet should result in adequate ingestion of Mg^{2+}. Nevertheless, there is evidence for continued insufficient dietary Mg^{2+} intake, resulting in many healthy people ingesting Mg^{2+} below RDA. The clinical impact of this malnutrition is not clear (123). In addition, vomiting and more often diarrhea are causes of malabsorption of Mg^{2+} (**Table 2**) (124). Frequently, drug use indirectly results in these gastrointestinal problems, however, impaired Mg^{2+} absorption can also be induced directly by characteristic diseases of this organ like gastrointestinal fistulas or inflammatory bowel disease (133). Unfortunately, hypomagnesemia is repeatedly diagnosed in patients with chronic diseases. Chronic alcohol abuse is related to hypomagnesemia, the prevalence is approximately 30% in alcoholic patients. This is caused by multiple factors, of which renal Mg^{2+} wastage and malnutrition are prominent (134). DM2, with an alarming prevalence in Western countries, related to overweight and obesity, is associated with hypomagnesemia as well. Probably, the development of insulin resistance during a Mg^{2+}-deficient state,

explains the underlying mechanism (135). A defect in TRPM6, might form the molecular basis (87). Heart and vascular diseases, another major contributor to decreased lifespan and rising health care costs, probably results in hypomagnesemia due to comorbidity, like renal insufficiency or via treatment with diuretics or surgery (136-138). In addition, it has been suggested that Mg^{2+} deficiency is a risk factor for some types of cancer and that it plays a role in progression of the disease or complicates (drug) therapy (139). Interestingly, a protective role of Mg^{2+} in various diseases, in particular cardiovascular pathology and subarachnoid hemorrhage, has been demonstrated (82, 135, 140-143).

Mg^{2+} in relation to other electrolytes

Mg^{2+} and Ca^{2+} are lookalikes, concerning the divalent state and chemical reactivity of these cations. Some binding proteins like PV can, although the affinities are generally quite different, interact with both divalents (55, 57). Subsequently, active transport of these electrolytes is executed by transporters of the same transient receptor potential (TRP)-family (144). In addition, diffusion through the tight junctions in TAL for example does not discriminate between Ca^{2+} and Mg^{2+} ions (145). However, often these ions exert antagonistic biological actions or modulate each other's actions (146-148). Mainly, because Ca^{2+} ions dehydrate easily compared to Mg^{2+}, which is more soluble, these ions can act differently. Mg^{2+} transporters require specific characteristics to recognize the highly hydrophilic state and finally to transport Mg^{2+} (149).

Close interaction of Mg^{2+} and Ca^{2+} homeostasis

Maintenance of the Ca^{2+} balance is of vital importance, especially for a lot of brain and heart physiological functions (35). Similar to the regulation of the Mg^{2+} balance, the concerted role of bone, intestine and kidney is vital. Ca^{2+} is in part absorbed more proximal in the intestine compared to Mg^{2+}, in fact largely in the duodenum (35, 150). This process is dependent on the gradient created by the Na^{+} and H_2O absorption (151). In addition, renal Ca^{2+} reabsorption is slightly different from Mg^{2+} reabsorption. The PT reabsorbs ~65% and the TAL an additional ~20% of the amount of Ca^{2+} filtered by the glomerulus, in a passive paracellular manner. Ca^{2+} is actively transported in DCT2 and the connecting tubule (CNT), resulting in the absorption of the final ~15%. From the pro-urine, Ca^{2+} enters these cells via the epithelial Ca^{2+} channel TRPV5. It is transported through the cytosol, in association with calbindin-D_{28K} to the basolateral cell membrane, where it is extruded by the Na^{+}, Ca^{2+}-exchanger (NCX1) and the plasma membrane ATPase type 1b (PMCA1b) (35, 152). Ca^{2+} homeostasis is maintained by the four calciotropic hormones: i) PTH; ii) $1,25(OH)_2D_3$; iii) calcitonin and; klotho (35, 151, 153, 154). Ca^{2+} influx via TRPV5 and its relative TRPV6 is an important regulatory target of PTH and $1,25(OH)_2D_3$ (155). PTH activates TRPV5 via protein kinase A (PKA) signaling and subsequent phosphorylation of the carboxyl tail (156). Besides, PTH is involved in the mobilization of Ca^{2+} from in bone and stimulation of Ca^{2+} absorption in the intestine via $1,25(OH)_2D_3$ (157). PTH release is regulated by the parathyroid gland, in response to changes in the plasma Ca^{2+} concentration. The CaSR has a central role in this process (157, 158). In response to a reduced extracellular Ca^{2+} or Mg^{2+} level, the CaSR is less activated, which results in a relatively low intracellular Ca^{2+} concentration ($[Ca^{2+}]_i$) and subsequent release of PTH into

the circulation from the cells of the parathyroid gland (157, 159, 160). This hormonal regulation is of special interest, since there is a lot of evidence that these hormones influence Mg^{2+} homeostasis as well (161). Besides, it has been shown that dietary Mg^{2+} restriction not only leads to renal Mg^{2+} conservation, but also to Ca^{2+} conservation and that vise versa, a Mg^{2+}-enriched diet leads to increased excretion of both electrolytes (21). This close interaction of Mg^{2+} and Ca^{2+} homeostasis is in line with the longstanding observation of the development of hypocalcemia, in patients and animals with hypomagnesemia (25). The disease HSH, in which patients are affected by a non-functional TRPM6 channel, represents an example of this phenomenon (103, 104). It has been suggested that hypocalcemia is secondary to PTH and/or $1,25(OH)_2D_3$ failure resulting from Mg^{2+} deficiency (162, 163). In addition, a direct role for Mg^{2+} affecting Ca^{2+} metabolism, including regulation of TRPV5, forms an alternative pathway (164).

Hypomagnesemia: its effect on K^+ balance

Hypokalemia is probably the most common electrolyte disturbance encountered in hospitalized patients, with an incidence of around 20%. The clinical importance is, that severe aberrations in K^+ balance may predispose the patient to cardiac arrhythmias and paralysis (165). The extracellular and intracellular K^+ concentrations are essential components in skeletal muscle, cardiovascular and respiratory function by setting the membrane potential and propagation of action potentials (166). Like for Mg^{2+}, the kidney is the most important overall regulator of K^+ homeostasis, by adjusting the rate of K^+ excretion. Hypokalemia is in most patients of multifactorial nature, with gastrointestinal losses due to vomiting or diarrhea, or increased renal excretion of K^+ initiated by thiazide or loop diuretics like furosemide, usually included. In around 60% of the patients diagnosed with hypokalemia, hypomagnesemia co-exists (167). Importantly, Mg^{2+} deficiency can be the primary inducer of hypokalemia and also aggravates the situation. Low $[Mg^{2+}]_i$ impairs the Na^+, K^+-ATPase activity (168), likely via decreased MgATP substrate abundance (169). In addition, $[Mg^{2+}]_i$ can directly affect the activity of ROMK channels (170). This results in K^+-leakage from epithelial cells of TAL and CD into the tubular lumen (168, 171). In addition, inward-rectification of ROMK, facilitated by a proper Mg^{2+} balance is essential to limit K^+ excretion (168). Finally, many researchers have shown, using various experimental settings, that Mg^{2+} replacement should be considered as co-treatment in hypokalemic patients (140, 168).

Outline of this thesis

The main focus of this thesis is the molecular mechanisms underlying the development of hypomagnesemia. As described in the previous paragraphs, recent studies considerably increased our knowledge of renal reabsorption of Mg^{2+} in DCT. Especially, the essential role of TRPM6 in this process and its regulation by interacting proteins has been studied intensively. Nevertheless, many details still need to be unraveled. By challenging the Mg^{2+} balance in animal models, using multifarious approaches, this thesis reports new insights and consequently increases our physiological understanding of Mg^{2+} transport. In **Chapter 2** the molecular mechanism by which the antineoplastic drug cisplatin causes hypomagnesemia was investigated *in vivo*. In particular the tubular toxicity of cisplatin to

the DCT was examined by measuring renal mRNA and protein levels of TRPM6, NCC and PV in mice. **Chapter 3** describes the effect of another drug, the loop diuretic furosemide, on Mg^{2+} homeostasis. It is reported that the chronic use of this compound in mice is accompanied by polyuria, whereas serum Mg^{2+} was not affected. Likely, enhanced reabsorption of Mg^{2+}, via the upregulated TRPM6 channel, compensates for the reduced reabsorption of Mg^{2+} in TAL. The impact of 2-week dietary Mg^{2+} restriction, on Mg^{2+} and Ca^{2+} handling in mice was evaluated in **Chapter 4.** Magnesiotropic genes were analysed for their susceptibility to dietary Mg^{2+} content. Besides TRPM6, HNF1B was shown to be upregulated in hypomagnesemic mice. It was demonstrated that NCC and PV, both expressed in DCT, were affected by the Mg^{2+} status. In addition, molecular players responsible for the association of renal Ca^{2+} and Mg^{2+} transport were examined. In **Chapter 5** the fate of the mutation in pro-EGF, causing hypomagnesemia in patients was investigated. The cellular sorting of pro-EGF and secretion of its different cleavage products was studied in transfected cell lines and the surrounding culture medium. To unravel this shedding process in detail, immunoblotting, enzyme-linked immunosorbent assay and immunocytochemistry followed by confocal microscopy analysis, were used. Finally, in **Chapter 6** the main findings of this thesis are summarized, and the conclusions and future directions are discussed.

References

1. Stwertka, A. A guide to the elements, second edition. *Oxford*. 1996.
2. Horst, E., and Mordike, B.L. Magnesium Technology, Metallurgy, Design Data, Applications. *Springer*. 2006.
3. Nishizawa, M., Durlach. New perspectives in Magnesium Research. *Springer*. 2007.
4. Letzig, D., Swiostek, J., Bohlen, J., et al. Wrought magnesium alloys for structural applications. *Materials Science and Technology* 24:991-996(996). 2008.
5. Rude, R.K. Magnesium deficiency: a cause of heterogeneous disease in humans. *J Bone Miner Res* 13:749-758. 1998.
6. Grubbs, R.D. Intracellular magnesium and magnesium buffering. *Biometals* 15:251-259. 2002.
7. Veloso, D., Guynn, R.W., Oskarsson, M., et al. The concentrations of free and bound magnesium in rat tissues. Relative constancy of free Mg 2+ concentrations. *J Biol Chem* 248:4811-4819. 1973.
8. Quamme, G.A. Magnesium homeostasis and renal magnesium handling. *Miner Electrolyte Metab* 19:218-225. 1993.
9. Musso, C.G. Magnesium metabolism in health and disease. *Int Urol Nephrol* 41:357-362. 2009.
10. Thienpont, L.M., Dewitte, K., and Stockl, D. Serum complexed magnesium--a cautionary note on its estimation and its relevance for standardizing serum ionized magnesium. *Clin Chem* 45:154-155. 1999.
11. Kulpmann, W.R., and Gerlach, M. Relationship between ionized and total magnesium in serum. *Scand J Clin Lab Invest Suppl* 224:251-258. 1996.
12. Grubbs, R.D., and Maguire, M.E. Magnesium as a regulatory cation: criteria and evaluation. *Magnesium* 6:113-127. 1987.
13. Wacker, W.E., and Parisi, A.F. Magnesium metabolism. *N Engl J Med* 278:712-717. 1968.
14. National Research Council (US). Recommended dietary allowances, 10th ed. *Washington, DC: National Academy Press*. 1989.
15. Fine, K.D., Santa Ana, C.A., Porter, J.L., et al. Intestinal absorption of magnesium from food and supplements. *J Clin Invest* 88:396-402. 1991.
16. Brannan, P.G., Vergne-Marini, P., Pak, C.Y., et al. Magnesium absorption in the human small intestine. Results in normal subjects, patients with chronic renal disease, and patients with absorptive hypercalciuria. *J Clin Invest* 57:1412-1418. 1976.
17. Graham, L.A., Caesar, J.J., and Burgen, A.S. Gastrointestinal absorption and excretion of Mg 28 in man. *Metabolism* 9:646-659. 1960.
18. Quamme, G.A. Recent developments in intestinal magnesium absorption. *Curr Opin Gastroenterol* 24:230-235. 2008.
19. Voets, T., Nilius, B., Hoefs, S., et al. TRPM6 forms the Mg2+ influx channel involved in intestinal and renal Mg2+ absorption. *J Biol Chem* 279:19-25. 2004.
20. Schweigel, M., and Martens, H. Magnesium transport in the gastrointestinal tract. *Front Biosci* 5:D666-677. 2000.
21. Groenestege, W.M., Hoenderop, J.G., van den Heuvel, L., et al. The epithelial Mg2+ channel transient receptor potential melastatin 6 is regulated by dietary Mg2+ content and estrogens. *J Am Soc Nephrol* 17:1035-1043. 2006.
22. Alfrey, A.C., and Miller, N.L. Bone magnesium pools in uremia. *J Clin Invest* 52:3019-3027. 1973.
23. Wallach, S. Effects of magnesium on skeletal metabolism. *Magnes Trace Elem* 9:1-14. 1990.
24. Rude, R.K., Kirchen, M.E., Gruber, H.E., et al. Magnesium deficiency-induced osteoporosis in the rat: uncoupling of bone formation and bone resorption. *Magnes Res* 12:257-267. 1999.
25. Rude, R.K., Singer, F.R., and Gruber, H.E. Skeletal and hormonal effects of magnesium deficiency. *J Am Coll Nutr* 28:131-141. 2009.
26. Dai, L.J., Ritchie, G., Kerstan, D., et al. Magnesium transport in the renal distal

convoluted tubule. *Physiol Rev* 81:51-84. 2001.
27. Brunette, M.G., and Crochet, M.E. Fluormetric method for the determination of magnesium in renal tubular fluid. *Anal Biochem* 65:79-88. 1975.
28. Grimellec, C.L., Poujeol, P., and Rouffignia, C. 3H-inulin and electrolyte concentrations in Bowman's capsule in rat kidney. Comparison with artificial ultrafiltration. *Pflugers Arch* 354:117-131. 1975.
29. Yeaman, C., Grindstaff, K.K., and Nelson, W.J. New perspectives on mechanisms involved in generating epithelial cell polarity. *Physiol Rev* 79:73-98. 1999.
30. Dragsten, P.R., Blumenthal, R., and Handler, J.S. Membrane asymmetry in epithelia: is the tight junction a barrier to diffusion in the plasma membrane? *Nature* 294:718-722. 1981.
31. Rodriguez-Boulan, E., and Nelson, W.J. Morphogenesis of the polarized epithelial cell phenotype. *Science* 245:718-725. 1989.
32. de Rouffignac, C., and Quamme, G. Renal magnesium handling and its hormonal control. *Physiol Rev* 74:305-322. 1994.
33. Ruska, H., Moore, D.H., and Weinstock, J. The base of the proximal convoluted tubule cells of rat kidney. *J Biophys Biochem Cytol* 3:249-254. 1957.
34. Murayama, Y., Morel, F., and Le Grimellec, C. Phosphate, calcium and magnesium transfers in proximal tubules and loops of Henle, as measured by single nephron microperfusion experiments in the rat. *Pflugers Arch* 333:1-16. 1972.
35. Hoenderop, J.G., Nilius, B., and Bindels, R.J. Calcium absorption across epithelia. *Physiol Rev* 85:373-422. 2005.
36. Le Grimellec, C. Micropuncture study along the proximal convoluted tubule. Electrolyte reabsorption in first convolutions. *Pflugers Arch* 354:133-150. 1975.
37. Quamme, G.A., and Smith, C.M. Magnesium transport in the proximal straight tubule of the rabbit. *Am J Physiol* 246:F544-550. 1984.
38. Schneider, E.G., Strandhoy, J.W., Willis, L.R., et al. Relationship between proximal sodium reabsorption and excretion of calcium, magnesium and phosphate. *Kidney Int* 4:369-376. 1973.
39. Preisig, P.A., and Rector, F.C., Jr. Role of Na+-H+ antiport in rat proximal tubule NaCl absorption. *Am J Physiol* 255:F461-465. 1988.
40. Maunsbach, A.B., Marples, D., Chin, E., et al. Aquaporin-1 water channel expression in human kidney. *J Am Soc Nephrol* 8:1-14. 1997.
41. Preston, G.M., Carroll, T.P., Guggino, W.B., et al. Appearance of water channels in Xenopus oocytes expressing red cell CHIP28 protein. *Science* 256:385-387. 1992.
42. Quamme, G.A. Control of magnesium transport in the thick ascending limb. *Am J Physiol* 256:F197-210. 1989.
43. Greger, R. Ion transport mechanisms in thick ascending limb of Henle's loop of mammalian nephron. *Physiol Rev* 65:760-797. 1985.
44. Amemiya, M., Loffing, J., Lotscher, M., et al. Expression of NHE-3 in the apical membrane of rat renal proximal tubule and thick ascending limb. *Kidney Int* 48:1206-1215. 1995.
45. Simon, D.B., Lu, Y., Choate, K.A., et al. Paracellin-1, a renal tight junction protein required for paracellular Mg2+ resorption. *Science* 285:103-106. 1999.
46. Konrad, M., Schaller, A., Seelow, D., et al. Mutations in the tight-junction gene claudin 19 (CLDN19) are associated with renal magnesium wasting, renal failure, and severe ocular involvement. *Am J Hum Genet* 79:949-957. 2006.
47. Hou, J., Renigunta, A., Konrad, M., et al. Claudin-16 and claudin-19 interact and form a cation-selective tight junction complex. *J Clin Invest* 118:619-628. 2008.
48. Houillier, P., and Paillard, M. Calcium-sensing receptor and renal cation handling. *Nephrol Dial Transplant* 18:2467-2470. 2003.
49. Brown, E.M., and MacLeod, R.J. Extracellular calcium sensing and

extracellular calcium signaling. *Physiol Rev* 81:239-297. 2001.
50. Linss, W., and Geyer, G. [the Electron Microscopic Structure of the Kidney Tubule in Rana Esculenta]. *Anat Anz* 115:281-296. 1964.
51. Doucet, A., Katz, A.I., and Morel, F. Determination of Na-K-ATPase activity in single segments of the mammalian nephron. *Am J Physiol* 237:F105-113. 1979.
52. Wilson, F.H., Hariri, A., Farhi, A., et al. A cluster of metabolic defects caused by mutation in a mitochondrial tRNA. *Science* 306:1190-1194. 2004.
53. Loffing, J., Loffing-Cueni, D., Valderrabano, V., et al. Distribution of transcellular calcium and sodium transport pathways along mouse distal nephron. *Am J Physiol Renal Physiol* 281:F1021-1027. 2001.
54. Ikura, M., and Ames, J.B. Genetic polymorphism and protein conformational plasticity in the calmodulin superfamily: two ways to promote multifunctionality. *Proc Natl Acad Sci U S A* 103:1159-1164. 2006.
55. Yang, W., Lee, H.W., Hellinga, H., et al. Structural analysis, identification, and design of calcium-binding sites in proteins. *Proteins* 47:344-356. 2002.
56. Cates, M.S., Teodoro, M.L., and Phillips, G.N., Jr. Molecular mechanisms of calcium and magnesium binding to parvalbumin. *Biophys J* 82:1133-1146. 2002.
57. Eberhard, M., and Erne, P. Calcium and magnesium binding to rat parvalbumin. *Eur J Biochem* 222:21-26. 1994.
58. Belge, H., Gailly, P., Schwaller, B., et al. Renal expression of parvalbumin is critical for NaCl handling and response to diuretics. *Proc Natl Acad Sci U S A* 104:14849-14854. 2007.
59. Flatman, P.W. Mechanisms of magnesium transport. *Annu Rev Physiol* 53:259-271. 1991.
60. Obermuller, N., Bernstein, P., Velazquez, H., et al. Expression of the thiazide-sensitive Na-Cl cotransporter in rat and human kidney. *Am J Physiol* 269:F900-910. 1995.
61. Glaudemans, B., van der Wijst, J., Scola, R.H., et al. A missense mutation in the Kv1.1 voltage-gated potassium channel-encoding gene KCNA1 is linked to human autosomal dominant hypomagnesemia. *J Clin Invest* 119:936-942. 2009.
62. Simon, D.B., Bindra, R.S., Mansfield, T.A., et al. Mutations in the chloride channel gene, CLCNKB, cause Bartter's syndrome type III. *Nat Genet* 17:171-178. 1997.
63. Adachi, S., Uchida, S., Ito, H., et al. Two isoforms of a chloride channel predominantly expressed in thick ascending limb of Henle's loop and collecting ducts of rat kidney. *J Biol Chem* 269:17677-17683. 1994.
64. Lourdel, S., Paulais, M., Cluzeaud, F., et al. An inward rectifier K(+) channel at the basolateral membrane of the mouse distal convoluted tubule: similarities with Kir4-Kir5.1 heteromeric channels. *J Physiol* 538:391-404. 2002.
65. Stuiver, M., Lainez, S., Will, C., et al. CNNM2, encoding a basolateral protein required for renal Mg2+ handling, is mutated in dominant hypomagnesemia. *Am J Hum Genet* 88:333-343. 2011.
66. de Baaij, J.H., Stuiver, M., Meij, I.C., et al. Membrane topology and intracellular processing of cyclin M2 (CNNM2). *J Biol Chem* 287:13644-13655. 2012.
67. Adalat, S., Woolf, A.S., Johnstone, K.A., et al. HNF1B mutations associate with hypomagnesemia and renal magnesium wasting. *J Am Soc Nephrol* 20:1123-1131. 2009.
68. Clapham, D.E., Runnels, L.W., and Strubing, C. The TRP ion channel family. *Nat Rev Neurosci* 2:387-396. 2001.
69. Chubanov, V., Waldegger, S., Mederos y Schnitzler, M., et al. Disruption of TRPM6/TRPM7 complex formation by a mutation in the TRPM6 gene causes hypomagnesemia with secondary hypocalcemia. *Proc Natl Acad Sci U S A* 101:2894-2899. 2004.
70. Schmitz, C., Perraud, A.L., Johnson, C.O., et al. Regulation of vertebrate cellular Mg2+ homeostasis by TRPM7. *Cell* 114:191-200. 2003.

71. Schmitz, C., Dorovkov, M.V., Zhao, X., et al. The channel kinases TRPM6 and TRPM7 are functionally nonredundant. *J Biol Chem* 280:37763-37771. 2005.
72. Xie, J., Sun, B., Du, J., et al. Phosphatidylinositol 4,5-bisphosphate (PIP(2)) controls magnesium gatekeeper TRPM6 activity. *Sci Rep* 1:146. 2011.
73. Li, M., Jiang, J., and Yue, L. Functional characterization of homo- and heteromeric channel kinases TRPM6 and TRPM7. *J Gen Physiol* 127:525-537. 2006.
74. Montell, C. Mg2+ homeostasis: the Mg2+nificent TRPM chanzymes. *Curr Biol* 13:R799-801. 2003.
75. van der Wijst, J., Hoenderop, J.G., and Bindels, R.J. Epithelial Mg2+ channel TRPM6: insight into the molecular regulation. *Magnes Res* 22:127-132. 2009.
76. Cao, G., Thebault, S., van der Wijst, J., et al. RACK1 inhibits TRPM6 activity via phosphorylation of the fused alpha-kinase domain. *Curr Biol* 18:168-176. 2008.
77. Cao, G., van der Wijst, J., van der Kemp, A., et al. Regulation of the epithelial Mg2+ channel TRPM6 by estrogen and the associated repressor protein of estrogen receptor activity (REA). *J Biol Chem* 284:14788-14795. 2009.
78. Cao, G., Lee, K.P., van der Wijst, J., et al. Methionine sulfoxide reductase B1 (MsrB1) recovers TRPM6 channel activity during oxidative stress. *J Biol Chem* 285:26081-26087. 2010.
79. Walder, R.Y., Yang, B., Stokes, J.B., et al. Mice defective in Trpm6 show embryonic mortality and neural tube defects. *Hum Mol Genet* 18:4367-4375. 2009.
80. Woudenberg-Vrenken, T.E., Sukinta, A., van der Kemp, A.W., et al. Transient receptor potential melastatin 6 knockout mice are lethal whereas heterozygous deletion results in mild hypomagnesemia. *Nephron Physiol* 117:p11-19. 2011.
81. Kazaks, A.G., Uriu-Adams, J.Y., Albertson, T.E., et al. Effect of oral magnesium supplementation on measures of airway resistance and subjective assessment of asthma control and quality of life in men and women with mild to moderate asthma: a randomized placebo controlled trial. *J Asthma* 47:83-92. 2010.
82. Barbagallo, M., Dominguez, L.J., Galioto, A., et al. Role of magnesium in insulin action, diabetes and cardio-metabolic syndrome X. *Mol Aspects Med* 24:39-52. 2003.
83. Quamme, G.A. Renal handling of magnesium: drug and hormone interactions. *Magnesium* 5:248-272. 1986.
84. Ritchie, G., Kerstan, D., Dai, L.J., et al. 1,25(OH)(2)D(3) stimulates Mg2+ uptake into MDCT cells: modulation by extracellular Ca2+ and Mg2+. *Am J Physiol Renal Physiol* 280:F868-878. 2001.
85. al-Ghamdi, S.M., Cameron, E.C., and Sutton, R.A. Magnesium deficiency: pathophysiologic and clinical overview. *Am J Kidney Dis* 24:737-752. 1994.
86. Nijenhuis, T., Renkema, K.Y., Hoenderop, J.G., et al. Acid-base status determines the renal expression of Ca2+ and Mg2+ transport proteins. *J Am Soc Nephrol* 17:617-626. 2006.
87. Nair, A.V., Hocher, B., Verkaart, S., et al. Loss of insulin-induced activation of TRPM6 magnesium channels results in impaired glucose tolerance during pregnancy. *Proc Natl Acad Sci U S A* 109:11324-11329. 2012.
88. Groenestege, W.M., Thebault, S., van der Wijst, J., et al. Impaired basolateral sorting of pro-EGF causes isolated recessive renal hypomagnesemia. *J Clin Invest* 117:2260-2267. 2007.
89. Thebault, S., Alexander, R.T., Tiel Groenestege, W.M., et al. EGF increases TRPM6 activity and surface expression. *J Am Soc Nephrol* 20:78-85. 2009.
90. Ikari, A., Okude, C., Sawada, H., et al. TRPM6 expression and cell proliferation are up-regulated by phosphorylation of ERK1/2 in renal epithelial cells. *Biochem Biophys Res Commun* 369:1129-1133. 2008.
91. Touitou, Y., Auzeby, A., Camus, F., et al. Twenty-four-hour profiles of urinary excretion of calcium, magnesium, phosphorus, urea, and creatinine in healthy prepubertal boys. *Clin Biochem* 43:102-105. 2010.

92. Wong, E.T., Rude, R.K., Singer, F.R., et al. A high prevalence of hypomagnesemia and hypermagnesemia in hospitalized patients. *Am J Clin Pathol* 79:348-352. 1983.
93. Syedmoradi, L., Ghasemi, A., Zahediasl, S., et al. Prevalence of hypo- and hypermagnesemia in an Iranian urban population. *Ann Hum Biol* 38:150-155. 2011.
94. Whang, R., and Ryder, K.W. Frequency of hypomagnesemia and hypermagnesemia. Requested vs routine. *JAMA* 263:3063-3064. 1990.
95. Topf, J.M., and Murray, P.T. Hypomagnesemia and hypermagnesemia. *Rev Endocr Metab Disord* 4:195-206. 2003.
96. Kanbay, M., Goldsmith, D., Uyar, M.E., et al. Magnesium in chronic kidney disease: challenges and opportunities. *Blood Purif* 29:280-292.
97. Onishi, S., and Yoshino, S. Cathartic-induced fatal hypermagnesemia in the elderly. *Intern Med* 45:207-210. 2006.
98. Agus, Z.S. Hypomagnesemia. *J Am Soc Nephrol* 10:1616-1622. 1999.
99. Chernow, B., Bamberger, S., Stoiko, M., et al. Hypomagnesemia in patients in postoperative intensive care. *Chest* 95:391-397. 1989.
100. Ryzen, E. Magnesium homeostasis in critically ill patients. *Magnesium* 8:201-212. 1989.
101. Swaminathan, R. Magnesium metabolism and its disorders. *Clin Biochem Rev* 24:47-66. 2003.
102. Sontia, B., and Touyz, R.M. Role of magnesium in hypertension. *Arch Biochem Biophys* 458:33-39. 2007.
103. Schlingmann, K.P., Weber, S., Peters, M., et al. Hypomagnesemia with secondary hypocalcemia is caused by mutations in TRPM6, a new member of the TRPM gene family. *Nat Genet* 31:166-170. 2002.
104. Walder, R.Y., Landau, D., Meyer, P., et al. Mutation of TRPM6 causes familial hypomagnesemia with secondary hypocalcemia. *Nat Genet* 31:171-174. 2002.
105. Meij, I.C., Koenderink, J.B., van Bokhoven, H., et al. Dominant isolated renal magnesium loss is caused by misrouting of the Na(+),K(+)-ATPase gamma-subunit. *Nat Genet* 26:265-266. 2000.
106. Scholl, U.I., Choi, M., Liu, T., et al. Seizures, sensorineural deafness, ataxia, mental retardation, and electrolyte imbalance (SeSAME syndrome) caused by mutations in KCNJ10. *Proc Natl Acad Sci U S A* 106:5842-5847. 2009.
107. Bockenhauer, D., Feather, S., Stanescu, H.C., et al. Epilepsy, ataxia, sensorineural deafness, tubulopathy, and KCNJ10 mutations. *N Engl J Med* 360:1960-1970. 2009.
108. Bell, G.I., Fong, N.M., Stempien, M.M., et al. Human epidermal growth factor precursor: cDNA sequence, expression in vitro and gene organization. *Nucleic Acids Res* 14:8427-8446. 1986.
109. Seyberth, H.W., and Schlingmann, K.P. Bartter- and Gitelman-like syndromes: salt-losing tubulopathies with loop or DCT defects. *Pediatr Nephrol* 26:1789-1802. 2011.
110. Unwin, R.J., and Capasso, G. Bartter's and Gitelman's syndromes: their relationship to the actions of loop and thiazide diuretics. *Curr Opin Pharmacol* 6:208-213. 2006.
111. Bartter, F.C., Pronove, P., Gill, J.R., Jr., et al. Hyperplasia of the juxtaglomerular complex with hyperaldosteronism and hypokalemic alkalosis. A new syndrome. *Am J Med* 33:811-828. 1962.
112. Pollak, M.R., Brown, E.M., Estep, H.L., et al. Autosomal dominant hypocalcaemia caused by a Ca(2+)-sensing receptor gene mutation. *Nat Genet* 8:303-307. 1994.
113. Schlingmann, K.P., Konrad, M., and Seyberth, H.W. Genetics of hereditary disorders of magnesium homeostasis. *Pediatr Nephrol* 19:13-25. 2004.
114. Konrad, M., Vollmer, M., Lemmink, H.H., et al. Mutations in the chloride channel gene CLCNKB as a cause of classic Bartter syndrome. *J Am Soc Nephrol* 11:1449-1459. 2000.
115. Dimke, H., Hoenderop, J.G., and Bindels, R.J. Hereditary tubular transport disorders: implications for renal handling

of Ca2+ and Mg2+. *Clin Sci (Lond)* 118:1-18. 2010.
116. Gitelman, H.J., Graham, J.B., and Welt, L.G. A new familial disorder characterized by hypokalemia and hypomagnesemia. *Trans Assoc Am Physicians* 79:221-235. 1966.
117. Pearce, S.H., Williamson, C., Kifor, O., et al. A familial syndrome of hypocalcemia with hypercalciuria due to mutations in the calcium-sensing receptor. *N Engl J Med* 335:1115-1122. 1996.
118. Lameris, A.L., Monnens, L.A., Bindels, R.J., et al. Drug-induced alterations in Mg2+ homoeostasis. *Clin Sci (Lond)* 123:1-14. 2012.
119. Hendry, B.M., and Ellory, J.C. Molecular sites for diuretic action. *Trends Pharmacol Sci* 9:416-421. 1988.
120. Nijenhuis, T., Vallon, V., van der Kemp, A.W., et al. Enhanced passive Ca2+ reabsorption and reduced Mg2+ channel abundance explains thiazide-induced hypocalciuria and hypomagnesemia. *J Clin Invest* 115:1651-1658. 2005.
121. Schilsky, R.L., and Anderson, T. Hypomagnesemia and renal magnesium wasting in patients receiving cisplatin. *Ann Intern Med* 90:929-931. 1979.
122. Buckley, J.E., Clark, V.L., Meyer, T.J., et al. Hypomagnesemia after cisplatin combination chemotherapy. *Arch Intern Med* 144:2347-2348. 1984.
123. Ford, E.S., and Mokdad, A.H. Dietary magnesium intake in a national sample of US adults. *J Nutr* 133:2879-2882. 2003.
124. Tong, G.M., and Rude, R.K. Magnesium deficiency in critical illness. *J Intensive Care Med* 20:3-17. 2005.
125. Nielsen, S.P., Andersen, O., and Steven, K.E. Magnesium and calcium metabolism during prolonged furosemide (Lasix) administration to normal rats. *Acta Pharmacol Toxicol (Copenh)* 27:469-479. 1969.
126. van Meyel, J.J., Smits, P., and Gribnau, F.W. Absence of magnesium sparing effect of a single dose of triamterene in combination with frusemide in healthy male adults. *Br J Clin Pharmacol* 30:774-777. 1990.
127. Davies, D.L., and Fraser, R. Do diuretics cause magnesium deficiency? *Br J Clin Pharmacol* 36:1-10. 1993.
128. Cohen, N., Almoznino-Sarafian, D., Zaidenstein, R., et al. Serum magnesium aberrations in furosemide (frusemide) treated patients with congestive heart failure: pathophysiological correlates and prognostic evaluation. *Heart* 89:411-416. 2003.
129. Dussol, B., Moussi-Frances, J., Morange, S., et al. A randomized trial of furosemide vs hydrochlorothiazide in patients with chronic renal failure and hypertension. *Nephrol Dial Transplant* 20:349-353. 2005.
130. Loon, N.R., Wilcox, C.S., and Unwin, R.J. Mechanism of impaired natriuretic response to furosemide during prolonged therapy. *Kidney Int* 36:682-689. 1989.
131. Costa, A., Tejpar, S., Prenen, H., et al. Hypomagnesaemia and targeted anti-epidermal growth factor receptor (EGFR) agents. *Target Oncol* 6:227-233. 2011.
132. Hess, M.W., Hoenderop, J.G., Bindels, R.J., et al. Systematic review: hypomagnesaemia induced by proton pump inhibition. *Aliment Pharmacol Ther* 36:405-413. 2012.
133. Mouw, D.R., Latessa, R.A., and Hickner, J. Clinical inquiries. What are the causes of hypomagnesemia? *J Fam Pract* 54:174-176. 2005.
134. Shane, S.R., and Flink, E.B. Magnesium deficiency in alcohol addiction and withdrawal. *Magnes Trace Elem* 10:263-268. 1991.
135. Barbagallo, M., and Dominguez, L.J. Magnesium metabolism in type 2 diabetes mellitus, metabolic syndrome and insulin resistance. *Arch Biochem Biophys* 458:40-47. 2007.
136. Reyes, A.J., and Leary, W.P. Cardiovascular toxicity of diuretics related to magnesium depletion. *Hum Toxicol* 3:351-371. 1984.
137. Aglio, L.S., Stanford, G.G., Maddi, R., et al. Hypomagnesemia is common following cardiac surgery. *J Cardiothorac Vasc Anesth* 5:201-208. 1991.
138. Abbott, K.C., and Bakris, G.L. Cardiology patient page. Kidney failure and

cardiovascular disease. *Circulation* 108:e114-115. 2003.
139. Castiglioni, S., and Maier, J.A. Magnesium and cancer: a dangerous liason. *Magnes Res* 24:S92-100. 2011.
140. Chakraborti, S., Chakraborti, T., Mandal, M., et al. Protective role of magnesium in cardiovascular diseases: a review. *Mol Cell Biochem* 238:163-179. 2002.
141. Akhtar, M.I., Ullah, H., and Hamid, M. Magnesium, a drug of diverse use. *J Pak Med Assoc* 61:1220-1225. 2011.
142. Cunha, A.R., Umbelino, B., Correia, M.L., et al. Magnesium and vascular changes in hypertension. *Int J Hypertens* 2012:754250. 2012.
143. van den Bergh, W.M., Algra, A., van der Sprenkel, J.W., et al. Hypomagnesemia after aneurysmal subarachnoid hemorrhage. *Neurosurgery* 52:276-281; discussion 281-272. 2003.
144. Hoenderop, J.G., and Bindels, R.J. Calciotropic and magnesiotropic TRP channels. *Physiology (Bethesda)* 23:32-40. 2008.
145. Monnens, L., Starremans, P., and Bindels, R. Great strides in the understanding of renal magnesium and calcium reabsorption. *Nephrol Dial Transplant* 15:568-571. 2000.
146. Altura, B.M., Altura, B.T., Carella, A., et al. Mg2+-Ca2+ interaction in contractility of vascular smooth muscle: Mg2+ versus organic calcium channel blockers on myogenic tone and agonist-induced responsiveness of blood vessels. *Can J Physiol Pharmacol* 65:729-745. 1987.
147. Jenkinson, D.H. The nature of the antagonism between calcium and magnesium ions at the neuromuscular junction. *J Physiol* 138:434-444. 1957.
148. Wang, H., Gopalakrishnan, V., McNeill, J.R., et al. Calcium antagonizes the magnesium-induced high affinity state of the hepatic vasopressin receptor for the agonist interaction. *Br J Pharmacol* 100:5-10. 1990.
149. Maguire, M.E., and Cowan, J.A. Magnesium chemistry and biochemistry. *Biometals* 15:203-210. 2002.
150. Christakos, S. Recent advances in our understanding of 1,25-dihydroxyvitamin D(3) regulation of intestinal calcium absorption. *Arch Biochem Biophys* 523:73-76. 2012.
151. Wasserman, R.H., and Fullmer, C.S. Vitamin D and intestinal calcium transport: facts, speculations and hypotheses. *J Nutr* 125:1971S-1979S. 1995.
152. Nijenhuis, T., Hoenderop, J.G., and Bindels, R.J. TRPV5 and TRPV6 in Ca(2+) (re)absorption: regulating Ca(2+) entry at the gate. *Pflugers Arch* 451:181-192. 2005.
153. Reichel, H., Koeffler, H.P., and Norman, A.W. The role of the vitamin D endocrine system in health and disease. *N Engl J Med* 320:980-991. 1989.
154. Chang, Q., Hoefs, S., van der Kemp, A.W., et al. The beta-glucuronidase klotho hydrolyzes and activates the TRPV5 channel. *Science* 310:490-493. 2005.
155. Friedman, P.A., Coutermarsh, B.A., Kennedy, S.M., et al. Parathyroid hormone stimulation of calcium transport is mediated by dual signaling mechanisms involving protein kinase A and protein kinase C. *Endocrinology* 137:13-20. 1996.
156. de Groot, T., Lee, K., Langeslag, M., et al. Parathyroid hormone activates TRPV5 via PKA-dependent phosphorylation. *J Am Soc Nephrol* 20:1693-1704. 2009.
157. Brown, E.M., Gamba, G., Riccardi, D., et al. Cloning and characterization of an extracellular Ca(2+)-sensing receptor from bovine parathyroid. *Nature* 366:575-580. 1993.
158. Riccardi, D., and Brown, E.M. Physiology and pathophysiology of the calcium-sensing receptor in the kidney. *Am J Physiol Renal Physiol* 298:F485-499. 2009.
159. Shoback, D., Thatcher, J., Leombruno, R., et al. Effects of extracellular Ca++ and Mg++ on cytosolic Ca++ and PTH release in dispersed bovine parathyroid cells. *Endocrinology* 113:424-426. 1983.
160. Friedman, P.A., and Goodman, W.G. PTH(1-84)/PTH(7-84): a balance of power. *Am J Physiol Renal Physiol* 290:F975-984. 2006.

161. Zofkova, I., and Kancheva, R.L. The relationship between magnesium and calciotropic hormones. *Magnes Res* 8:77-84. 1995.
162. Anast, C.S., Mohs, J.M., Kaplan, S.L., et al. Evidence for parathyroid failure in magnesium deficiency. *Science* 177:606-608. 1972.
163. Rude, R.K., Adams, J.S., Ryzen, E., et al. Low serum concentrations of 1,25-dihydroxyvitamin D in human magnesium deficiency. *J Clin Endocrinol Metab* 61:933-940. 1985.
164. Bonny, O., Rubin, A., Huang, C.L., et al. Mechanism of urinary calcium regulation by urinary magnesium and pH. *J Am Soc Nephrol* 19:1530-1537. 2008.
165. Gennari, F.J. Hypokalemia. *N Engl J Med* 339:451-458. 1998.
166. Sejersted, O.M., and Sjogaard, G. Dynamics and consequences of potassium shifts in skeletal muscle and heart during exercise. *Physiol Rev* 80:1411-1481. 2000.
167. Crop, M.J., Hoorn, E.J., Lindemans, J., et al. Hypokalaemia and subsequent hyperkalaemia in hospitalized patients. *Nephrol Dial Transplant* 22:3471-3477. 2007.
168. Huang, C.L., and Kuo, E. Mechanism of hypokalemia in magnesium deficiency. *J Am Soc Nephrol* 18:2649-2652. 2007.
169. Sachs, J.R. Interaction of magnesium with the sodium pump of the human red cell. *J Physiol* 400:575-591. 1988.
170. Yang, L., Frindt, G., and Palmer, L.G. Magnesium modulates ROMK channel-mediated potassium secretion. *J Am Soc Nephrol* 21:2109-2116. 2010.
171. Nichols, C.G., Ho, K., and Hebert, S. Mg(2+)-dependent inward rectification of ROMK1 potassium channels expressed in Xenopus oocytes. *J Physiol* 476:399-409. 1994.

Chapter 2

Cisplatin-induced injury of the renal distal convoluted tubule is associated with hypomagnesemia in mice

Annelies A. van Angelen*, Bob Glaudemans*, AnneMiete W.C.M. van der Kemp, Joost G.J. Hoenderop and René J.M. Bindels

* These authors contributed equally to this work

Department of Physiology, Radboud University Medical Center, Nijmegen, The Netherlands.

Nephrol Dial Transplant 28: 879–889, 2013

Abstract

Background. Cisplatin is an effective antineoplastic drug, but its clinical use is limited due to dose-dependent nephrotoxicity. The majority of cisplatin-treated patients develop hypomagnesemia, often associated with a reduced glomerular filtration rate (GFR), polyuria and other electrolyte disturbances. The aim of this study is to unravel the molecular mechanism responsible for these particular electrolyte disturbances.

Methods. Two groups of 10 mice were injected intraperitoneally three times, once every 4 days, with cisplatin (5 mg/kg body weight,) or vehicle. Serum and urine electrolyte concentrations were determined. Next, renal mRNA levels of distal convoluted tubule (DCT) genes epithelial Mg^{2+} channel TRPM6, the Na^{+}, Cl^{-} cotransporter (NCC), and parvalbumin (PV), as well as marker genes for other tubular segments were measured by real-time quantitative polymerase chain reaction (qPCR). Subsequently, renal protein levels of NCC, PV, aquaporin 1 and aquaporin 2 were determined using immunoblotting and immunohistochemistry (IHC).

Results. The cisplatin-treated mice developed significant polyuria (2.5 ± 0.3 and 0.9 ± 0.1 mL/24h, cisplatin versus control, $P < 0.05$), reduced creatinine clearance rate (C_{Cr}) (0.18 ± 0.02 and 0.26 ± 0.02 mL/min, cisplatin versus control, $P < 0.05$) and a substantially reduced serum level of Mg^{2+} (1.23 ± 0.03 and 1.58 ± 0.03 mmol/L, cisplatin versus control, $P < 0.05$), whereas serum Ca^{2+}, Na^{+} and K^{+} values were not altered. Measurements of 24 h urinary excretion demonstrated markedly increased Mg^{2+}, Ca^{2+}, Na^{+} and K^{+} levels in the cisplatin-treated group, whereas P_i levels were not changed. The mRNA levels of TRPM6, NCC and PV were significantly reduced in the cisplatin group. The expression levels of the marker genes for other tubular segments were unaltered, except for claudin-16, which was significantly upregulated by the cisplatin treatment. The observed DCT-specific downregulation was confirmed at the protein level.

Conclusions. The present study identified the DCT as an important cisplatin-affected renal segment, explaining the high prevalence of hypomagnesemia following treatment.

Introduction

Cis-Diamminedichloroplatinum(II) (Cisplatin) is a widely used cytotoxic agent with a broad range of actions in the treatment of solid tumours, including ovarian, endometrial, cervical, urothelial, testicular, head/neck and lung cancer (1). Cisplatin causes cytotoxic lesions in rapidly dividing cells, such as tumour cells, due to the formation of cross-links with RNA, DNA and protein (2). Despite its effect as an anti-cancer agent, clinical use is limited as ~20% of the patients who receive high-dose cisplatin develop severe renal dysfunction, often leading to acute renal failure (3-5). DNA-damaging agents usually have a less toxic effect on non-proliferating cells, yet, selective tubular epithelial cell damage has been demonstrated. Treatment with cisplatin or related compounds cause tissue damage by inflammation, oxidative stress injury, necrosis and/or apoptosis (4) of particularly the renal proximal tubule (PT) (6, 7) and/or the distal convoluted tubule (DCT) (8-13) in humans and a variety of animal models. The renal phenotype associated with treatment of cisplatin is multifold. The majority of cisplatin-treated patients suffer from hypomagnesemia (14, 15), often associated with a reduced glomerular filtration rate (GFR), polyuria and electrolyte disturbances such as sodium (Na^+), calcium (Ca^{2+}) and magnesium (Mg^{2+}) wasting and/or hypokalemic alkalosis (16-19). Previously, it was suggested that the DCT could play a prominent role in causing cisplatin-induced hypomagnesemia (20-22).

The observed nephrotoxicity likely results from cisplatin accumulation in the kidneys, which is five times higher in comparison with other tissues. Although platinum compounds are bound to proteins in the plasma, most cisplatin is unbound (5) and is freely filtered by the glomerulus. Next to filtration, renal cells secrete cisplatin from the blood to the tubular lumen (23). The extent to which either pathway is responsible for the induction of cisplatin-induced renal cell death is unclear. Cisplatin is rapidly removed from the body as ~65% of the cisplatin is excreted via the urine within the first 4 h following treatment (24). Cisplatin enters the tubular cell by passive diffusion and active uptake via specific transport mechanisms (25).

The present study aims to elucidate the molecular mechanism responsible for the cisplatin-induced hypomagnesemia. In recent years, the study of patients with hypomagnesaemia has led to the identification of genes involved in Mg^{2+} handling. A large fraction of these genes localize to the early part of the DCT (DCT1), indicating its prominent role in Mg^{2+} reabsorption (26). Examples are the transient receptor potential channel melastatin subtype 6 (TRPM6), the epidermal growth factor, the voltage-gated K^+ channel Kv1.1 and the Na^+, K^+-ATPase γ-subunit. We hypothesize that cisplatin-induced hypomagnesemia is caused by specific damage to the DCT. The effect of chronic cisplatin treatment on serum Na^+, potassium (K^+), Ca^{2+} and Mg^{2+} and urine Na^+, K^+, Ca^{2+}, Mg^{2+} and phosphate (P_i) levels was evaluated in mice. The mRNA and protein levels of renal Mg^{2+} and Na^+ transporting proteins were studied to indicate which segments of the tubule were affected.

Methods

Animal studies

Female C57BL/6J mice (10 weeks of age) were purchased from Charles River (L'Arbresle Cedex, France) and housed in a temperature- and light-controlled room with *ad libitum* access to standard pellet chow (SSNIFF spezialdiäten GmbH, Soest, Germany) and drinking water. Mice were randomly assigned to a control and a cisplatin treatment group (n = 10 per group). Cisplatin was administered using an intraperitoneal injection (5 mg/kg body weight per injection), while control animals received an intraperitoneal injection of vehicle only (0.9% (w/v) NaCl solution). The injections were administrated on days 0, 4 and 8. Before the start of the experiment, and on day 12, the mice were individually housed in metabolic cages enabling 24 h urine collections (under mineral oil to prevent evaporation) and to measure water and food intake. On day 13, blood samples were taken under isoflurane anaesthesia, after which the mice were sacrificed. Subsequently, kidneys were frozen immediately in liquid nitrogen or incubated in periodate-lysine-paraformaldehyde (PLP) solution for the isolation of mRNA and protein or immunohistochemistry (IHC) analysis, respectively. Blood was led to clot at room temperature, incubated overnight at 4°C and spun down for 5' at 13 250 × g. The serum was collected and used for analytical procedures. The animal ethics board of the Radboud University Nijmegen approved all experimental procedures.

Analytical procedures

Serum and urinary Mg^{2+} concentrations were determined using a colorimetric assay kit according to the manufacturer's protocol (Roche Diagnostics, Woerden, The Netherlands). Serum and urine Ca^{2+} concentrations were measured as described previously (27). A flame spectrophotometer (FCM 6343; Eppendorf) was used to measure serum and urine Na^{+} and K^{+} concentrations. Urine P_i concentrations were measured by the phosphomolybdate method with an Aeroset analyser (Abbott Diagnostics, Abbott Park, IL, USA).

Total kidney RNA isolation and cDNA synthesis

Total RNA was extracted from kidney using TriZol Total RNA isolation reagent according to standard procedures (Gibco BRL, Breda, The Netherlands). The obtained RNA was subjected to DNase treatment (Promega, Madison, WI, USA) to prevent genomic DNA contamination. All samples were resolved on a 1% w/v formaldehyde agarose gel to evaluate the RNA quality, while RNA concentration was determined by measuring the ratio of the UV absorbance at 260 and 280 nm using the NANODROP 2000c (Thermo scientific, Wilmington, DE, USA). Thereafter, 1.5 µg of RNA was reverse transcribed by Molony-Murine Leukemia Virus-Reverse Transcriptase (Invitrogen, Breda, The Netherlands) into cDNA according to the manufacturer's recommendations.

SYBR Green real-time quantitative polymerase chain reaction

Total kidney cDNA was used to determine the mRNA expression levels of genes of interest, as well as the reference gene glyceraldehyde 3-phosphate dehydrogenase (GAPDH). Primer3 software (http://frodo.wi.mit.edu/primer3/) was used to design real-time quantitative polymerase chain reaction (qPCR) primers according to the general criteria for real-time primers. All primer sequences used in this study are listed in **Table 1**

and **Figure 1** shows an overview of all markers used. Prior to real-time qPCR reactions the efficiency (95-105%) and dynamic range (R^2>0.98) were evaluated for each primer set. Real-time qPCR reactions were performed on a Bio-Rad CFX96™ Real-Time qPCR and Bio-Rad C1000™ Thermal Cycler system, using Bio-Rad iQ™ SYBR® Green Supermix. All amplicons showed the correct sizes after gel electrophoresis and the dissociation curves showed one distinct melting peak, ensuring the absence of a non-specific by-product or primer dimers. Moreover, no reverse transcription and no template controls were taken along.

Table 1. Sequences of mouse primers used for real-time qPCR

Gene	*Forward primer*	*Reverse primer*
GAPDH	5'-TAACATCAAATGGGGTGAGG-3'	5'-GGTTCACACCCATCACAAAC-3'
Kim-1	5'-TGTCGAGTGGAGATTCCTGGATGGT-3'	5'-GGTCTTCCTGTAGCTGTGGGCC-3'
TRPM6	5'-AAAGCCATGCGAGTTATCAGC-3'	5'-CTTCACAATGAAAACCTGCCC-3'
PV	5'-CGCTGAGGACATCAAGAAGG-3'	5'-CCGGGTTCTTTTTCTTCAGG-3'
NCC	5'-CTTCGGCCACTGGCATTCTG-3'	5'-GATGGCAAGGTAGGAGATGG-3'
NKCC2	5'-GGCTTGATCTTTGCTTTTGC-3'	5'-CCATCATTGAATCGCTCTCC-3'
NHE3	5'-TGCCTTGGTGGTACTTCTGG-3'	5'-TCGCTCCTCTTCACCTTCAG-3'
CLDN16	5'-GTTGCAGGGACCACATTAC-3'	5'-GAGGAGCGTTCGACGTAAAC-3'
CLDN19	5'-GGTTCCTTTCTCTGCTGCAC-3'	5'-CGGGCAACTTAACAACAGG-3'
AQP1	5'-CCGAGACTTAGGTGGCTCAG-3'	5'-TGATACCGCAGCCAGTGTAG-3'
SGLT1	5'-ATCTTCAACAGCGCCAGTAC-3'	5'-TCAGCACGAGGATGAACAAC-3'
TRPV5	5'-CCACAGTGATGCTGGAGAGG-3'	5'-GGATTCTGCTCCTGGTGGTG-3'
α-ENaC	5'-CATGCCTGGAGTCAACAATG-3'	5'-CCATAAAAGCAGGCTCATCC-3'
AQP2	5'-CTCCACAACAATGCAACAGC-3'	5'-GAGCAGCCGGTGAAATAGAT-3'
OCT2	5'-AAAATCGGTGCCAGTCTCTC-3'	5'-GACCAAGTCCAGGAACGAAG-3'
CTR1	5'-ACCACCTCAGCCTCACACTC-3'	5'-TCTCGGGCTATCTTGAGTCC-3'

Mouse primers used to perform SYBR Green real-time qPCR. GAPDH, glyceraldehyde 3-phosphate dehydrogenase; Kim-1, Kidney injury molecule-1; TRPM6, transient receptor potential melastatin member 6; PV, parvalbumin; NCC, Na^+, Cl^- cotransporter; NKCC2, Na^+, K^+, Cl^- cotransporter; NHE3, Na^+, H^+ exchanger 3; CLDN16, claudin-16; CLDN19, claudin-19; AQP1, aquaporin 1; SGLT1, sodium-glucose cotransporter 1; TRPV5, transient receptor potential vanilloid member; α-ENaC, epithelial Na^+ channel alfa subunit; AQP2, aquaporin 2; OCT2, organic cation transporter; CTR1, copper transporter 1.

Immunoblotting

Kidneys of control and cisplatin-treated mice were homogenized in homogenization buffer A (HbA; 20 mM Tris/HCl (pH = 7.4), 5 mM $MgCl_2$, 5 mM NaH_2PO_4, 1 mM EDTA, 80 mM sucrose, 1 mM PMSF, 1 μg/ml leupeptin and 10 μg/ml pepstatin). Protein concentration of the homogenates was determined using the Bio-Rad Protein Assay, (Bio-Rad, Munich, Germany). The proteins were solubilized by 30' incubation at 37°C in Laemmli buffer. Each

protein sample (60 μg) was separated on a SDS-PAGE gel and blotted to a PVDF-nitrocellulose membrane (Immobilon-P, Millipore Corporation, Bedford, MA, USA)

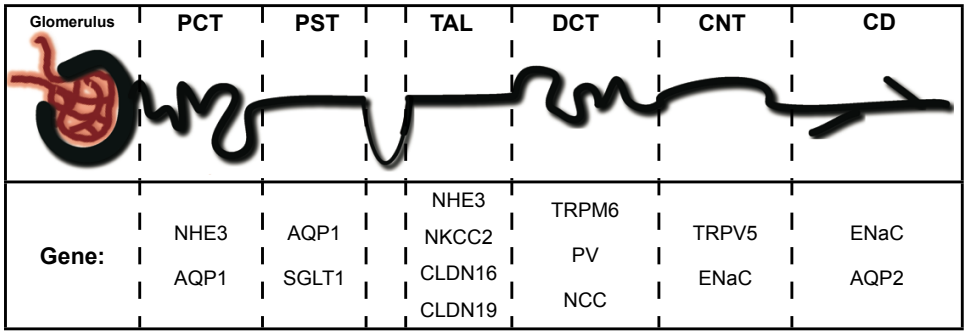

Figure 1. Schematic overview of a nephron depicting the expression of gene products used as marker to determine in which segments cisplatin exerts its effect. Nephron segments: PCT, proximal convoluted tubule; PST, proximal straight tubule; TAL, thick ascending limb of Henle's loop; DCT, distal convoluted tubule; CNT, connecting tubule; CD, collecting duct. Gene products used as marker: NHE3, Na^+, H^+ exchanger 3; AQP1, aquaporin 1; SGLT1, sodium-glucose cotransporter 1; NKCC2, Na^+, K^+, Cl^- cotransporter; CLDN16, claudin-16; CLDN19, claudin-19; TRPM6, transient receptor potential melastatin member 6; PV, parvalbumin; NCC, Na^+, Cl^- cotransporter; TRPV5, transient receptor potential vanilloid member 5; ENaC, epithelial Na^+ channel; AQP2, aquaporin 2.

Blots were incubated for 16 h with either a rabbit NCC antibody (1:500 dilution; Millipore, Billerica, MA, USA), a rabbit parvalbumin antibody (PV-28, 1:500 dilution; Swant, Bellinzona, Switzerland), and a mouse monoclonal aquaporin 1 (AQP1) antibody (1:100 dilution) (28), a rabbit aquaporin 2 (AQP2) antibody (1:500 dilution) or a mouse tubulin antibody (1:20 000 dilution); (these antibodies were provided by Prof. Deen). Thereafter, blots were incubated with peroxidase-conjugated secondary antibodies after which proteins were visualized by chemiluminescence (Pierce, Rockford, IL, USA). Immunopositive bands were scanned using ChemiDoc XRS (Bio-Rad) and signals were analysed with the Quantity One software (Bio-Rad). The amount of NCC, PV, AQP1 and AQP2 protein was normalized for the corresponding total amount of protein, using tubulin protein levels or coomassie staining. Data are based on two independent experiments in which four samples per group were analysed.

Immunohistochemistry

IHC staining was performed on 7-μm cryosections PLP-fixed kidney samples. Sections were stained with rabbit anti-NCC (29) and rabbit PV antibody (1:200; PV-28, Swant, Bellinzona, Switzerland), following standard procedures. Images were made using a Zeiss fluorescence microscope (Sliedrecht, the Netherlands) equipped with an AxioCam digital photo camera.

Statistical analysis

Data are expressed as mean ± SEM. Overall statistical analyses were performed by Student's *t*-test. $P < 0.05$ was considered statistically significant. All calculations were accomplished using the InStat 3 for Macintosh software.

Results

Serum and urine electrolyte levels of cisplatin-treated mice

Ten-week-old C57Bl/6J mice were intraperitoneally injected with either 5 mg/kg body weight cisplatin on days 0, 4 and 8 or vehicle. After 12 days, the animals were placed into metabolic cages for the collection of 24 h urine. Subsequently, the mice were sacrificed to collect blood and to harvest the kidneys. Serum electrolyte and creatinine levels and body weight are displayed in **Table 2**, while urinary electrolyte levels are presented in **Table 3**. The body weight was significantly decreased in the cisplatin group compared with the control group (**Table 2**).

Table 2. Serum analysis and body weight of control and cisplatin-treated mice

Measurement	*Control*	*Cisplatin*
$[Mg^{2+}]$ (mmol/L)	1.58 ± 0.03	1.23 ± 0.03[a]
$[Ca^{2+}]$ (mmol/L)	2.12 ± 0.03	2.19 ± 0.03
$[Na^{+}]$ (mmol/L)	137.1 ± 0.5	138.7 ± 0.8
$[K^{+}]$ (mmol/L)	6.7 ± 0.1	6.7 ± 0.2
[Creatinine] (μmol/L)	6.4 ± 0.3	10.4 ± 0.9 [a]
Weight loss (g)	0.1 ± 0.1	2.3 ± 0.8[a]

Control, mice receiving vehicle injections only; cisplatin, mice receiving 5 mg/kg cisplatin injections on days 0, 4 and 8. Values are presented as average ± SEM. [a] $P < 0.05$ versus control.

Besides the weight loss, no signals of severe illness were perceived. Compared with control mice, serum Mg^{2+} levels were substantially reduced in the cisplatin-treated mice (*n* = 10), while no differences were observed in serum Ca^{2+}, Na^{+} and K^{+} levels (**Table 2**). The mice chronically treated with cisplatin displayed polyuria (**Table 3**). Moreover, these mice showed markedly increased serum creatinine levels (**Table 2**) in combination with reduced urinary creatinine excretion (**Table 3**), indicating a significantly reduced creatinine clearance (C_{Cr}) (**Table 3**). The excretion of Mg^{2+}, Ca^{2+}, Na^{+}, K^{+} and P_i was corrected by urinary concentration of creatinine to compensate for changes in GFR. In comparison with the control group, the renal excretion of Mg^{2+}, Ca^{2+}, Na^{+} and K^{+} was increased on treatment with cisplatin, whereas the excretion of P_i was not affected (**Table 3**). The urinary osmolality was substantially decreased when the mice were treated with cisplatin (**Table 3**).

The effect of cisplatin on proximal tubular injury

To evaluate whether cisplatin treatment caused tubular injury, the expression level of kidney injury molecule-1 (Kim-1) was measured. Kim-1 is a type 1 membrane protein, which is expressed at very low levels in normal kidney. As a result of renal injury Kim-1 is strongly upregulated in predominantly PT cells (30). Compared with the control group, our study showed markedly increased Kim-1 mRNA levels upon treatment with cisplatin (3378 ± 1101 and 100 ± 30%, cisplatin versus control, $P < 0.05$) (**Figure 2**).

Table 3. Urine analysis of control and cisplatin-treated mice

Measurement	*Control*	*Cisplatin*
Urine volume (mL/24 h)	0.9 ± 0.1	2.5 ± 0.3[a]
[Creatinine] (mmol/L)	2.4 ± 0.2	0.9 ± 0.1[a]
Mg^{2+} excretion (µmol/24 h)	24 ± 2	42 ± 2[a]
Mg^{2+}/creatinine	10.6 ± 0.3	16.0 ± 0.5[a]
Ca^{2+} excretion (µmol/24 h)	4.7 ± 0.4	7.2 ± 0.3[a]
Ca^{2+}/creatinine	2.1 ± 0.1	3.2 ± 0.4[a]
Na^{+} excretion (µmol/24 h)	110 ± 13	163 ± 18[a]
Na^{+}/creatinine	48 ± 3	69 ± 3[a]
K^{+} excretion (µmol/24 h)	344 ± 38	464 ± 21
K^{+}/creatinine	150 ± 6	186 ± 4[a]
P_i excretion (µmol/24 h)	43 ± 8	45 ± 4
P_i /creatinine	17 ± 2	21 ± 2
Urinary pH	6.7 ± 0.2	6.7 ± 0.2
Urinary osmolality (Osmol/kg)	2.8 ± 0.1	1.4 ± 0.1[a]
C_{Cr} (mL/min)	0.26 ± 0.02	0.18 ± 0.02[a]

Control, mice receiving vehicle injections only; cisplatin, mice receiving 5 mg/kg cisplatin injections on days 0, 4 and 8; $C_{Cr,}$ creatinine clearance. Values are presented as average ± SEM. [a] $P < 0.05$ versus control.

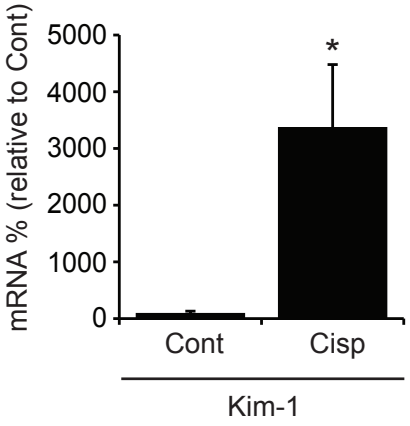

Figure 2. Effect of cisplatin treatment on kidney injury. The effect of cisplatin (5 mg/kg/injection on days 0, 4 and 8) on mRNA expression levels of kidney injury molecule-1 (Kim-1). Results are presented as average ± SEM (n = 10), relative to the control group. * $P < 0.05$ compared with control. Cont, control; Cisp, cisplatin.

The effect of cisplatin on mRNA expression of renal electrolyte transporters

The mRNA expression levels of TRPM6, NCC and parvalbumin (PV) and different Ca^{2+} and Na^{+} transporters as well as AQP2, were determined by real-time qPCR (**Figure 3**). The cisplatin group showed significantly lower expression levels of TRPM6 (60 ± 7 and 100 ± 5%, cisplatin versus control, $P < 0.05$) and NCC (63 ± 7 and 100 ± 5%, cisplatin versus control, $P < 0.05$). Additionally, the DCT specific protein PV was markedly downregulated in cisplatin-treated mice (38 ± 12 and 100 ± 6%, cisplatin versus control, $P < 0.05$). Subsequently, the mRNA expression levels of the Na^{+}, K^{+}, $2Cl^{-}$ cotransporter (NKCC2) and the tight junction proteins claudin-16 (CLDN16) and claudin-19 (CLDN19) (31), all located in the thick ascending limb of Henle's loop (TAL), were determined. The NKCC2 and CLDN19 expression levels were not significantly changed (103 ± 5 versus 100 ± 5% for NKCC2 and 120 ± 9 versus 100 ± 5% for CLDN19, cisplatin versus control, $P > 0.2$), whereas CLDN16 was substantially upregulated in the cisplatin-treated group (163 ± 16 and 100 ± 3%, cisplatin versus control, $P < 0.05$). The mRNA level of the Na^{+}, H^{+} exchanger 3 (NHE3), which is expressed in the proximal convoluted tubule (PCT) and the TAL (32, 33) was not affected by cisplatin (100 ± 4 and 100 ± 3%, cisplatin versus control, $P > 0.2$).

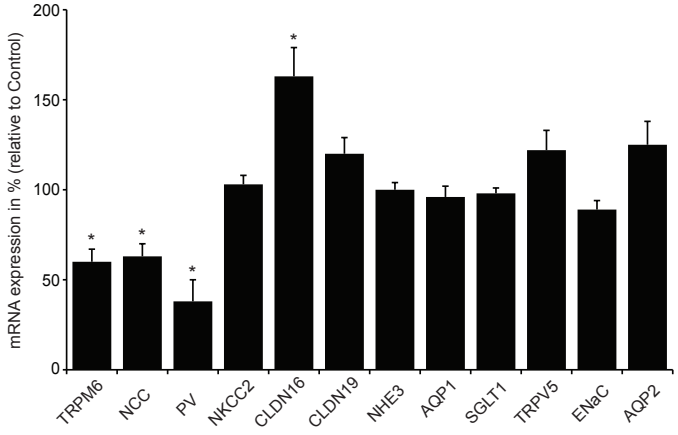

Figure 3. Effect of cisplatin treatment on mRNA expression levels of renal electrolyte transporters. The effect of cisplatin (5 mg/kg/injection on days 0, 4 and 8) on mRNA expression levels of renal transport proteins, which reside in the distal convoluted tubule (DCT), such as the epithelial Mg^{2+} channel TRPM6, the Na^{+}, Cl^{-} cotransporter (NCC) and parvalbumin (PV) or are located in other tubule segments, including the Na^{+}, K^{+}, Cl^{-} cotransporter (NKCC2), claudin-16, (CLDN16), claudin-19 (CLDN19), the Na^{+}, H^{+} exchanger 3 (NHE3), aquaporin 1 (AQP1), the sodium-glucose cotransporter 1 (SGLT1), the epithelial Ca^{2+} channel TRPV5, the epithelial Na^{+} channel (ENaC) and aquaporin 2 (AQP2). Results are presented as average ± SEM (n = 10), corrected for GAPDH and as ratio of the expression level in the control group. * $P < 0.05$ compared with control.

Moreover, the mRNA expression levels of AQP1, expressed in the PCT and the proximal straight tubule (PST) and of the sodium-glucose cotransporter 1 (SGLT1), exclusively expressed in the PST, were also unaffected by cisplatin treatment (96 ± 6 versus 100 ± 5% for AQP1 and 98 ± 3 versus 100 ± 5% for SGLT1, cisplatin versus control, $P > 0.2$). The mRNA level of the late DCT (DCT2) and CNT marker TRPV5 was not changed either upon cisplatin treatment (122 ± 11 and 100 ± 5%, cisplatin versus control, $P > 0.2$). Furthermore, the mRNA level of the epithelial Na^+ channel (ENaC), which localizes to the connecting tubule (CNT) and collecting duct (CD), was not significantly changed by cisplatin (89 ± 5 and 100 ± 5%, cisplatin versus control, $P > 0.2$). Finally, the mRNA level of AQP2, as a measure of CD integrity, was unchanged (125 ± 13 and 100 ± 7%, cisplatin versus control, $P > 0.2$).

The effect of cisplatin on protein expression of renal electrolyte transporters

The effect of cisplatin treatment on NCC, PV, AQP1 and AQP2 protein expression was investigated by immunoblotting. We were able to confirm the DCT-specific downregulation on protein level. NCC and PV were significantly reduced in the cisplatin-treated group (38 ± 9 versus 100 ± 19% for NCC and 62 ± 5 versus 100 ± 6% for PV, cisplatin versus control, $P < 0.05$) (**Figures 4A and B**), whereas the AQP1 and AQP2 protein expression in the cisplatin-treated group did not significantly differ from the control group (116 ± 23 and 100 ± 10% for AQP1 and 120 ± 18 and 100 ± 16% for AQP2, cisplatin versus control, $P > 0.2$) (**Figures 4C and D**).

Next, to establish whether the reduction of mRNA encoding for DCT transporters is dependent on protein downregulation or on cellular damage immunohistochemical staining was performed for NCC and PV. **Figure 5** shows that NCC and PV are localized in the same cell compartment when treated with cisplatin, compared with control mice. It is clear that the tubules of the cisplatin-treated mice have a larger lumen and that the epithelial cells are more flat. In addition, there were indications of minor tubular damage with individual necrotic tubular epithelial cells in the cisplatin kidneys (data not shown).

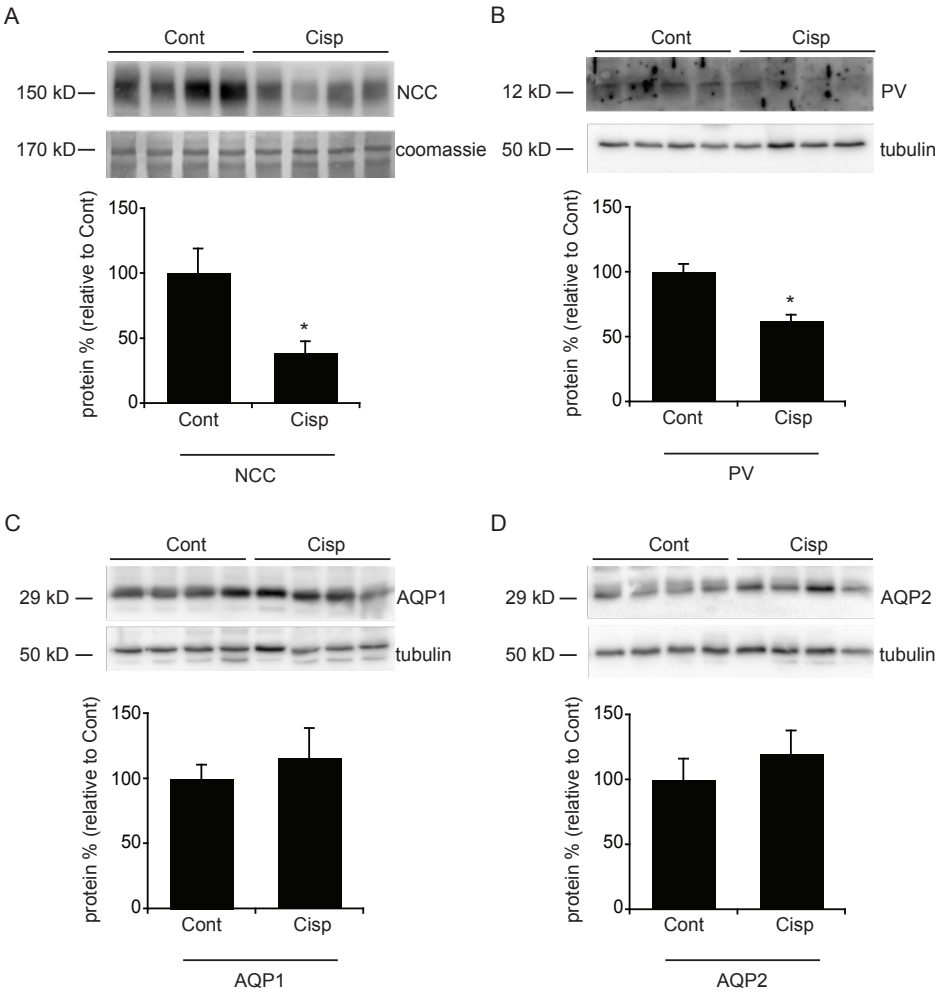

Figure 4. Effect of cisplatin on protein expression levels of renal marker proteins. The effect of cisplatin (Cisp) (5 mg/kg/injection on days 0, 4 and 8) on protein expression levels of the Na^+, Cl^- cotransporter (NCC) (**A**), parvalbumin (PV) (**B**), aquaporin 1 (AQP1) (**C**) and aquaporin 2 (AQP2) (**D**). The upper part of each figure shows the immunoblot, with on the left side the molecular mass (in kDa) and the lower parts depict the expression levels as percentage of control (Cont). Values are presented as average ± SEM (*n* = 4), while experiments are performed in duplicate. * $P < 0.05$ compared with control.

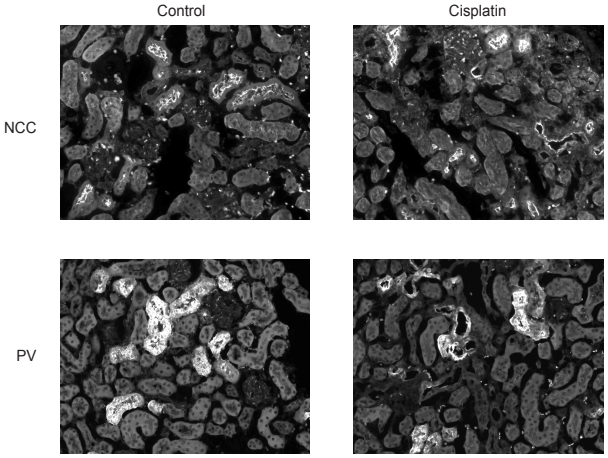

Figure 5. Effect of cisplatin on protein expression of NCC and PV in kidney. The effect of cisplatin (5 mg/kg/injection on days 0, 4 and 8) on protein expression levels and localization of the Na^+, Cl^- cotransporter (NCC) and parvalbumin (PV) in mice kidney was studied. This figure shows representative images of kidney cortex slides of control and cisplatin-treated mice.

The effect of cisplatin on mRNA expression of known cisplatin transporters

Previous studies suggested that the uptake of cisplatin is mediated by a specific transport mechanism (34, 35). Exclusive expression of cisplatin transporters to the DCT may explain the damage to particularly this tubule segment. The organic cation transporter 2 (OCT2) and the copper transporter 1 (CTR1) are identified to contribute to the uptake of cisplatin (36, 37). The mRNA expression level of OCT2 was not changed in the cisplatin group, compared with the control group (93 ± 10 and 100 ± 7%, cisplatin versus control, $P > 0.2$) (**Figure 6A**). In contrast, the mRNA level of CTR1 was significantly downregulated by treatment with cisplatin (82 ± 4 and 100 ± 6%, cisplatin versus control, $P < 0.05$) (**Figure 6B**).

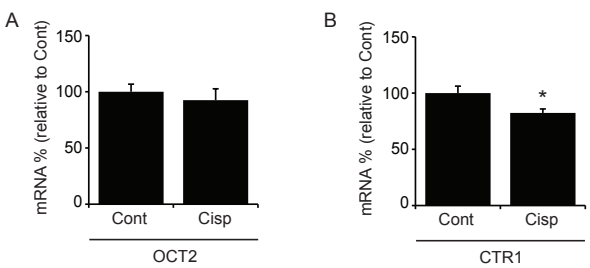

Figure 6. Effect of cisplatin on mRNA expression levels of cisplatin transporters. The effect of cisplatin (5 mg/kg/injection on days 0, 4 and 8) on mRNA expression levels of cisplatin transporters organic cation transporter 2 (OCT2) (**A)** and copper transporter 1 (CTR1) (**B**). Expression levels are shown as percentage of control. Values are presented as average ± SEM (n = 10). * $P < 0.05$ compared with control. Cont, control; Cisp, cisplatin.

Discussion

Our study provides further evidence that the DCT segment is affected by cisplatin treatment. We demonstrated that cisplatin treatment in mice induces hypomagnesemia, whereas serum Ca^{2+}, Na^{+} and K^{+} levels were unaffected. The mice developed polyuria, reduced C_{Cr} and the renal excretion of Mg^{2+}, Ca^{2+}, Na^{+} and K^{+} was increased, whereas P_i excretion was not changed, after the chronic treatment with cisplatin. Investigation of the mRNA expression levels of the DCT marker genes NCC, TRPM6 and PV showed a significant decline in the cisplatin-treated mouse group. In line with these data, we observed markedly reduced NCC and PV protein levels by immunoblotting experiments. IHC staining for NCC and PV suggested that specific protein downregulation rather than major cellular damage explains the underlying mechanism.

The DCT plays a key role in determining the final plasma Mg^{2+} concentration, as the more distal parts of the tubule are largely impermeable to Mg^{2+}. In DCT, Mg^{2+} reabsorption occurs in an active transcellular manner initiated by TRPM6 (38). TRPM6 localizes to the luminal membrane where it facilitates transport of Mg^{2+} from the pro-urine into the cell (39). The importance of Mg^{2+} in cisplatin-induced renal injury has been underlined by several studies. A recent study demonstrated that cisplatin-induced nephrotoxicity is enhanced due to Mg^{2+} depletion (21, 40). In addition, nephroprotection can be attained in patients who are supplemented with Mg^{2+} during and between courses of cisplatin treatment (41). In addition, NCC is responsible for the reabsorption of 10-15% of the filtered NaCl (42). Its importance is illustrated by the fact that NCC is the target of the thiazide diuretics, which are commonly prescribed drugs in the treatment of high blood pressure (43).

Furthermore, the effect of cisplatin treatment on mRNA and protein expression in other tubule segments, including PT, TAL, CNT and CD, was investigated. The PT can be severely affected by cisplatin treatment, especially morphological changes in the PST have been observed (6, 7). The cisplatin-induced increase of the Kim-1 expression level suggests that the PST segment is also affected in our study (30, 44). The NHE3 expression levels were similar in the kidneys of control and cisplatin-treated groups. IHC for NHE3 previously showed strong staining on the apical membrane of the PCT, while staining was absent in the PST (32). Therefore, we also determined the mRNA expression level of SGLT1, which is exclusively expressed in the PST segment (45), and of AQP1, which is present throughout the PT (46). However, also for these genes we did not observe a significant effect by cisplatin treatment. Moreover, the urinary excretion level of P_i was not affected in cisplatin-treated mice. P_i is mainly reabsorbed in the PT in a transcellular, Na^{+}-dependent manner (47). These results suggest that cisplatin injury to the PST might be less severe or different from injury to the DCT.

We did not observe expression differences for the CNT marker TRPV5 or for the CNT and CD marker ENaC, suggesting that these tubular segments are not significantly affected by cisplatin treatment in our study. Additionally, the mRNA expression level of NKCC2 was unchanged following cisplatin treatment. Our observations are in line with a study by Ecelbarger *et al*. which showed normal protein expression of NKCC2 in the medullary TAL segment (48). The same study also demonstrated that the protein abundance of NHE3, the renal outer medullary K^{+} channel (ROMK), localized in TAL and CNT and the α-subunit of the Na^{+}, K^{+}-ATPase, expressed throughout the nephron, were not affected. On the

other hand, the expression of IMCD proteins AQP2 and AQP3 and urea transporters (UT-A) was reduced. This is in contrast with our results, which showed no effect of cisplatin treatment on AQP2 mRNA and protein level. Remarkably, a study by Lajer *et al*. displayed lower protein abundance for all investigated proteins, including the α-subunit of the Na^+, K^+-ATPase, NHE3, NKCC2, AQP1 and AQP2 (40). It is important to note that these discrepancies may result from a species-specific effect because they all used rats reporting a more severe polyuria. Proper interaction of CLDN16 and CLDN19 in TAL is essential for the cation selectivity of paracellular route and consequently reabsorption of divalent cations in this tubule segment (31). Upregulation of CLDN16 levels in our cisplatin-treated mouse group suggested that TAL might compensate for decreased reabsorption of Mg^{2+} in DCT. Altogether, our results suggest a specific downregulation of proteins that reside in the DCT. To our knowledge, this is the first study that specifically investigates the expression levels of transport proteins in the DCT following cisplatin treatment.

There are several mechanisms that can explain the polyuria, which is caused by cisplatin administration. In rats it has been shown that polyuria is associated with decreased expression of AQP1, 2 and 3 (49). However, we did not observe a change in mRNA or protein level of AQP1 and AQP2. Additionally, IHC staining displayed similar AQP2 localization and quantity in kidneys of cisplatin-treated or control animals (data not shown). We also determined whether the polyuria might be secondary to osmotic diuresis. As depicted in **Table 3**, the urinary osmolality is markedly reduced after cisplatin treatment that renders this assumption unlikely. Reduced urinary osmolality in combination with a decline of C_{Cr} indicate decreased GFR due to acute kidney failure in the cisplatin-treated animals. Another explanation might, therefore, be that a decreased GFR, secondary to cisplatin-induced nephrotoxicity, is associated with medullary urea cycling defect. This results in reduced tonicity of the medulla and as a consequence increased excretion of water (4). Moreover, we showed that cisplatin treatment causes hypomagnesemia and increased urinary excretion of K^+ and Na^+ in combination with polyuria. Interestingly, in patients suffering from Gitelman Syndrome (GS), besides tetany and muscle weakness, similar findings were observed (16, 18, 50). GS results from homozygous loss-of-function mutations in NCC (51). Absence of NCC causes renal NaCl wasting and activation of the renin-angiotensin-aldosterone system (52, 53). The high Na^+ load in the CNT/CD region will cause increased reabsorption by ENaC, in exchange for K^+ (54). The present study demonstrated a lower NCC mRNA and protein expression levels, following treatment with cisplatin. Another characteristic of GS is hypocalciuria. Nijenhuis *et al.* demonstrated that hypocalciuria in NCC-deficient mice is caused by enhanced Ca^{2+} reabsorption in the PT, secondary to the hypovolemia (55). The fact that we did observe hypercalciuria in the cisplatin-treated mice, instead of hypocalciuria as shown in GS, suggests tubular damage to the PT, as also confirmed by the upregulation of Kim-1. Hence, it might be that the polyuria is primarily caused by impaired NaCl reabsorption via NCC, in combination with insufficient compensation via ENaC, AQP2 and NHE-3.

Taken together, our study identified for the first time a specific effect of cisplatin on the expression level of DCT markers. It is unclear whether this is caused by specific downregulation of Na^+ and Mg^{2+} transport proteins in the DCT or a cisplatin-induced DCT-specific cell death. The procedure for cisplatin-mediated cell death is still unknown. Apoptosis can be induced by the formation of chromosomal DNA/cisplatin adducts and/or mitochondria-induced pathways (56, 57). Mitochondria-induced apoptosis is of interest as

the large size and high density of mitochondria characterizes DCT cells (58). For that reason, the DCT may be more susceptible to mitochondria-induced apoptosis, as shown for cell lines with a relatively high density of mitochondria (59). Alternatively, as only minor cellular damage was detected, specific down-regulation of proteins in DCT might indeed be the mechanism causing loss of function of this part of the nephron.

Research focuses on the identification of cisplatin transport mechanism contributing to its segment specific nephrotoxicity and ways to block these in a competitive manner. Recent studies identified OCT2 (36) and the copper transporter 1 (CTR1) (37) as cisplatin-transporting proteins. Interestingly, both OCT2 and CTR1 are expressed in the kidney as well as in malignant tissues (60-62) and are, for that reason, candidates to facilitate the entry of cisplatin into renal cells. Our results showed that the mRNA level of OCT2 was not affected, whereas the CTR1 expression level was slightly but significantly decreased by cisplatin treatment. Recently, Pabla *et al*. identified PKCδ as a critical regulator of cisplatin nephrotoxicity (63). Future studies are needed to confirm the role of CTR1 in the entry of cisplatin in DCT cells and if targeting PKCδ could be an effective way to reduce cisplatin-induced side effects.

In summary, cisplatin treatment results in polyuria, hypomagnesemia and renal Mg^{2+}, Ca^{2+}, Na^{+} and K^{+} wasting. These defects likely arise from impaired functionality of the renal PCT and DCT segments. As long as the exact mechanism that causes hypomagnesemia is not resolved, it's important that patients treated with cisplatin are frequently checked for their serum Mg^{2+} level and supplemented with Mg^{2+} accordingly.

Acknowledgements. The expert help of Dr. S. Florquin was appreciated with respect to evaluation of the nephrotoxicity of the renal sections. This research was financially supported by the Dutch Organization for Scientific Research (ZonMw 9120.8026; ALW 818.02.001), a European Young Investigator award from the European Science Foundation.

References

1. Rosenberg, B., VanCamp, L., Trosko, J.E., et al. Platinum compounds: a new class of potent antitumour agents. Nature 222:385-386. 1969.
2. Roberts, J.J., and Pascoe, J.M. Cross-linking of complementary strands of DNA in mammalian cells by antitumour platinum compounds. Nature 235:282-284. 1972.
3. Rosenberg, B. Platinum coordination complexes in cancer chemotherapy. Naturwissenschaften 60:399-406. 1973.
4. Yao, X., Panichpisal, K., Kurtzman, N., et al. Cisplatin nephrotoxicity: a review. Am J Med Sci 334:115-124. 2007.
5. Arany, I., and Safirstein, R.L. Cisplatin nephrotoxicity. Semin Nephrol 23:460-464. 2003.
6. Dobyan, D.C., Levi, J., Jacobs, C., et al. Mechanism of cis-platinum nephrotoxicity: II. Morphologic observations. J Pharmacol Exp Ther 213:551-556. 1980.
7. Mavichak, V., Wong, N.L., Quamme, G.A., et al. Studies on the pathogenesis of cisplatin-induced hypomagnesemia in rats. Kidney Int 28:914-921. 1985.
8. Daugaard, G., Abildgaard, U., Larsen, S., et al. Functional and histopathological changes in dog kidneys after administration of cisplatin. Ren Physiol 10:54-64. 1987.
9. Gonzales-Vitale, J.C., Hayes, D.M., Cvitkovic, E., et al. The renal pathology in clinical trials of cis-platinum (II) diamminedichloride. Cancer 39:1362-1371. 1977.
10. Magil, A.B., Mavichak, V., Wong, N.L., et al. Long-term morphological and biochemical observations in cisplatin-induced hypomagnesemia in rats. Nephron 43:223-230. 1986.
11. Takashi, M., Zhu, Y., Miyake, K., et al. Urinary 28-kD calbindin-D as a new marker for damage to distal renal tubules caused by cisplatin-based chemotherapy. Urol Int 56:174-179. 1996.
12. Orfila, C., Bompart, G., Lepert, J.C., et al. Renal immunolocalization of kallikrein in cisplatin nephrotoxicity in rats. Histochem J 25:772-777. 1993.
13. Bompart, G., Orfila, C., and Girolami, J.P. Distal nephrotoxicity of cisplatin demonstrated by urinary kallikrein excretion and morphological study in rats. Toxicology 69:121-132. 1991.
14. Lam, M., and Adelstein, D.J. Hypomagnesemia and renal magnesium wasting in patients treated with cisplatin. Am J Kidney Dis 8:164-169. 1986.
15. Schilsky, R.L., and Anderson, T. Hypomagnesemia and renal magnesium wasting in patients receiving cisplatin. Ann Intern Med 90:929-931. 1979.
16. Ariceta, G., Rodriguez-Soriano, J., Vallo, A., et al. Acute and chronic effects of cisplatin therapy on renal magnesium homeostasis. Med Pediatr Oncol 28:35-40. 1997.
17. Jones, D.P., and Chesney, R.W. Renal toxicity of cancer chemotherapeutic agents in children: ifosfamide and cisplatin. Curr Opin Pediatr 7:208-213. 1995.
18. Panichpisal, K., Angulo-Pernett, F., Selhi, S., et al. Gitelman-like syndrome after cisplatin therapy: a case report and literature review. BMC Nephrol 7:10. 2006.
19. Vassal, G., Rubie, H., Kalifa, C., et al. Hyponatremia and renal sodium wasting in patients receiving cisplatinum. Pediatr Hematol Oncol 4:337-344. 1987.
20. Dai, L.J., Ritchie, G., Kerstan, D., et al. Magnesium transport in the renal distal convoluted tubule. Physiol Rev 81:51-84. 2001.
21. Lajer, H., and Daugaard, G. Cisplatin and hypomagnesemia. Cancer Treat Rev 25:47-58. 1999.
22. Mavichak, V., Coppin, C.M., Wong, N.L., et al. Renal magnesium wasting and hypocalciuria in chronic cis-platinum nephropathy in man. Clin Sci (Lond) 75:203-207. 1988.

23. Ludwig, T., Riethmuller, C., Gekle, M., et al. Nephrotoxicity of platinum complexes is related to basolateral organic cation transport. Kidney Int 66:196-202. 2004.
24. Litterst, C.L., Gram, T.E., Dedrick, R.L., et al. Distribution and disposition of platinum following intravenous administration of cis-diamminedichloroplatinum(II) (NSC 119875) to dogs. Cancer Res 36:2340-2344. 1976.
25. Hall, M.D., Okabe, M., Shen, D.W., et al. The role of cellular accumulation in determining sensitivity to platinum-based chemotherapy. Annu Rev Pharmacol Toxicol 48:495-535. 2008.
26. Glaudemans, B., Knoers, N.V., Hoenderop, J.G., et al. New molecular players facilitating Mg(2+) reabsorption in the distal convoluted tubule. Kidney Int 77:17-22.
27. Hoenderop, J.G., Muller, D., Van Der Kemp, A.W., et al. Calcitriol controls the epithelial calcium channel in kidney. J Am Soc Nephrol 12:1342-1349. 2001.
28. Jennings, M.L. Monoclonal antibody against red blood cell CHIP28 protein. J Gen Physiol 100:21A. 1992.
29. Nijenhuis, T., Hoenderop, J.G., Loffing, J., et al. Thiazide-induced hypocalciuria is accompanied by a decreased expression of Ca2+ transport proteins in kidney. Kidney Int 64:555-564. 2003.
30. Ichimura, T., Hung, C.C., Yang, S.A., et al. Kidney injury molecule-1: a tissue and urinary biomarker for nephrotoxicant-induced renal injury. Am J Physiol Renal Physiol 286:F552-563. 2004.
31. Hou, J., Renigunta, A., Konrad, M., et al. Claudin-16 and claudin-19 interact and form a cation-selective tight junction complex. J Clin Invest 118:619-628. 2008.
32. Amemiya, M., Loffing, J., Lotscher, M., et al. Expression of NHE-3 in the apical membrane of rat renal proximal tubule and thick ascending limb. Kidney Int 48:1206-1215. 1995.
33. Nishinaga, H., Komatsu, R., Doi, M., et al. Circadian expression of the Na+/H+ exchanger NHE3 in the mouse renal medulla. Biomed Res 30:87-93. 2009.
34. Andrews, P.A., Velury, S., Mann, S.C., et al. cis-Diamminedichloroplatinum(II) accumulation in sensitive and resistant human ovarian carcinoma cells. Cancer Res 48:68-73. 1988.
35. Mann, S.C., Andrews, P.A., and Howell, S.B. Modulation of cis-diamminedichloroplatinum(II) accumulation and sensitivity by forskolin and 3-isobutyl-1-methylxanthine in sensitive and resistant human ovarian carcinoma cells. Int J Cancer 48:866-872. 1991.
36. Ciarimboli, G., Ludwig, T., Lang, D., et al. Cisplatin nephrotoxicity is critically mediated via the human organic cation transporter 2. Am J Pathol 167:1477-1484. 2005.
37. Ishida, S., Lee, J., Thiele, D.J., et al. Uptake of the anticancer drug cisplatin mediated by the copper transporter Ctr1 in yeast and mammals. Proc Natl Acad Sci U S A 99:14298-14302. 2002.
38. Schlingmann, K.P., Weber, S., Peters, M., et al. Hypomagnesemia with secondary hypocalcemia is caused by mutations in TRPM6, a new member of the TRPM gene family. Nat Genet 31:166-170. 2002.
39. Voets, T., Nilius, B., Hoefs, S., et al. TRPM6 forms the Mg2+ influx channel involved in intestinal and renal Mg2+ absorption. J Biol Chem 279:19-25. 2004.
40. Lajer, H., Kristensen, M., Hansen, H.H., et al. Magnesium depletion enhances cisplatin-induced nephrotoxicity. Cancer Chemother Pharmacol 56:535-542. 2005.
41. Willox, J.C., McAllister, E.J., Sangster, G., et al. Effects of magnesium supplementation in testicular cancer patients receiving cis-platin: a randomised trial. Br J Cancer 54:19-23. 1986.
42. Reilly, R.F., and Ellison, D.H. Mammalian distal tubule: physiology, pathophysiology, and molecular anatomy. Physiol Rev 80:277-313. 2000.
43. Chobanian, A.V., Bakris, G.L., Black, H.R., et al. The Seventh Report of the Joint National Committee on Prevention, Detection, Evaluation, and Treatment of High Blood Pressure: the JNC 7 report. Jama 289:2560-2572. 2003.

44. Zhang, J., Goering, P.L., Espandiari, P., et al. Differences in immunolocalization of Kim-1, RPA-1, and RPA-2 in kidneys of gentamicin-, cisplatin-, and valproic acid-treated rats: potential role of iNOS and nitrotyrosine. Toxicol Pathol 37:629-643. 2009.
45. Sabolic, I., Skarica, M., Gorboulev, V., et al. Rat renal glucose transporter SGLT1 exhibits zonal distribution and androgen-dependent gender differences. Am J Physiol Renal Physiol 290:F913-926. 2006.
46. Maunsbach, A.B., Marples, D., Chin, E., et al. Aquaporin-1 water channel expression in human kidney. J Am Soc Nephrol 8:1-14. 1997.
47. Murer, H., Hernando, N., Forster, I., et al. Proximal tubular phosphate reabsorption: molecular mechanisms. Physiol Rev 80:1373-1409. 2000.
48. Ecelbarger, C.A., Sands, J.M., Doran, J.J., et al. Expression of salt and urea transporters in rat kidney during cisplatin-induced polyuria. Kidney Int 60:2274-2282. 2001.
49. Kishore, B.K., Krane, C.M., Di Iulio, D., et al. Expression of renal aquaporins 1, 2, and 3 in a rat model of cisplatin-induced polyuria. Kidney Int 58:701-711. 2000.
50. Gitelman, H.J., Graham, J.B., and Welt, L.G. A new familial disorder characterized by hypokalemia and hypomagnesemia. Trans Assoc Am Physicians 79:221-235. 1966.
51. Simon, D.B., and Lifton, R.P. The molecular basis of inherited hypokalemic alkalosis: Bartter's and Gitelman's syndromes. Am J Physiol 271:F961-966. 1996.
52. Barker, N.W., Carey, B., and Brough, W. Effect of chlorothiazide on patients with edema of the lower extremities of local origin. Minn Med 42:227-230. 1959.
53. Poutsiaka, J.W., Madissoo, H., Millstein, L.G., et al. Effects of benzydroflumethiazide (Naturetin) on the renal excretion of calcium and magnesium by dogs. Toxicol Appl Pharmacol 3:455-458. 1961.
54. Greger, R. Why do loop diuretics cause hypokalaemia? Nephrol Dial Transplant 12:1799-1801. 1997.
55. Nijenhuis, T., Vallon, V., van der Kemp, A.W., et al. Enhanced passive Ca2+ reabsorption and reduced Mg2+ channel abundance explains thiazide-induced hypocalciuria and hypomagnesemia. J Clin Invest 115:1651-1658. 2005.
56. Yang, Z., Schumaker, L.M., Egorin, M.J., et al. Cisplatin preferentially binds mitochondrial DNA and voltage-dependent anion channel protein in the mitochondrial membrane of head and neck squamous cell carcinoma: possible role in apoptosis. Clin Cancer Res 12:5817-5825. 2006.
57. Wang, D., and Lippard, S.J. Cellular processing of platinum anticancer drugs. Nat Rev Drug Discov 4:307-320. 2005.
58. Linss, W., and Geyer, G. [the Electron Microscopic Structure of the Kidney Tubule in Rana Esculenta]. Anat Anz 115:281-296. 1964.
59. Qian, W., Nishikawa, M., Haque, A.M., et al. Mitochondrial density determines the cellular sensitivity to cisplatin-induced cell death. Am J Physiol Cell Physiol 289:C1466-1475. 2005.
60. Kuo, Y.M., Gybina, A.A., Pyatskowit, J.W., et al. Copper transport protein (Ctr1) levels in mice are tissue specific and dependent on copper status. J Nutr 136:21-26. 2006.
61. Beretta, G.L., Gatti, L., Tinelli, S., et al. Cellular pharmacology of cisplatin in relation to the expression of human copper transporter CTR1 in different pairs of cisplatin-sensitive and -resistant cells. Biochem Pharmacol 68:283-291. 2004.
62. Filipski, K.K., Mathijssen, R.H., Mikkelsen, T.S., et al. Contribution of organic cation transporter 2 (OCT2) to cisplatin-induced nephrotoxicity. Clin Pharmacol Ther 86:396-402. 2009.
63. Pabla, N., Dong, G., Jiang, M., et al. Inhibition of PKCdelta reduces cisplatin-induced nephrotoxicity without blocking chemotherapeutic efficacy in mouse models of cancer. J Clin Invest 121. 2011.

Chapter 3

Increased expression of renal TRPM6 compensates for Mg^{2+} wasting during furosemide treatment

Annelies A. van Angelen, AnneMiete W. van der Kemp,
Joost G. Hoenderop and René J. Bindels

Department of Physiology, Radboud University Nijmegen Medical Centre,
Nijmegen, The Netherlands.

Clin Kidney J 5: 535-544, 2012

Abstract

Background. Furosemide is a loop diuretic, which blocks the Na^+, K^+, $2Cl^-$ cotransporter (NKCC2) in the thick ascending limb of Henle's loop (TAL). By diminishing sodium (Na^+) reabsorption, loop diuretics reduce the lumen-positive transepithelial voltage and consequently diminish paracellular transport of magnesium (Mg^{2+}) and calcium (Ca^{2+}) in TAL. Indeed, furosemide promotes urinary Mg^{2+} excretion; however, it is unclear whether this leads, especially during prolonged treatment, to hypomagnesemia. The aim of the present study was, therefore, to determine the effect of chronic furosemide application on renal Mg^{2+} handling in mice.

Methods. Two groups of 10 mice received an osmotic minipump subcutaneously for 7 days with vehicle or 30 mg/kg/day furosemide. Serum and urine electrolyte concentrations were determined. Next, renal mRNA levels of the epithelial Mg^{2+} channel (TRPM6), the Na^+, Cl^- cotransporter (NCC), the epithelial Ca^{2+} channel (TRPV5), the cytosolic Ca^{2+}-binding protein calbindin-D_{28K}, as well parvalbumin (PV), claudin-7 (CLDN7) and claudin-8 (CLDN8), the epithelial Na^+ channel (ENaC) and the Na^+, H^+ exchanger 3 (NHE3) were determined by real-time quantitative polymerase chain reaction (qPCR). Renal protein levels of NCC, TRPV5, calbindin-D_{28K} and ENaC were also measured using semi-quantitative immunohistochemistry (IHC) and immunoblotting.

Results. The mice chronically treated with 30 mg/kg/day furosemide displayed a significant polyuria (2.1 ± 0.3 and 1.3 ± 0.2 mL/24h, furosemide versus control respectively, $P < 0.05$). Furosemide treatment resulted in increased serum concentrations of Na^+ (158 ± 3 (treated) and 147 ± 1 mmol/L (control), $P < 0.01$), whereas serum K^+, Ca^{2+} and Mg^{2+} values were not significantly altered in mice treated with furosemide. Urinary excretion of Na^+, K^+, Ca^{2+} and Mg^{2+} was not affected by chronic furosemide treatment. The present study shows specific renal upregulation of TRPM6, NCC, TRPV5 and calbindin-D_{28K}.

Conclusions. During chronic furosemide treatment, enhanced active reabsorption of Mg^{2+} via the epithelial channel TRPM6 in DCT compensates for the reduced reabsorption of Mg^{2+} in TAL.

Introduction

Furosemide is a loop diuretic, which blocks the Na^+, K^+, $2Cl^-$ cotransporter (NKCC2) in the thick ascending limb of Henle's loop (TAL) (1) by competing for the chloride site on the transporter (2). Interestingly, most magnesium (Mg^{2+}) reabsorption takes place in TAL (~60 %) in a passive, paracellular way (3, 4). This reabsorption is driven by the transepithelial potential mediated by transport via NKCC2. Furosemide treatment is usually prescribed primarily for its natriuretic action as treatment of edematous status and hypertension (5). By diminishing sodium (Na^+) reabsorption, the concentrating process that occurs in the renal medulla is impaired and fluid loss ensues. On the short term, this results in diminished Na^+ and chloride (Cl^-) reabsorption and as a consequence, due to increased distal Na^+ delivery and increased levels of aldosterone, potassium (K^+) loss. In TAL, the generation of a lumen-positive transepithelial voltage by NKCC2 is diminished by treatment with furosemide, consequently paracellular transport of Mg^{2+} and calcium (Ca^{2+}) is reduced resulting in increased urinary excretion of these ions (6-8). Chronic effects of furosemide treatment sometimes result in hypercalciuria, but only rarely leading to hypocalcemia (9, 10). Long-term effects of treatment with furosemide on urinary and serum Mg^{2+} values vary, in such a way that hypomagnesemia is sometimes observed in patients with heart failure or other serious diseases, while especially during sufficient Mg^{2+} intake disturbances in Mg^{2+} balance are not generally observed (9, 11, 12). However, data of chronic furosemide treatment in healthy volunteers or animal models are scarce and seem to lack analysis of Mg^{2+} homeostasis in relation to other electrolytes.

A complicating factor of chronic furosemide use is the development of resistance, which decreases the long-term efficacy (13). On the one hand, decreased efficacy with time occurs because of the 'braking phenomenon' (14). This phenomenon is the result of adaptation in the distal convoluted tubule (DCT) and connecting tubule (CNT), due to the chronically increased Na^+ delivery to these nephron segments (15-17). On the other hand, resistance develops due to the short-acting characteristic of furosemide, with a peak plasma concentration after ~1 h of furosemide treatment (18, 19). Thus, increased reabsorption of Na^+ can be observed rapidly, know as the 'rebound phase' (14). As an indicator of resistance to chronic furosemide treatment, particularly the impaired natriuretic response was determined by measuring renal Na^+ excretion levels (15). It is interesting to unravel if the excretion of in particular Mg^{2+} is affected similarly. Like the clinical implications for furosemide use, hypomagnesemia is only sporadically observed in antenatal Bartter syndrome (20). This disorder is caused by mutations in genes facilitating transcellular NaCl reabsorption in TAL including the gene encoding NKCC2 (*SLC12AI*). This hereditary recessive disease, which impairs the transport function of the TAL, is characterized by prenatal onset, a severe salt-wasting state with low blood pressure, hypokalemic metabolic alkalosis, hyperreninemia, polyuria, hyperprostaglandinuria and often hypercalciuria (21).

The aim of the present study was to unravel whether chronic furosemide treatment leads to hypomagnesemia or that other parts of the nephron can compensate for the reduced Mg^{2+} reabsorption in TAL. For this purpose, the chronic effect of furosemide on renal handling of Mg^{2+} was studied in mice. The fine-tuning of Mg^{2+} excretion is mediated by the early DCT (DCT1), where active transcellular reabsorption takes place via the epithelial Mg^{2+} channel (TRPM6) (22). Therefore, the expression level of TRPM6 was

measured as well as the level of the Na^+, Cl^- cotransporter (NCC). This protein is, like TRPM6, expressed exclusively along the apical membrane of the DCT (23).

Subjects and methods

Animal studies

Male C57BL/6J mice (10 weeks of age) were purchased from Harlan/CPB (Zeist, The Netherlands) and roomed in a temperature- and light-controlled room with *ad libitum* access to standard pellet chow (0.19% w/w Mg^{2+}, SSNIFF spezialdiäten GmbH, Soest, Germany) and drinking water. Mice were randomly assigned to a control and a furosemide treatment group (n = 10 per group). Furosemide (Sigma, St Louis, MO, USA) was administered using osmotic minipumps (Alzet, Cupertino, CA, USA) subcutaneously for 7 days with vehicle or 30 mg/kg/day furosemide. Before and after the treatment the mice were individually housed in metabolic cages enabling 24 h urine collections under mineral oil (to prevent evaporation) and to measure their water and food intake. At the end of the experiment, blood samples were taken under isoflurane anaesthesia and the mice were sacrificed. Subsequently, kidneys were frozen immediately in liquid nitrogen or incubated in periodate-lysine-paraformaldehyde (PLP) solution for RNA isolation, immunoblotting and immunohistochemistry (IHC) analysis, respectively. Blood was led to clot at room temperature, incubated overnight at 4°C and spun down for 5' at 13 250 × g, and the collected serum was subsequently used for analytical procedures. The animal ethics board of the Radboud University Nijmegen approved all experimental procedures.

Analytical procedures

Serum Mg^{2+} concentration and urinary Mg^{2+} excretion were determined using a colorimetric assay kit according to the manufacturer's protocol (Roche Diagnostics, Woerden, The Netherlands). Serum and urine Ca^{2+} concentrations were measured colorimetrically as described previously (24). A flame spectrophotometer (FCM 6343; Eppendorf) was used to measure serum and urine Na^+ and K^+ concentrations.

Total kidney RNA isolation and cDNA synthesis

Total RNA was extracted from the kidney using TriZol Total RNA isolation reagent according to standard procedures (Gibco BRL, Breda, The Netherlands). The obtained RNA was subjected to DNase treatment (Promega, Madison, WI, USA) to prevent genomic DNA contamination. All samples were resolved on 1% w/v formaldehyde agarose gel to evaluate the RNA quality, while RNA concentration was determined by measuring the ratio of the UV absorbance at 260 and 280 nm using the NANODROP 2000c (Thermo scientific, Wilmington, DE, USA). Thereafter, 1.5 µg of RNA was reverse transcribed by Molony-Murine Leukemia Virus-Reverse Transcriptase (Invitrogen, Breda, The Netherlands) into cDNA according to the manufacturer's recommendations.

SYBR Green real-time quantitative polymerase chain reaction

The cDNA was used to determine the mRNA expression levels of genes of interest, as well as mRNA levels of the reference gene glyceraldehyde 3-phosphate dehydrogenase (GAPDH) as an endogenous control. Primer3 software (http://frodo.wi.mit.edu/primer3/)

was used to design real-time quantitative polymerase chain reaction (qPCR) primers according to the general criteria for real-time primers. All primer sets were intron-overspanning, except for *CLDN8*, because this gene consists of only one exon. All primer sequences used in this study are listed in **Table 1**. Prior to real-time qPCR, the efficiency (95-105%) and dynamic range (R^2>0.98) were evaluated for each primer set. Real-time qPCRs were performed on a Bio-Rad CFX96™ real-time PCR and Bio-Rad C1000™ Thermal Cycler system. Reactions were performed in duplicate using 6.25 μL of SYBR®-Green Master Mix (Applied Biosystems, Foster City, CA, USA), 12.5 ng of template cDNA and 400 nM each primer in a final volume of 12.5 μL. All amplicons showed the correct sizes after gel electrophoresis and the dissociation curves showed one distinct melting peak, ensuring the absence of a non-specific byproduct or primer dimers. Moreover, no reverse transcription controls and no template controls were taken and the difference between the samples was at least eight ct-values, but most of the times >40 cycles (data not shown).

Table 1. Sequences of mouse primers used for real-time qPCR

Gene	*Forward primer*	*Reverse primer*
GAPDH	5'-TAACATCAAATGGGGTGAGG-3'	5'-GGTTCACACCCATCACAAAC-3'
TRPM6	5'-CCTTGGGGAGTCATTGAGAAC-3'	5'-CAGTCCCATCATCACACAGG-3'
NCC	5'-CTTCGGCCACTGGCATTCTG-3'	5'-GATGGCAAGGTAGGAGATGG-3'
TRPV5	5'-CCACAGTGATGCTGGAGAGG-3'	5'-GGATTCTGCTCCTGGTGGTG-3'
Calbindin-D_{28K}	5'-AACTGACAGAGATGGCCAGGTTA-3'	5'-TGAACTCTTTCCCACACATTTTGAT-3'
PV	5'-CGCTGAGGACATCAAGAAGG-3'	5'-CCGGGTTCTTTTTCTTCAGG-3'
CLDN7	5'-GGATTGGTCATCAGATTGTCACA-3'	5'-TGGCAGGTCCAAACTCGTACT-3'
CLDN8	5'-CATGCCTCAGTGGAGAGTG-3'	5'-GACCTTGCACTGCATTCTG-3'
ENaC	5'-CATGCCTGGAGTCAACAATG-3'	5'-CCATAAAAGCAGGCTCATCC-3'
NHE3	5'-TGCCTTGGTGGTACTTCTGG-3'	5'-TCGCTCCTCTTCACCTTCAG-3'

Mouse primers used to perform SYBR Green real-time qPCR. GAPDH, glyceraldehyde 3-phosphate dehydrogenase; TRPM6, transient receptor potential melastatin member 6; NCC, Na^+, Cl^- cotransporter; TRPV5, transient receptor potential vanilloid member 5; Calbindin-D_{28K}, Ca^{2+}-binding protein D_{28K}; PV, parvalbumin; CLDN7, claudin-7; CLDN8, claudin-8; ENaC: epithelial Na^+ channel; NHE3, Na^+, H^+ exchanger 3.

Immunohistochemistry

Immunohistochemical staining was performed on 7-μm cryosections PLP-fixed kidney samples. Sections were stained with guinea pig anti-TRPV5 (25), rabbit anti–calbindin-D_{28K} (Swant, Bellinzona, Switzerland) and rabbit anti-NCC (26), as described previously (27, 28). Images representing the entire kidney cortex were made using a Zeiss fluorescence microscope (Sliedrecht, the Netherlands) equipped with an AxioCam digital photo camera. For semi-quantitative determination of protein levels as the mean of integrated optical density (28), images were analysed with the Fiji ImageJ image analysis software (http://pacific.mpi-cbg.de).

Immunoblotting

Kidneys of control and furosemide-treated mice were homogenized in homogenization buffer A (HbA; 20 mmol/L Tris/HCl (pH = 7.4), 5 mmol/L $MgCl_2$, 5 mmol/L NaH_2PO_4, 1 mmol/L EDTA, 80 mmol/L sucrose, 1 mmol/L PMSF, 1 μg/mL leupeptin and 10 μg/mL pepstatin). Protein concentration of the homogenates was determined using the Bio-Rad Protein Assay (Bio-Rad, Munich, Germany). The proteins were solubilized by 30' incubation at 37°C in Laemmli buffer. Sixty micrograms of each protein sample were separated on an SDS-PAGE gel and blotted to a PVDF-nitrocellulose membrane (Immobilon-P, Millipore Corporation, Bedford, MA, USA). Blots were incubated for 16 h with either a rabbit NCC antibody (1:500 dilution; Millipore, Billerica, MA, USA), a rabbit anti–calbindin-D_{28K} (1:10 000 dilution; Swant, Bellinzona, Switzerland), a rabbit anti-αENaC antibody (1:1000 dilution; StressMarq, Victoria, Canada) or a mouse tubulin antibody (1:20 000 dilution; Invitrogen, Camarillo, CA, USA). Thereafter, blots were incubated with peroxidase-conjugated secondary antibodies after which proteins were visualized by chemiluminescence (Pierce, Rockford, IL, USA). Immunopositive bands were scanned using ChemiDoc XRS (Bio-Rad) and signals were analysed with the Quantity One software (Bio-Rad). The amount of NCC, calbindin-D_{28K} and ENaC protein was normalized for the corresponding total amount of protein, using tubulin protein levels or Coomassie staining. Data are based on two independent experiments in which four samples per group were analysed.

Statistical analysis

Data are expressed as mean ± SEM. Statistical analyses were performed by Student's *t*-test. $P < 0.05$ was considered statistically significant. All calculations were accomplished using the InStat 3 for Macintosh software.

Results

Serum and urine electrolyte levels of furosemide-treated mice

Ten-week-old C57Bl/6J mice were administered furosemide or vehicle using osmotic minipumps for 7 days. Before and after the treatment the mice were individually housed in metabolic cages enabling 24 h urine collections and to measure their water and food intake. Urinary volume and serum electrolyte concentrations and urinary electrolyte levels are displayed in **Table 2**. The mice treated with furosemide displayed a significant polyuria (2.1 ± 0.3 and 1.3 ± 0.2 mL/24h, furosemide versus control, respectively, $P < 0.05$). Serum determinations showed that furosemide treatment resulted in substantially increased levels of Na^+ (158 ± 3 (furosemide) and 147 ± 1 mmol/L (control), $P < 0.01$) whereas serum Ca^{2+}, Mg^{2+} and K^+ values were not significantly altered in mice treated with furosemide. Moreover, furosemide treatment did not affect the urinary Mg^{2+}, Ca^{2+}, Na^+ and K^+ excretion (μmol/24h). Body weight, food intake, water intake and production of feces were not significantly influenced by the chronic furosemide treatment.

Table 2. Serum electrolyte concentrations and urine analysis of mice following chronic furosemide treatment

Measurement	*Control*	*Furosemide*
Serum		
[Mg^{2+}] (mmol/L)	1.65 ± 0.03	1.57 ± 0.04
[Ca^{2+}] (mmol/L)	2.25 ± 0.04	2.27 ± 0.02
[Na^{+}] (mmol/L)	147 ± 1	158 ± 3[a]
[K^{+}] (mmol/L)	7.7 ± 0.1	8.5 ± 0.4
Urine		
Volume (mL/24h)	1.3 ± 0.2	2.1 ± 0.3[a]
Mg^{2+} excretion (µmol/24h)	33 ± 3	36 ± 4
Ca^{2+} excretion (µmol/24h)	7.1 ± 0.7	8.9 ± 0.7
Na^{+} excretion (µmol/24h)	165 ± 12	194 ± 16
K^{+} excretion (µmol/24h)	435 ± 34	490 ± 25

Controls, mice receiving vehicle only; Furosemide, mice receiving 30 mg/kg/day furosemide. Values are presented as means ± SEM. [a] $P < 0.05$ compared with control.

Effect of furosemide treatment on renal expression of TRPM6 and NCC

The effect of furosemide treatment on the renal expression level of TRPM6 was determined by real-time qPCR. A significant increase in renal TRPM6 mRNA expression was observed in mice chronically treated with furosemide (129 ± 9 and 100 ± 6%, furosemide versus control, $P < 0.05$) (**Figure 1**).

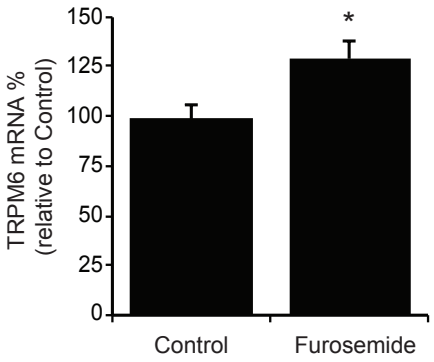

Figure 1. Effect of chronic furosemide treatment on renal TRPM6 mRNA expression level. Real-time qPCR was used to determine the epithelial Mg^{2+} channel TRPM6 mRNA expression level in the kidneys of mice chronically treated with furosemide (30 mg/kg/day for 7 days). Expression levels are corrected for GAPDH and presented as relative percentage of expression in control mice. Values are presented as means ± SEM (n = 10). * $P < 0.05$ compared with control.

Next, the renal mRNA expression level and protein abundance of the thiazide-sensitive NCC were determined. Chronic furosemide treatment had no effect on mRNA expression of NCC (98 ± 4% and 100 ± 5%, furosemide versus control, P > 0.2) (**Figure 2A**). The renal protein abundance of NCC was examined by IHC. In order to semi-quantify the protein expression, the amount of immunopositive tubules in the total kidney cortex was determined for each experimental group. The averaged values of the furosemide treated group are presented as relative percentage of expression in control mice. In contrast with the mRNA level, the protein abundance of NCC was substantially increased (176 ± 9% and 100 ± 8%, furosemide versus control, P < 0.01) (**Figure 2B**).

Specificity of increased levels of Mg^{2+} transporters in response to furosemide administration

To determine the specificity of the upregulation of TRPM6 and NCC in response to furosemide treatment, renal mRNA expression levels of other genes specifically expressed in the DCT and CNT were quantified. To evaluate the effect of furosemide treatment on Ca^{2+} handling, renal expression levels of TRPV5 and the cytosolic Ca^{2+}-binding protein calbindin-D_{28K} in the late DCT (DCT2) and CNT were determined. Furosemide significantly increased the mRNA expression levels of TRPV5 (125 ± 6 and 100 ± 6%, furosemide versus control, P < 0.01) (**Figure 3A**) and calbindin-D_{28K} (153 ± 14 and 100 ± 10%, furosemide versus control, P < 0.01) (**Figure 3B**).

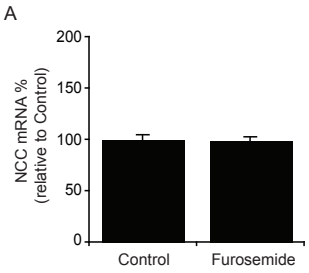

Figure 2. Effect of chronic furosemide treatment on renal NCC expression levels. Real-time quantitative PCR was used to determine the mRNA level of the thiazide-dependent Na^+, Cl^- cotransporter (NCC) in the kidneys of mice chronically treated with furosemide (30 mg/kg/day for 7 days). Expression levels are corrected for GAPDH and presented as relative percentage of expression in control mice (**A**). NCC protein abundance was determined by computerized analysis of immunohistochemical images and presented as relative percentage of control mice (**B**). Values are presented as means ± SEM (*n* = 10). * P < 0.05 compared with control.

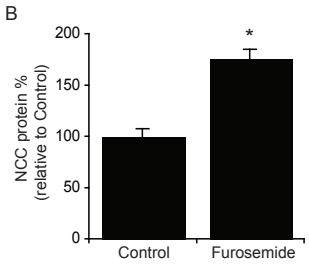

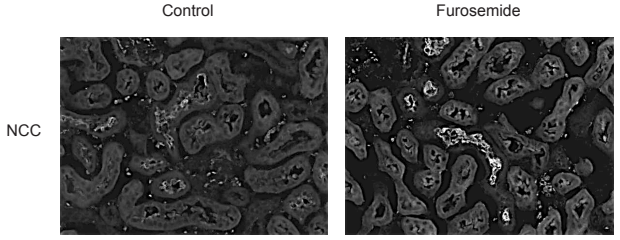

Subsequently, the renal protein abundance of TRPV5 and calbindin-D_{28K} was examined by IHC. In accordance with the mRNA levels, the protein levels of TRPV5 (171 ± 18 and 100 ± 10%, furosemide versus control, P < 0.01) (**Figure 3C**) and calbindin-D_{28K} (173 ± 13 and 100 ± 8%, furosemide versus control, P < 0.01) (**Figure 3D**) were markedly increased. Subsequently, the mRNA abundance of parvalbumin (PV), a DCT-specific Ca^{2+}- and Mg^{2+}-binding protein (29), the tight junction proteins claudin-7 (CLDN7) and claudin-8 (CLDN8)

expressed along the entire aldosterone-sensitive part of the nephron (30) and the epithelial Na^+ channel (ENaC) in the CNT and collecting duct (CD), were determined by real-time qPCR. Furosemide treatment had no significant effect on the mRNA expression levels of these genes; PV (122 ± 9 and 100 ± 8%) (**Figure 4A**), CLDN7 (115 ± 6 and 100 ± 11%) (**Figure 4B**), CLDN8 (103 ± 9 and 100 ± 8%) (**Figure 4C**) and ENaC (122 ± 13 and 100 ± 7%) (**Figure 4D**), for all these four genes; furosemide versus control, $P > 0.05$. Finally, the mRNA expression level of the Na^+, H^+ exchanger 3 (NHE3) in the proximal tubule (PT) and to a minor extent in TAL (31, 32) was determined to define whether chronic furosemide treatment increased Na^+ reabsorption in the PT. Furosemide treatment did not substantially change the renal mRNA level of NHE3 (125 ± 17 and 100 ± 6%, furosemide versus control, $P > 0.1$) (**Figure 4E**).

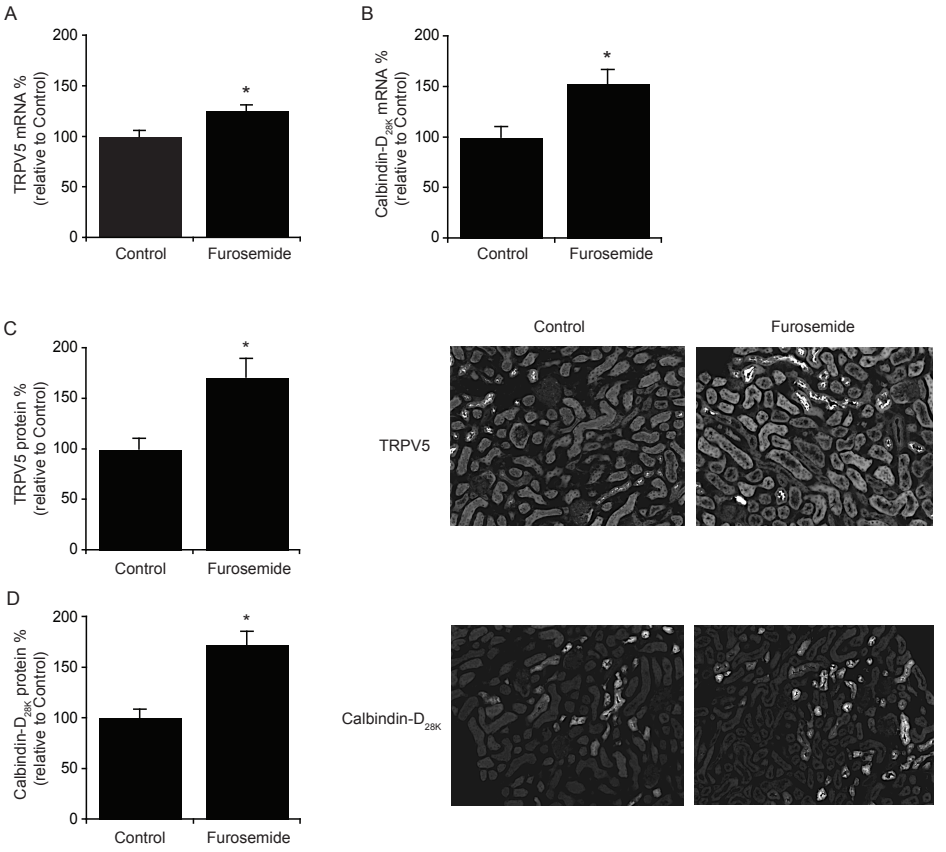

Figure 3. Effect of chronic furosemide treatment on renal TRPV5 and calbindin-D_{28K} expression levels. Real-time qPCR was used to determine the mRNA expression levels of the epithelial Ca^{2+} channel TRPV5 (**A**) and the cytosolic Ca^{2+}-binding protein calbindin-D_{28K} (**B**) in the kidneys of mice chronically treated with furosemide (30 mg/kg/day for 7 days). Expression levels are corrected for GAPDH and presented as relative percentage of expression in control mice. TRPV5 and calbindin-D_{28K} protein abundance were determined by computerized analysis of immunohistochemical images and presented as relative percentage of control mice (**C and D**). Values are presented as means ± SEM ($n = 10$). * $P < 0.05$ compared with control.

Ultimately, to confirm our data obtained by real-time qPCR and IHC, we performed immunoblotting for NCC, calbindin-D_{28K} and αENaC. Quantification of the immunoblots revealed that NCC (165 ± 15 and 100 ± 10%, furosemide versus control, P < 0.01) (**Figure 5A**) and calbindin-D_{28K} (180 ± 23 and 100 ± 12%, furosemide versus control, P < 0.01) (**Figure 5B**) were markedly upregulated in the furosemide-treated group, confirming the results obtained using IHC. Moreover, the immunoblot for ENaC further substantiated the result obtained on the mRNA level, showing that αENaC protein expression is not affected by furosemide treatment as well (122 ± 17 and 100 ± 14%, furosemide versus control, P > 0.2) (**Figure 5C**).

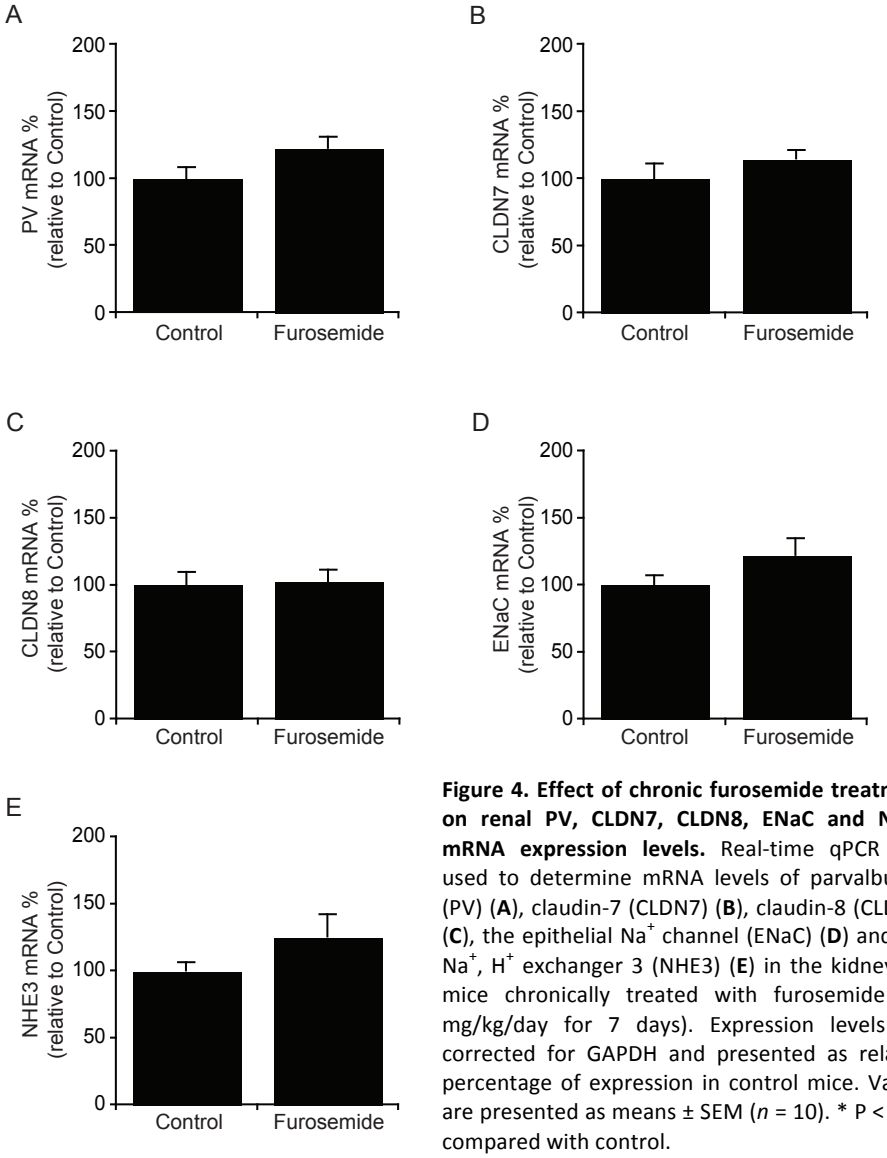

Figure 4. Effect of chronic furosemide treatment on renal PV, CLDN7, CLDN8, ENaC and NHE3 mRNA expression levels. Real-time qPCR was used to determine mRNA levels of parvalbumin (PV) (**A**), claudin-7 (CLDN7) (**B**), claudin-8 (CLDN8) (**C**), the epithelial Na^+ channel (ENaC) (**D**) and the Na^+, H^+ exchanger 3 (NHE3) (**E**) in the kidneys of mice chronically treated with furosemide (30 mg/kg/day for 7 days). Expression levels are corrected for GAPDH and presented as relative percentage of expression in control mice. Values are presented as means ± SEM (*n* = 10). * P < 0.05 compared with control.

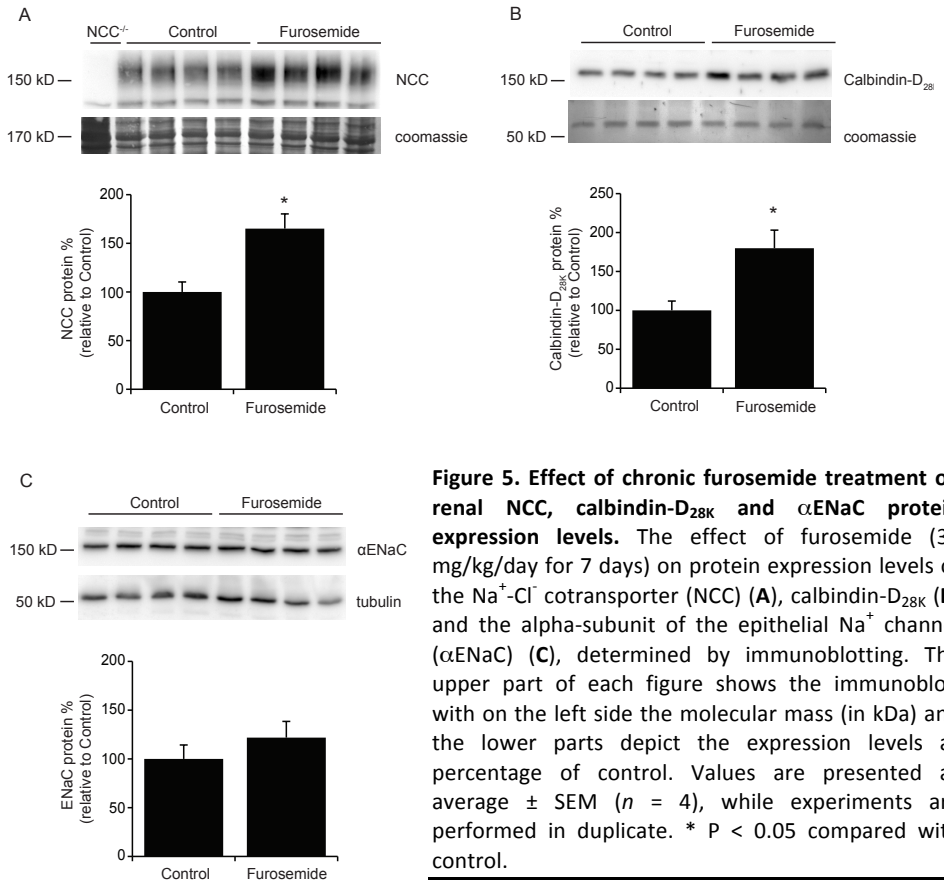

Figure 5. Effect of chronic furosemide treatment on renal NCC, calbindin-D_{28K} and αENaC protein expression levels. The effect of furosemide (30 mg/kg/day for 7 days) on protein expression levels of the Na^+-Cl^- cotransporter (NCC) (**A**), calbindin-D_{28K} (**B**) and the alpha-subunit of the epithelial Na^+ channel (αENaC) (**C**), determined by immunoblotting. The upper part of each figure shows the immunoblot, with on the left side the molecular mass (in kDa) and the lower parts depict the expression levels as percentage of control. Values are presented as average ± SEM (*n* = 4), while experiments are performed in duplicate. * $P < 0.05$ compared with control.

Discussion

Our study demonstrated that chronic furosemide treatment induces a robust polyuria. This effect, which is well known for blocking NKCC2, is the consequence of a defect in the urinary concentrating process due to diminished Na^+, K^+ and Cl^- cotransport in the TAL. Importantly, serum Na^+ values were significantly increased, whereas serum Mg^{2+}, Ca^{2+} and K^+ levels remained constant. The renal excretion of these electrolytes was not affected by chronic furosemide administration. Apparently, the abolished reabsorption in the TAL during chronic furosemide treatment is compensated by an enhanced transport of Mg^{2+} and Na^+ in the DCT and of Ca^{2+} in the DCT2 and CNT, via TRPM6, NCC and TRPV5, respectively. These findings demonstrate a large adaptive capacity of the distal part of the nephron during a chronic diuretic regime.

Our furosemide-treated mice did not develop a significant hypokalemia, hypercalciuria or renal K^+ wasting as usually observed for patients treated with furosemide or affected by Bartter syndrome (33, 34). In contrast, we observed hypernatremia in the furosemide-

treated group. Dehydration is a well-recognized characteristic of Bartter syndrome (34). Besides, in a mouse model of Bartter syndrome, it was shown that these mice suffer from uncompensated polyuria reflected by extracellular volume depletion and hypernatremia (35). Our data suggest that the significant difference in urinary volume was balanced by a smaller, and therefore not significant, compound changes in faeces, water intake and body weight. Consequently, the hypernatremia probably reflects a loss of water in the furosemide group. Importantly, this could have affected the other electrolyte levels as well. Likewise, NCC-deficient mice appear almost normal since no hypokalemia was observed and just a mild form of Gitelman syndrome (GS) (36). This latter finding is unanticipated as well and could indicate that in some cases the mouse is not an optimal model for the human situation.

Our study demonstrated increased mRNA expression level of TRPM6 in response to chronic furosemide treatment. This novel finding unraveled increased active reabsorption of Mg^{2+} in the DCT as a responsible molecular mechanism for the compensation of impaired Mg^{2+} reabsorption in the TAL. The upregulation of TRPM6 in this study demonstrates, like shown before during dietary Mg^{2+} deprivation (37), the gatekeeper function of this channel in the maintenance of the Mg^{2+} balance. Studies on the effect of chronic furosemide application on Mg^{2+} homeostasis are scarce. A minor but significant drop (0.95 +/- 0.01 mmol/L and 0.99 +/- 0.01 mmol/L, furosemide versus control, respectively) in plasma Mg^{2+} was found in rats treated with furosemide for several months (38). In healthy volunteers, oral administration of torasemide (an analogue of furosemide) for 3 weeks did not modify total plasma Mg^{2+}, plasma ionized Mg^{2+} or the free-Mg^{2+} fraction (39). The sufficient intake of Mg^{2+} during furosemide treatment seems to be fundamental to optimal compensation (9) and aberrations in Mg^{2+} balance probably occur only due to comorbidity (11, 12).

NCC facilitates cotransport of Na^{+} and Cl^{-} into DCT cells. Mutations in the gene encoding NCC cause GS, a salt-losing disorder characterized by hypokalemic metabolic alkalosis, hypomagnesemia and hypocalciuria (36, 40). Moreover, NCC-deficient mice have a similar phenotype, including hypomagnesemia (36, 40, 41). This indicates the importance of NCC for Mg^{2+} homeostasis, although it might be an indirect effect since it was not proven that decreased Mg^{2+} reabsorption in TAL is a direct stimulus for upregulation of NCC.

Next, the expression levels of the Ca^{2+} transporter TRPV5 and calbindin-D_{28K}, which are expressed in DCT2 and CNT, were determined. TRPV5 constitutes the apical entry step in active Ca^{2+} reabsorption and is a key player in determining the final urinary Ca^{2+} concentration (42). TRPV5 and calbindin-D_{28K} were on mRNA as well as on the protein level substantially upregulated, which suggests that like Mg^{2+} transport also active Ca^{2+} transport in the distal part of the nephron is increased upon chronic administration of furosemide. Our results are consistent with the results of Lee *et al.* concerning the compensatory adaptation of Ca^{2+} reabsorption mediated by an increase in Ca^{2+} transporter abundance in the kidney during chronic furosemide treatment. In contrast with our results obtained after 7 days of treatment, they observed increased urinary excretion of Ca^{2+} after 3 days of furosemide (10). This apparent discrepancy suggests that the adaptation of the DCT/CNT to chronic furosemide treatment takes more than 3 days to fully compensate for decreased Ca^{2+} reabsorption in the TAL.

Previous studies performed in rats have demonstrated that 6-8 days of continuous furosemide infusion causes hypertrophy of the DCT, CNT and principal cells of the CD (16, 17). Microperfusion experiments in rats have shown an enhanced capacity for Na^+ reabsorption and K^+ secretion by the DCT, CNT and initial CD (ICD) in this adapted state. Furosemide treatment did not affect the length of these tubule segments, but the fractional volumes of the DCT, CNT and ICD were increased, since these cells have increased height of lateral cell processes and larger nuclei (16). In the study by Ellison *et al*., the effect of furosemide was more dramatic, concerning urinary volume, Na^+ excretion and weight loss of the rats compared with our study. This is probably caused by the higher concentration of furosemide used in the former study. We cannot exclude which part/percentage of the compensated reabsorption observed in our study is caused by increased cell volume of the DCT and CNT. However, our results suggest that specific upregulation of TRPM6, NCC and the Ca^{2+} transporters TRPV5 and calbindin-D_{28K} contributes to the increased reabsorption. Additionally, the mRNA expression levels of PV, CLDN7, CLDN8, ENaC and NHE3, as well as the protein level of ENaC were not affected by furosemide treatment. This suggests that the response of the above-mentioned Ca^{2+} and Mg^{2+} transport proteins is rather specific.

In line with our findings, Dussol *et al*. observed in patients that furosemide treatment for 1 month did not significantly increase urinary Na^+ excretion (14, 43). Loon *et al*. showed that continued renal Na^+ loss during furosemide treatment, also for 1 month and in patients, could be prevented. This was mediated by increased renal Na^+ reabsorption and by a decreased natriuretic response to furosemide (15). They explained their findings by the negative impact of both the rebound and the braking phenomena. In contrast with those studies where they used once-daily injections, we used osmotic minipumps resulting in continuous release of furosemide. Our procedure makes the occurrence of a rebound period very unlikely, and thus is the compensation probably exclusively mediated by the braking phenomenon. Remarkably, an experiment in rats comparable with our study showed an almost seven times increased urinary volume and four times increased urinary Na^+ excretion levels. Moreover, they observed increased levels of all thee subunits of ENaC, whereas the NCC protein levels were unchanged upon furosemide treatment (44). In many other studies, furosemide has been shown to increase the abundance and activity of NCC (16, 45, 46). Interestingly, northern blot analysis of NCC mRNA demonstrated no significant effect of furosemide, similar to our real-time qPCR results, indicating that NCC is specifically regulated on the protein level (46). The significantly increased serum levels of Na^+ after chronic furosemide treatment found in our study suggest that the furosemide-treated mice developed net water loss, possibly leading to a hypovolemic state and activation of the renin-angiotensin-aldosterone system (RAAS).

Recently, van der Lubbe *et al*. (47) demonstrated that angiotensin II, independently of aldosterone, can increase the abundance and phosphorylation of NCC. This effect is probably mediated in a with-no-lysine kinase (WNK)4-STE20/SPS1-related, proline alanine-rich kinase (SPAK)-dependent manner (48). Specific activation of NCC, as measured in the present study, is a likely explanation for the fact that we did not observe compensated Na^+ reabsorption in the PT via NHE3 as shown for chronic thiazide treatment (26) or stimulation of ENaC in the CNT and CD. Finally, we could not exclude that increased phosphorylation of NCC is mediated by arginine vasopressin, the hormone that primarily

serves to control extracellular fluid homeostasis, via the WNK-SPAK/OSR1 pathway (49, 50).

In summary, this study showed that mice adapt to chronic furosemide treatment, by the upregulation of transporters distal to the furosemide target segment, including TRPM6, NCC and TRPV5. In this way, urinary wasting of especially Mg^{2+} and the subsequent development of hypomagnesemia is prevented. Extrapolating these findings to patients on continuous furosemide treatment, with normal kidney function and consuming an adequate diet, suggests that it is unlikely that they develop hypomagnesemia. Intriguing remains why patients with mutations in CLDN16 and CLDN19, tight junction proteins located in the TAL, develop hypomagnesemia due to progressive renal Mg^{2+} wasting (51, 52), while blockade of NKCC2 does not result in hypomagnesemia. It might be that the effect of mutations in CLDN16 and CLDN19 is more effective compared with blocking NKCC2 by furosemide. Another possible explanation is that CLDN16 and CLDN19 are expressed in more segments than only the TAL.

Acknowledgements. This research was financially supported by the Dutch Organization for Scientific Research (ZonMw 9120.8026; ALW 818.02.001), a European Young Investigator award from the European Science Foundation.

References

1. Hendry, B.M., and Ellory, J.C. Molecular sites for diuretic action. *Trends Pharmacol Sci* 9:416-421. 1988.
2. Rose, B.D. Diuretics. *Kidney Int* 39:336-352. 1991.
3. Quamme, G.A. Renal handling of magnesium: drug and hormone interactions. *Magnesium* 5:248-272. 1986.
4. Dimke, H., Hoenderop, J.G., and Bindels, R.J. Hereditary tubular transport disorders: implications for renal handling of Ca2+ and Mg2+. *Clin Sci (Lond)* 118:1-18.
5. Ellison, D.H. Diuretic drugs and the treatment of edema: from clinic to bench and back again. *Am J Kidney Dis* 23:623-643. 1994.
6. Di Stefano, A., Roinel, N., de Rouffignac, C., et al. Transepithelial Ca2+ and Mg2+ transport in the cortical thick ascending limb of Henle's loop of the mouse is a voltage-dependent process. *Ren Physiol Biochem* 16:157-166. 1993.
7. Quamme, G.A. Effect of furosemide on calcium and magnesium transport in the rat nephron. *Am J Physiol* 241:F340-347. 1981.
8. Lee, A.J., Chen, Y.H., Chu, M.L., et al. [Effect of furosemide on renal magnesium and calcium excretion of different ages (II)]. *Zhonghua Min Guo Xiao Er Ke Yi Xue Hui Za Zhi* 35:215-220. 1994.
9. Caddell, J.L. Protection by magnesium of renal calcinosis in furosemide-treated weanling rats with moderate magnesium deficiency. *Biol Neonate* 48:49-58. 1985.
10. Lee, C.T., Chen, H.C., Lai, L.W., et al. Effects of furosemide on renal calcium handling. *Am J Physiol Renal Physiol* 293:F1231-1237. 2007.
11. Cohen, N., Almoznino-Sarafian, D., Zaidenstein, R., et al. Serum magnesium aberrations in furosemide (frusemide) treated patients with congestive heart failure: pathophysiological correlates and prognostic evaluation. *Heart* 89:411-416. 2003.
12. Davies, D.L., and Fraser, R. Do diuretics cause magnesium deficiency? *Br J Clin Pharmacol* 36:1-10. 1993.
13. Jentzer, J.C., DeWald, T.A., and Hernandez, A.F. Combination of loop diuretics with thiazide-type diuretics in heart failure. *J Am Coll Cardiol* 56:1527-1534. 2010.
14. Ellison, D.H. The physiologic basis of diuretic synergism: its role in treating diuretic resistance. *Ann Intern Med* 114:886-894. 1991.
15. Loon, N.R., Wilcox, C.S., and Unwin, R.J. Mechanism of impaired natriuretic response to furosemide during prolonged therapy. *Kidney Int* 36:682-689. 1989.
16. Ellison, D.H., Velazquez, H., and Wright, F.S. Adaptation of the distal convoluted tubule of the rat. Structural and functional effects of dietary salt intake and chronic diuretic infusion. *J Clin Invest* 83:113-126. 1989.
17. Kaissling, B., Bachmann, S., and Kriz, W. Structural adaptation of the distal convoluted tubule to prolonged furosemide treatment. *Am J Physiol* 248:F374-381. 1985.
18. Branch, R.A., Homeida, M., Levine, D., et al. Pharmacokinetics of frusemide related to diuretic response [proceedings]. *Br J Pharmacol* 57:442P-443P. 1976.
19. Andreasen, F., Lauridsen, I.N., Hansen, F.A., et al. Dose dependency of furosemide-induced sodium excretion. *J Pharmacol Exp Ther* 248:1182-1188. 1989.
20. Schlingmann, K.P., Konrad, M., and Seyberth, H.W. Genetics of hereditary disorders of magnesium homeostasis. *Pediatr Nephrol* 19:13-25. 2004.
21. Simon, D.B., Karet, F.E., Hamdan, J.M., et al. Bartter's syndrome, hypokalaemic alkalosis with hypercalciuria, is caused by mutations in the Na-K-2Cl cotransporter NKCC2. *Nat Genet* 13:183-188. 1996.
22. Voets, T., Nilius, B., Hoefs, S., et al. TRPM6 forms the Mg2+ influx channel involved in intestinal and renal Mg2+ absorption. *J Biol Chem* 279:19-25. 2004.

23. Bachmann, S., Velazquez, H., Obermuller, N., et al. Expression of the thiazide-sensitive Na-Cl cotransporter by rabbit distal convoluted tubule cells. *J Clin Invest* 96:2510-2514. 1995.
24. Hoenderop, J.G., Muller, D., Van Der Kemp, A.W., et al. Calcitriol controls the epithelial calcium channel in kidney. *J Am Soc Nephrol* 12:1342-1349. 2001.
25. Hoenderop, J.G., Hartog, A., Stuiver, M., et al. Localization of the epithelial Ca(2+) channel in rabbit kidney and intestine. *J Am Soc Nephrol* 11:1171-1178. 2000.
26. Nijenhuis, T., Hoenderop, J.G., Loffing, J., et al. Thiazide-induced hypocalciuria is accompanied by a decreased expression of Ca2+ transport proteins in kidney. *Kidney Int* 64:555-564. 2003.
27. Hoenderop, J.G., van Leeuwen, J.P., van der Eerden, B.C., et al. Renal Ca2+ wasting, hyperabsorption, and reduced bone thickness in mice lacking TRPV5. *J Clin Invest* 112:1906-1914. 2003.
28. Nijenhuis, T., Hoenderop, J.G., and Bindels, R.J. Downregulation of Ca(2+) and Mg(2+) transport proteins in the kidney explains tacrolimus (FK506)-induced hypercalciuria and hypomagnesemia. *J Am Soc Nephrol* 15:549-557. 2004.
29. Bindels, R.J., Timmermans, J.A., Hartog, A., et al. Calbindin-D9k and parvalbumin are exclusively located along basolateral membranes in rat distal nephron. *J Am Soc Nephrol* 2:1122-1129. 1991.
30. Li, W.Y., Huey, C.L., and Yu, A.S. Expression of claudin-7 and -8 along the mouse nephron. *Am J Physiol Renal Physiol* 286:F1063-1071. 2004.
31. Amemiya, M., Loffing, J., Lotscher, M., et al. Expression of NHE-3 in the apical membrane of rat renal proximal tubule and thick ascending limb. *Kidney Int* 48:1206-1215. 1995.
32. Nishinaga, H., Komatsu, R., Doi, M., et al. Circadian expression of the Na+/H+ exchanger NHE3 in the mouse renal medulla. *Biomed Res* 30:87-93. 2009.
33. Suki, W.N., Eknoyan, G., and Martinez-Maldonado, M. Tubular sites and mechanisms of diuretic action. *Annu Rev Pharmacol* 13:91-106. 1973.
34. Bartter, F.C., Pronove, P., Gill, J.R., Jr., et al. Hyperplasia of the juxtaglomerular complex with hyperaldosteronism and hypokalemic alkalosis. A new syndrome. *Am J Med* 33:811-828. 1962.
35. Takahashi, N., Chernavvsky, D.R., Gomez, R.A., et al. Uncompensated polyuria in a mouse model of Bartter's syndrome. *Proc Natl Acad Sci U S A* 97:5434-5439. 2000.
36. Schultheis, P.J., Lorenz, J.N., Meneton, P., et al. Phenotype resembling Gitelman's syndrome in mice lacking the apical Na+-Cl- cotransporter of the distal convoluted tubule. *J Biol Chem* 273:29150-29155. 1998.
37. Groenestege, W.M., Hoenderop, J.G., van den Heuvel, L., et al. The epithelial Mg2+ channel transient receptor potential melastatin 6 is regulated by dietary Mg2+ content and estrogens. *J Am Soc Nephrol* 17:1035-1043. 2006.
38. Wong, N.L., Sutton, R.A., and Dirks, J.H. Is lymphocyte magnesium concentration a reflection of intracellular magnesium concentration? *J Lab Clin Med* 112:721-726. 1988.
39. Gozzi, T., Durler, S., Truttman, A.C., et al. Free circulating magnesium and loop diuretics in humans. *Eur J Clin Pharmacol* 53:275-276. 1997.
40. Simon, D.B., Nelson-Williams, C., Bia, M.J., et al. Gitelman's variant of Bartter's syndrome, inherited hypokalaemic alkalosis, is caused by mutations in the thiazide-sensitive Na-Cl cotransporter. *Nat Genet* 12:24-30. 1996.
41. Gitelman, H.J., Graham, J.B., and Welt, L.G. A new familial disorder characterized by hypokalemia and hypomagnesemia. *Trans Assoc Am Physicians* 79:221-235. 1966.
42. Hoenderop, J.G., van der Kemp, A.W., Hartog, A., et al. Molecular identification of the apical Ca2+ channel in 1, 25-dihydroxyvitamin D3-responsive epithelia. *J Biol Chem* 274:8375-8378. 1999.
43. Dussol, B., Moussi-Frances, J., Morange, S., et al. A randomized trial of furosemide vs hydrochlorothiazide in patients with chronic renal failure and hypertension. *Nephrol Dial Transplant* 20:349-353. 2005.

44. Na, K.Y., Oh, Y.K., Han, J.S., et al. Upregulation of Na+ transporter abundances in response to chronic thiazide or loop diuretic treatment in rats. *Am J Physiol Renal Physiol* 284:F133-143. 2003.
45. Stanton, B.A., and Kaissling, B. Adaptation of distal tubule and collecting duct to increased Na delivery. II. Na+ and K+ transport. *Am J Physiol* 255:F1269-1275. 1988.
46. Abdallah, J.G., Schrier, R.W., Edelstein, C., et al. Loop diuretic infusion increases thiazide-sensitive Na(+)/Cl(-)-cotransporter abundance: role of aldosterone. *J Am Soc Nephrol* 12:1335-1341. 2001.
47. van der Lubbe, N., Lim, C.H., Fenton, R.A., et al. Angiotensin II induces phosphorylation of the thiazide-sensitive sodium chloride cotransporter independent of aldosterone. *Kidney Int* 79:66-76. 2011.
48. San-Cristobal, P., Pacheco-Alvarez, D., Richardson, C., et al. Angiotensin II signaling increases activity of the renal Na-Cl cotransporter through a WNK4-SPAK-dependent pathway. *Proc Natl Acad Sci U S A* 106:4384-4389. 2009.
49. Mutig, K., Saritas, T., Uchida, S., et al. Short-term stimulation of the thiazide-sensitive Na+-Cl- cotransporter by vasopressin involves phosphorylation and membrane translocation. *Am J Physiol Renal Physiol* 298:F502-509. 2010.
50. Pedersen, N.B., Hofmeister, M.V., Rosenbaek, L.L., et al. Vasopressin induces phosphorylation of the thiazide-sensitive sodium chloride cotransporter in the distal convoluted tubule. *Kidney Int* 78:160-169. 2010.
51. Simon, D.B., Lu, Y., Choate, K.A., et al. Paracellin-1, a renal tight junction protein required for paracellular Mg2+ resorption. *Science* 285:103-106. 1999.
52. Konrad, M., Schaller, A., Seelow, D., et al. Mutations in the tight-junction gene claudin 19 (CLDN19) are associated with renal magnesium wasting, renal failure, and severe ocular involvement. *Am J Hum Genet* 79:949-957. 2006.

Chapter 4

The impact of dietary magnesium restriction on magnesiotropic and calciotropic genes

Annelies A. van Angelen, Pedro San-Cristobal, Wilco P. Pulskens,
Joost G. Hoenderop and René J. Bindels

Department of Physiology, Radboud University Nijmegen Medical Centre,
Nijmegen, The Netherlands.

Nephrol Dial Transplant 28: 2983-93, 2013

Abstract

Background. Magnesium (Mg^{2+}) is an essential electrolyte with important physiological functions. Consequently, hypomagnesemia, an electrolyte disorder frequently diagnosed in critically ill patients, can have life-threatening consequences. The kidney plays a central role in the regulation of the Mg^{2+} balance. The present study investigated the molecular consequences of dietary Mg^{2+} restriction on renal Mg^{2+} transporters.

Methods. Two groups of 10 mice were fed a Mg^{2+}-deficient diet or a Mg^{2+}-enriched diet for 2 weeks. Serum and urine electrolyte concentrations were assayed. Next, renal mRNA expression levels of Mg^{2+}-related genes were measured to determine their sensitivity to the dietary Mg^{2+} content. Subsequently, parvalbumin (PV) and the thiazide-sensitive Na^{+}, Cl^{-} cotransporter (NCC), both co-expressed in the distal convoluted tubule (DCT) with TRPM6, were further analysed at the protein level using immunoblotting and immunohistochemistry (IHC).

Results. Serum and urine electrolyte measurements revealed that dietary Mg^{2+} restriction resulted in significant reduction of serum Mg^{2+} and Ca^{2+} levels, and that the urinary excretion of these ions was also markedly reduced, while phosphate (P_i) excretion was significantly increased. In addition, the serum FGF23 level was markedly increased, whereas P_i was not significantly changed in the Mg^{2+}-restricted mouse group. The renal abundance of hepatocyte nuclear factor 1 homeobox B (HNF1B) and the epithelial Mg^{2+} channel TRPM6 were increased in response to dietary Mg^{2+} restriction, whereas other magnesiotropic transporters were not affected. PV abundance was upregulated, while NCC was significantly downregulated. Furthermore, the expression levels of the epithelial Ca^{2+} channel TRPV5 and calbindin-D_{28K} were markedly reduced in the low Mg^{2+} group.

Conclusion. Our data indicate an essential adaptive role for DCT during hypomagnesemia since TRPM6, HNF1B, PV and NCC expression levels were adjusted. Moreover, hypomagnesemia resulted in severe changes in Ca^{2+} and P_i reabsorption and expression levels of calciotropic proteins.

Introduction

Magnesium (Mg^{2+}) is the most prevalent intracellular divalent cation. It plays a critical role in diverse biochemical and physiological processes, especially in neuromuscular functioning (1). The plasma Mg^{2+} concentration represents 1% of total body Mg^{2+} and is regulated by the concerted action of intestinal absorption, storage in bone and reabsorption by the kidney (2). Hypomagnesemia is one of the most frequent electrolyte disturbances diagnosed in ~10% of the hospitalized patients and can be as high as 65% in intensive care patients (3, 4). Symptoms of hypomagnesemia frequently involve neuromuscular irritability, such as tetany and seizures, and if not corrected in time, cardiac arrhythmias (5).

The kidney is the unfailing organ for Mg^{2+} homeostasis (6). About 80% of the total plasma Mg^{2+} is ultrafiltrated through the glomerular membrane, of which 90-95% is reabsorbed in consecutive segments of the nephron (1). Most of the Mg^{2+} reabsorption takes place in a passive paracellular manner in the proximal tubules (PTs) and the thick ascending limb of Henle's loop (TAL) (10-30% and 40-70% of the filtered load, respectively). This transport is driven by a favourable concentration gradient for Mg^{2+} conditional on the Na^+-driven net water reabsorption in PT (7), and by the lumen-positive transepithelial potential in TAL, which is mainly generated by the Na^+, K^+, $2Cl^-$ cotransporter (NKCC2) (8). Approximately 5-10% of the filtered load is reabsorbed by the distal convoluted tubule (DCT), where fine-tuning of Mg^{2+} reabsorption occurs via an active reabsorption process (2). In this segment, the epithelial Mg^{2+} channel TRPM6 is conspicuously localized along the apical membrane, facilitating Mg^{2+} influx (9). After the DCT, Mg^{2+} is not further reabsorbed and consequently around 1-3% of the filtered Mg^{2+} is excreted in the urine (1).

During the last decade, isolated cases of hereditary disorders of Mg^{2+} homeostasis have played a major role in the identification of magnesiotropic proteins localized in the kidney, like the discovery of TRPM6 in autosomal-recessive disorder hypomagnesemia with secondary hypocalcemia (HSH) (10, 11). This resulted in the elucidation of additional genes responsible for maintenance of Mg^{2+} balance, including the Na^+, K^+-ATPase γ-subunit, a protein encoded by the *FXYD2* gene (12); the hepatocyte nuclear factor 1 homeobox B (HNF1B), which is shown to regulate the transcription of *FXYD2* (13); the *KCNJ10* gene (14, 15), encoding the inwardly rectifying K^+ channel 4.1 (Kir4.1) (16); the epidermal growth factor (EGF) (17); and finally, the *KCNA1* gene, encoding the voltage-gated K^+ channel 1.1 (Kv1.1) (18). Moreover, in TAL mutations in genes encoding the interacting tight junction proteins claudin-16 (CLDN16) (19) and claudin-19 (CLDN19) (20) were also linked to disturbances in Mg^{2+} homeostasis.

Previous studies have demonstrated that dietary Mg^{2+} restriction results in renal Mg^{2+} conservation, whereas a Mg^{2+}-enriched diet increases urinary Mg^{2+} excretion (21, 22). The dietary Mg^{2+} content affected the renal TRPM6 expression on mRNA as well as protein level (22). *A*lterations in the Mg^{2+} balance can also cause Ca^{2+} disturbances as a secondary adverse effect (23). Indeed, Groenestege *et al.* showed that dietary Mg^{2+} restriction not only leads to renal Mg^{2+} conservation, but also reduces Ca^{2+} wasting (22). Furthermore, the disease HSH displays a close interaction between Mg^{2+} and Ca^{2+} homeostasis. It has been suggested that hypocalcemia is secondary to parathyroid hormone (PTH) failure resulting from Mg^{2+} deficiency (24). However, the details of this mechanism remain largely

unknown. Maintenance of the Ca^{2+} balance is, like for Mg^{2+}, of vital importance for ample physiological functions (25). The Ca^{2+}-sensing receptor plays a central role in the homeostasis of both divalent ions (26).

The aim of the present study was to investigate which magnesiotropic players are affected by the dietary Mg^{2+} content. Furthermore, the effect on other electrolyte transporters present in the TRPM6-expressing DCT segment was investigated. To this end, C57BL/6J mice were fed a Mg^{2+}-deficient (0.003% w/w Mg^{2+}) and -enriched (0.48% w/w Mg^{2+}) diet and serum and urine electrolyte measurements were performed for Mg^{2+}, Ca^{2+}, Na^{+} and K^{+}. In addition, real-time quantitative polymerase chain reaction (qPCR) and immunohistochemistry (IHC) were used to determine the different mRNA and protein levels, respectively.

Materials and methods

Animal studies

C57BL/6J male mice (10 weeks of age) were purchased from Harlan/CPB (Zeist, The Netherlands) and maintained in a temperature-controlled and 12/12 h light-darkness room. To study the effect of dietary Mg^{2+}, mice (n = 10 per group) were fed for 14 days a Mg^{2+}-deficient (0.003% w/w) diet or a Mg^{2+}-enriched (0.48% w/w) diet (#TD.93106 and #TD.10531, respectively, Harlan-Teklad Madison, WI, USA). Both diets contained 0.6% w/w Ca^{2+}, 0.45% w/w phosphorus and 2200 IU/kg vitamin D. The diets and deionized drinking water were provided *ad libitum*. A diet containing 0.19% w/w Mg^{2+} is considered normal for rodents (22). Before the start of the experiment and on day 12, the mice were individually housed in metabolic cages enabling 24 h urine collections (mineral oil was used to prevent evaporation) and to measure their water and food intake. At the end of the experiment, blood samples were taken under isoflurane (3.5% v/v) anaesthesia, and the mice were sacrificed by cervical dislocation. Subsequently, kidneys and colon were immediately frozen in liquid nitrogen for RNA and protein isolation or incubated in periodate-lysine-paraformaldehyde (PLP)-solution for IHC analysis. Blood was led to clot at room temperature, incubated overnight at 4°C and spun down for 5' at 13 250 × g and the collected serum was used for analytical procedures. The animal ethics board of the Radboud University Nijmegen approved all experimental procedures.

Analytical procedures

Serum and urine Mg^{2+} concentrations were determined using a colorimetric assay kit according to the manufacturer's protocol (Roche Diagnostics, Woerden, The Netherlands). Serum and urine Ca^{2+} concentrations were measured as described previously (27). A flame spectrophotometer (FCM 6343; Eppendorf) was used to measure serum and urinary Na^{+} and K^{+} concentrations. Serum and urine phosphate (P_i) concentrations were measured by the phosphomolybdate method with an Aeroset analyser (Abbott Diagnostics, Abbott Park, IL, USA). Serum FGF23 levels were determined using an enzyme-linked immunosorbent assay kit (Immutopics, San Clemente, CA, USA).

Total kidney and colon RNA isolation and cDNA synthesis

Total RNA was extracted from the kidney and colon using TriZol Total RNA isolation reagent according to standard procedures (Gibco BRL, Breda, The Netherlands). The obtained RNA was subjected to DNase treatment (Promega, Madison, WI, USA) to prevent genomic DNA contamination. To determine RNA integrity, all samples were resolved on ethidium bromide gel 1% w/v formaldehyde agarose gel, while RNA concentrations were determined by measuring the ratio of the UV absorbance at 260 and 280 nm using the NANODROP 2000c (Thermo scientific, Wilmington, DE, USA). Next, 1.5 μg of RNA was reverse transcribed by Molony-Murine Leukemia Virus-Reverse Transcriptase (Invitrogen, Breda, The Netherlands) into complementary DNA (cDNA) according to the manufacturer's recommendations.

SYBR Green real-time quantitative polymerase chain reaction

cDNA was used to determine the mRNA expression levels of genes of the interest, as well as mRNA levels of the reference gene glyceraldehyde 3-phosphate dehydrogenase (GAPDH) as an endogenous control. Primer3 software (http://frodo.wi.mit.edu/primer3/) was used to design real-time qPCR primers according to the general criteria for these primers. All primer sequences used in this study are listed in **Table 1**. Prior to real-time qPCRs, the efficiency (95-105%) and dynamic range ($R^2 > 0.98$) were evaluated for each primer set. Real-time qPCRs were performed on a Bio-Rad CFX96™ Real-Time PCR and Bio-Rad C1000™ Thermal Cycler system. Reactions were performed in duplicate using a 6.25 μL SYBR®-Green Master Mix (Applied Biosystems, Foster City, CA, USA), 12.5 ng of template cDNA and 400 nM of each primer in a final volume of 12.5 μL. All amplicons showed the correct sizes after gel electrophoresis and the dissociation curves showed one distinct melting peak, ensuring the absence of a nonspecific byproduct or primer dimers. Moreover, no reverse transcription and no template controls were taken along.

Immunohistochemistry

IHC was performed as previously described (28). Briefly, immunohistochemical staining was executed on 7 μm cryosections PLP-fixed kidney samples. Sections were incubated for 16 h at 4°C with the primary antibodies: rabbit anti-parvalbumin (PV) antibody (1:200; PV-28, Swant, Bellinzona, Switzerland), guinea pig anti-TRPV5 (1:2000) (29), rabbit anti-calbindin-D_{28K} (1:300; Swant), and rabbit anti-NCC (1:100) (30). For detection, the sections were incubated with Alexa-conjugated secondary antibodies. Images representing the entire kidney cortex were made using a Zeiss fluorescence microscope (Sliedrecht, The Netherlands) equipped with an AxioCam digital photo camera. For semi-quantitative determination of protein levels as the mean of integrated optical density, images were analysed with the Fiji ImageJ image analysis software (http://pacific.mpi-cbg.de).

Immunoblotting

Total kidney sections of mice treated with both diets were homogenized in buffer A (HbA; 20 mM Tris/HCl (pH = 7.4), 5 mM $MgCl_2$, 5 mM NaH_2PO_4, 1 mM EDTA, 80 mM sucrose, 1 mM PMSF, 1 μg/mL leupeptin and 10 μg/mL pepstatin). Protein concentration of the homogenates was determined by Bio-Rad Protein Assay (Bio-Rad, Munich, Germany). The proteins were solubilized by 30' incubation at 37°C in Laemmli buffer. 60 micrograms of each protein sample was separated on a 10% w/v SDS-PAGE gel and blotted to a PVDF-

nitrocellulose membrane (Immobilon-P, Millipore Corporation, Bedford, MA, USA). Blots were incubated for 16 h with a rabbit HNF1B antibody (H-85, 1:500 dilution; Santa Cruz Biotechnology, Santa Cruz, CA, USA), or with a mouse tubulin antibody (1:20 000 dilution; Invitrogen, Camarillo, CA, USA). Thereafter, blots were incubated with peroxidase-coupled secondary antibodies, and proteins were visualized using the chemiluminescence method (Pierce, Rockford, IL, USA). Immunopositive bands were scanned using ChemiDoc XRS (Bio-Rad) and the signals were analysed using the Quantity One software (Bio-Rad). The amount of HNF1B protein was normalized for the corresponding total amount of protein, using tubulin protein levels.

Table 1. Sequences of mouse primers used for real-time qPCR

Gene	*Forward primer*	*Reverse primer*
GAPDH	5′-TAACATCAAATGGGGTGAGG-3′	5′-GGTTCACACCCATCACAAAC-3′
TRPM6	5′-AAAGCCATGCGAGTTATCAGC-3′	5′-CTTCACAATGAAAACCTGCCC-3′
TRPM7	5′-GGTTCCTCCTGTGGTGCCTT-3′	5′-CCCCATGTCGTCTCTGTCGT-3′
Kv1.1	5′-CTGTGACAATTGGAGGCAAGATC-3′	5′-GAGCAACTGAGCCTGCTCTTC-3′
EGF	5′-GAGTTGCCCTGACTCTACCG-3′	5′-CCACCATTGAGGCAGTATCC-3′
EGFR	5′-CAGAACTGGGCTTAGGGAAC-3′	5′-GGACGATGTCCCTCCACTG-3′
Kir4.1	5′-CCGCGATTTATCAGAGC-3′	5′-AGATCCTTGAGGTAGAGGAA-3′
HNF1B	5′-CAAGATGTCAGGAGTGCGCTAC-3′	5′-CTGGTCACCATGGCACTGTTAC-3′
FXYD2b	5′-GTACCTGGGTGGCAGTGCCAAG-3′	5′-CCTTTTGCTGAGAATGATGAGGAG-3′
CLDN16	5′-GTTGCAGGGACCACATTAC-3′	5′-GAGGAGCGTTCGACGTAAAC-3′
CLDN19	5′-GGTTCCTTTCTCTGCTGCAC-3′	5′-CGGGCAACTTAACAACAGG-3′
PV	5′-CGCTGAGGACATCAAGAAGG-3′	5′-CCGGGTTCTTTTTCTTCAGG-3′
NCC	5′-CTTCGGCCACTGGCATTCTG-3′	5′-GATGGCAAGGTAGGAGATGG-3′
TRPV5	5′-CCACAGTGATGCTGGAGAGG-3′	5′-GGATTCTGCTCCTGGTGGTG-3′
Calbindin-D_{28K}	5′-CCACAGTGATGCTGGAGAGG-3′	5′-GGATTCTGCTCCTGGTGGTG-3′
NHE3	5′-TGCCTTGGTGGTACTTCTGG-3′	5′-TCGCTCCTCTTCACCTTCAG-3′
ENaC	5′-CATGCCTGGAGTCAACAATG-3′	5′-CCATAAAAGCAGGCTCATCC-3′

Mouse primers used to perform SYBR Green real-time qPCR. GAPDH, glyceraldehyde 3-phosphate dehydrogenase; TRPM6, transient receptor potential melastatin member 6; TRPM7, transient receptor potential melastatin member 7; Kv1.1, voltage-gated K^+ channel, shaker, member 1.1; EGF, epidermal growth factor; EGFR, epidermal growth factor receptor; Kir4.1, inwardly rectifying K^+ (Kir) channel 4.1; HNF1B, hepatocyte nuclear factor 1B; FXYD2b, FXYD domain containing ion transport regulator 2, splice variant b; CLDN16, claudin-16; CLDN19, claudin-19; PV, parvalbumin; NCC, Na^+, Cl^- cotransporter; TRPV5, transient receptor potential vanilloid member 5; Calbindin-D_{28K}, Ca^{2+}-binding protein D_{28K}; NHE3, Na^+, H^+ exchanger 3, ENaC: epithelial Na^+ channel.

Statistical analysis

Data are expressed as mean ± SEM. Statistical analyses were performed by an unpaired Student's *t*-test. The low Mg^{2+} diet mouse group was compared with the high Mg^{2+} diet mouse group. $P < 0.05$ was considered statistically significant. All analyses were performed

using the InStat 3 software.

Results

Serum and urine electrolyte levels of mice fed a low or high Mg^{2+} diet

Before and after the diet period, mice were individually housed in metabolic cages to collect 24 h urine samples and to measure their water and food intake. Serum electrolyte concentrations, and urinary volumes and electrolyte levels are listed in **Table 2**.

Table 2. Serum electrolyte concentrations and urine analysis of mice following an Mg^{2+}-deficient or Mg^{2+}-enriched diet

Measurement	*0.003% w/w Mg^{2+}*	*0.48% w/w Mg^{2+}*	*Normal range[1]*
Serum			
[Mg^{2+}] (mmol/L)	0.63 ± 0.04[b]	1.80 ± 0.04	1.6-1.8
[Ca^{2+}] (mmol/L)	1.94 ± 0.02[b]	2.06 ± 0.02	2.2-2.4
[Na^{+}] (mmol/L)	139.6 ± 0.8[a]	136.2 ± 0.5	130-150
[K^{+}] (mmol/L)	7.60 ± 0.07[a]	7.93 ± 0.09	6-8
[P_i] (mmol/L)	2.4 ± 0.2	2.0 ± 0.1	2.2-2.7
[FGF23] (pg/mL)	157 ±19[b]	64 ± 8	60-140
Urine			
Volume (mL/24h)	1.3 ± 0.1	1.2 ± 0.1	~1.0
Mg^{2+} excretion (µmol/24h)	0.22 ± 0.04[b]	139 ±12	~30
Ca^{2+} excretion (µmol/24h)	0.9 ± 0.2[b]	23 ± 2	~7.0
Na^{+} excretion (µmol/24h)	91 ± 6	76 ± 9	~100
K^{+} excretion (µmol/24h)	166 ± 6	154 ± 10	~200
P_i excretion (µmol/24h)	79 ± 8[b]	1.9 ± 0.3	~2.8

0.003% w/w Mg^{2+}, mice receiving the deficient (0.003% w/w) Mg^{2+} diet; *0.48% w/w Mg^{2+}*, mice receiving the enriched (0.48% w/w) Mg^{2+} diet. Values are presented as means ± SEM. [1] Normal serum values in C57BL/6J mice in mmol/L based on the values determined by Harlan (Harlan-Teklad Madison, WI, USA), previous experiments performed in our lab and the metabolic cage data before the start of this experiment. The urinary excretion has a high variability. [a] $P < 0.05$ compared with the high Mg^{2+} diet, [b] $P < 0.001$ compared with the high Mg^{2+} diet.

The mouse group fed with the Mg^{2+}-deficient diet displayed a significant hypomagnesemia accompanied by a marked hypocalcemia compared with the mice receiving a Mg^{2+}-enriched diet. Moreover, serum Na^{+} and K^{+} were slightly, but significantly affected by the Mg^{2+}-deficient diet, resulting in an increased serum Na^{+} and a decreased K^{+} level. In

addition, the serum FGF23 level was markedly increased, whereas P_i was not significantly changed in the Mg^{2+}-restricted mouse group. Dietary Mg^{2+} restriction resulted in a substantial decreased urinary Mg^{2+} and Ca^{2+} excretion, whereas the Na^+ and K^+ excretions were not affected. Further, the urinary P_i excretion was markedly increased in the mouse group fed with the low Mg^{2+} diet (**Table 2**). Body weight, food intake, water intake and production of urine and faeces were not influenced by differences in the dietary Mg^{2+} content.

Effect of dietary Mg^{2+} deficiency on mRNA expression of magnesiotropic transporters

Table 3 shows the effect of dietary Mg^{2+} levels on renal mRNA abundance of TRPM6, the ubiquitously expressed Mg^{2+} channel TRPM7, Kv1.1, EGF, EGF receptor (EGFR), Kir4.1, HNF1B, FXYD domain-containing ion transport regulator 2, splice variants a and b (FXYD2a and FXYD2b), CLDN16 and CLDN19. The Mg^{2+}-deficient diet resulted in a significantly increased renal TRPM6 mRNA level.

Table 3. Effect of dietary Mg^{2+} content on the expression profile of magnesiotropic genes in kidney

Gene	*0.003% w/w Mg^{2+}*	*0.48% w/w Mg^{2+}*
TRPM6	204 ± 17%[a]	100 ± 7%
TRPM7	95 ± 5%	100 ± 7%
Kv1.1	109 ± 8%	100 ± 8%
EGF	112 ± 5%	100 ± 7%
EGFR	86 ± 4%	100 ± 6%
Kir4.1	97 ± 7%	100 ± 9%
HNF1B	185 ± 19%[a]	100 ± 8%
FXYD2b	103 ± 7%	100 ± 4%
CLDN16	99 ± 7%	100 ± 5%
CLDN19	100 ± 9%	100 ± 10%

A real-time qPCR was used to determine the mRNA expression levels of genes associated with Mg^{2+} homeostasis in total kidney lysate of mice on a Mg^{2+}-deficient diet (0.003% w/w), or an enriched Mg^{2+} diet (0.48% w/w). Expression levels are corrected for GAPDH and presented as a relative percentage of expression in mice put on the high Mg^{2+} diet. The mRNA levels of the following magnesiotropic genes were determined; the Mg^{2+} channels TRPM6 and TRPM7, the voltage-gated K^+ channel Kv1.1, the epidermal growth factor (EGF) and its receptor (EGFR), the inwardly rectifying K^+ channel Kir4.1, the hepatocyte nuclear factor 1B (HNF1B), the FXYD domain containing ion transport regulator 2, splice variant a (FXYD2a); the FXYD domain containing ion transport regulator 2, splice variant b (FXYD2b), claudin-16 (CLDN16) and claudin-19 (CLDN19). Values are presented as means ± SEM (n = 10). [a] $P < 0.05$ compared with the high Mg^{2+} diet.

Interestingly, dietary Mg^{2+} restriction markedly upregulated the HNF1B level. However, differences in dietary Mg^{2+} content did not significantly affect the renal abundance of TRPM7, Kv1.1, EGF, EGFR, Kir4.1, Fxyd2a, Fxyd2b, CLDN16 or CLDN19. Next, HNF1B protein levels of kidneys of the various dietary regimens were determined. In addition,

low dietary Mg^{2+} significantly increased TRPM6 mRNA level in colon, compared with the high Mg^{2+} diet (**Figure 1**).

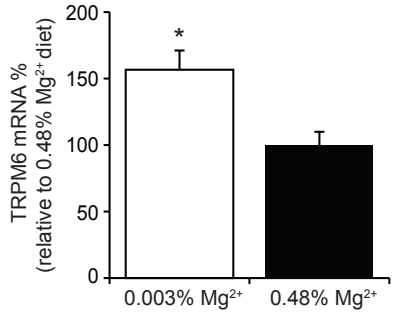

Figure 1. Effect of dietary Mg^{2+} content on the mRNA level of TRPM6 in colon. An real-time qPCR was used to determine the mRNA expression level of the epithelial Mg^{2+} channel TRPM6 in colon of mice on a Mg^{2+}-deficient diet (0.003% w/w, white bar), or an enriched Mg^{2+} diet (0.48% w/w, black bar). Expression level is corrected for GAPDH and presented as relative percentage of expression in mice put on the high Mg^{2+} diet (0.48% w/w). Values are presented as means ± SEM (n = 10). [a] $P < 0.05$ compared with the high Mg^{2+} diet.

Figure 2 depicts a representative immunoblot to detect HNF1B. The Mg^{2+}-deficient diet resulted in a markedly increased expression level of this protein (171 ± 19 and 100 ± 8% for low versus high Mg^{2+} diet, respectively, $P < 0.05$).

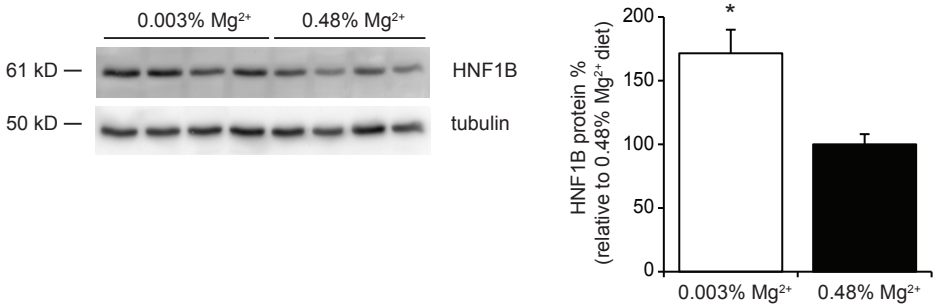

Figure 2. Effect of the dietary Mg^{2+} content on the protein level of HNF1B in kidney. The effect of dietary Mg^{2+} restriction (0.003% Mg^{2+}) on the protein expression level of the HNF1B, presented as the ratio of the expression level on the enriched Mg^{2+} diet (0.48% w/w). The left side of the figure depicts the immunoblot for HNF1B, with the molecular masses (in kD) indicated and the right side of the figure depicts the protein expression level as a percentage of the high Mg^{2+} diet. The white bar indicates the Mg^{2+}-deficient diet and the black bar the Mg^{2+}-enriched diet. Values are presented as means ± SEM (n = 4), the experiment is performed in duplicate. * $P < 0.05$ compared with the high Mg^{2+} diet.

Effect of dietary Mg^{2+} restriction on the expression levels of PV and NCC

The mRNA expression level of PV was considerably increased (701 ± 34 and 100 ± 7% for low versus high Mg^{2+} diet, respectively, $P < 0.05$) (**Figure 3A**), whereas NCC was not significantly altered by the dietary Mg^{2+} regimen (105 ± 4 and 100 ± 5% for low versus high Mg^{2+} diet, respectively, $P > 0.05$) (**Figure 3B**). Subsequently, immunohistochemical staining

was performed to determine the expression of PV and NCC at the protein level.

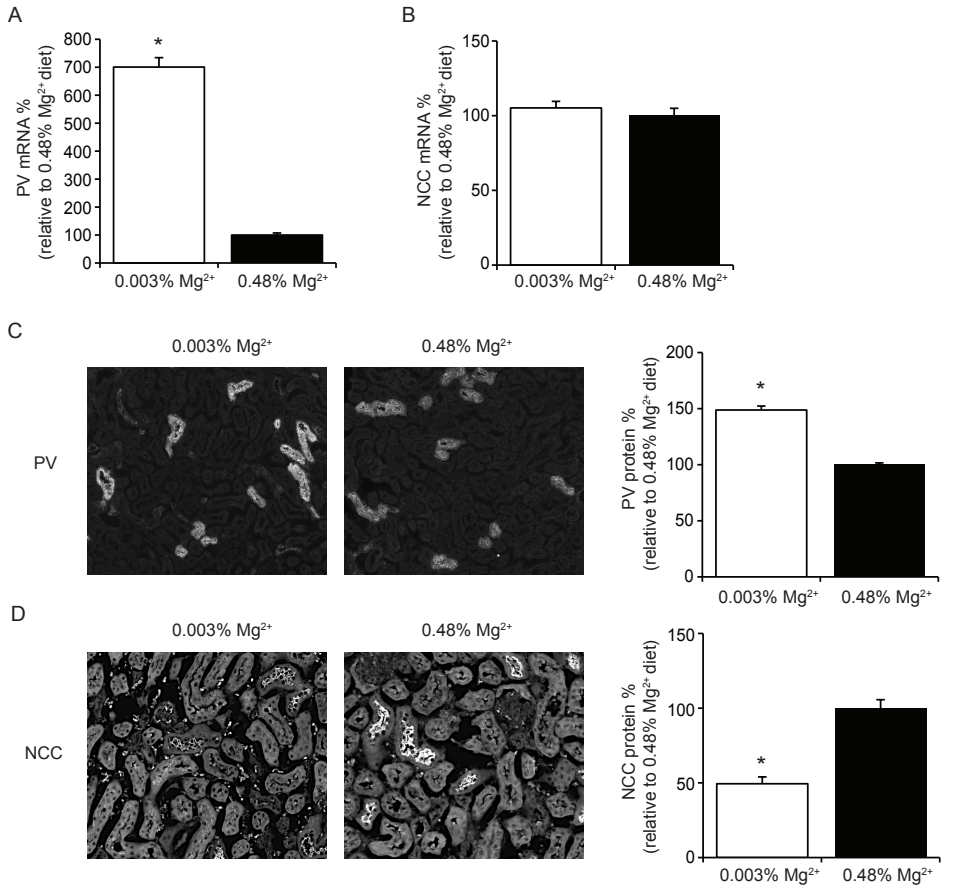

Figure 3. Effect of dietary Mg^{2+} content on PV and NCC mRNA and protein levels in kidney. An real-time qPCR was used to determine the mRNA expression levels of PV (**A**) and the thiazide-dependent NCC (**B**) in kidneys of mice on a Mg^{2+}-deficient diet (0.003% w/w), or an enriched Mg^{2+} diet (0.48% w/w). Expression levels are corrected for GAPDH and presented as relative percentage of expression in mice put on the high Mg^{2+} diet. Figures **C** and **D** show on the left side representative pictures of immunohistochemical staining for PV (**C**) and NCC (**D**) and on the right side the semi-quantification of these protein levels, relative to the high Mg^{2+} diet. The white bar indicates the Mg^{2+}-deficient diet and the black bar the Mg^{2+}-enriched diet. Values are presented as means ± SEM (*n* = 10 for real-time qPCR and *n* = 8 for IHC), experiment was performed in duplicate. * $P < 0.05$ compared with the high Mg^{2+} diet.

The Mg^{2+}-deficient diet resulted in a markedly increased expression level of PV (149 ± 4 and 100 ± 2% for low versus high Mg^{2+} diet, respectively, $P < 0.05$) (**Figure 3C**), while the NCC protein levels were significantly downregulated (49 ± 5 and 100 ± 6% for low versus high Mg^{2+} diet, respectively, $P < 0.05$) (**Figure 3D**), compared with the expression level in the mouse group fed the high Mg^{2+} diet.

Effect of dietary Mg^{2+} deficiency on the expression levels of Ca^{2+} transporters, NHE3 and ENaC

To investigate the underlying mechanism of the hypocalcemia and sharp decline of urinary Ca^{2+} excretion of mice fed a low Mg^{2+} diet, the renal expression levels of TRPV5, calbindin-D_{28K}, the Na^+, H^+ exchanger 3 (NHE3) and the epithelial Na^+ channel (ENaC) were determined. **Figure 4** shows that dietary Mg^{2+} restriction results in significantly lower mRNA levels of TRPV5 and calbindin-D_{28K}, compared with the kidneys of mice on the Mg^{2+}-enriched diet (45 ± 1 and 100 ± 7% for TRPV5 and 40 ± 2 and 100 ± 8% for calbindin-D_{28K} for low versus high Mg^{2+} diet, respectively, $P < 0.05$).

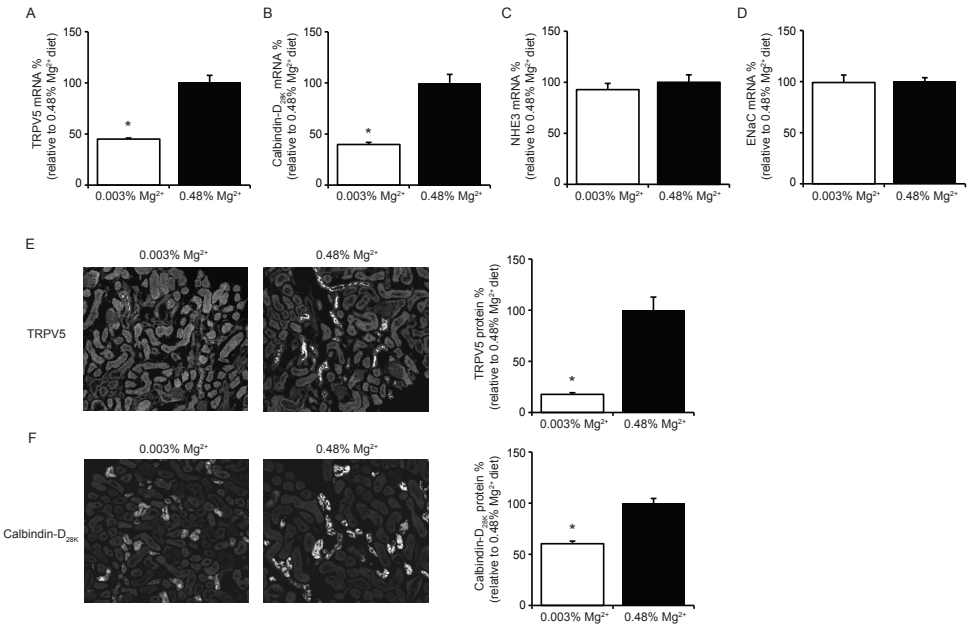

Figure 4. Effect of dietary Mg^{2+} content on calciotropic mRNA and protein levels in kidney. An real-time qPCR was used to determine the mRNA expression levels of the epithelial Ca^{2+} channel TRPV5 (**A**) the cytosolic Ca^{2+}-binding protein calbindin-D_{28K} (**B**) the Na^+, H^+ exchanger 3 (NHE3) (**C**) and the epithelial Na^+ channel (ENaC) (**D**) in kidneys of mice fed a Mg^{2+}-deficient diet (0.003% w/w), or an enriched Mg^{2+} diet (0.48% w/w). Expression levels are corrected for GAPDH and presented as a relative percentage of expression in mice on the high Mg^{2+} diet. TRPV5 and calbindin-D_{28K} protein abundance was determined by computerized analysis of immunohistochemical images and presented as a relative percentage of the abundance in the high Mg^{2+} diet (**E and F**). The white bar indicates the Mg^{2+}-deficient diet and the black bar the Mg^{2+}-enriched diet. Values are presented as means ± SEM (n = 10 for real-time qPCR and n = 8 for IHC). * $P < 0.05$ compared with the high Mg^{2+} diet.

In contrast, the mRNA levels of NHE3 and ENaC were not significantly affected by the dietary Mg^{2+} content (93 ± 6 and 100 ± 7% for NHE3 and 99 ± 7 and 100 ± 4% for ENaC for low versus high Mg^{2+} diet, respectively, $P > 0.05$). Next, the renal protein levels were determined for these calciotropic molecules. Semi-quantitative immunohistochemical

analysis showed a strikingly low TRPV5 expression level (18 ± 2 and 100 ± 13% for low versus high Mg^{2+} diet, respectively, $P < 0.05$) (**Figure 4E**) and calbindin-D_{28K} (60 ± 3 and 100 ± 5% for low versus high Mg^{2+} diet, respectively, $p < 0.05$) (**Figure 4F**) in kidneys of mice fed a low Mg^{2+} diet.

Discussion

The present study demonstrated that dietary Mg^{2+} restriction results in hypomagnesemia accompanied by hypocalcemia. Moreover, the serum Na^+:K^+ ratio was slightly but significantly increased under dietary Mg^{2+} restriction. As renal adaptive response, the urinary excretion of Mg^{2+} as well as Ca^{2+} was markedly reduced in these mice. Interestingly, the urinary level of P_i was regulated in opposite direction compared with Ca^{2+} and also serum FGF23 was increased in the Mg^{2+}-restricted mice. Analysis of expression levels revealed that the dietary Mg^{2+} content regulated TRPM6 and HNF1B abundance, while the other magnesiotropic transporters were not affected. In addition, the expression of TRPV5 and calbindin-D_{28K} was markedly lower in the Mg^{2+}-restricted diet compared with the enriched Mg^{2+} diet. Finally, renal PV was upregulated and NCC downregulated as a consequence of the low Mg^{2+} diet. These results clearly indicate profound effects of Mg^{2+} restriction on gene expression levels in the distal part of the nephron. The hypomagnesemia and hypomagnesuria confirmed that the 2-week dietary Mg^{2+} restriction was effective. Furthermore, we revealed that the mRNA level of TRPM6 in kidney as well as in colon was upregulated during Mg^{2+} restriction. This suggests that a diminished Mg^{2+} excretion in kidney is accompanied by an enhanced absorption of Mg^{2+} in the large intestine. Whether the direct trigger for TRPM6 upregulation during a hypomagnesemic state is intrinsic (sensing of Mg^{2+} concentration by TRPM6 itself) or external (like hormonal regulation) remains elusive. Interestingly, the other magnesiotropic genes tested (TRPM7, Kv1.1, EGF, EGFR, Kir4.1, FXYD2a, FXYD2b, CLDN16 and CLDN19) were not affected by the amount of dietary Mg^{2+} intake. Although, we cannot exclude changes on protein level of these players, these results emphasize the physiologic importance of TRPM6, as a gatekeeper in Mg^{2+} balance. In our previous dietary studies, we did not observe a reduced serum Ca^{2+} level nor an increased level of TRPM6 in colon during Mg^{2+} restriction (22). This difference can be due to the extended dietary period or to the more severe Mg^{2+} restriction in the current study. In addition, our data on TRPM6 regulation in kidney and colon are in line with the study of Rondon *et al.* (31).

HNF1B plays an essential role during renal embryonic development. Besides, it has been shown to be particularly important for the maintenance of Mg^{2+} and Ca^{2+} balance once maturated, since mutations in HNF1B caused hypomagnesemia and hypocalciuria (13). The upregulation of HNF1B during dietary Mg^{2+} restriction is, therefore, of special interest. HNF1B regulates the transcription of FXYD2 (32), which encodes the γ-subunit of the Na^+, K^+-ATPase. This latter transmembrane protein has been shown to be important for maintainance of Na^+, K^+-ATPase capacity (33). Probably, impaired capacity to set the basolateral membrane potential, which ultimately hinders reabsorption of Mg^{2+} via TRPM6, seems to be the mechanism by which decreased expression of the γ-subunit resulted in hypomagnesemia (32, 34). However, the expression level of both FXYD2 transcription variants remained constant during the Mg^{2+} restriction. This suggests that

HNF1B needs a co-factor to promote transcription of the γa-subunit or that HNF1B is responsible for maintaining the Mg^{2+} balance by other means.

The effect of dietary Mg^{2+} restriction is not limited to Mg^{2+} homeostasis since it seriously affected the renal handling of Ca^{2+} as well as of P_i. P_i is required for cellular functions and skeletal mineralization (35), and its homeostasis is closely related to that of Ca^{2+} (36). The combination of a trend for increased serum P_i, significantly increased serum FGF23 and increased urinary P_i excretion, suggest profound effects of dietary Mg^{2+} restriction on phosphate balance. Likely, the increased FGF23 level decreases P_i reabsorption in the PT (37). Borderline increased serum P_i is the stimulus of the elevated FGF23 level in our mice (38); however, the underlying mechanism for changes in serum P_i, remains elusive. The cascade observed in patients of persistent hypomagnesemia causing hypoparathyroidism and consequently hypocalcemia in combination with hyperphosphatemia (39, 40), is in line with our data.

Hypomagnesemia in patients is frequently accompanied by hypocalciuria when the NCC activity is also diminished, i.e. Gitelman syndrome (GS) or chronic thiazide use (41). Increased passive Ca^{2+} reabsorption in the PT, accompanied by an increased level of NHE3, responsible for Na^{+} and subsequent paracellular Ca^{2+} reabsorption (42), accounts for the underlying mechanism (43). This is implicated via extracellular volume contraction and activation of the renin-angiotensin-aldosterone system (RAAS) (43). In our study, the mRNA expression level of NHE3 was not affected by dietary Mg^{2+} intake, which implies that Ca^{2+} reabsorption in PT was not increased. Since, angiotensin II is a direct stimulator of ENaC activity (44), our observation that ENaC mRNA level was not regulated further supports that RAAS signaling is not activated. However, this finding also implicates that the causative factor for the Na:K imbalances, remains elusive.

The significant downregulation of TRPV5 and calbindin-$D_{28K,}$ for which localization is restricted to DCT and connecting tubules (CNT), indicates that active Ca^{2+} reabsorption in these tubule segments is decreased. This could be the consequence of increased reabsorption of Ca^{2+} in TAL. Here, Ca^{2+} and Mg^{2+} transport compete for the same paracellular route. Given the hypomagnesemia, a more favourable situation is possibly created to reabsorb Ca^{2+} in TAL (45). Van Abel *et al*. showed that the TRPV5 and calbindin-D_{28K} expression levels are dependent on PTH stimulation (46). The reduced TRPV5 and calbindin-D_{28K} levels as measured in the present study indicate a defect in the regulation of these proteins by PTH. Subsequently, the co-existence of hypocalciuria and a decreased serum Ca^{2+} level in the low Mg^{2+} diet group suggests a disturbed bone metabolism. This is possibly induced by end-organ resistance to PTH also known as pseudohypoparathyroidism (47). The latter, mediated by the continuously high levels of PTH, induced by the Mg^{2+}-deficient state (48). Disturbances in enzyme activity might form the underlying mechanism for the secondary effects on Ca^{2+} balance. Probably, defects in PTH secretion only occur after more prolonged periods of Mg^{2+} deficiency (49), like the experimental period of 2 weeks used in this study.

To obtain more insight into the function of DCT during hypomagnesemia, the expression of other DCT-specific markers was investigated including NCC and PV. PV is known as a Ca^{2+}-binding protein with versatile functions in cellular processes (50) and was predominantly studied for its role in neurons and muscle fibres. In kidney, PV is exclusively expressed in the early DCT (DCT1), where it co-localizes with TRPM6 and NCC (9, 51). To our knowledge, this is the first study showing a markedly increased mRNA and protein

expression level of PV during dietary Mg^{2+} deficiency. Analysis of the renal phenotype of PV knockout mice showed polyuria and some aberrations in electrolyte homeostasis, however, not for Mg^{2+} (51). Interestingly, Belge *et al*. (51) observed reduced expression levels of NCC in the PV knockout mice, possibly mediated by diminished capacity to buffer intracellular Ca^{2+}. NCC forms the apical entry mechanism for Na^{+} and Cl^{-} in DCT. Mutations in the NCC gene cause GS, a salt-wasting renal disorder characterized by hypokalemia, metabolic alkalosis, hypomagnesemia and hypocalciuria (52). Besides, NCC-deficient mice have a similar phenotype, including hypomagnesemia (53). This suggests that NCC is important for the maintenance of the Mg^{2+} balance. Interestingly, our data displayed that a Mg^{2+}-deficient state results in decreased protein expression levels of NCC. Assembling these findings concerning PV and NCC, we hypothesize that hypomagnesemia results in an increased $[Ca^{2+}]_i$ in DCT cells (resembling Ca^{2+} mobilization in heart or smooth muscle cells (49)) which downregulates the expression of NCC. Further, the upregulation of PV aimed to counteract the effect of $[Ca^{2+}]_i$ on NCC. The increased $[Ca^{2+}]_i$ might be mediated by a release from ER or mitochondria (54). However, a role for $[Mg^{2+}]_i$ itself in the regulation of PV and/or NCC could not be excluded.

Figure 5 presents the main results of the present study and a schematic model of adaptations in the nephron in response to dietary Mg^{2+} restriction. In short, this study revealed that HNF1B and TRPM6 act as unique regulators of Mg^{2+} homeostasis. In addition, we observed more configurations during the hypomagnesemic state in DCT, namely changed PV and NCC expression levels. The detailed regulation of these proteins and their possible interaction via $[Ca^{2+}]_i$ remains to be established. Moreover, our results once again pinpoint the close interaction of the Mg^{2+} and Ca^{2+} balance. Downregulation of TRPV5 and calbindin-D_{28K} combined with the decreased serum Ca^{2+} level, increased serum FGF23 level and increased urinary P_i excretion in Mg^{2+}-restricted mice suggests disturbances in control by PTH. Further experiments are needed to unravel the detailed triggers inducing the adaptations in DCT and the role of PTH during hypomagnesemia.

Acknowledgements. The authors are grateful to our colleagues Titia Woudenberg-Vrenken, and AnneMiete van der Kemp for technical assistance and helpful suggestions. This research was financially supported by the Dutch Organization for Scientific Research (VENI ZonMw 916.12.046), the Dutch Kidney foundation (C08.2252) and an European Young Investigator award from the European Science Foundation.

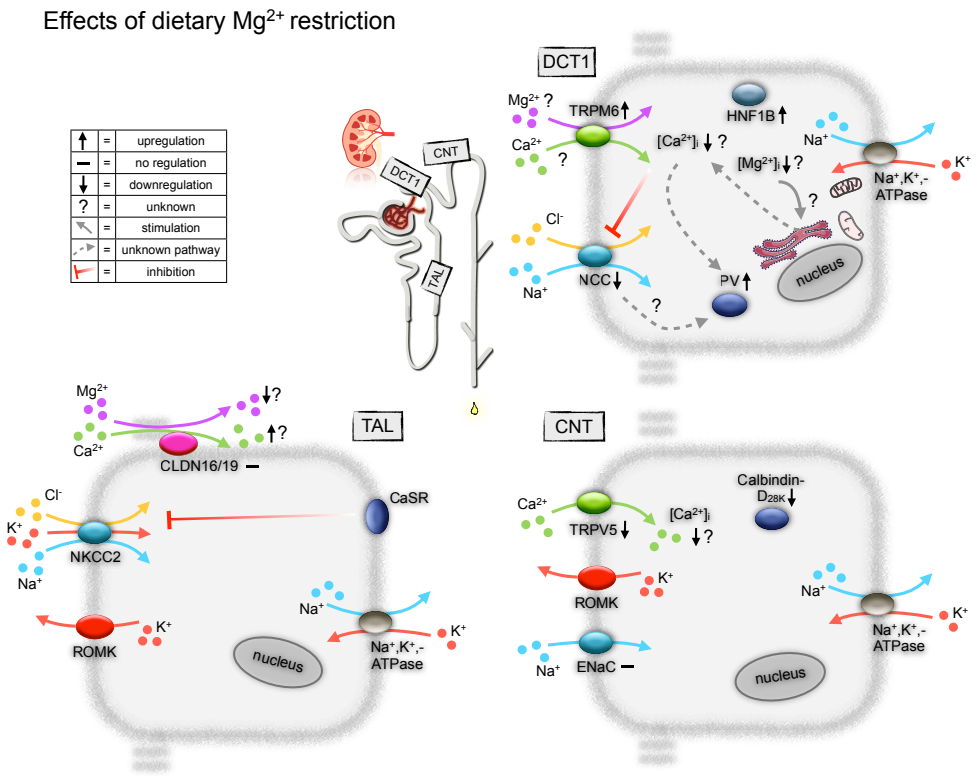

Figure 5. Schematic overview of the effects of dietary Mg^{2+} restriction in TAL, DCT1 and CNT. In the middle of this figure, the functional unit of the kidney, the nephron is shown. The different segments affected by dietary Mg^{2+} restriction are indicated in this nephron and enlarged cells of these respective segments surround the nephron. In TAL, passive reabsorption of Ca^{2+} is increased due to lack of competition of Mg^{2+} ions. CLDN16 and CLDN19 mRNA expression levels were not affected. In DCT1, TRPM6 mRNA and HNF1B mRNA and protein expression levels are increased. The detailed physiological relevance of HNF1B concerning Mg^{2+} balance is still unknown. HNF1B probably plays an important role in the stabilization of the Na^{+}, K^{+}-ATPase in the basolateral membrane. In addition, NCC is downregulated and PV is upregulated. We hypothesize that this is to counteract increased $[Ca^{2+}]_i$, which in turn is the consequence of release of Ca^{2+} from the ER or mitochondria, triggered by a decreased $[Mg^{2+}]_i$ level. Alternatively, the presumed lower $[Mg^{2+}]_i$ level, resulting from the dietary Mg^{2+} restriction, possibly exerts more direct effects on these proteins. More distal in the CNT, TRPV5 and calbindin-D_{28K} are downregulated; however, the underlying mechanism still needs to be unraveled. In addition, the ENaC mRNA level is not affected by the dietary Mg^{2+} content, so the factor causing Na:K imbalances remains unknown.

References

1. Dai, L.J., Ritchie, G., Kerstan, D., et al. Magnesium transport in the renal distal convoluted tubule. *Physiol Rev* 81:51-84. 2001.
2. Quamme, G.A. Renal handling of magnesium: drug and hormone interactions. *Magnesium* 5:248-272. 1986.
3. Chernow, B., Bamberger, S., Stoiko, M., et al. Hypomagnesemia in patients in postoperative intensive care. *Chest* 95:391-397. 1989.
4. Ryzen, E. Magnesium homeostasis in critically ill patients. *Magnesium* 8:201-212. 1989.
5. Topf, J.M., and Murray, P.T. Hypomagnesemia and hypermagnesemia. *Rev Endocr Metab Disord* 4:195-206. 2003.
6. Elin, R.J. Magnesium: the fifth but forgotten electrolyte. *Am J Clin Pathol* 102:616-622. 1994.
7. Le Grimellec, C. Micropuncture study along the proximal convoluted tubule. Electrolyte reabsorption in first convolutions. *Pflugers Arch* 354:133-150. 1975.
8. Greger, R. Ion transport mechanisms in thick ascending limb of Henle's loop of mammalian nephron. *Physiol Rev* 65:760-797. 1985.
9. Voets, T., Nilius, B., Hoefs, S., et al. TRPM6 forms the Mg2+ influx channel involved in intestinal and renal Mg2+ absorption. *J Biol Chem* 279:19-25. 2004.
10. Schlingmann, K.P., Weber, S., Peters, M., et al. Hypomagnesemia with secondary hypocalcemia is caused by mutations in TRPM6, a new member of the TRPM gene family. *Nat Genet* 31:166-170. 2002.
11. Walder, R.Y., Landau, D., Meyer, P., et al. Mutation of TRPM6 causes familial hypomagnesemia with secondary hypocalcemia. *Nat Genet* 31:171-174. 2002.
12. Meij, I.C., Koenderink, J.B., van Bokhoven, H., et al. Dominant isolated renal magnesium loss is caused by misrouting of the Na(+),K(+)-ATPase gamma-subunit. *Nat Genet* 26:265-266. 2000.
13. Adalat, S., Woolf, A.S., Johnstone, K.A., et al. HNF1B mutations associate with hypomagnesemia and renal magnesium wasting. *J Am Soc Nephrol* 20:1123-1131. 2009.
14. Scholl, U.I., Choi, M., Liu, T., et al. Seizures, sensorineural deafness, ataxia, mental retardation, and electrolyte imbalance (SeSAME syndrome) caused by mutations in KCNJ10. *Proc Natl Acad Sci U S A* 106:5842-5847. 2009.
15. Bockenhauer, D., Feather, S., Stanescu, H.C., et al. Epilepsy, ataxia, sensorineural deafness, tubulopathy, and KCNJ10 mutations. *N Engl J Med* 360:1960-1970. 2009.
16. Ito, M., Inanobe, A., Horio, Y., et al. Immunolocalization of an inwardly rectifying K+ channel, K(AB)-2 (Kir4.1), in the basolateral membrane of renal distal tubular epithelia. *FEBS Lett* 388:11-15. 1996.
17. Groenestege, W.M., Thebault, S., van der Wijst, J., et al. Impaired basolateral sorting of pro-EGF causes isolated recessive renal hypomagnesemia. *J Clin Invest* 117:2260-2267. 2007.
18. Glaudemans, B., van der Wijst, J., Scola, R.H., et al. A missense mutation in the Kv1.1 voltage-gated potassium channel-encoding gene KCNA1 is linked to human autosomal dominant hypomagnesemia. *J Clin Invest* 119:936-942. 2009.
19. Simon, D.B., Lu, Y., Choate, K.A., et al. Paracellin-1, a renal tight junction protein required for paracellular Mg2+ resorption. *Science* 285:103-106. 1999.
20. Konrad, M., Schaller, A., Seelow, D., et al. Mutations in the tight-junction gene claudin 19 (CLDN19) are associated with renal magnesium wasting, renal failure, and severe ocular involvement. *Am J Hum Genet* 79:949-957. 2006.
21. Dunn, M.J., and Walser, M. Magnesium depletion in normal man. *Metabolism* 15:884-895. 1966.
22. Groenestege, W.M., Hoenderop, J.G., van den Heuvel, L., et al. The epithelial Mg2+ channel transient receptor potential

melastatin 6 is regulated by dietary Mg2+ content and estrogens. *J Am Soc Nephrol* 17:1035-1043. 2006.
23. Rude, R.K., Singer, F.R., and Gruber, H.E. Skeletal and hormonal effects of magnesium deficiency. *J Am Coll Nutr* 28:131-141. 2009.
24. Anast, C.S., Mohs, J.M., Kaplan, S.L., et al. Evidence for parathyroid failure in magnesium deficiency. *Science* 177:606-608. 1972.
25. Hoenderop, J.G., Nilius, B., and Bindels, R.J. Calcium absorption across epithelia. *Physiol Rev* 85:373-422. 2005.
26. Brown, E.M., Gamba, G., Riccardi, D., et al. Cloning and characterization of an extracellular Ca(2+)-sensing receptor from bovine parathyroid. *Nature* 366:575-580. 1993.
27. Hoenderop, J.G., Muller, D., Van Der Kemp, A.W., et al. Calcitriol controls the epithelial calcium channel in kidney. *J Am Soc Nephrol* 12:1342-1349. 2001.
28. Hoenderop, J.G., van Leeuwen, J.P., van der Eerden, B.C., et al. Renal Ca2+ wasting, hyperabsorption, and reduced bone thickness in mice lacking TRPV5. *J Clin Invest* 112:1906-1914. 2003.
29. Hoenderop, J.G., Hartog, A., Stuiver, M., et al. Localization of the epithelial Ca(2+) channel in rabbit kidney and intestine. *J Am Soc Nephrol* 11:1171-1178. 2000.
30. Nijenhuis, T., Hoenderop, J.G., Loffing, J., et al. Thiazide-induced hypocalciuria is accompanied by a decreased expression of Ca2+ transport proteins in kidney. *Kidney Int* 64:555-564. 2003.
31. Rondon, L.J., Groenestege, W.M., Rayssiguier, Y., et al. Relationship between low magnesium status and TRPM6 expression in the kidney and large intestine. *Am J Physiol Regul Integr Comp Physiol* 294:R2001-2007. 2008.
32. Ferre, S., Veenstra, G.J., Bouwmeester, R., et al. HNF-1B specifically regulates the transcription of the gammaa-subunit of the Na+/K+-ATPase. *Biochem Biophys Res Commun* 404:284-290.
33. Mishra, N.K., Peleg, Y., Cirri, E., et al. FXYD proteins stabilize Na,K-ATPase: amplification of specific phosphatidylserine-protein interactions. *J Biol Chem* 286:9699-9712.
34. Sha, Q., Pearson, W., Burcea, L.C., et al. Human FXYD2 G41R mutation responsible for renal hypomagnesemia behaves as an inward-rectifying cation channel. *Am J Physiol Renal Physiol* 295:F91-99. 2008.
35. Takeda, E., Taketani, Y., Sawada, N., et al. The regulation and function of phosphate in the human body. *Biofactors* 21:345-355. 2004.
36. Renkema, K.Y., Alexander, R.T., Bindels, R.J., et al. Calcium and phosphate homeostasis: concerted interplay of new regulators. *Ann Med* 40:82-91. 2008.
37. Segawa, H., Onitsuka, A., Furutani, J., et al. Npt2a and Npt2c in mice play distinct and synergistic roles in inorganic phosphate metabolism and skeletal development. *Am J Physiol Renal Physiol* 297:F671-678. 2009.
38. Perwad, F., Azam, N., Zhang, M.Y., et al. Dietary and serum phosphorus regulate fibroblast growth factor 23 expression and 1,25-dihydroxyvitamin D metabolism in mice. *Endocrinology* 146:5358-5364. 2005.
39. Hermans, C., Lefebvre, C., Devogelaer, J.P., et al. Hypocalcaemia and chronic alcohol intoxication: transient hypoparathyroidism secondary to magnesium deficiency. *Clin Rheumatol* 15:193-196. 1996.
40. Monteleone, J.A., Lee, J.B., Tashjian, A.H., Jr., et al. Transient neonatal hypocalcemia, hypomagnesemia, and high serum parathyroid hormone with maternal hyperparathyroidism. *Ann Intern Med* 82:670-672. 1975.
41. Monroy, A., Plata, C., Hebert, S.C., et al. Characterization of the thiazide-sensitive Na(+)-Cl(-) cotransporter: a new model for ions and diuretics interaction. *Am J Physiol Renal Physiol* 279:F161-169. 2000.
42. Pan, W., Borovac, J., Spicer, Z., et al. The epithelial sodium/proton exchanger, NHE3, is necessary for renal and intestinal calcium (re)absorption. *Am J Physiol Renal Physiol* 302:F943-956. 2012.
43. Nijenhuis, T., Vallon, V., van der Kemp, A.W., et al. Enhanced passive Ca2+ reabsorption and reduced Mg2+ channel

abundance explains thiazide-induced hypocalciuria and hypomagnesemia. *J Clin Invest* 115:1651-1658. 2005.

44. Peti-Peterdi, J., Warnock, D.G., and Bell, P.D. Angiotensin II directly stimulates ENaC activity in the cortical collecting duct via AT(1) receptors. *J Am Soc Nephrol* 13:1131-1135. 2002.
45. Ikari, A., Hirai, N., Shiroma, M., et al. Association of paracellin-1 with ZO-1 augments the reabsorption of divalent cations in renal epithelial cells. *J Biol Chem* 279:54826-54832. 2004.
46. van Abel, M., Hoenderop, J.G., van der Kemp, A.W., et al. Coordinated control of renal Ca(2+) transport proteins by parathyroid hormone. *Kidney Int* 68:1708-1721. 2005.
47. Butterworth, C.E., Jr., Hamilton, L.C., and Zheutlin, N. Pseudohypoparathyroidism. *Am J Med* 21:644-648. 1956.
48. Shoback, D., Thatcher, J., Leombruno, R., et al. Effects of extracellular Ca++ and Mg++ on cytosolic Ca++ and PTH release in dispersed bovine parathyroid cells. *Endocrinology* 113:424-426. 1983.
49. Rude, R.K. Magnesium deficiency: a cause of heterogeneous disease in humans. *J Bone Miner Res* 13:749-758. 1998.
50. Ikura, M., and Ames, J.B. Genetic polymorphism and protein conformational plasticity in the calmodulin superfamily: two ways to promote multifunctionality. *Proc Natl Acad Sci U S A* 103:1159-1164. 2006.
51. Belge, H., Gailly, P., Schwaller, B., et al. Renal expression of parvalbumin is critical for NaCl handling and response to diuretics. *Proc Natl Acad Sci U S A* 104:14849-14854. 2007.
52. Simon, D.B., Nelson-Williams, C., Bia, M.J., et al. Gitelman's variant of Bartter's syndrome, inherited hypokalaemic alkalosis, is caused by mutations in the thiazide-sensitive Na-Cl cotransporter. *Nat Genet* 12:24-30. 1996.
53. Schultheis, P.J., Lorenz, J.N., Meneton, P., et al. Phenotype resembling Gitelman's syndrome in mice lacking the apical Na+-Cl- cotransporter of the distal convoluted tubule. *J Biol Chem* 273:29150-29155. 1998.
54. Swaminathan, R. Magnesium metabolism and its disorders. *Clin Biochem Rev* 24:47-66. 2003.

Chapter 5

Sorting and cleavage of pro-EGF in MDCK cells

Annelies A. van Angelen, Joost G.J. Hoenderop and René J.M. Bindels

Department of Physiology, Radboud University Medical Center,
Nijmegen, The Netherlands.

Manuscript in preparation

Abstract

Background. Magnesium (Mg^{2+}) is essential for many functions in our body and the plasma Mg^{2+} concentration is tightly regulated. The identification of a mutation in the epidermal growth factor (*EGF*) gene in two sisters with isolated autosomal recessive renal hypomagnesemia (IRH), linked this hormone to Mg^{2+} homeostasis. This homozygous P1070L mutation in precursor EGF (pro-EGF) specifically prevents secretion of pro-EGF to the basolateral side in polarized Madin-Darby canine kidney (MDCK) cells. As a consequence of this mutation, the renal EGF receptor (EGFR) is not adequately activated, resulting in impaired stimulation of the epithelial Mg^{2+} channel TRPM6 and thereby causing renal Mg^{2+} loss. The aim of the present study was to investigate the underlying molecular defect in more detail.

Methods. Using the inducible Tetracycline-Regulated Expression (T-REx) system we were able to study the sorting and processing of pro-EGF and the mutant in polarized MDCK cell lines. The membrane fraction was studied using cell surface biotinylation and immunoblotting techniques. The different cleavage products of pro-EGF in the secreted fraction were separated into two fractions, one containing the 3-50 kD (pro)-EGF products and a fraction containing pro-EGF proteins larger than 50 kD, concentrated and analysed by enzyme-linked immunosorbent assay (ELISA) and immunoblotting. In addition, subcellular localization of wild-type pro-EGF-GFP (pro-EGF-WT) and pro-EGF-P1070L-GFP (pro-EGF-P1070L) was determined by immunocytochemistry and confocal microscopy.

Results. Immunocytochemical detection of the extracellular EGF-epitope revealed that pro-EGF-WT and pro-EGF-P1070L are both predominantly present on the apical membrane. Moreover, immunoblotting and ELISA experiments of the secreted (pro)EGF fractions showed that this protein is mainly secreted to the apical side of the cell and processed into mature EGF. Impaired secretion of the mutant, which affected both the apical and basolateral compartment, was demonstrated. In addition, our data revealed that the abundance of EGF in the apical 3-50 kD fraction was three-four times higher in MDCKI cells and similar in MDCKII cells, to the amount of (pro-)EGF in the > 50 kD fraction. In contrast, at the basolateral side the EGF abundance was two-six times lower in the 3-50 kD fraction when compared with the > 50 kD fraction. Finally, addition of the metalloprotease inhibitor phenanthroline did not affect the secretion of pro-EGF.

Conclusions. Pro-EGF-WT and pro-EGF-P1070L are principally sorted to the apical side of MDCK cells and secreted and processed into the apical medium. The P1070L mutation likely results in impaired secretion of pro-EGF and consequently inadequate stimulation of the EGFR. This results in a physiological defect at the basolateral side due to the lower amount of pro-EGF at this side, as a consequence of preferential sorting to the apical membrane.

Introduction

Magnesium (Mg^{2+}) plays a critical role in many biochemical and physiological processes, including DNA synthesis, neurotransmission, and hormone receptor binding (1). The plasma Mg^{2+} concentration is maintained within a narrow range by adapting the urinary Mg^{2+} excretion in response to altered absorption by the intestine (2). However, hypomagnesemia (plasma Mg^{2+} < 0.7 mmol/L) is a frequent problem, observed in ~10% of the general population and can affect up to 65% of intensive care patients (3). This is of special interest given the correlation between hypomagnesemia and common chronic diseases such as diabetes and cardiac disturbances (4, 5). Although hypomagnesemia is often asymptomatic, patients may suffer from neuromuscular, cardiovascular and metabolic disturbances like tremor, convolutions and cardiac arrhythmias (6).

One important aspect of Mg^{2+} homeostasis is the transcellular Mg^{2+} transport through the TRPM6 channel, which is predominantly expressed in the distal convoluted tubule (DCT) of the kidney and in the distal part of the intestine (7, 8). Recently, our group identified a homozygous mutation (P1070L) in the epidermal growth factor (*EGF*) gene, encoding precursor EGF (pro-EGF) in two sisters with isolated autosomal recessive renal hypomagnesemia (IRH) (9). Moreover, this study revealed that activation of the EGF receptor (EGFR), located at the basolateral membrane of DCT cells (10), by EGF is the essential upstream point towards TRPM6 activation (9). Follow-up experiments demonstrated that EGFR-mediated stimulation of TRPM6 is affected by redistribution of vesicular TRPM6 and its insertion into the apical plasma membrane (11). Other studies reported that patients develop hypomagnesemia when treated with an EGFR antagonist (cetuximab) (12-15). EGFR is a useful target in chemotherapy since this receptor is often upregulated in solid tumours, and EGFR participates in signaling cascades that are disturbed in cancer cells (16).

EGF is known for its growth-promoting effects on epithelial cells and it has been demonstrated to be an effective inhibitor of gastric acid and pepsin secretion (17). In the kidney, EGF also affects the glomerular filtration and it decreases the activity of the epithelial Na^{+} channel (ENaC) (18, 19). Renal EGF expression is localized to the apical side of the DCT and the thick ascending limb of Henle's loop (TAL) (9, 20). EGF is principally synthesized by the kidney (21), and secreted and maturated in large amounts in the urine (22, 23). Groenestege *et al*. showed that the P1070L mutation in pro-EGF specifically prevents secretion of this protein to the basolateral side in polarized MDCKI cells (9). As a consequence of this mutation, the renal EGFR is inadequately activated, resulting in impaired stimulation of TRPM6, and thereby causing renal Mg^{2+} loss. The aberrant secretion of pro-EGF may be the result of defective targeting of pro-EGF-P1070L to the basolateral membrane, or abnormal processing by proteases.

The *EGF* gene consists of 24 exons which encode the large type I membrane-associated pro-EGF protein of 1207 amino acid residues (24). The 190 kD pro-EGF is cleaved, releasing soluble pro-EGF of 170 kD, which is further processed into a 45-70 kD pro-EGF intermediate, to finally generate the 6 kD mature peptide hormone EGF (25, 26). Measurements of EGF in urine and other bodily fluids, using different approaches, confirmed the presence of these different forms of (pro-)EGF *in vivo* (23, 25, 27, 28).

The P1070L mutation is located in the cytoplasmic domain of pro-EGF. This carboxyl-tail has been shown to be important for specific distribution to the plasma membrane and

cleavage of the large precursor protein (29, 30). The proline affected by the mutation represents the second proline of the basolateral-sorting motif PXXP (with X being an arbitrary amino acid) (9, 31). This indicated that the P1070L mutation in the carboxyl-tail of pro-EGF might result in impaired sorting of the protein to the basolateral membrane. Alternatively, cleavage of the mutated protein at the basolateral side can cause impaired stimulation of EGFR in DCT cells. Supposedly, proteolytical release of pro-EGF ligand is critical for activation of EGFR via autocrine and/or juxtacrine signalling (32, 33). Processing of pro-EGF is likely mediated by a disintegrin and metalloprotease (ADAM) (34, 35), which also needs to be activated via cleavage. The ectodomain shedding of pro-EGF resulting in its release from the plasma membrane is probably executed by ADAM10, whereas ADAM17 is responsible for processing of other EGFR ligands (35, 36). The regulation of ADAM10 remains elusive; however, it might be that shedding can be stimulated by phorbol esters like phorbol myristate acetate (PMA), as reported for ADAM17 (34), and decreased by metalloprotease inhibitors (36).

The main objective of this study was to delineate the function of (pro-)EGF in the molecular regulation of the renal Mg^{2+} handling. For this purpose MDCK cells were stably transfected with wild-type pro-EGF and pro-EGF-P1070L tagged with green fluorescent protein (GFP) using the inducible T-REx system. The sorting and processing of pro-EGF and the mutant was analysed by detection of these proteins or cleavage products in different cellular compartments and in the surrounding culture medium, using different biochemical approaches.

Methods

Constructs

Full-length pro-EGF (pro-EGF-WT) and mutant (P1070L) pro-EGF both tagged with *GFP* expressed in vector plasmid CB7 (pCB7) (9) were cloned into the inducible expression plasmid (pcDNA4/TO/myc-HisA) (gift of Dr. Nijtmans), using the KpnI and AgeI restriction enzymes. Constructs were verified by sequence analysis. The regulatory plasmid (pcDNA6/TR) (gift of Dr. Nijtmans), which encodes the Tet repressor (TetR), complements the inducible T-REx system (Invitrogen, Breda, The Netherlands).

Cell culture

Human Embryonic Kidney 293 (HEK293) cells were seeded at a density of 3.0×10^6 cells/petri dish in Dulbecco's modified Eagle's medium (DMEM) (BioWhittaker, Verviers, Belgium) supplemented with 10% (v/v) fetal calf serum (FCS) (PAA, Linz, Austria), 2 mM L-glutamine, 0.1 mM non-essential amino acids (Invitrogen) and 10 ug/mL ciproxin at 37°C in a humidity-controlled incubator with 5% (v/v) CO_2 in air. The next day, the cells were transiently transfected with pro-EGF-WT-GFP or pro-EGF-P1070L-GFP in the pCB7 vector using polyethylenimine (PEI) (Brunschwig, Basel, Switzerland) with a DNA:PEI ratio of 1:6.

Madin-Darby canine kidney type I (MDCKI) and II (MDCKII) cells were seeded at a density of 1.5×10^5 cells/12-well in DMEM supplemented with 5% (v/v) FCS, 2 mM L-glutamine, 0.1 mM non-essential amino acids (Invitrogen) and 10 ug/mL ciproxin at 37°C in a humidity-controlled incubator with 5% (v/v) CO_2 in air. They were transiently transfected with pro-EGF-WT-GFP or pro-EGF-P1070L-GFP in the pCB7 vector using the

following transfection agents: *i*) Lipofectamine 2000 (Invitrogen) DNA:Lipofectamine ratio of 1:2; *ii*) PEI with a DNA:PEI ratio of 1:6; *ii*) Metafectene Pro (Biontex, Martinsried/Planegg, Germany) with a DNA:Metafectene Pro ratio of 1:3 and; *iv*) FuGENE HD (Roche, Penzberg, Germany) DNA: FuGENE HD ratio of 1:2.5. The percentage of positive cells for pro-EGF expression was determined by counting the "green" cells in a representative area of cells, using fluorescent microscopy.

For transient transfection of MDCKI cells using T-REx, cells were seeded on petri d ishes (2.0×10^6 cells/dish) or on 6-well plates (3.0×10^5 cells/well). The next day, these cells were transiently co-transfected with pcDNA6/TR and pro-EGF-WT-GFP, pro-EGF-P1070L-GFP or the empty expression vector, using the pcDNA6/TR plasmid and the inducible expression construct at a ratio of 6:1 (w:w) and FuGENE HD, DNA: FuGENE HD ratio of 1:2.5. These cells were used for biotinylation or detection of pro-EGF in the medium.

For the generation of stable expression of MDCKI and MDCKII cells, pro-EGF-WT-GFP or pro-EGF-P1070L-GFP in the pCB7 vector, pro-EGF-WT-GFP or pro-EGF-P1070L-GFP in the pcDNA4/TO/myc-HisA plasmid and pcDNA6/TR were transfected using the calcium-phosphate method as previously described (37). In short, 1.0×10^6 cells were plated in a petri dish. The next day, the cells were transfected using 25 μg of circular DNA, followed by a glycerol shock once small crystals were observed. First, transfection with the regulatory plasmid pcDNA6/TR was performed, using 5 μg/mL blasticidin (Invitrogen) as selection medium. Second, these cells were transfected with the inducible expression vector: pcDNA4/TO/myc-HisA containing pro-EGF-WT-GFP or pro-EGF-P1070L-GFP. 125 μg/mL Zeocin (Invitrogen) was added to the medium for selection of positive co-transfected inducible clones. 75 μg/mL hygromycin B (Invitrogen) was used to select for positive clones of cells transfected with pro-EGF-WT-GFP or pro-EGF-P1070L-GFP in the pCB7 vector. Within 14 days after transfection, individual colonies were selected (using cloning rings) and expanded.

For experiments on semi-permeable filters (Transwell®, 0.4 μm pore size, Corning Costar, Cambridge, MA, USA), using the stably transfected MDCK cells, these exponentially growing cells were trypsinized and seeded at a density of 5.0×10^5 cells/6-well and 1.5×10^5 cells/12-well. The 6-well filters were used for immunoblotting in combination with sampling of the medium and the 12-well filters for immunocytochemistry. After 3-5 days, depending on the transcellular resistance, the cells were induced with 100 ng/mL doxycycline (Sigma, St Louis, MO, USA) for 24 h. For experiments with non-polarized MDCKI cells, protein expression was induced the day after transfection. If applied, 10 μmol/L phenanthroline (Sigma) together with fresh doxycycline was added, to both the apical and basolateral compartment, 6 h after initial induction for the remaining 18 h.

Validation of the inducible T-REx system

Figure 1 shows a schematic model of the T-REx system as used for this study. In short, upon addition of doxycycline, the tetR homodimers were released from the Tet operator sequences in the promoter of the inducible expression vector, and production of pro-EGF-WT-GFP or pro-EGF-P1070L-GFP was induced.

We determined whether this system was useful to express pro-EGF-GFP. Therefore, PcDNA6/TR + pcDNA4/TO/myc-HisA containing pro-EGF-WT-GFP, pro-EGF-P1070L-GFP or empty or together with a positive control (pcDNA6/TO/Luciferase) were transiently co-

transfected at a ratio of 6:1 into MDCK cells using FuGENE HD, DNA: FuGENE HD ratio of 1:2.5 and the expression was tested using immunoblotting.

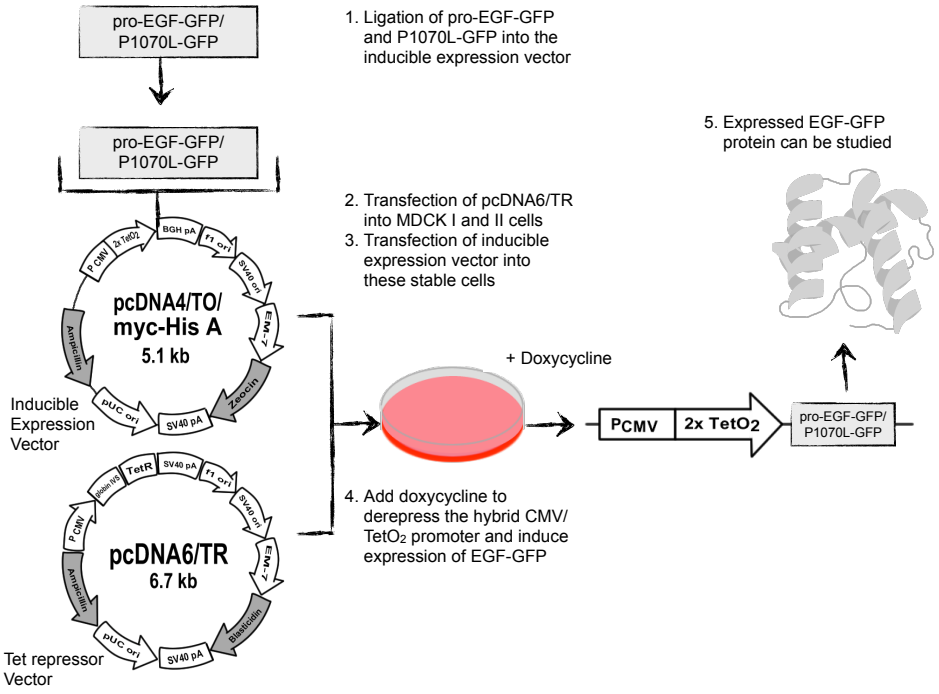

Figure 1. Tetracycline-Regulated Expression (T-REx) system. Schematic overview of the different steps necessary for creating inducible transcription of pro-EGF-WT-GFP and pro-EGF-P1070L-GFP, using the T-REx system. Pro-EGF-WT-GFP and pro-EGF-P1070L-GFP are cloned into the inducible expression vector and these constructs are co-transfected with the regulatory plasmid, pcDNA6/TR, into MDCKI or MDCKII cells. Subsequently, cells are incubated with doxycycline to remove repression of the promoter and induce transcription of pro-EGF-GFP, allowing us to perform experiments. Figure adapted from Life Technologies Corporation (48), used under permission (Copyright © 2013 Life Technologies Corporation).

For selection of stably-transfected MDCK cells, positive clones containing the TetR (pcDNA6/TR) were transiently co-transfected with pcDNA6/TO/Luciferase and induced with doxycycline (100 ng/mL) or not, and screened using the Luciferase Assay System (Promega, Madison, WI, USA). The clones expressing the highest expression of TetR after induction with doxycycline and the lowest basal expression were used as hosts for the inducible expression construct.

To determine the optimal amount of antibiotics needed for our system, “kill curves” were made (**Figure 2**). For this purpose, cells were seeded in 6-well plates, with a confluency of approximately 25%. The antibiotics (0-10 µg/mL blasticidin and 0-250 µg/mL Zeocin) were immediately added (i.e. before the cells were attached to the well), and replenished every 3-4 days. **Figure 2** showed that 5 µg/mL blasticidin and 125 µg/mL

Zeocin were the optimal concentrations for MDCK cell culture to kill the non-transfected cells.

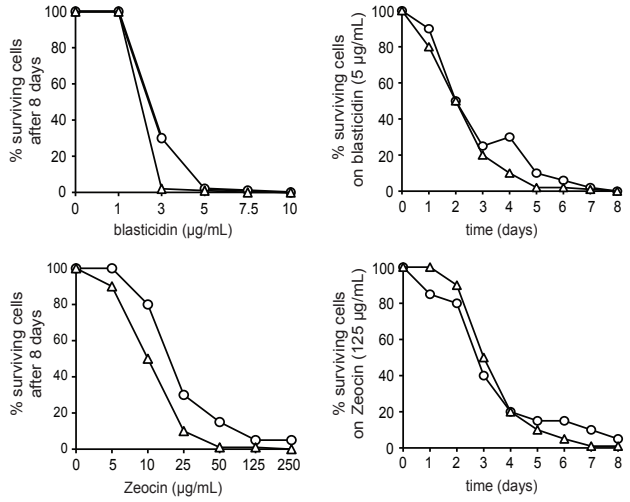

Figure 2. Validation of the T-REx inducible protein expression system. The concentration of the antibiotics blasticidin and Zeocin, necessary to select for MDCKI (triangles) and MDCKII (circles) clones expressing the transfected plasmids and for continued culture of these selected clones, was tested making use of "kill-curves" (n = 1).

Collection and concentration of conditioned culture media

24 h after induction the medium was replaced for FCS-free culture medium. When used, 1 µmol/L PMA (Sigma) was added to this medium. At 4, 16 or 48 h after the replacement, the FCS-free media were collected from the petri dishes or the apical and the basolateral compartments when cells were grown on filters, and proteinase inhibitors were added (1 mM PMSF, 1 µg/mL pepstatin A, and 10 ng/mL leupeptin). Subsequently, the proteins collected in the FCS-free culture media were separated and concentrated using the YM-50 and YM-3 Centriprep devices (Millipore Corporation, Bedford, MA, USA), consecutively. The proteins were detected using immunoblotting or ELISA.

Cell surface biotinylation

Two days after transfection of HEK293 cells or 24 h after induction of MDCK cells, surface proteins were biotinylated for 30' at 4°C using 0.5 mg/mL sulfo-NHS-LC-LC-biotin (Pierce, Rockford, IL, USA) as described previously (38). In short, cells were lysed in 150 mM NaCl, 5 mM EDTA, 50 mM Tris-HCl pH 7.5, 1% (v/v) NP-40 and protease inhibitors at 4°C, scraped from the filter or well and spun down for 10' at 14 000 × g. Finally, biotinylated proteins in the supernatant were precipitated using neutravidin-coupled beads (Pierce) and analysed by immunoblotting.

Immunoblotting

The collected proteins from the cell lysates or media were denatured by incubation in Laemmli/DTT buffer for 30' at 37°C. Each protein sample (60 µg) was separated using sodium dodecyl sulfate polyacrylamide gel electrophoresis (SDS–PAGE) and blotted to a PVDF-nitrocellulose membrane (Immobilon-P, Millipore). Blots were incubated for 16 h with either rabbit anti-GFP antibody (1:5000 dilution; Transduction Laboratories), rabbit

anti-EGF (1:1000 dilution; Ab-3, Calbiochem, Millipore), or mouse anti-β-actin (1:10 000 dilution; Sigma) antibody, in Tris-Buffered Saline Tween-20 (TBS-T) pH 7.6 supplemented with 1% w/v non-fat dried milk. Blots were incubated for 1 h with 1:5000 diluted goat anti-rabbit IgG's or 1:2000 diluted goat anti-mouse IgG's (Sigma) as secondary antibodies coupled to horseradish peroxidase. Proteins were visualized using enhanced chemiluminescence (Pierce). Immunopositive bands were scanned using ChemiDoc XRS (Bio-Rad) and signals were analysed with the Quantity One software (Bio-Rad). The amount of GFP or EGF protein was normalized for the corresponding total amount of protein.

EGF enzyme-linked immunosorbent assay (ELISA)

EGF concentrations were measured using the DuoSet ELISA for human EGF (DY236, (R&D Systems, Minneapolis, MN, USA), according to manufacturer's protocol. For this sandwich ELISA, the monoclonal anti-human EGF antibody (MAB636) was used as the capture antibody and for detection the biotinylated anti-human EGF Antibody (BAF236).

Immunocytochemistry and confocal laser scanning microscopy (CLSM)

24 h after induction the MDCK cells were fixed in 4% w/v paraformaldehyde in PBS. Next, cells were permeabilized using 0.1% v/v Triton X-100 in PBS for 15'. Importantly, for extracellular EGF staining, cells were not permeabilized. Cells were subsequently blocked with 5% w/v non-fat dried milk in PBS for 1 h at 3 temperature (RT). Then, cells were incubated with rabbit anti-EGF (1: 500; Ab-3, Calbiochem) or rat anti-E-cadherin (1:500; Abcam) primary antibody in PBS supplemented with 5% w/v non-fat dried milk for 1 h at RT. After washing in PBS three times, cells were incubated with anti-rat or anti-rabbit Alexa Fluor 594 (1:1000; Jackson ImmunoResearch Laboratories) secondary antibody in PBS supplemented with 5% w/v non-fat dried milk for 1 h at RT. Individual filters were cut out of their supports and the slides were mounted in MOWIOL 4-88 solution supplemented with DABCO (Calbiochem) and examined with CLSM (Olympus FV1000).

Statistical analysis

Data are presented as mean ± standard error of the mean (SEM). Overall statistical significance was determined by one-way ANOVA, followed by a Tukey post-hoc test. $P < 0.05$ was considered statistically significant. All analyses were performed using the InStat 3 for Macintosh software.

Results

Expression of pro-EGF in cells using various transfection methods

First, we studied the fate of wild-type pro-EGF-GFP (pro-EGF-WT) and pro-EGF-P1070L-GFP (pro-EGF-P1070L) expressed in non-polarized HEK293 cells. To this end, these cells were transiently transfected using polyethylenimine (PEI), resulting in a transfection efficiency of 30-50%, which persisted for at least one week. To compare the cell surface expression of pro-EGF to total expression, biotinylation experiments were performed. Immunoblotting of both fractions, using the GFP antibody, showed robust plasma

membrane localization, while the expression of pro-EGF-P1070L was not different from pro-EGF-WT (**Figure 4A**).

Second, a polarized cell model was employed to study the fate of these proteins in more detail. We attempted a stable transfection of MDCK cells with pro-EGF-WT and P1070L in the pCB7 plasmid (9), using the calcium-phosphate precipitation technique. However, some pilot experiments taught us that the expression of pro-EGF in these cells was undetectable by immunoblotting (data not shown). Next, different transient transfection strategies were tested using various transfection reagents under variable conditions. The percentage of transfected (GFP-expressing) cells was determined using fluorescence microscopy. The results showed that a transfection efficiency of 10% was the maximum, with only 5% of the cells being positive three days later (the earliest stage to perform experiments) (**Table 1**). Finally, an inducible cell expression system was tested, namely the tetracycline-regulated mammalian expression system (T-REx, Invitrogen), for expression of pro-EGF-WT and pro-EGF-P1070L protein.

Table 1. Overview of transfection methods and cell types used

Cell line and transfection method	*Transfection efficiency*	*Transfected cells after 3 days*
HEK293		
Polyethylenimine (PEI)	30-50%	30-50%
MDCKI		
Polyethylenimine (PEI)	2-5%	0-2%
FuGENE HD	~10%	2-5%
Metafectene Pro	~5%	0-1%
Lipofectamine 2000	0-3%	0-2%

The pCB7 vector containing the pro-EGF-WT-GFP or pro-EGF-P1070L-GFP construct or empty vector was used for transfection. The transfection efficiency was determined by counting the percentage of transfected “green” cells, using fluorescent microscopy.

Expression of pro-EGF in MDCK cells using the T-REx inducible system

To address the optimal dose of doxycyline to induce expression of pro-EGF-WT and pro-EGF-P1070L in MDCK cells, immunoblotting was performed. **Figure 3** shows that 100 ng/mL doxycycline is necessary and sufficient for inducing transcription of pro-EGF. Moreover, using fluorescent microscopy we observed that of the transiently transfected inducible MDCK cells around 10% was expressing the protein, whereas stable expression of the protein resulted in up to 100% positive cells, after induction with doxycycline (data not shown).

The T-REx system provided expression levels high enough to immunoblot pro-EGF-WT-GFP and pro-EGF-P1070L-GFP using the GFP-antibody and even to determine the total (apical and basolateral) plasma membrane fraction, using biotinylation (**Figure 4B)**. Cell-surface biotinylation showed a similar fraction of pro-EGF-WT and pro-EGF-P1070L on the plasma membrane, comparable to the experiment in HEK293 cells. These experiments

showed that the inducible system is suitable for the expression of pro-EGF-WT-GFP and pro-EGF-P1070L-GFP in MDCK cells.

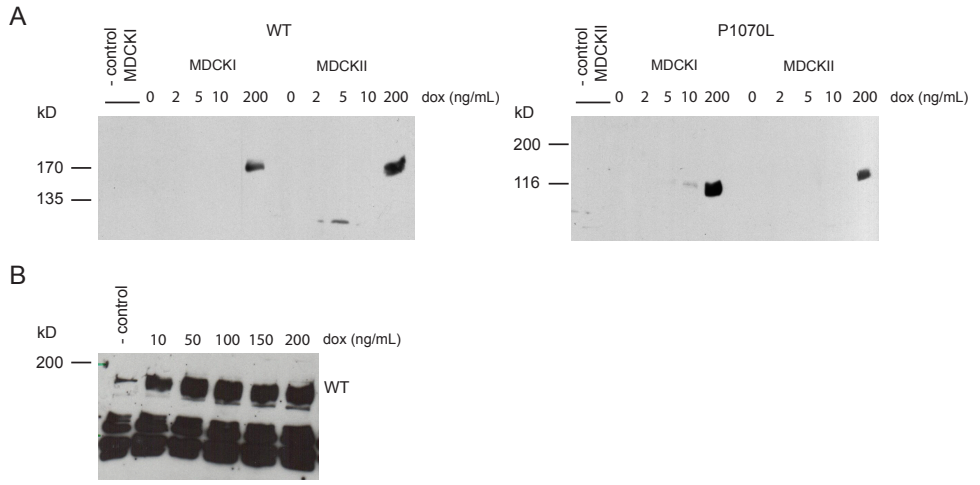

Figure 3. Optimization of the doxycycline concentration necessary for inducible protein expression using the T-REx system. The optimal dosage of doxycycline (dox) needed to induce pro-EGF-WT-GFP (WT) and pro-EGF-P1070L-GFP (P1070L) transcription was determined, using immunoblotting with the GFP-antibody. For this purpose, MDCKI and MDCKII cell lines were transiently transfected with WT and P1070L. (**A**) The expression of WT as well as P1070L in MDCKI and MDCKII cells was tested using a broad range of doxycycline concentrations. (**B**) The exact concentration of doxycycline needed was determined for the expression of WT in MDCKI cells.

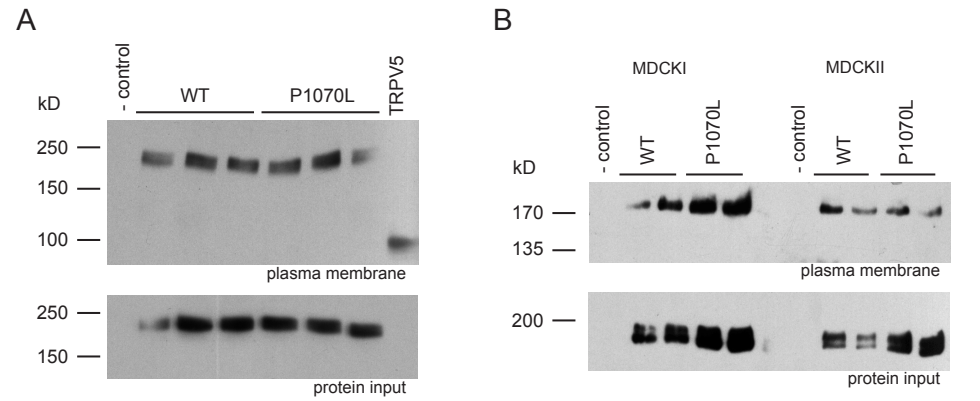

Figure 4. Plasma membrane localization of pro-EGF-WT and pro-EGF-P1070L in HEK293 and MDCK cells. HEK293 and MDCK cells were transiently co-transfected with pcDNA6/TR and pro-EGF-WT-GFP (WT), pro-EGF-P1070L-GFP (P1070L), empty vector or with TRPV5-GFP (TRPV5) as positive control. The next day, expression of pro-EGF was induced using 100 ng/mL doxycycline. Cell-surface biotinylation of these proteins was analysed in HEK293 cells (**A**) and MDCKI and MDCKII cells (**B**), using the GFP-antibody. Protein input represents pro-EGF-WT-GFP or pro-EGF-P1070L-GFP expression in total cell lysate. The protein mass scale (in kD) is indicated on the left. – control, cells transfected with empty vector.

Secretion of pro-EGF-WT and pro-EGF-P1070L from MDCKI cells

MDCKI cells transiently expressing pro-EGF-WT, pro-EGF-P1070L or the empty vector were induced with 100 ng/mL doxycycline. The following day, FCS-free medium was added with or without 1 μmol/L PMA. The media and cells were collected separately at 4 or 16 h. The media were concentrated and fractionated in a 3-50 kD and a > 50 kD protein fraction. **Figure 5** shows the results of two individual and slightly different experiments.

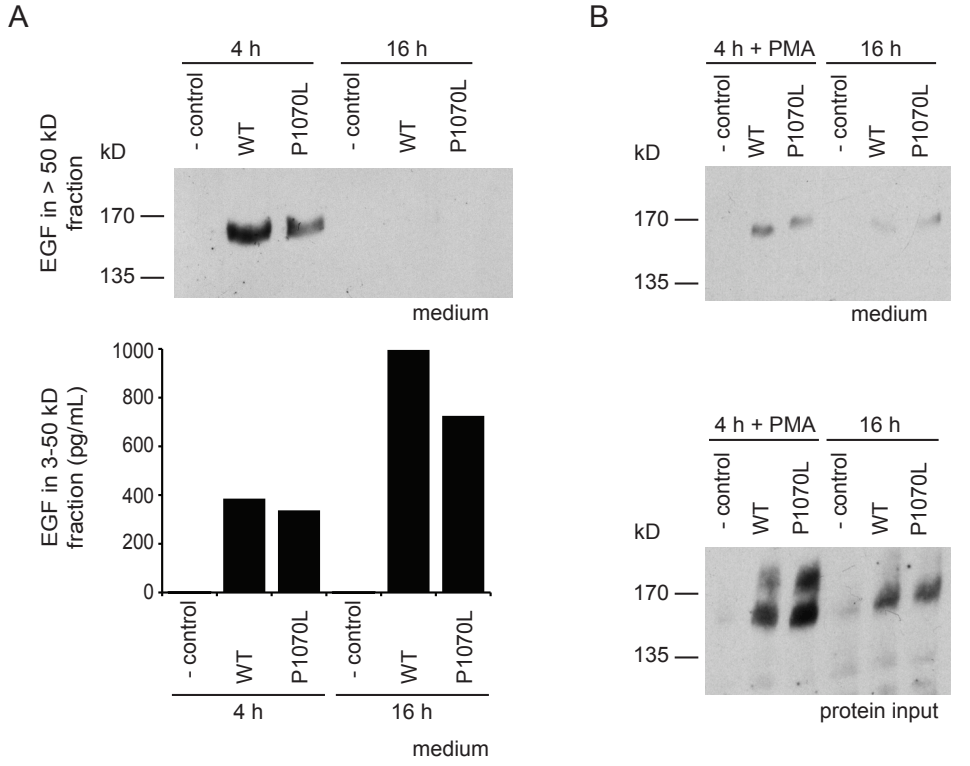

Figure 5. Detection of (pro-)EGF in the medium of non-polarized MDCKI cells using immunoblotting and ELISA. MDCKI cells transiently co-transfected with pcDNA6/TR and pro-EGF-WT-GFP (WT), pro-EGF-P1070L-GFP (P1070L) or empty vector were seeded on petri dishes. The next day, expression of pro-EGF was induced using 100 ng/mL doxycycline. 24 h later, FCS-free medium was added in the presence or absence of 1 μmol/L phorbol myristate acetate (PMA). After 4 or 16 h, medium was collected and the protein fractions were separated (in a > 50 kD fraction and a 3-50 kD fraction) and concentrated using centriprep columns. This figure represents two individual experiments. (**A**) The first experiment measured (pro-)EGF after 4 h and after 16 h in the > 50 kD medium of MDCKI cells using immunoblotting (upper part) and in the 3-50 kD fraction by ELISA (lower part) in the corresponding samples. (**B**) The second experiment determined pro-EGF after 4 h with PMA and after 16 h in the absence of PMA, in the > 50 kD medium. In addition, the total lysate was blotted, using the EGF antibody, to determine the input. The protein mass scale (in kD) is indicated on the left side of the immunoblots. – control, cells transfected with empty vector, (n = 1).

The first experiment revealed that after 4 h pro-EGF-WT and pro-EGF-P1070L are detectable in the > 50 kD fraction by immunoblotting, whereas after 16 h these proteins were not detected. In addition the ELISA, which determined EGF in the 3-50 kD fraction, detected twice as much EGF after 16 h compared with 4 h (**Figure 5A**). This indicates that after 16 h most of the excreted pro-EGF is processed into mature EGF. The second experiment examined the influence of PMA on secretion of pro-EGF. **Figure 5B** shows that stimulation with PMA for 4 h does not significantly increase secreted pro-EGF.

Polarized secretion of pro-EGF-WT and pro-EGF-P1070L

Figure 6A shows an overview of the side-specific secretion and processing of pro-EGF and the mutant. In short, MDCK cells stably expressing pro-EGF-WT and pro-EGF-P1070L were seeded on semi-permeable filters. Five days later, protein expression was induced with 100 ng/mL doxycycline. The following day, FCS-free medium was added to both compartments and collected after 4, 16 or 48 h. In addition, the cells were scraped from the filter supports to quantify protein expression levels. The media were concentrated and separated in a 3-50 kD and a > 50 kD protein fraction. Immunoblotting analysis of the > 50 kD medium fraction revealed that the 170 kD pro-EGF and P1070L proteins are predominantly secreted into the apical compartment (**Figure 6B** and **C,** upper parts). This immunoblot revealed that no pro-EGF is detectable in the basolateral medium of MDCKI cells, whereas in MDCKII cells the full-length protein was excreted at this side, although the amount was approximately 25-50% of the level found in the apical compartment.

The excretion of P1070L was around 20% lower in both compartments, when compared with wild-type. However, the whole cell lysate protein expression showed that expression of pro-EGF-P1070L was 50% lower in MDCKI cells and 25% lower in MDCKII cells. In addition, the total protein expression in MDCKI cells, represented by the β-actin levels, was 25% lower for the mutant, whereas in MDCKII cells this was equal for pro-EGF-WT and pro-EGF-P1070L (**Figure 6B** and **C,** lower parts). Therefore, this experiment was repeated, using different stable clones. As depicted in **Figure 7A,** pro-EGF-WT and pro-EGF-P1070L were again secreted predominantly into the apical compartment; however, the abundance of pro-EGF-P1070L was around 40% of wild-type. In this experiment 5% of the apical pro-EGF released was found in the basolateral medium, whereas pro-EGF-P1070L was not detectable in the basolateral compartment. Subsequent immunoblotting of the total cell lysate, using anti-GFP and β-actin antibodies, showed that the abundance in pro-EGF-P1070L expressing cells was 85% and 75% of the wild-type, respectively (**Figure 7B**). In addition, in all individual experiments only the large 170 kD pro-EGF fragment was perceived in the > 50 kD fraction or in the total medium fraction; no smaller (pro-)EGF intermediates were observed.

To assess the processing of pro-EGF-WT and pro-EGF-P1070L, detection of EGF in the various medium fractions was performed by ELISA. In MDCKI cells, the putative 170 kDa pro-EGF-WT and pro-EGF-P1070L are largely secreted into the apical compartment, similar to the results obtained by immunoblotting. After 16 h the pro-EGF abundance in the medium was triple the amount of the 4 h medium. Moreover, the 3-50 kD fraction contained approximately three times higher EGF concentrations compared with the > 50 kD protein fraction (**Figure 6D**). In addition, pro-EGF secretion by MDCKII cells showed a

comparable profile, except in two areas: *i*) the EGF concentrations were approximately two-four times lower in all fractions and; *ii*) EGF was detected in all basolateral medium fractions of pro-EGF-WT and pro-EGF-P1070L transfected MDCKII cells (**Figure 6E**).

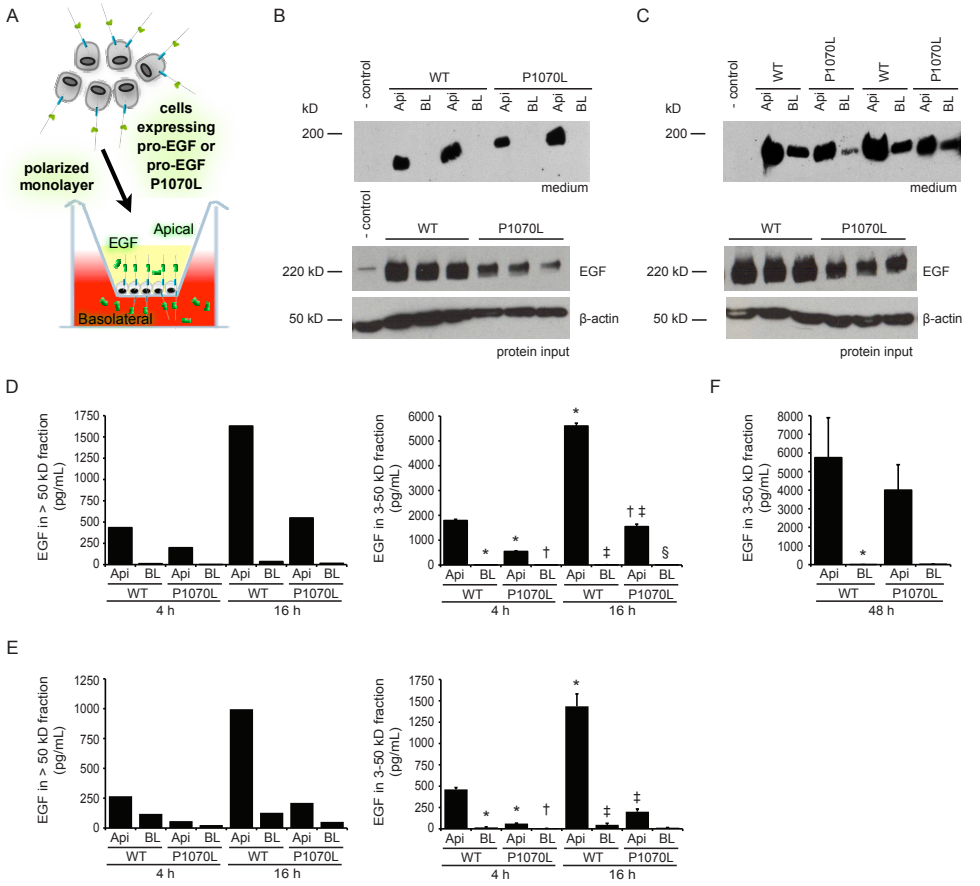

Figure 6. Detection of (pro-)EGF in the medium of polarized MDCK cells using immunoblotting and ELISA. (**A**) MDCK cells stably transfected with pro-EGF-WT-GFP (WT) or pro-EGF-P1070L-GFP (P1070L) were seeded on filters. Once the cells were polarized, expression of pro-EGF was induced using 100 ng/mL doxycycline. 24 h later, FCS-free medium was added and after 4, 16 or 48 h medium was collected and the protein fractions were separated and concentrated using centriprep columns. Detection of pro-EGF after 16 h in the medium of MDCKI (**B**) and MDCKII (**C**) cells by immunoblotting. Total lysate was also blotted, using the EGF and β-actin antibodies to determine the expression levels of WT and P1070L and the total protein input. The protein mass scale (in kD) is indicated on the left. Side specific excretion of WT and P1070L after 4 or 16 h in MDCKI (**D**) and MDCKII (**E**) was determined by ELISA for the 3-50 kD (*n* = 3) and > 50 kD (*n* = 1) fractions. In a separate experiment, the excretion was assayed after 48 h on FCS-free medium in MDCKI cells for the < 50 kD fraction (*n* = 4) (**F**). Values of ELISA are presented as mean ± SEM. * P < 0.05 versus Api WT 4/48 h. † P < 0.05 versus Api P1070L 4 h. ‡ P < 0.05 versus Api WT 16 h. § P < 0.05 versus Api P1070L 16h. – control, cells transfected with empty vector; Api, apical; BL, basolateral.

In agreement with the immunoblotting results, two-three and three-seven times lower concentrations were measured for the P1070L mutant in the secreted fractions of MDCKI and MDCKII cells, respectively. Moreover, an additional experiment showed that after 48 h incubation in FCS-free medium, the presence of EGF on the basolateral side was marginal compared with the apical side for MDCKI cells (**Figure 6F**).

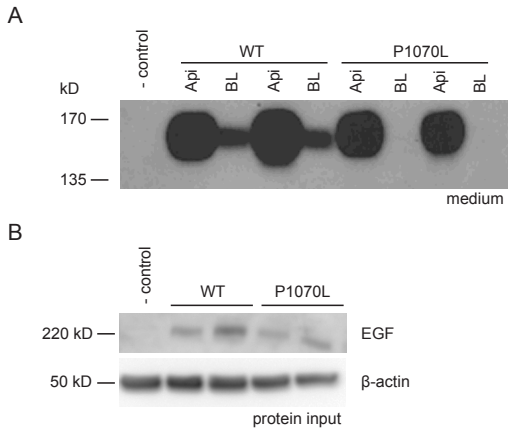

Figure 7. Detection of pro-EGF in the medium of polarized MDCK cells using immunoblotting. Detection of pro-EGF-WT-GFP (WT) and pro-EGF-P1070L-GFP (P1070L) after 16 h in the medium of MDCKI cells by immunoblotting (**A**), also the total lysate was blotted, using the EGF and β-actin antibodies to determine the input (**B**). The protein mass scale (in kD) is indicated on the left. – control, cells transfected with empty vector; Api, apical; BL, basolateral.

Subcellular localization of pro-EGF-WT and pro-EGF-P1070L

To investigate the subcellular localization of pro-EGF-WT and pro-EGF-P1070L, immunocytochemistry followed by confocal microscopy was performed. Hence, MDCK cells stably-transfected with pro-EGF-WT and pro-EGF-P1070L were seeded on semi-permeable filters and protein expression was induced after three days. The next day, cells were stained using an anti-E-cadherin or anti-EGF antibody; the latter was used for staining of the extracellular EGF epitopes only (**Figure 8A**). MDCKII cells expressing pro-EGF formed a tight monolayer, whereas MDCKI cells expressing pro-EGF did not establish confluent monolayers. Wild-type pro-EGF and the P1070L mutant were both principally expressed at the apical membrane, which is most clearly visualized by the MDCKII cells. Minor basolateral expression of pro-EGF-WT and pro-EGF-P1070L was detected in both MDCK cell lines as well (**Figures 8B and C**). Finally, the effect of the metalloproteinase inhibitor phenanthroline was tested. As shown in the right panels of **Figures 8B** and **C**, incubation with 10 μmol/L phenanthroline for 18 h had no substantial effect on membrane expression and/or localization of pro-EGF-WT and pro-EGF-P1070L.

Discussion

Fluorescent staining and consecutive confocal analysis of polarized MDCK cells showed that pro-EGF-WT and pro-EGF-P1070L are predominantly sorted to the apical plasma membrane. Moreover, pro-EGF-WT and pro-EGF-P1070L are secreted by MDCK cells and processed to produce the mature 6 kD EGF hormone, presumably in proportion to their abundance. Finally, abated secretion of pro-EGF-P1070L, into the apical as well as the basolateral compartment was observed, in comparison with wild-type.

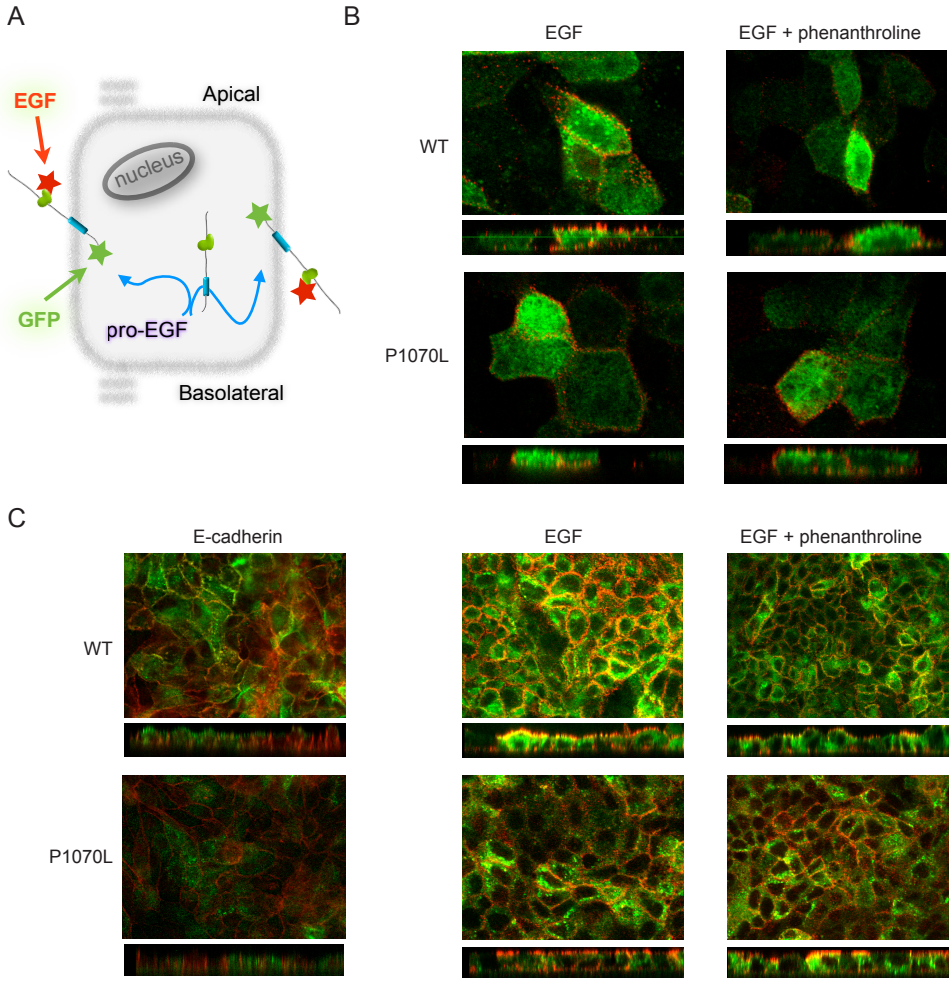

Figure 8. Analysis of subcellular localization of pro-EGF-WT-GFP (WT) and pro-EGF P1070L-GFP (P1070L) in MDCK cells, using immunocytochemistry and confocal laser scanning microscopy (CLSM). (**A**) Schematic overview of fluorescent procedure used; the EGF-antibody is used for detection of the membrane expressed WT and P1070L only. Confluent monolayers of the MDCKI (**B**) and MDCKII cells (**C**) were stimulated with 100 ng/mL doxycycline to induce WT or P1070L expression. MDCKI and MDCKII cells expressing WT or P1070L were left untreated or incubated with 10 μmol/L phenanthroline for 18 h. Cells were subjected to immunocytochemistry, using the E-cadherin or EGF antibody followed by Alexa-594-conjugated IgG's. Top view (XY) CLSM images and their corresponding cross sections (XZ) are shown.

In contrast to transfection of HEK293 cells with pro-EGF-WT-GFP or pro-EGF-P1070L-GFP, the overexpression of these large proteins in MDCK cells and the maintenance of these cells was laborious. The transfection efficiency of MDCK cells with pro-EGF-WT-GFP and the mutant was low regardless of the transfection method used. In addition, the

expression of these proteins decreased over time, impeding the study of these proteins. As postulated by Voldborg *et al*., co-expression of EGFR and its ligand pro-EGF might result in an autocrine loop, resulting in continuous activation of EGFR, leading to uncontrolled cell growth (39). Consequently, it is possible that in our cell system apoptosis or senescence was induced.

However, in the past MDCK cells stably expressing pro-EGF-WT and pro-EGF-P1070L were successfully used by our group for patch clamp analysis (9). It is important to note that for these patch clamp experiments a low expression of pro-EGF was sufficient. Furthermore, the transfection used pro-EGF constructs without GFP attached to the carboxyl-terminus, and the expression of an even larger protein in the present study might explain the problems we encountered.

Difficulties with overexpression of pro-EGF, especially in a polarized cell model, are also evident from the literature. In some studies, specific tags were applied, or cells were treated with sodium butyrate to increase expression of pro-EGF, followed by pulse-chase experiments and immunoprecipitation, to enable detection (30, 40, 41). Fortunately, the inducible T-REx system, which composes an additional regulatory DNA plasmid, provided us with expression levels of pro-EGF-GFP high enough to perform the outlined experiments.

Using the T-REx system, we showed that pro-EGF-WT-GFP and pro-EGF-P1070L-GFP are equally located in the total plasma membrane fractions of HEK293 cells and transiently-transfected non-polarized MDCK cells. Furthermore, secretion of pro-EGF from transiently-transfected non-polarized MDCK cells was observed from 4 h onwards. Our data indicated that after 16 h most of the full-length pro-EGF is processed and that secretion is decreased at that time point.

Additional experiments performed using stably-transfected, polarized MDCK cells, found that pro-EGF-WT and the P1070L mutant were both principally expressed at the apical membrane. However, substantial basolateral localization of these proteins was detected in both MDCK cell models. Secretion of pro-EGF was predominantly observed on the apical side, although, significant release of pro-EGF-WT and the mutant was noticed in the basolateral compartment of MDCKII cells. Furthermore, we observed that full-length pro-EGF was processed into a smaller than 50 kD protein.

In contrast to the results obtained with the non-polarized transiently-transfected cells, the secretion of pro-EGF seems to be prolonged. In polarized MDCK cells, after 16 h higher concentrations of pro-EGF and P1070L were detected in the 3-50 and > 50 kD fractions, compared with 4 h. Within 4 h, the quantity of (pro-)EGF in the 3-50 kD protein fraction was two-three times higher in the apical compartment of polarized MDCKI cells, suggesting that pro-EGF is en masse processed into mature EGF within hours upon secretion. Importantly, in MDCKII cells the apical EGF concentration was similar or slightly increased in the 3-50 kD apical fraction. In the basolateral compartment of MDCKI and MDCKII cells the abundance of EGF was two-six times lower compared with the > 50 kD fraction. These results suggest that processing at the apical and basolateral side are different processes.

Interestingly, although we observed a comparable processing of pro-EGF-WT and pro-EGF-P1070L in MDCKI and MDCKII cells, there are some specific differences. Both MDCK cell lines are generally used for experiments in which polarization is important. The major difference between these cell lines is that a monolayer of MDCKI cells has a higher

transepithelial electrical resistance, compared with an MDCKII cell monolayer (42). Whereas pro-EGF was virtually undetectable in the basolateral medium of MDCKI cells, the basolateral media of MDCKII cells contained significant amounts of pro-EGF-WT and pro-EGF- P1070L. However, as indicated by the immunoblot (**Figure 7**), MDCKI cells are capable of releasing pro-EGF as well, suggesting no differences between the two cell types with respect to pro-EGF shedding.

Remarkably, Dempsey *et al*. showed, that human pro-EGF overexpressed in MDCK cells was equally delivered to the apical and basolateral membrane. The authors demonstrated that after 2 h, 6 h and 4 days, pro-EGF is predominantly detected at the apical membrane domain, while pro-EGF concentrations in the basolateral medium are approximately two times higher compared with the apical medium. They proposed that preferential ectodomain cleavage at the basolateral surface explains the apparent abundant apical localization of pro-EGF (40). This is in conflict with our results, which show increased abundance in the apical medium of pro-EGF and mature EGF. Regardless of the different detection method, they used the MDCKII cell type as well, and a similar time-span for collection of the medium. However, our observations agree more readily with *in vivo* data. The impressive amounts of pro-EGF of renal origin found in urine, is the consequence of pro-EGF release from the apical side of renal kidney cells (21, 22, 27, 28). Interestingly, the physiological relevance of EGF in urine is not clear, considering that EGFR localization is restricted to the basolateral side (10). It has been proposed that urinary EGF plays a role in the recovery following renal damage, by immediate stimulation of the EGFRs via the damaged tight junctions (43).

Our results suggest that the impaired plasma membrane cleavage of pro-EGF-P1070L explains the insufficient activation of EGFR and consequently Mg^{2+} loss (**Figure 9**). It seems unlikely that disturbed sorting to the basolateral membrane is responsible for the phenotype caused by the mutation. The observed secretion defect of pro-EGF-P1070L probably only impacts the physiological effect of pro-EGF at the basolateral side for the following reasons: *i*) the "threshold" for activation of EGFR is not reached due to the preferential sorting of pro-EGF to the apical side, or *ii*) (pro-)EGF is only physiologically active the basolateral side of the DCT, since EGFRs are supposed to be located only at this domain. The experiments performed in HEK293 and transiently-transfected MDCK cells demonstrated equal expression of pro-EGF-GFP and P1070L-GFP. In contrast, in some experiments performed with the stably-transfected MDCK cells lower total expression of the mutant was observed. However, this difference was inferior to the effect observed for the excreted abundance of pro-EGF-P1070L, indicating reduced secretion of the mutant in this model as well.

In the present study we showed that secretion of pro-EGF is not markedly affected by PMA stimulation or phenanthroline inhibition. This suggests that shedding of membrane-anchored pro-EGF is of constitutive origin and/or can be mediated by proteases, which are endogenously present in MDCK cells. Several papers reported an effect on cleavage of pro-EGF by modulating PKC activity or metalloprotease inhibitors (35, 40), whereas others showed no effect (25, 30, 41). It might be that the cell type or metalloprotease inhibitor used accounts for these different outcomes. Besides, constitutive activity was reported in most experiments (25, 30, 40, 44), suggesting that additional stimulation is not necessary for the release of pro-EGF. This further supports the probability that pro-EGF is not cleaved by ADAM17, but possibly by ADAM10. ADAM10 contains significant basal activity

towards its substrate (36). Cleavage of pro-EGF is likely to be independent of other regulators and determined mainly by the expression level of this protease (34). ADAM10 is constitutively expressed at the basolateral membrane of human DCT (45). In addition endogenous ADAM10 was detected in this membrane domain, primarily at cell-cell contacts, in MDCK cells (46). Furthermore, insulin has been indicated to enhance proteolytic activity of ADAM10 (47) and also to activate TRPM6 (5). Altogether, our data and the existing literature are in line with shedding of pro-EGF in kidney by ADAM10.

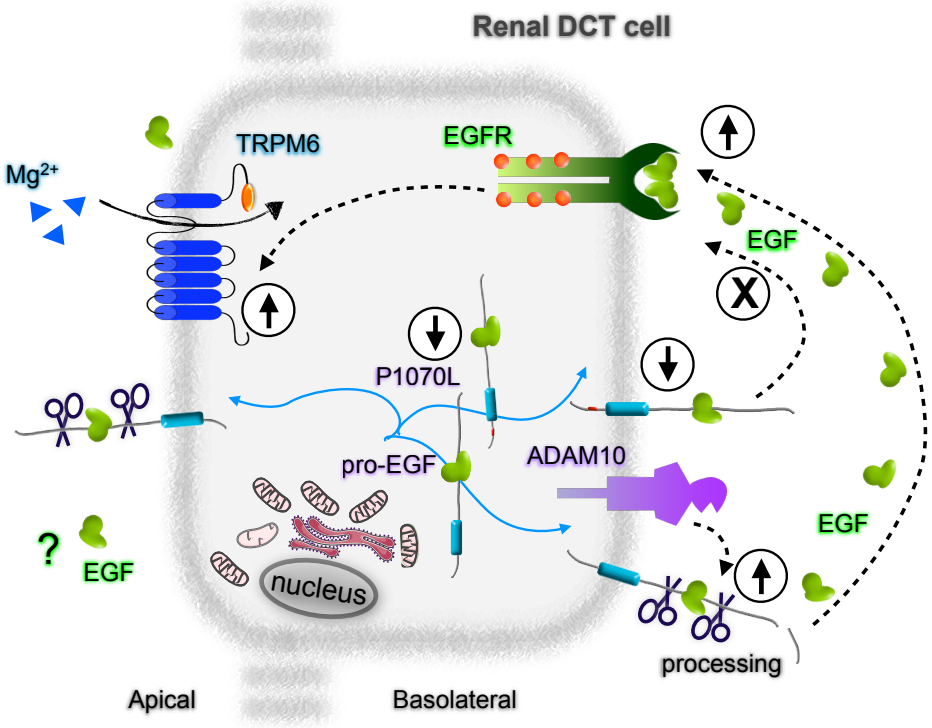

Figure 9. Schematic model of the hypothesis of the defect in pro-EGF due to the P1070L mutation in renal DCT cells. We showed that secretion of P1070L to the apical as well as the basolateral compartment is impaired in polarized MDCK cells. This indicates that the shedding of P1070L is hindered; however, we could not exclude lower total expression of the mutant. Consequently, the EGF receptor (EGFR), located at the basolateral membrane of the distal convoluted tubule (DCT), is inadequately activated, resulting in impaired stimulation of the epithelial Mg^{2+} channel TRPM6 and thereby causing renal Mg^{2+} loss. Since it is not clear whether EGF has a physiological role at the apical side, the consequence of reduced levels of (pro)EGF in pro-urine due to the P1070L mutation remains ambiguous. In addition, our results indicated that the processing of pro-EGF might be dependent on activity of the metalloprotease ADAM10.

As schematically visualized in **Figure 9**, we demonstrated that pro-EGF-WT and the P1070L mutant are both predominantly sorted to the apical membrane of MDCK cells. Moreover,

pro-EGF and P1070L were secreted at the apical domain and further processed to mature EGF. Our results indicate that endogenously present proteases adequately cleave (pro-)EGF in renal kidney cells. Cell models more closely resembling the *in vivo* situation could be instrumental in studying the sorting and shedding process of pro-EGF and the fate of the P1070L mutant.

Acknowledgements. The expert advice of Dr. H. van Goor was appreciated with respect to ELISA measurements. This research was financially supported by the Dutch Organization for Scientific Research (ZonMw 9120.8026; ALW 818.02.001).

References

1. Dai, L.J., Ritchie, G., Kerstan, D., et al. Magnesium transport in the renal distal convoluted tubule. *Physiol Rev* 81:51-84. 2001.
2. Quamme, G.A. Renal handling of magnesium: drug and hormone interactions. *Magnesium* 5:248-272. 1986.
3. Wong, E.T., Rude, R.K., Singer, F.R., et al. A high prevalence of hypomagnesemia and hypermagnesemia in hospitalized patients. *Am J Clin Pathol* 79:348-352. 1983.
4. Swaminathan, R. Magnesium metabolism and its disorders. *Clin Biochem Rev* 24:47-66. 2003.
5. Nair, A.V., Hocher, B., Verkaart, S., et al. Loss of insulin-induced activation of TRPM6 magnesium channels results in impaired glucose tolerance during pregnancy. *Proc Natl Acad Sci U S A* 109:11324-11329. 2012.
6. Topf, J.M., and Murray, P.T. Hypomagnesemia and hypermagnesemia. *Rev Endocr Metab Disord* 4:195-206. 2003.
7. Voets, T., Nilius, B., Hoefs, S., et al. TRPM6 forms the Mg2+ influx channel involved in intestinal and renal Mg2+ absorption. *J Biol Chem* 279:19-25. 2004.
8. Groenestege, W.M., Hoenderop, J.G., van den Heuvel, L., et al. The epithelial Mg2+ channel transient receptor potential melastatin 6 is regulated by dietary Mg2+ content and estrogens. *J Am Soc Nephrol* 17:1035-1043. 2006.
9. Groenestege, W.M., Thebault, S., van der Wijst, J., et al. Impaired basolateral sorting of pro-EGF causes isolated recessive renal hypomagnesemia. *J Clin Invest* 117:2260-2267. 2007.
10. Gesualdo, L., Di Paolo, S., Calabro, A., et al. Expression of epidermal growth factor and its receptor in normal and diseased human kidney: an immunohistochemical and in situ hybridization study. *Kidney Int* 49:656-665. 1996.
11. Thebault, S., Alexander, R.T., Tiel Groenestege, W.M., et al. EGF increases TRPM6 activity and surface expression. *J Am Soc Nephrol* 20:78-85. 2009.
12. Cao, Y., Liao, C., Tan, A., et al. Meta-analysis of incidence and risk of hypomagnesemia with cetuximab for advanced cancer. *Chemotherapy* 56:459-465. 2010.
13. Tejpar, S., Piessevaux, H., Claes, K., et al. Magnesium wasting associated with epidermal-growth-factor receptor-targeting antibodies in colorectal cancer: a prospective study. *Lancet Oncol* 8:387-394. 2007.
14. Vickers, M.M., Karapetis, C.S., Tu, D., et al. Association of hypomagnesemia with inferior survival in a phase III, randomized study of cetuximab plus best supportive care versus best supportive care alone: NCIC CTG/AGITG CO.17. *Ann Oncol* 24:953-960. 2013.
15. Schrag, D., Chung, K.Y., Flombaum, C., et al. Cetuximab therapy and symptomatic hypomagnesemia. *J Natl Cancer Inst* 97:1221-1224. 2005.
16. Cunningham, D., Humblet, Y., Siena, S., et al. Cetuximab monotherapy and cetuximab plus irinotecan in irinotecan-refractory metastatic colorectal cancer. *N Engl J Med* 351:337-345. 2004.
17. Carpenter, G., and Cohen, S. Epidermal growth factor. *Annu Rev Biochem* 48:193-216. 1979.
18. Melenhorst, W.B., Mulder, G.M., Xi, Q., et al. Epidermal growth factor receptor signaling in the kidney: key roles in physiology and disease. *Hypertension* 52:987-993. 2008.
19. Tong, Q., and Stockand, J.D. Receptor tyrosine kinases mediate epithelial Na(+) channel inhibition by epidermal growth factor. *Am J Physiol Renal Physiol* 288:F150-161. 2005.
20. Salido, E.C., Barajas, L., Lechago, J., et al. Immunocytochemical localization of epidermal growth factor in mouse kidney. *J Histochem Cytochem* 34:1155-1160. 1986.
21. Rall, L.B., Scott, J., Bell, G.I., et al. Mouse prepro-epidermal growth factor synthesis by the kidney and other tissues. *Nature* 313:228-231. 1985.

22. Jorgensen, P.E., Hilchey, S.D., Nexo, E., et al. Urinary epidermal growth factor is excreted from the rat isolated perfused kidney in the absence of plasma. *J Endocrinol* 139:227-234. 1993.
23. Aybay, C., Karakus, R., and Yucel, A. Characterization of human epidermal growth factor in human serum and urine under native conditions. *Cytokine* 35:36-43. 2006.
24. Bell, G.I., Fong, N.M., Stempien, M.M., et al. Human epidermal growth factor precursor: cDNA sequence, expression in vitro and gene organization. *Nucleic Acids Res* 14:8427-8446. 1986.
25. Le Gall, S.M., Meneton, P., Mauduit, P., et al. The sequential cleavage of membrane anchored pro-EGF requires a membrane serine protease other than kallikrein in rat kidney. *Regul Pept* 122:119-129. 2004.
26. Journe, F., Wattiez, R., Piron, A., et al. Renal epidermal growth factor precursor: proteolytic processing in an in vitro cell-free system. *Biochim Biophys Acta* 1357:18-30. 1997.
27. Lakshmanan, J., Salido, E.C., Lam, R., et al. Epidermal growth factor prohormone is secreted in human urine. *Am J Physiol* 263:E142-150. 1992.
28. Mroczkowski, B., and Reich, M. Identification of biologically active epidermal growth factor precursor in human fluids and secretions. *Endocrinology* 132:417-425. 1993.
29. Wiley, H.S., Woolf, M.F., Opresko, L.K., et al. Removal of the membrane-anchoring domain of epidermal growth factor leads to intracrine signaling and disruption of mammary epithelial cell organization. *J Cell Biol* 143:1317-1328. 1998.
30. Dong, J., and Wiley, H.S. Trafficking and proteolytic release of epidermal growth factor receptor ligands are modulated by their membrane-anchoring domains. *J Biol Chem* 275:557-564. 2000.
31. He, C., Hobert, M., Friend, L., et al. The epidermal growth factor receptor juxtamembrane domain has multiple basolateral plasma membrane localization determinants, including a dominant signal with a polyproline core. *J Biol Chem* 277:38284-38293. 2002.
32. Dong, J., Opresko, L.K., Chrisler, W., et al. The membrane-anchoring domain of epidermal growth factor receptor ligands dictates their ability to operate in juxtacrine mode. *Mol Biol Cell* 16:2984-2998. 2005.
33. Singh, A.B., and Harris, R.C. Autocrine, paracrine and juxtacrine signaling by EGFR ligands. *Cell Signal* 17:1183-1193. 2005.
34. Blobel, C.P. ADAMs: key components in EGFR signalling and development. *Nat Rev Mol Cell Biol* 6:32-43. 2005.
35. Le Gall, S.M., Auger, R., Dreux, C., et al. Regulated cell surface pro-EGF ectodomain shedding is a zinc metalloprotease-dependent process. *J Biol Chem* 278:45255-45268. 2003.
36. Sahin, U., Weskamp, G., Kelly, K., et al. Distinct roles for ADAM10 and ADAM17 in ectodomain shedding of six EGFR ligands. *J Cell Biol* 164:769-779. 2004.
37. Deen, P.M., Nielsen, S., Bindels, R.J., et al. Apical and basolateral expression of aquaporin-1 in transfected MDCK and LLC-PK cells and functional evaluation of their transcellular osmotic water permeabilities. *Pflugers Arch* 433:780-787. 1997.
38. van de Graaf, S.F., Rescher, U., Hoenderop, J.G., et al. TRPV5 is internalized via clathrin-dependent endocytosis to enter a Ca2+-controlled recycling pathway. *J Biol Chem* 283:4077-4086. 2008.
39. Voldborg, B.R., Damstrup, L., Spang-Thomsen, M., et al. Epidermal growth factor receptor (EGFR) and EGFR mutations, function and possible role in clinical trials. *Ann Oncol* 8:1197-1206. 1997.
40. Dempsey, P.J., Meise, K.S., Yoshitake, Y., et al. Apical enrichment of human EGF precursor in Madin-Darby canine kidney cells involves preferential basolateral ectodomain cleavage sensitive to a metalloprotease inhibitor. *J Cell Biol* 138:747-758. 1997.
41. Mroczkowski, B., Reich, M., Chen, K., et al. Recombinant human epidermal growth

factor precursor is a glycosylated membrane protein with biological activity. *Mol Cell Biol* 9:2771-2778. 1989.

42. Richardson, J.C., Scalera, V., and Simmons, N.L. Identification of two strains of MDCK cells which resemble separate nephron tubule segments. *Biochim Biophys Acta* 673:26-36. 1981.
43. Humes, H.D., Cieslinski, D.A., Coimbra, T.M., et al. Epidermal growth factor enhances renal tubule cell regeneration and repair and accelerates the recovery of renal function in postischemic acute renal failure. *J Clin Invest* 84:1757-1761. 1989.
44. Mroczkowski, B., Reich, M., Whittaker, J., et al. Expression of human epidermal growth factor precursor cDNA in transfected mouse NIH 3T3 cells. *Proc Natl Acad Sci U S A* 85:126-130. 1988.
45. Schramme, A., Abdel-Bakky, M.S., Gutwein, P., et al. Characterization of CXCL16 and ADAM10 in the normal and transplanted kidney. *Kidney Int* 74:328-338. 2008.
46. Wild-Bode, C., Fellerer, K., Kugler, J., et al. A basolateral sorting signal directs ADAM10 to adherens junctions and is required for its function in cell migration. *J Biol Chem* 281:23824-23829. 2006.
47. Chen, C.D., Podvin, S., Gillespie, E., et al. Insulin stimulates the cleavage and release of the extracellular domain of Klotho by ADAM10 and ADAM17. *Proc Natl Acad Sci U S A* 104:19796-19801. 2007.
48. Life Technologies Corporation. T-REx™ System: A Tetracycline-Regulated Expression System for Mammalian Cells. *MAN0000105* www.lifetechnologies.com. 2011.

Chapter 6

Summary and General Discussion

Introduction

The regulation of the Mg^{2+} balance in the human body and the maintenance of a plasma Mg^{2+} concentration between 0.7-1.1 mmol/L, is of vital importance. This is achieved by the concerted actions of intestinal absorption, exchange with bone and renal reabsorption. Renal adaptation of urinary Mg^{2+} excretion to fluctuating circumstances is the most important of these mechanisms for maintaining a constant plasma Mg^{2+} concentration (1). In the proximal tubule (PT) and thick ascending limb of Henle's loop (TAL) Mg^{2+} reabsorption takes place in a passive and paracellular manner, secondary to Na^+ and H_2O transport. However, fine-tuning takes place in the distal convoluted tubule (DCT), where active Mg^{2+} reabsorption occurs (2). The epithelial Mg^{2+} channel transient receptor potential subfamily melastatin, member 6 (TRPM6) expressed in DCT has been identified as gatekeeper of active transcellular Mg^{2+} reabsorption (3). In recent years the molecular regulation of TRPM6 became evident via the discovery and characterization of several modifying proteins (4). In addition, linkage and DNA analysis of patients suffering from isolated autosomal recessive renal hypomagnesemia (IRH) uncovered a role for epidermal growth factor (EGF) as the first magnesiotropic hormone (5). Moreover, several other hereditary disorders, which have hypomagnesemia as a component of the phenotype, indicated additional proteins essential for Mg^{2+} reabsorption in DCT or TAL (6). For most of them, their function has been (largely) unraveled, whereas for others the exact function remains obscure. This thesis focused on the impact of several drug treatments and dietary Mg^{2+} content on systemic Mg^{2+} balance. The function and importance of individual "magnesiotropic players", and the capacity of the kidney to adapt to challenging physiological situations was investigated. The outcome of these studies are summarized and discussed in this chapter.

Impact of drugs on the Mg^{2+} balance

Nowadays drug development is directed against defined molecular targets and when a new drug is successfully launched, the molecular pathway is known. However, in the last century, when most of the drugs still in use today were discovered, plural approaches were used. Often, trial-and-error experiments were involved and compounds were of synthetic as well as natural origin, resulting in many effective drugs where the mechanism of action remained elusive (7). As a consequence, the adverse effects of several drugs, uncovered after the drug was already marketed, accelerated insight into human physiology (8, 9). The annual worldwide spending on medications is expected to exceed 1 trillion dollars in 2015 (10). In particular, elderly and chronically ill patients use a variety of drugs (11). For certain drugs, aberrations in Mg^{2+} handling have been described as side effect. For instance, some antineoplastic agents and calcineurin inhibitors can cause hypomagnesemia in up to 100% of the patients in a cohort (12). For other chemical substances, side effects concerning the Mg^{2+} balance are observed in a smaller percentage of patients (12).

Cisplatin

In **Chapter 2** the mechanism by which Cis-Diamminedichloroplatinum(II) (Cisplatin) treatment causes hypomagnesemia was studied. Cisplatin is a widely used cytostatic drug with a broad range of actions in the treatment of solid tumors (13). This chemical kills cancer cells by cross linking RNA, DNA and protein in rapidly dividing cells (14). Unfortunately, renal toxicity, and more specifically damage to the PT and DCT segments of the nephron, restricts treatment (15-18). Around 20% of the patients treated with high-dose cisplatin develop renal dysfunction, which frequently leads to acute renal failure (19-21). However, most of the patients treated with cisplatin develop severe hypomagnesemia (22, 23), often associated with a reduced glomerular filtration rate (GFR), polyuria and other electrolyte disturbances (24-27). It was previously suggested that toxicity to the DCT is responsible for cisplatin-induced hypomagnesemia (1, 28, 29). Therefore, the purpose of our study was to unravel the pathway by which cisplatin therapy causes renal Mg^{2+} wasting. For this experiment, mice were treated with 3 intraperitoneal injections containing 5 mg/kg body weight cisplatin or vehicle, with 3 non-treatment days between injections and after the last treatment.

The mice treated with cisplatin developed significant polyuria, reduced creatinine clearance rates (C_{Cr}) and substantially reduced serum Mg^{2+} levels, whereas serum Ca^{2+}, Na^{+} and K^{+} concentrations were not changed. The renal excretion of Mg^{2+}, Ca^{2+}, Na^{+} and K^{+} was increased in the cisplatin-treated group, whereas the excretion of P_i was not affected. Analysis of the mRNA expression levels of different ion transporters and associated proteins revealed specific downregulation of TRPM6, the Na^{+}, Cl^{-} cotransporter (NCC) and parvalbumin (PV), which are typically expressed in the DCT. Experiments measuring corresponding protein levels confirmed the decreased expression of these proteins. These results strongly support an increased susceptibility of the DCT to cisplatin. It is likely that downregulation of TRPM6 in the DCT causes the observed Mg^{2+} loss, since active reabsorption of Mg^{2+} through this channel determines the final plasma Mg^{2+} concentration, and other parts of the tubule are largely impermeable to Mg^{2+}. Interestingly, several genes specifically expressed in the PT were not affected. Although kidney injury molecule-1 (Kim-1) mRNA levels were impressively upregulated upon treatment with cisplatin, aquaporin 1 (AQP1), the Na^{+}, H^{+} exchanger 3 (NHE3) and the sodium-glucose cotransporter 1 (SGLT1) expression levels were equal between the cisplatin-treated group and the control group. Possible explanations are that PT damage is less severe, or that it is different from DCT toxicity, in that general destruction via oxidative stress and necrosis prevail in PT (20).

Theoretically, two mechanisms could explain DCT-specific toxicity: *i*) local entry of cisplatin in these tubular cells or; *ii*) specific sensitivity of these cells to cisplatin. We showed that the expression of the copper transporter 1 (CTR1), which was postulated as mediator of cisplatin uptake (30) and shown to be involved in causing ototoxicity (31), was significantly decreased at the mRNA level in the cisplatin-treated mice. This transporter is localized in DCT cells (unpublished results) and in malignant tumors (32). We hypothesize that this transporter is responsible for cisplatin toxicity in the DCT. Confirmation that CTR1 is downregulated on protein level in the cisplatin group would be essential. Blocking the entry of cisplatin via this transporter, using copper sulfate (31), could verify its contribution to cisplatin-induced toxicity in the kidney. Alternatively, mitochondrial-induced apoptosis could be another pathway by which cisplatin causes DCT-specific cell

death (33, 34). DCT cells are characterized by the large size and multiplicity of mitochondria (35). Augmented sensitivity to cisplatin based on mitochondrial density has been shown *in vitro* (36). Immunohistochemical staining of cisplatin-treated kidney sections for NCC and PV suggested that specific protein downregulation, rather than major cellular damage, is responsible for cell death. This was confirmed by light microscopy, showing clear indications of individual necrotic tubular epithelial cells, detachment of cells and some urinary casts; however, this damage was limited (**Chapter 2**; unpublished results).

Finally, discovering how to block uptake or targeting of cisplatin to the DCT in a clinically practical manner would be the ultimate route to reduce renal side effects. Alternatively, inhibition of PKCδ (37) and infusion of adipose tissue-derived mesenchymal stem cells (38) have been proposed as candidate strategies to attenuate cisplatin-induced damage and to restore kidney function. Cisplatin will likely remain the best treatment option for different solid tumors, as it is highly efficacious. However, the continued search for the optimal combination with other platinum-based drugs, non-platinum anticancer agents and/or specific cellular targets, might further improve its potential (34, 39).

In conclusion, specific downregulation of certain proteins in the DCT, rather than massive hypotrophy or apoptosis in these cells explains the high sensitivity of this part of the nephron to cisplatin and the subsequent development of hypomagnesemia.

Furosemide

Furosemide has been widely used since the 1960s for treating hypertension and edema (9). Today, this compound is still regularly prescribed, often in combination with other diuretics (40, 41). Furosemide blocks the Na^+, K^+, $2Cl^-$ cotransporter (NKCC2) in TAL (42). Consequently, Na^+ reabsorption is diminished, which results in decreased urine concentration and fluid loss. It is generally accepted that the other well-known diuretic, thiazide, which affects NCC in the DCT, results in Mg^{2+} wasting (43). Although urinary Mg^{2+} excretion was enhanced immediately after furosemide administration (44-46), chronic use does not necessarily result in hypomagnesemia (47-49). Usually, studies that investigated the clinical effect of furosemide were performed in cohorts of patients with a specific disease.

Chapter 3 examined the effect of chronic furosemide use on the total Mg^{2+} status, focusing on reabsorption of Mg^{2+} by the kidney. Mice were treated for 7 days with furosemide using osmotic minipumps, which subcutaneously released the dissolved drug in a continuous manner. The mice chronically treated with furosemide developed a significant polyuria. In addition, these mice displayed increased serum concentrations of Na^+, whereas serum K^+, Ca^{2+} and Mg^{2+} values were not significantly altered in those animals. Moreover, the urinary excretion of Na^+, K^+, Ca^{2+} and Mg^{2+} was not affected by the furosemide treatment. Our results, obtained with mRNA and/or protein level measurements, revealed specific upregulation of TRPM6, NCC, the epithelial Ca^{2+} channel (TRPV5) and calbindin-D_{28K}, whereas PV, claudin-7 (CLDN7) and claudin-8 (CLDN8), the epithelial Na^+ channel (ENaC) and NHE3 were not affected.

These findings suggested that the DCT can compensate for impaired paracellular reabsorption of Mg^{2+} in the TAL by increasing TRPM6-mediated transcellular Mg^{2+} transport during blockade of NKCC2 by furosemide. The increased Mg^{2+} delivered to the DCT results in a luminal Mg^{2+} concentration favourable to Mg^{2+} transport, and in

combination with increased abundance of TRPM6, facilitates increased Mg^{2+} reabsorption in the DCT. A decent experiment to prove this hypothesis would be to measure fractional Mg^{2+} delivery along the tubule using the *in vivo* micropuncture technique. Reabsorption of Na^{+} in DCT via NCC, and of Ca^{2+} in the late DCT and connecting tubule (CNT) via TRPV5 are likely to be enhanced. In conclusion, this study found a large adaptive capacity of the distal part of the nephron during a chronic diuretic regime.

The urinary Na^{+} excretion was not significantly higher in the furosemide-treated group compared with the control group. This indicates that these mice develop resistance to this drug (50). Our findings regarding the compensatory adaptation of Na^{+} and Ca^{2+} reabsorption are in line with the upregulation and/or increased activity of NCC and calciotropic players in response to furosemide, as reported by others (46, 51-53). As far as we know, our study is the first to describe the upregulation of TRPM6 in mice treated with furosemide. Future experiments showing increased Mg^{2+} reabsorption via TRPM6 would further support the current data. Administration of furosemide in TRPM6 knockout mice would be a suitable model, as well as the application of a specific TRPM6 antagonist, to test this hypothesis. Unfortunately, these knockout mice are not viable (54) and a specific TRPM6 blocker has not yet been discovered or designed. A conditional knockout model might offer a solution. Alternatively, assessing the co-treatment of furosemide and thiazide, might confirm the adaptive role of the DCT as observed in this chapter. Hypomagnesemia induced by thiazide treatment and in the NCC knockout mice has been associated with downregulation of TRPM6 (43). Previous publications indicate that combination therapy enhances Na^{+} excretion and urinary production (41). Moreover, urinary Mg^{2+} excretion is likely in between the amounts of Mg^{2+} excreted upon treatment with thiazide or the loop diuretic furosemide alone (43, 55); however, the effect on the Mg^{2+} balance needs to be further established, especially on the long term.

The present study found that mice treated with furosemide effectively lose fluid without serious electrolyte imbalances. Adequate renal function is an essential requisite for adapting reabsorption of Mg^{2+}, as well as Na^{+}, K^{+} and Ca^{2+}, to avoid electrolyte imbalances. However, renal function is critical in many patients treated with furosemide. Hypertension is a common cause of chronic kidney disease (CKD) and vice versa (56), which explains why electrolyte aberrations might be diagnosed in this cohort (57). In addition to sufficient renal function, an adequate diet is also of vital importance for optimal treatment with furosemide. Dietary intake of Mg^{2+} is often problematic in seriously ill patients or the elderly (58-60); again, the very people who are prescribed furosemide. Altogether, these data indicate that monitoring Mg^{2+} status of patients treated with loop diuretics such as furosemide, will improve their clinical outcomes.

Dietary Mg^{2+} intake

Human beings are dependent on sufficient dietary Mg^{2+} intake from the external environment. Fortunately, Mg^{2+} is an essential element of biological systems in general, providing us with a broad range of products containing Mg^{2+}, which are appropriate as nourishment. In this section, dietary Mg^{2+} intake and absorption will be discussed in more detail as it pertains to health and disease.

Sensitivity of magnesiotropic players to the dietary Mg^{2+} content

Insight into the network of proteins essential for Mg^{2+} reabsorption has significantly increased in the past decade. Several proteins involved in Mg^{2+} homeostasis were uncovered, as well as part of their interactions and regulating factors. In **Chapter 4** the sensitivity of these recently discovered magnesiotropic players to changes in dietary Mg^{2+} content was determined. Mice were placed on a Mg^{2+}-deficient or a Mg^{2+}-enriched diet for two weeks. Dietary Mg^{2+} restriction resulted in a significant hypomagnesemia in combination with markedly reduced urinary excretion of Mg^{2+}, in line with previous studies (61, 62). This study revealed that in addition to TRPM6, the renal abundance of hepatocyte nuclear factor 1 homeobox B (HNF1B) and PV were substantially upregulated, at both the mRNA and protein levels, during dietary Mg^{2+} constraint. However, the other genes involved in Mg^{2+} homeostasis were not affected by the different Mg^{2+} regimes. The detailed molecular pathway by which HNF1B affects Mg^{2+} handling in DCT needs further investigation. Regulation of HNF1B indicates that basolateral Mg^{2+} transport in DCT is a critical process. Further research into HNF1B could uncover the mechanism for Mg^{2+} extrusion into the blood compartment (1). PV has been originally classified as Ca^{2+}-binding protein (63); however, the present study suggests that its role in the DCT might be more extensive. It likely affects the activity of NCC and/or can bind Mg^{2+} and consequently is directly or indirectly entangled in Mg^{2+} reabsorption. Although PV knockout mice were normomagnesemic, they showed increased diuresis, urinary K^+ excretion and elevated aldosterone levels (64). In addition, the level of NCC in the PV knockout mice was reduced, which might be a consequence of impaired $[Ca^{2+}]_i$ buffering. Electrolyte reabsorption by NCC has been suggested to be essential for Mg^{2+} transport in DCT (65, 66). Since we found that NCC levels were downregulated and PV levels upregulated in our dietary Mg^{2+}-restricted mice, we propose that the hypomagnesemic state affected the $[Ca^{2+}]_i$ in DCT cells. Intracellular Ca^{2+} measurements are necessary to test this hypothesis in combination with intracellular Ca^{2+} channel blockers to discover which Ca^{2+} store(s) might contribute to increased $[Ca^{2+}]_i$.

The fact that the other magnesiotropic players were not regulated on the mRNA level does not necessarily devaluate their importance in Mg^{2+} balance, because: *i*) they might be regulated on protein level; *ii*) post-transcriptional activation is of major importance for these transcripts (67) or; *iii*) their activity might be regulated by internal dynamics or protein-protein interactions (68, 69). Furthermore, the mRNA expression level of TRPM6 in the colon was also markedly increased during dietary Mg^{2+} restriction. This indicates that regardless of the renal adaptations, the capacity for transcellular Mg^{2+} absorption is enhanced.

Finally, TRPM6 expression was not only observed in kidney and intestine, it has also been attributed to lung tissue (62). Our unpublished PCR data showed that TRPM6 is expressed in the trachea as well. Immunohistochemical staining was performed for TRPM6; unfortunately, the specificity of the antibody in these samples was questionable. Therefore, in situ hybridization would be an appropriate tool to localize TRPM6 and subsequently define its function in the respiratory system. This is clinically interesting, since Mg^{2+} treatment has been shown to induce relaxation of bronchial cells and ameliorate obstructive lung diseases like asthma (70, 71). It might be that TRPM6 plays an essential role in Mg^{2+} signaling in the lung and that more insight into pulmonary TRPM6 could contribute to improved lung function of many patients.

The entanglement of Mg^{2+} and Ca^{2+} reabsorption

The dietary Mg^{2+} experiment performed in **Chapter 4**, showed that Mg^{2+} intake and/or the body Mg^{2+} status is closely connected to Ca^{2+} homeostasis. The considerable reduction in urinary Ca^{2+} excretion, along with the almost abolished excretion of Mg^{2+} in dietary Mg^{2+}-restricted mice, remains fascinating. The observation that Ca^{2+} reabsorption is affected by the Mg^{2+} status has been shown before (62, 72, 73); however, this study revealed several interesting clues about the regulation of Ca^{2+} and Mg^{2+} reabsorption. First of all, we observed that dietary Mg^{2+} intake affects not only renal Ca^{2+} reabsorption, but also P_i reabsorption, albeit in the opposite direction. The serum P_i level was increased in the Mg^{2+}-deficient mice compared with the Mg^{2+}-enriched mice. Second, the serum FGF23 level was two and a half times higher in the mice fed the low Mg^{2+} diet. These results indicated that the postulated reduction in renal P_i reabsorption in the PT is preceded by the increased FGF23 in the hypomagnesemic mice (74). It might be that increased serum P_i stimulates the elevation of FGF23 (75). Further investigation is needed to establish the mechanism by which serum P_i and FGF23 are linked. Importantly, the electrolyte imbalances observed in our dietary Mg^{2+}-restricted mice correspond to the clinical picture of patients with persistent hypomagnesemia accompanied by hypoparathyroidism, and consequently hypocalcemia in combination with hyperphosphatemia (76, 77). Third, the expression of TRPV5 and calbindin-D_{28K} was markedly downregulated during dietary Mg^{2+} restriction on both the mRNA and protein levels. Nearly all Ca^{2+} is reabsorbed by the kidney when dietary Mg^{2+} is restricted, predominantly by paracellular transport in TAL, due to lack of competition from Mg^{2+} ions. The result will be that little Ca^{2+} remains in the pro-urine in DCT/CNT to be actively transported. However, the physiological stimulus for the downregulation of these calciotropic proteins is indistinct, considering the existence of secondary hypocalcemia in the hypomagnesemic mice. Parathyroidectomized rats had similarly reduced TRPV5 and calbindin-D_{28K} levels, which were normalized upon injection with parathyroid hormone (PTH) (78). Unfortunately, it was not possible to directly measure PTH levels, since we collected serum from our mice and plasma is required for a PTH assay. Nevertheless, in patients hypomagnesemia is often accompanied by low PTH levels, which could be restored by Mg^{2+} supplementation (72, 79, 80). Most likely, Mg^{2+} depletion causes impaired secretion and/or synthesis of PTH (81) and resistance to PTH (82, 83), resulting in downregulation of TRPV5 and calbindin-D_{28K}. This, combined with disordered bone metabolism, explains the secondary hypocalcaemia (73).

The binding of PTH to its receptors in bone is hindered during hypomagnesemia. It was demonstrated that decreased uptake of PTH and reduced PTH-stimulated cAMP production by bone causes skeletal resistance to PTH in chronically Mg^{2+}-restricted dogs (83). The mechanism by which chronic hypomagnesemia affects PTH secretion by the parathyroid gland remains intriguing, particularly since acute hypomagnesemia stimulates the release of PTH (84), and it is supposed that PTH release can be triggered by a reduced extracellular Mg^{2+} level (85, 86). It seems that only a prolonged hypomagnesemic state will impair PTH secretion (87), as seen in our mouse study. The reduction of intracellular Mg^{2+} seems to obstruct PTH secretion (87), perhaps by limiting the function of Mg^{2+} as a second-messenger (88); however, the details are not yet elucidated. *In vitro* and *in vivo* experiments of PTH release by the parathyroid gland via Ca^{2+}-sensing receptor (CaSR) stimulation, under various Mg^{2+} conditions, would be necessary to unravel the role of PTH during hypomagnesemia.

Mg^{2+} supplementation

Large surveys investigating whether daily Mg^{2+} intake is adequate amongst healthy people are scarce. Interestingly, the research that has been conducted indicated that insufficient dietary Mg^{2+} intake affects many people worldwide, especially those of a lower socioeconomic status, and woman and the elderly are especially at risk (89-94). The consumption of a well-balanced diet, which includes a variety of fruits, vegetables, legumes and cereals (like for the "Healthy Eating Pyramid") should fulfill the Mg^{2+} needs (91, 95). Unfortunately, many people do not consume such a diet. In industrialized countries, the average diet contains too much added sugar, saturated fat and insufficient nutrients (96). Education campaigns, and maybe even measures like financial incentives to consume certain foods should be considered. Mg^{2+} supplementation has been shown to be beneficial for different physiological processes (97-100). Further research is needed to determine whether standard Mg^{2+} supplementation in specific population groups, like the elderly, should be advised. Some people, such as elite athletes and pregnant women, likely have an increased daily Mg^{2+} requirement (101, 102). Mg^{2+} supplementation has been shown to be beneficial in the treatment of muscle cramps and to reduce the occurrence of pre-eclampsia (103, 104).

Although cardiac and metabolic health is likely affected by insufficient dietary Mg^{2+} intake (99, 100), the clinical impact is not completely assessed. However, as described in the general introduction of this thesis, different groups of patients are at risk of developing severe hypomagnesemia, with potentially life-threatening consequences. When drugs affecting Mg^{2+} homeostasis are prescribed and/or patients have impaired kidney function, regular monitoring of the Mg^{2+} status is especially crucial (105, 106).

Various methods exist to determine Mg^{2+} deficiency; unfortunately each of them has limitations. Some methods accurately reflect the total body Mg^{2+} level, including muscle or blood cell measurements; however, they are neither practical nor widely applicable. The assessment of only ionized serum Mg^{2+} might better reflect the Mg^{2+} status than total serum Mg^{2+} (107), but the large same-day variability requires multiple measurements (108). Therefore, determination of the total serum Mg^{2+} concentration in combination with 24-hour urinary Mg^{2+} excretion is advised. This often provides a good clinical indication of the patient's Mg^{2+} status and currently is best practice, especially when considering feasibility, costs, duration and impact for the patient (12, 109). Moreover, this method was supported by the reflection of the effect of dietary Mg^{2+} restriction in serum and urine in **Chapter 4.**

Once the indication for Mg^{2+} supplementation is assessed, different routes of Mg^{2+} administration are possible. Depending on the underlying disease(s) and severity of hypomagnesemia, the condition of the patient and whether or not the patient is hospitalized, the attending physician can opt for oral supplementation, intramuscular injections or intravenous infusions (12, 110). For patients treated with cisplatin, supplementation of the pre- and post-hydration fluids with Mg^{2+}, combined with oral supplementation in between courses had beneficial treatment outcomes (28, 106, 111). For patients treated chronically with diuretics, oral Mg^{2+} supplementation could normalize body Mg^{2+} (112, 113). Co-treatment with Mg^{2+} was positively applied in many other treatment strategies (114-116). Importantly, regular monitoring of all these patients is essential to ascertain the intended effect and to adapt the therapy when necessary.

Adaptability of the DCT

The animal experiments performed in this thesis highlight the instrumental role of the DCT in Mg^{2+} homeostasis. Treatment with the cytostatic agent cisplatin resulted in downregulation of the DCT specific proteins TRPM6, PV and NCC, providing a plausible explanation for development of hypomagnesemia. It is likely that the decreased abundance of TRPM6 following cisplatin treatment is mediated indirectly, perhaps via alterations in the mitochondria resulting in impaired energy metabolism, or by a shift in the electrochemical gradient (117). The cisplatin study also revealed that CLDN16 is upregulated. This suggests that there is compensatory paracellular Mg^{2+} reabsorption in TAL; however, this cannot completely compensate for the disturbed Mg^{2+} transport in the DCT.

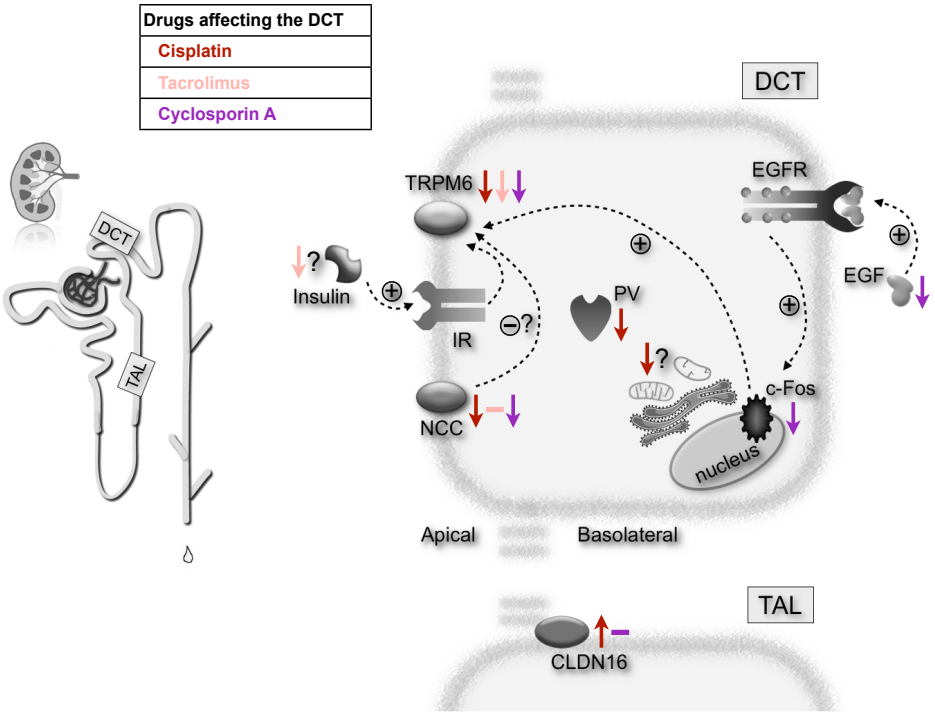

Figure 1. Schematic representation of effects evoked by drugs affecting Mg^{2+} reabsorption in DCT. Mg^{2+} wasting caused by treatment with the drugs cisplatin, tacrolimus and cyclosporin A is probably induced by decreased expression of TRPM6 in the distal convoluted tubule (DCT). The upstream molecular pathways for TRPM6 downregulation are different. Cyclosporin A results in reduced transcription of c-Fos, whereas the triggers for TRPM6 downregulation upon cisplatin and tacrolimus therapy remain elusive. Impaired energy release by mitochondria and a reduced insulin level might be involved, respectively. NCC expression level was downregulated in cisplatin and cyclosporin A-treated rodents; however, it was not affected in tacrolimus-treated rats. Whether NCC expression level and/or activity influences Mg^{2+} transport via TRPM6 needs to be investigated.

A decade ago, our group investigated the Mg^{2+} imbalances regularly diagnosed in patients treated with the immunosuppressant tacrolimus. They found that tacrolimus-induced hypomagnesemia is associated with downregulation of TRPM6, whereas NCC abundance was not affected (118). Moreover, *in vitro* and *in vivo* experiments revealed that cyclosporin A, another immunosuppressant drug affecting Mg^{2+} homeostasis (119), downregulates TRPM6 (120, 121). Cyclosporin A also downregulates NCC and reduces aldosterone levels (121). These drug studies revealed that when the DCT is affected and TRPM6 is downregulated, there are radical consequences for Mg^{2+} balance. However, the molecular pathway leading to the downregulation of TRPM6 in tacrolimus-treated rats has not yet been unraveled. The significantly increased serum glucose levels found (118), might offer a clue, via impaired insulin secretion. Since insulin has been shown to bind to the insulin receptor in the DCT and stimulate TRPM6 activity, failure to stimulate TRPM6 activity might be the underlying cause of hypomagnesemia in these patients (122). In addition, decreased expression of TRPM6 by cyclosporin A is likely mediated by inhibited transcription of c-Fos (120), and this could not be overcome by stimulation with EGF (121) (**Figure 1)**. In contrast the following studies highlight the enormous adaptability of the DCT when dietary Mg^{2+} is restricted, and in response to drugs affecting Mg^{2+} reabsorption in PT/TAL.

The dietary restriction experiment described in this thesis showed a tight correlation in the serum Mg^{2+} level with the urinary Mg^{2+} excretion in the experimental mice. The upregulation of TRPM6, HNF1B and PV and the downregulation of NCC indicated the adaptability of the DCT, in minimizing the body's Mg^{2+} loss during the low dietary Mg^{2+} regime. In addition, enhanced Mg^{2+} reabsorption in the DCT via upregulation of TRPM6 and NCC was sufficient to compensate for the decrease in Mg^{2+} reabsoprtion in the TAL during furosemide treatment, to prevent a hypomagnesemic state (**Figure 2)**.

Moreover, in rats treated with the immunosuppressant dexamethasone, TRPM6 was upregulated as well (118). This indicates compensation by the DCT and that the observed hypomagnesemia and hypermagnesiuria were caused elsewhere, likely further upstream, in the nephron. Interestingly, NCC was also upregulated in the rats treated with dexamethasone (118). The antibiotic drug gentamycin induces Mg^{2+} and Ca^{2+} wasting, which rarely results in serious effects on serum levels of these ions. This is conceivably effectuated by stimulation of CaSR and the subsequent reduced reabsorption of Mg^{2+} and Ca^{2+} via NKCC2 in TAL (123, 124). Compensation by DCT/CNT, similar to what was observed in our furosemide study, was observed for gentamycin treatment by upregulation of TRPM6 and TRPV5 (125). Interestingly, the NCC abundance was not affected by treatment with this aminoglycoside drug (124), (125) (**Figure 2)**.

Upregulation of TRPM6 and NCC in furosemide and dexamethasone-treated mice, and downregulation of TRPM6 and NCC upon cisplatin and cyclosporin A treatment suggests that these proteins might be similarly regulated, for example via the acid-base status. However, the observation that TRPM6 is downregulated in response to chronic metabolic acidosis (126) while NCC is upregulated (127) makes this co-regulation less likely. In addition, the dietary Mg^{2+} study revealed that although limiting Mg^{2+} results in the upregulation of TRPM6, NCC is not regulated on the mRNA level and even downregulated on the protein level. Moreover, in the tacrolimus-treated rats the NCC protein level was not affected, as observed in the cisplatin and cyclosporin A experiments. Alternatively, since TRPM6 and NCC are co-localized on the apical membrane of DCT cells, TRPM6

expression might be directly dependent on the amount of Na^+ reabsorption by NCC. Downregulation of TRPM6 during thiazide treatment and in NCC knockout mice is a clear indication that the regulation of these channels is intertwined (43).

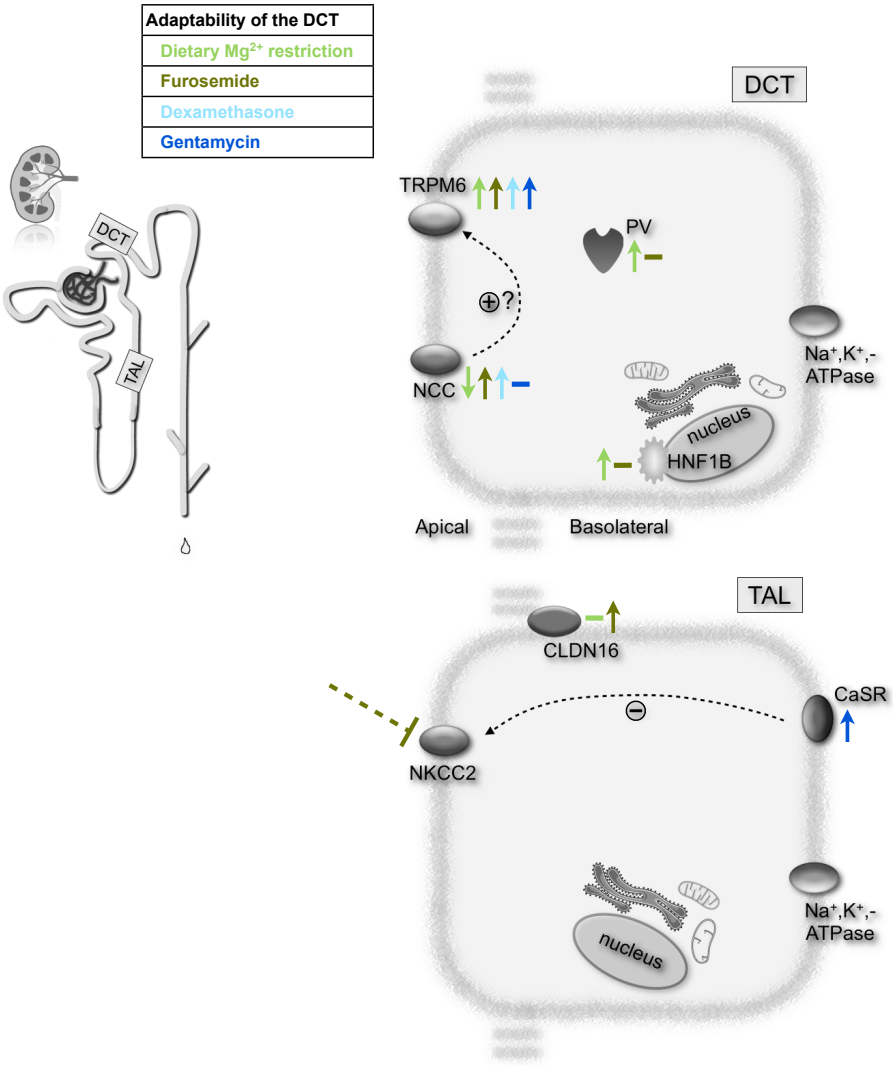

Figure 2. **Schematic representation of the adaptability of the DCT to dietary Mg^{2+} restriction and drugs affecting Mg^{2+} reabsorption in PT/TAL.** Aberrations of the Mg^{2+} balance induced by dietary Mg^{2+} restriction and treatment with the drugs furosemide, dexamethasone and gentamycin are accompanied by increased expression of TRPM6 in the distal convoluted tubule (DCT). Furosemide directly blocks NKCC2 in the thick ascending limb of Henle's loop (TAL), and gentamycin likely reduces the activity of this channel via activation of CaSR. As is the case for downregulation of TRPM6 (**Figure 1**), the influence of NCC expression level and/or activity on Mg^{2+} transport via TRPM6 needs to be determined.

Decreased Na^+ reabsorption in PT/TAL and the concomitant increased distal Na^+ load might be the initiator of increased Na^+ reabsorption via NCC, followed by upregulation of TRPM6. In the case of limiting dietary Mg^{2+}, furosemide, dexametasone and gentamycin experiments, this hypothesis appears to be valid, but direct confirmation is missing. Otherwise, Fanestil *et al*. showed that the NCC abundance is directly related to Mg^{2+} intake and to the plasma concentration of Mg^{2+} (128). It might be that the upregulation of PV in our hypomagnesemic mice, possibly mediated by increased $[Ca^{2+}]_i$ in DCT, overruled another NCC upregulating stimulus.

Whereas TRPM6 upregulation and adaptation of the DCT in general is quite well established, in response to factors affecting Mg^{2+} reabsorption in the kidney, the adaptability of the TAL is less clear. Interestingly, besides the observed upregulation of CLDN16 expression in the cisplatin study, the mRNA level of CLDN16 was also significantly upregulated in the furosemide-treated mouse group (194 ± 12 and 100 ± 8%, furosemide versus control, $P < 0.01$, data not shown). However, the mouse group fed the Mg^{2+}-restricted diet and the cyclosporin A-treated rats displayed no CLDN16 (or CLDN19) upregulation, compared with the enriched Mg^{2+} diet mouse group. Obviously, the abundance of tight junctions cannot be increased; changing the expression profile of the CLDNs affects only the selectivity of the permeability to the different electrolytes (129). The ionic composition of the pro-urine in combination with the electrochemical membrane potential probably determines the paracellular transport characteristics. Nevertheless, the presence of functional CLDN16 and CLDN19 proteins is essential, since mutations in both tight junction members disturb Mg^{2+} reabsorption (130, 131).

Finally, the EGFR antagonist cetuximab, prescribed for the treatment of cancer, has been associated with hypomagnesemia and corresponding lower survival rates (132-134), likely due to the blockage of TRPM6 activation via EGF (5, 135). Unfortunately, the expression levels of TRPM6 and NCC during this treatment remain to be investigated. Ironically, the efficiency of Panitumumab, a look-alike of cetuximab and also targeting the EGFR, can be determined by the occurrence of hypomagnesemia during treatment (136). More research is necessary to unravel whether there exists a certain degree of interdependence between TRPM6, NCC and/or PV and if upstream co-regulators of these proteins play a role in this.

In summary, the results presented in this thesis, together with many other studies investigating the effect of other Mg^{2+} homeostasis affecting drugs in the literature, indicate an enormous adaptability of the DCT for Mg^{2+} reabsorption. The pernicious outcome of treatment with different drugs affecting the DCT, illustrates how indispensable this nephron segment is in the maintenance of Mg^{2+} balance.

Regulation of TRPM6 by (pro-)EGF

In 2007, our group found that EGF can act as a magnesiotropic hormone; Groenestege *et al*. found that IRH is caused by a mutation in the *EGF* gene encoding the large precursor EGF (pro-EGF) (5). The authors suggested that the observed hypomagnesemia in these patients is the consequence of impaired activation of EGFR, located in the basolateral plasma membrane of the DCT, and subsequent impaired stimulation of TRPM6 (5). In **Chapter 5,** the fate of the P1070L mutation in the cytoplasmic tail of pro-EGF was studied

in more detail, using different biochemical approaches. Stable MDCKI and MDCKII cells were made, using the Tetracycline-Regulated Expression (T-REx) system. Interestingly, in HEK293 cells and in non-polarized MDCK cells, pro-EGF-P1070L plasma membrane expression and secretion showed the same profile compared with wild-type pro-EGF (pro-EGF-WT). In polarized cells both proteins were predominantly located on the apical membrane and secreted and processed into 6 kD EGF at this side of the cell. However, the MDCK cell lines also sorted pro-EGF-P1070L and pro-EGF-WT to the basolateral membrane, and these proteins were secreted into the basolateral compartment. Importantly, the secretion of the mutant was decreased on both the apical as well as the basolateral side. Our results suggested that the point mutation results in impaired cleavage of pro-EGF-P1070L. The hypomagnesemia diagnosed in the patients affected by the mutation is probably caused by the impaired stimulation of EGFR at the basolateral side due to the failure to reach a threshold concentration of secreted EGF, which is needed for stimulation of EGFR at this side of the cell. It has been suggested that pro-EGF contains a basolateral sorting motif (5), or that it is equally distributed on both plasma membrane compartments and the abundant apical expression is caused by preferential basolateral shedding (137). In contrast, in our study, the distribution of (pro-)EGF-WT and (pro-)EGF-P1070L was chiefly apical. Therefore, the presence of an apical sorting motif in pro-EGF would physiologically be more attractive. However, the rationale for predominant excretion and processing of pro-EGF ligand in the pro-urine, versus the localization of the EGFR on the basolateral membrane, remains elusive. A role of EGF in P_i transport in PT and of inhibition of ENaC has been postulated; however, both require activation of EGFR's (138, 139). The suggested repair function for EGF, after renal damage when tight junction integrity is abolished and EGF can diffuse to the basolateral side (140), would make sense from a physiological perspective.

A main limitation of this study and of related (pro-)EGF studies is the *in vitro* character of the experiments. In addition, many researches used a non-polarized cell model (137, 141), and sometimes not of renal origin (142-145), which makes it difficult to integrate all the data. Furthermore, it is unclear to what extent these data can be extrapolated to the *in vivo* situation. We observed that secretion of pro-EGF-P1070L and pro-EGF-WT in polarized MDCK cells was prolonged when compared with non-polarized transiently-transfected cells, indicating that the process of sorting and/or cleavage is different. In addition, Hobert *et al*. created an increased apical fraction of EGFR, by overexpression of this receptor, and found that apical EGF activation was less mitogenic when compared with the basolateral effect. They suggest that this difference could be due to plasma membrane domain-specific factors, such as the organization of the cytoskeleton (146). Moreover, the study model is also of major importance to investigate the shedding of pro-EGF by ADAM10 or another metalloprotease. The abundance of endogenous proteases could be limiting, given the nature of the overexpression system and this could potentially affect the outcome of our experiments. Hence, the exact physiological pathway of EGFR stimulation should be revealed by future studies including *in vivo* imaging of fluorescent (pro-)EGF mice with confocal microscopy. Finally, the construction of a transgenic kidney specific P1070L mouse model would be valuable to gain more insight into regulation of Mg^{2+} transport in DCT. These efforts will conceivably reveal the specific conditions under which activation of the EGFR by EGF is of crucial importance for the stimulation of TRPM6 activity. Furthermore, the initial trigger stimulating this (pro-)EGF(R) signaling cascade

might be discovered, resulting in a possible treatment target for patients suffering from Mg^{2+} imbalances.

The mouse as research model

Most research conducted for this thesis was performed using the mouse as a model for human beings. The mouse genomic sequence is highly similar to that of humans, due to the small evolutionary distance (147). Although species like primates are even more closely related to humans, mice are easy to handle and less expensive to maintain. Their short life span and reproductive cycle make it possible to study disease processes and generate (transgenic) mice relatively quickly. The scientific questions addressed in this thesis were often focused on a specific mechanism, which could not be studied without considering the physiological environment, i.e. the whole organism and its natural behavior. Unfortunately, complete artificial kidneys and especially ways to study their interactions with other organs are not yet available, to study physiological mechanisms as described in this thesis. Researchers should always be careful with their extrapolation of mouse data. However, for the moment, the mouse model is indispensable for biomedical research, supported by the massive knowledge this model already brought us (148). In addition, availability of humanized mouse models, this means mice that received human genes, cells tissues or even whole organs, further increased the suitability of mice for biomedical science (149).

The metabolic cage

In the mice studies described in this thesis (**Chapters 2, 3 and 4**) we made use of metabolic cages. In 1988 Campbell and Oldham patented the metabolic cage unit, in the configuration still used today. This equipment enabled researchers to house their mice individually, collect urine and feces, and accurately monitor their water and food intake. Individual 24-hour urine analysis is valuable to determine different parameters of kidney function. In addition, the other parameters provide an important tool, in combination with body weight and observation, to deduce general well being, and when necessary to exclude a particular mouse. The disadvantage that is coupled to the use of these cages is the stress it entails for the mice. This is mainly induced by isolation, the unpredictable situation and by the fact that they have to reside on a grid for optimal collection of excrement, which prevents them from behaving naturally (150). To minimize the discomfort, mice were acclimatized to the metabolic cage before the start of the experiment, the room temperature was increased and concaves were provided (151).

Male versus female mice

Traditionally, male mice are preferentially used for biomedical research (152). The main reason is the widely held belief that female mice are intrinsically more variable than males, due to their cyclical reproductive hormones. Although this influence is probably minor, the employment of both genders would be preferential in research, to create a reflection of the human population (153). The major disadvantage to using male mice is aggression, which might affect the experimental outcome. Fortunately, there exist ways to minimize aggressive behavior, for example by spraying lavender scent. For the

experiments described in **Chapters 3** and **4** of this thesis, male mice were used, whereas for **Chapter 2** female mice were used. We anticipated serious distress due to cisplatin treatment, and preferred to use female mice to minimize the chance of dropouts due to fighting in combination with their weakened condition. Different studies have reported gender-related differences on several parameters measured during cisplatin treatment. For example, it has been shown that estrogen blocks the protective effect of erythropoietin on cisplatin-induced nephrotoxicity (154). In contrast, other studies reported lower sensitivity of female tissue or patients to this cytostatic agent (155, 156). We assumed that the development of renal toxicity and hypomagnesemia would be equal in male mice. However, it would be best to test these effects of cisplatin in both genders. In male and female mice, hydrochlorothiazide and furosemide were found to be similarly effective, whereas a higher peak sodium excretion rate in male subjects was observed compared with female subjects (157). Strikingly, in rats the peak sodium excretion rate appeared to be higher for female mice (158).

The age of the mice

Age is likely a more important parameter than gender, especially concerning treatment with diuretics, like furosemide (159, 160). The indication for furosemide treatment is highest in the elderly (161, 162), as the prevalence of hypertension increases with age (163). This cohort of patients often suffers from multiple chronic diseases. The consequence is that the elderly take multiple medications, which increases the danger of complications due to drug-drug interactions (164). Multiple medications, in combination with declined organ function, especially of liver and kidney, further hampers successful loop diuretic treatment in the elderly (160). Therefore, a mouse study investigating the effects of chronic furosemide use on Mg^{2+} balance, using mice of different age-categories and/or specific infirmities of old age, would be interesting.

Conclusions

Figure 3 summarizes the main findings and limitations of the experiments presented in this thesis. Clinical recommendations concerning Mg^{2+} balance and future research challenges are listed. The discovery of mutations in the DCT resulting in a phenotype that includes hypomagnesemia confirms the major role of transcellular Mg^{2+} reabsorption by the kidney in Mg^{2+} homeostasis. The experiments performed in this thesis showed that the DCT has an impressive capacity to adapt to external factors that affect the Mg^{2+} balance. Conversely, when the DCT itself is damaged, for example by cisplatin treatment, this has immediate negative consequences for Mg^{2+} balance. Furthermore, dietary Mg^{2+} restriction of mice indicated that PV and HNF1B play an essential role in Mg^{2+} reabsorption. Future investigations should examine the process of Mg^{2+} transport to the basolateral side of the DCT and extrusion over the plasma membrane. In addition, increasing awareness amongst physicians for recognition and monitoring patients at risk for hypomagnesemia is desired, especially since hypomagnesemia can cause secondary hypocalcemia and hypokalemia, which can only be corrected by Mg^{2+} supplementation.

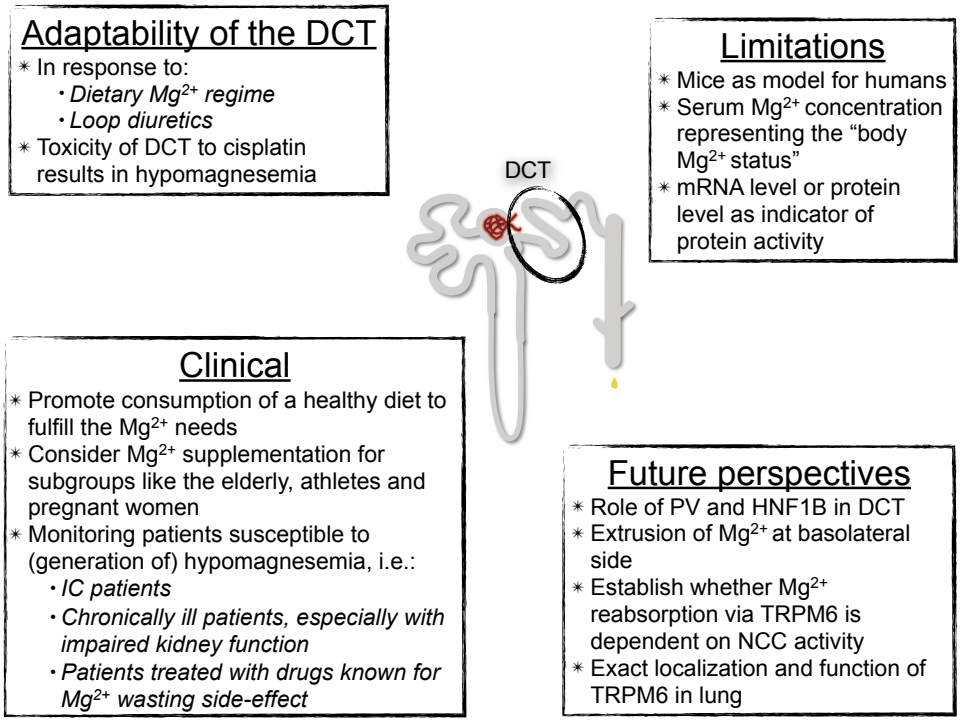

Figure 3. Overview of most important results, limitations, recommendations and future perspectives as described in more detail in this chapter.

References

1. Dai, L.J., Ritchie, G., Kerstan, D., et al. Magnesium transport in the renal distal convoluted tubule. *Physiol Rev* 81:51-84. 2001.
2. Quamme, G.A. Renal magnesium handling: new insights in understanding old problems. *Kidney Int* 52:1180-1195. 1997.
3. Voets, T., Nilius, B., Hoefs, S., et al. TRPM6 forms the Mg2+ influx channel involved in intestinal and renal Mg2+ absorption. *J Biol Chem* 279:19-25. 2004.
4. van der Wijst, J., Hoenderop, J.G., and Bindels, R.J. Epithelial Mg2+ channel TRPM6: insight into the molecular regulation. *Magnes Res* 22:127-132. 2009.
5. Groenestege, W.M., Thebault, S., van der Wijst, J., et al. Impaired basolateral sorting of pro-EGF causes isolated recessive renal hypomagnesemia. *J Clin Invest* 117:2260-2267. 2007.
6. Dimke, H., Hoenderop, J.G., and Bindels, R.J. Hereditary tubular transport disorders: implications for renal handling of Ca2+ and Mg2+. *Clin Sci (Lond)* 118:1-18. 2010.
7. Rang, H.P. Drug discovery and development. *Chruchill Livingstone Elsevier*. 2006.
8. Loriot, Y., Perlemuter, G., Malka, D., et al. Drug insight: gastrointestinal and hepatic adverse effects of molecular-targeted agents in cancer therapy. *Nat Clin Pract Oncol* 5:268-278. 2008.
9. Ellison, D.H. Diuretic drugs and the treatment of edema: from clinic to bench and back again. *Am J Kidney Dis* 23:623-643. 1994.
10. Informatics, I.I.f.H. The Global Use of Medicines: Outlook Through 2015. 2011.
11. Hajjar, E.R., Cafiero, A.C., and Hanlon, J.T. Polypharmacy in elderly patients. *Am J Geriatr Pharmacother* 5:345-351. 2007.
12. Lameris, A.L., Monnens, L.A., Bindels, R.J., et al. Drug-induced alterations in Mg2+ homoeostasis. *Clin Sci (Lond)* 123:1-14. 2012.
13. Rosenberg, B., VanCamp, L., Trosko, J.E., et al. Platinum compounds: a new class of potent antitumour agents. *Nature* 222:385-386. 1969.
14. Roberts, J.J., and Pascoe, J.M. Cross-linking of complementary strands of DNA in mammalian cells by antitumour platinum compounds. *Nature* 235:282-284. 1972.
15. Dobyan, D.C., Levi, J., Jacobs, C., et al. Mechanism of cis-platinum nephrotoxicity: II. Morphologic observations. *J Pharmacol Exp Ther* 213:551-556. 1980.
16. Mavichak, V., Wong, N.L., Quamme, G.A., et al. Studies on the pathogenesis of cisplatin-induced hypomagnesemia in rats. *Kidney Int* 28:914-921. 1985.
17. Daugaard, G., Abildgaard, U., Larsen, S., et al. Functional and histopathological changes in dog kidneys after administration of cisplatin. *Ren Physiol* 10:54-64. 1987.
18. Gonzales-Vitale, J.C., Hayes, D.M., Cvitkovic, E., et al. The renal pathology in clinical trials of cis-platinum (II) diamminedichloride. *Cancer* 39:1362-1371. 1977.
19. Rosenberg, B. Platinum coordination complexes in cancer chemotherapy. *Naturwissenschaften* 60:399-406. 1973.
20. Yao, X., Panichpisal, K., Kurtzman, N., et al. Cisplatin nephrotoxicity: a review. *Am J Med Sci* 334:115-124. 2007.
21. Arany, I., and Safirstein, R.L. Cisplatin nephrotoxicity. *Semin Nephrol* 23:460-464. 2003.
22. Lam, M., and Adelstein, D.J. Hypomagnesemia and renal magnesium wasting in patients treated with cisplatin. *Am J Kidney Dis* 8:164-169. 1986.
23. Schilsky, R.L., and Anderson, T. Hypomagnesemia and renal magnesium wasting in patients receiving cisplatin. *Ann Intern Med* 90:929-931. 1979.
24. Vassal, G., Rubie, H., Kalifa, C., et al. Hyponatremia and renal sodium wasting in patients receiving cisplatinum. *Pediatr Hematol Oncol* 4:337-344. 1987.
25. Ariceta, G., Rodriguez-Soriano, J., Vallo, A., et al. Acute and chronic effects of cisplatin

therapy on renal magnesium homeostasis. *Med Pediatr Oncol* 28:35-40. 1997.
26. Jones, D.P., and Chesney, R.W. Renal toxicity of cancer chemotherapeutic agents in children: ifosfamide and cisplatin. *Curr Opin Pediatr* 7:208-213. 1995.
27. Panichpisal, K., Angulo-Pernett, F., Selhi, S., et al. Gitelman-like syndrome after cisplatin therapy: a case report and literature review. *BMC Nephrol* 7:10. 2006.
28. Lajer, H., and Daugaard, G. Cisplatin and hypomagnesemia. *Cancer Treat Rev* 25:47-58. 1999.
29. Mavichak, V., Coppin, C.M., Wong, N.L., et al. Renal magnesium wasting and hypocalciuria in chronic cis-platinum nephropathy in man. *Clin Sci (Lond)* 75:203-207. 1988.
30. Ishida, S., Lee, J., Thiele, D.J., et al. Uptake of the anticancer drug cisplatin mediated by the copper transporter Ctr1 in yeast and mammals. *Proc Natl Acad Sci U S A* 99:14298-14302. 2002.
31. More, S.S., Akil, O., Ianculescu, A.G., et al. Role of the copper transporter, CTR1, in platinum-induced ototoxicity. *J Neurosci* 30:9500-9509. 2010.
32. Beretta, G.L., Gatti, L., Tinelli, S., et al. Cellular pharmacology of cisplatin in relation to the expression of human copper transporter CTR1 in different pairs of cisplatin-sensitive and -resistant cells. *Biochem Pharmacol* 68:283-291. 2004.
33. Yang, Z., Schumaker, L.M., Egorin, M.J., et al. Cisplatin preferentially binds mitochondrial DNA and voltage-dependent anion channel protein in the mitochondrial membrane of head and neck squamous cell carcinoma: possible role in apoptosis. *Clin Cancer Res* 12:5817-5825. 2006.
34. Wang, D., and Lippard, S.J. Cellular processing of platinum anticancer drugs. *Nat Rev Drug Discov* 4:307-320. 2005.
35. Linss, W., and Geyer, G. [the Electron Microscopic Structure of the Kidney Tubule in Rana Esculenta]. *Anat Anz* 115:281-296. 1964.
36. Qian, W., Nishikawa, M., Haque, A.M., et al. Mitochondrial density determines the cellular sensitivity to cisplatin-induced cell death. *Am J Physiol Cell Physiol* 289:C1466-1475. 2005.
37. Pabla, N., Dong, G., Jiang, M., et al. Inhibition of PKCdelta reduces cisplatin-induced nephrotoxicity without blocking chemotherapeutic efficacy in mouse models of cancer. *J Clin Invest* 121. 2011.
38. Kim, J.H., Park, D.J., Yun, J.C., et al. Human adipose tissue-derived mesenchymal stem cells protect kidneys from cisplatin nephrotoxicity in rats. *Am J Physiol Renal Physiol* 302:F1141-1150. 2012.
39. Galluzzi, L., Senovilla, L., Vitale, I., et al. Molecular mechanisms of cisplatin resistance. *Oncogene* 31:1869-1883. 2012.
40. O'Brien, J.G., Chennubhotla, S.A., and Chennubhotla, R.V. Treatment of edema. *Am Fam Physician* 71:2111-2117. 2005.
41. Jentzer, J.C., DeWald, T.A., and Hernandez, A.F. Combination of loop diuretics with thiazide-type diuretics in heart failure. *J Am Coll Cardiol* 56:1527-1534. 2010.
42. Hendry, B.M., and Ellory, J.C. Molecular sites for diuretic action. *Trends Pharmacol Sci* 9:416-421. 1988.
43. Nijenhuis, T., Vallon, V., van der Kemp, A.W., et al. Enhanced passive Ca2+ reabsorption and reduced Mg2+ channel abundance explains thiazide-induced hypocalciuria and hypomagnesemia. *J Clin Invest* 115:1651-1658. 2005.
44. Di Stefano, A., Roinel, N., de Rouffignac, C., et al. Transepithelial Ca2+ and Mg2+ transport in the cortical thick ascending limb of Henle's loop of the mouse is a voltage-dependent process. *Ren Physiol Biochem* 16:157-166. 1993.
45. Quamme, G.A. Effect of furosemide on calcium and magnesium transport in the rat nephron. *Am J Physiol* 241:F340-347. 1981.
46. Lee, A.J., Chen, Y.H., Chu, M.L., et al. [Effect of furosemide on renal magnesium and calcium excretion of different ages (II)]. *Zhonghua Min Guo Xiao Er Ke Yi Xue Hui Za Zhi* 35:215-220. 1994.

47. Davies, D.L., and Fraser, R. Do diuretics cause magnesium deficiency? *Br J Clin Pharmacol* 36:1-10. 1993.
48. Caddell, J.L. Protection by magnesium of renal calcinosis in furosemide-treated weanling rats with moderate magnesium deficiency. *Biol Neonate* 48:49-58. 1985.
49. Cohen, N., Almoznino-Sarafian, D., Zaidenstein, R., et al. Serum magnesium aberrations in furosemide (frusemide) treated patients with congestive heart failure: pathophysiological correlates and prognostic evaluation. *Heart* 89:411-416. 2003.
50. Loon, N.R., Wilcox, C.S., and Unwin, R.J. Mechanism of impaired natriuretic response to furosemide during prolonged therapy. *Kidney Int* 36:682-689. 1989.
51. Ellison, D.H., Velazquez, H., and Wright, F.S. Adaptation of the distal convoluted tubule of the rat. Structural and functional effects of dietary salt intake and chronic diuretic infusion. *J Clin Invest* 83:113-126. 1989.
52. Stanton, B.A., and Kaissling, B. Adaptation of distal tubule and collecting duct to increased Na delivery. II. Na+ and K+ transport. *Am J Physiol* 255:F1269-1275. 1988.
53. Abdallah, J.G., Schrier, R.W., Edelstein, C., et al. Loop diuretic infusion increases thiazide-sensitive Na(+)/Cl(-)-cotransporter abundance: role of aldosterone. *J Am Soc Nephrol* 12:1335-1341. 2001.
54. Woudenberg-Vrenken, T.E., Sukinta, A., van der Kemp, A.W., et al. Transient receptor potential melastatin 6 knockout mice are lethal whereas heterozygous deletion results in mild hypomagnesemia. *Nephron Physiol* 117:p11-19. 2011.
55. Knauf, H., Mutschler, E., Velazquez, H., et al. Torasemide significantly reduces thiazide-induced potassium and magnesium loss despite supra-additive natriuresis. *Eur J Clin Pharmacol* 65:465-472. 2009.
56. Tedla, F.M., Brar, A., Browne, R., et al. Hypertension in chronic kidney disease: navigating the evidence. *Int J Hypertens* 2011:132405. 2011.
57. Wu, X., Ackermann, U., and Sonnenberg, H. Potassium depletion and salt-sensitive hypertension in Dahl rats: effect on calcium, magnesium, and phosphate excretions. *Clin Exp Hypertens* 17:989-1008. 1995.
58. Martin, B.J., and Milligan, K. Diuretic-associated hypomagnesemia in the elderly. *Arch Intern Med* 147:1768-1771. 1987.
59. Wong, E.T., Rude, R.K., Singer, F.R., et al. A high prevalence of hypomagnesemia and hypermagnesemia in hospitalized patients. *Am J Clin Pathol* 79:348-352. 1983.
60. Ryzen, E. Magnesium homeostasis in critically ill patients. *Magnesium* 8:201-212. 1989.
61. Dunn, M.J., and Walser, M. Magnesium depletion in normal man. *Metabolism* 15:884-895. 1966.
62. Groenestege, W.M., Hoenderop, J.G., van den Heuvel, L., et al. The epithelial Mg2+ channel transient receptor potential melastatin 6 is regulated by dietary Mg2+ content and estrogens. *J Am Soc Nephrol* 17:1035-1043. 2006.
63. Ikura, M., and Ames, J.B. Genetic polymorphism and protein conformational plasticity in the calmodulin superfamily: two ways to promote multifunctionality. *Proc Natl Acad Sci U S A* 103:1159-1164. 2006.
64. Belge, H., Gailly, P., Schwaller, B., et al. Renal expression of parvalbumin is critical for NaCl handling and response to diuretics. *Proc Natl Acad Sci U S A* 104:14849-14854. 2007.
65. Simon, D.B., Nelson-Williams, C., Bia, M.J., et al. Gitelman's variant of Bartter's syndrome, inherited hypokalaemic alkalosis, is caused by mutations in the thiazide-sensitive Na-Cl cotransporter. *Nat Genet* 12:24-30. 1996.
66. Schultheis, P.J., Lorenz, J.N., Meneton, P., et al. Phenotype resembling Gitelman's syndrome in mice lacking the apical Na+-Cl- cotransporter of the distal convoluted tubule. *J Biol Chem* 273:29150-29155. 1998.

67. Goodarzi, H., Najafabadi, H.S., Oikonomou, P., et al. Systematic discovery of structural elements governing stability of mammalian messenger RNAs. *Nature* 485:264-268. 2012.
68. Tzeng, S.R., and Kalodimos, C.G. Protein activity regulation by conformational entropy. *Nature* 488:236-240. 2012.
69. Beltrao, P., Albanese, V., Kenner, L.R., et al. Systematic functional prioritization of protein posttranslational modifications. *Cell* 150:413-425. 2012.
70. Britton, J., Pavord, I., Richards, K., et al. Dietary magnesium, lung function, wheezing, and airway hyperreactivity in a random adult population sample. *Lancet* 344:357-362. 1994.
71. Gontijo-Amaral, C., Ribeiro, M.A., Gontijo, L.S., et al. Oral magnesium supplementation in asthmatic children: a double-blind randomized placebo-controlled trial. *Eur J Clin Nutr* 61:54-60. 2007.
72. Anast, C.S., Mohs, J.M., Kaplan, S.L., et al. Evidence for parathyroid failure in magnesium deficiency. *Science* 177:606-608. 1972.
73. Reddy, C.R., Coburn, J.W., Hartenbower, D.L., et al. Studies on mechanisms of hypocalcemia of magnesium depletion. *J Clin Invest* 52:3000-3010. 1973.
74. Segawa, H., Onitsuka, A., Furutani, J., et al. Npt2a and Npt2c in mice play distinct and synergistic roles in inorganic phosphate metabolism and skeletal development. *Am J Physiol Renal Physiol* 297:F671-678. 2009.
75. Perwad, F., Azam, N., Zhang, M.Y., et al. Dietary and serum phosphorus regulate fibroblast growth factor 23 expression and 1,25-dihydroxyvitamin D metabolism in mice. *Endocrinology* 146:5358-5364. 2005.
76. Hermans, C., Lefebvre, C., Devogelaer, J.P., et al. Hypocalcaemia and chronic alcohol intoxication: transient hypoparathyroidism secondary to magnesium deficiency. *Clin Rheumatol* 15:193-196. 1996.
77. Monteleone, J.A., Lee, J.B., Tashjian, A.H., Jr., et al. Transient neonatal hypocalcemia, hypomagnesemia, and high serum parathyroid hormone with maternal hyperparathyroidism. *Ann Intern Med* 82:670-672. 1975.
78. van Abel, M., Hoenderop, J.G., van der Kemp, A.W., et al. Coordinated control of renal Ca(2+) transport proteins by parathyroid hormone. *Kidney Int* 68:1708-1721. 2005.
79. Duran, M.J., Borst, G.C., 3rd, Osburne, R.C., et al. Concurrent renal hypomagnesemia and hypoparathyroidism with normal parathormone responsiveness. *Am J Med* 76:151-154. 1984.
80. Rude, R.K., Oldham, S.B., and Singer, F.R. Functional hypoparathyroidism and parathyroid hormone end-organ resistance in human magnesium deficiency. *Clin Endocrinol (Oxf)* 5:209-224. 1976.
81. Suh, S.M., Tashjian, A.H., Jr., Matsuo, N., et al. Pathogenesis of hypocalcemia in primary hypomagnesemia: normal end-organ responsiveness to parathyroid hormone, impaired parathyroid gland function. *J Clin Invest* 52:153-160. 1973.
82. Singh, R., Bhat, M.H., and Bhansali, A. Hypomagnesaemia masquerading as hypoparathyroidism. *J Assoc Physicians India* 54:411-412. 2006.
83. Freitag, J.J., Martin, K.J., Conrades, M.B., et al. Evidence for skeletal resistance to parathyroid hormone in magnesium deficiency. Studies in isolated perfused bone. *J Clin Invest* 64:1238-1244. 1979.
84. Rude, R.K., Oldham, S.B., Sharp, C.F., Jr., et al. Parathyroid hormone secretion in magnesium deficiency. *J Clin Endocrinol Metab* 47:800-806. 1978.
85. Shoback, D., Thatcher, J., Leombruno, R., et al. Effects of extracellular Ca++ and Mg++ on cytosolic Ca++ and PTH release in dispersed bovine parathyroid cells. *Endocrinology* 113:424-426. 1983.
86. Ferment, O., Garnier, P.E., and Touitou, Y. Comparison of the feedback effect of magnesium and calcium on parathyroid hormone secretion in man. *J Endocrinol* 113:117-122. 1987.

87. Rude, R.K. Magnesium deficiency: a cause of heterogeneous disease in humans. *J Bone Miner Res* 13:749-758. 1998.
88. Ferre, S., Hoenderop, J.G., and Bindels, R.J. Sensing mechanisms involved in Ca2+ and Mg2+ homeostasis. *Kidney Int* 82:1157-1166. 2012.
89. Ford, E.S. Race, education, and dietary cations: findings from the Third National Health And Nutrition Examination Survey. *Ethn Dis* 8:10-20. 1998.
90. Vaquero, M.P. Magnesium and trace elements in the elderly: intake, status and recommendations. *J Nutr Health Aging* 6:147-153. 2002.
91. Wu, S.J., Chang, Y.H., Wei, I.L., et al. Intake levels and major food sources of energy and nutrients in the Taiwanese elderly. *Asia Pac J Clin Nutr* 14:211-220. 2005.
92. Franz, K.B. Magnesium intake during pregnancy. *Magnesium* 6:18-27. 1987.
93. Galan, P., Preziosi, P., Durlach, V., et al. Dietary magnesium intake in a French adult population. *Magnes Res* 10:321-328. 1997.
94. Schimatschek, H.F., and Rempis, R. Prevalence of hypomagnesemia in an unselected German population of 16,000 individuals. *Magnes Res* 14:283-290. 2001.
95. Reedy, J., and Krebs-Smith, S.M. A comparison of food-based recommendations and nutrient values of three food guides: USDA's MyPyramid, NHLBI's Dietary Approaches to Stop Hypertension Eating Plan, and Harvard's Healthy Eating Pyramid. *J Am Diet Assoc* 108:522-528. 2008.
96. Siervo, M., Montagnese, C., Mathers, J.C., et al. Sugar consumption and global prevalence of obesity and hypertension: an ecological analysis. *Public Health Nutr*:1-10. 2013.
97. Chacko, S.A., Sul, J., Song, Y., et al. Magnesium supplementation, metabolic and inflammatory markers, and global genomic and proteomic profiling: a randomized, double-blind, controlled, crossover trial in overweight individuals. *Am J Clin Nutr* 93:463-473. 2011.
98. Hruby, A., Ngwa, J.S., Renstrom, F., et al. Higher magnesium intake is associated with lower fasting glucose and insulin, with no evidence of interaction with select genetic loci, in a meta-analysis of 15 CHARGE Consortium Studies. *J Nutr* 143:345-353. 2013.
99. Larsson, S.C., and Wolk, A. Magnesium intake and risk of type 2 diabetes: a meta-analysis. *J Intern Med* 262:208-214. 2007.
100. Ford, E.S., Li, C., McGuire, L.C., et al. Intake of dietary magnesium and the prevalence of the metabolic syndrome among U.S. adults. *Obesity (Silver Spring)* 15:1139-1146. 2007.
101. Nielsen, F.H., and Lukaski, H.C. Update on the relationship between magnesium and exercise. *Magnes Res* 19:180-189. 2006.
102. Durlach, J., Pages, N., Bac, P., et al. New data on the importance of gestational Mg deficiency. *Magnes Res* 17:116-125. 2004.
103. Altman, D., Carroli, G., Duley, L., et al. Do women with pre-eclampsia, and their babies, benefit from magnesium sulphate? The Magpie Trial: a randomised placebo-controlled trial. *Lancet* 359:1877-1890. 2002.
104. Supakatisant, C., and Phupong, V. Oral magnesium for relief in pregnancy-induced leg cramps: a randomised controlled trial. *Matern Child Nutr*. 2012.
105. do Pazo-Oubina, F., Estefanell-Tejero, A., Riu-Viladoms, G., et al. Magnesium monitoring practice in monoclonal anti-epidermal growth factor receptor antibodies therapy. *J Clin Pharm Ther* 38:101-103. 2013.
106. Lajer, H., Kristensen, M., Hansen, H.H., et al. Magnesium depletion enhances cisplatin-induced nephrotoxicity. *Cancer Chemother Pharmacol* 56:535-542. 2005.
107. Ben Rayana, M.C., Burnett, R.W., Covington, A.K., et al. IFCC guideline for sampling, measuring and reporting ionized magnesium in plasma. *Clin Chem Lab Med* 46:21-26. 2008.
108. Newhouse, I.J., Johnson, K.P., Montelpare, W.J., et al. Variability within individuals of plasma ionic magnesium concentrations. *BMC Physiol* 2:6. 2002.
109. Arnaud, M.J. Update on the assessment of magnesium status. *Br J Nutr* 99 Suppl 3:S24-36. 2008.

110. Agus, Z.S. Hypomagnesemia. *J Am Soc Nephrol* 10:1616-1622. 1999.
111. Willox, J.C., McAllister, E.J., Sangster, G., et al. Effects of magnesium supplementation in testicular cancer patients receiving cis-platin: a randomised trial. *Br J Cancer* 54:19-23. 1986.
112. Dorup, I., Skajaa, K., and Thybo, N.K. Oral magnesium supplementation restores the concentrations of magnesium, potassium and sodium-potassium pumps in skeletal muscle of patients receiving diuretic treatment. *J Intern Med* 233:117-123. 1993.
113. Ceremuzynski, L., Gebalska, J., Wolk, R., et al. Hypomagnesemia in heart failure with ventricular arrhythmias. Beneficial effects of magnesium supplementation. *J Intern Med* 247:78-86. 2000.
114. Barragan-Rodriguez, L., Rodriguez-Moran, M., and Guerrero-Romero, F. Efficacy and safety of oral magnesium supplementation in the treatment of depression in the elderly with type 2 diabetes: a randomized, equivalent trial. *Magnes Res* 21:218-223. 2008.
115. Agarwal, R., Iezhitsa, I., Awaludin, N.A., et al. Effects of magnesium taurate on the onset and progression of galactose-induced experimental cataract: In vivo and in vitro evaluation. *Exp Eye Res* 110C:35-43. 2013.
116. Song, Y., He, K., Levitan, E.B., et al. Effects of oral magnesium supplementation on glycaemic control in Type 2 diabetes: a meta-analysis of randomized double-blind controlled trials. *Diabet Med* 23:1050-1056. 2006.
117. Garrido, N., Perez-Martos, A., Faro, M., et al. Cisplatin-mediated impairment of mitochondrial DNA metabolism inversely correlates with glutathione levels. *Biochem J* 414:93-102. 2008.
118. Nijenhuis, T., Hoenderop, J.G., and Bindels, R.J. Downregulation of Ca(2+) and Mg(2+) transport proteins in the kidney explains tacrolimus (FK506)-induced hypercalciuria and hypomagnesemia. *J Am Soc Nephrol* 15:549-557. 2004.
119. Sabbagh, F., El Tawil, Z., Lecerf, F., et al. Impact of cyclosporine A on magnesium homeostasis: clinical observation in lung transplant recipients and experimental study in mice. *Transplantation* 86:436-444. 2008.
120. Ikari, A., Okude, C., Sawada, H., et al. Down-regulation of TRPM6-mediated magnesium influx by cyclosporin A. *Naunyn Schmiedebergs Arch Pharmacol* 377:333-343. 2008.
121. Ledeganck, K.J., Boulet, G.A., Horvath, C.A., et al. Expression of renal distal tubule transporters TRPM6 and NCC in a rat model of cyclosporine nephrotoxicity and effect of EGF treatment. *Am J Physiol Renal Physiol* 301:F486-493. 2011.
122. Nair, A.V., Hocher, B., Verkaart, S., et al. Loss of insulin-induced activation of TRPM6 magnesium channels results in impaired glucose tolerance during pregnancy. *Proc Natl Acad Sci U S A* 109:11324-11329. 2012.
123. Ward, D.T., McLarnon, S.J., and Riccardi, D. Aminoglycosides increase intracellular calcium levels and ERK activity in proximal tubular OK cells expressing the extracellular calcium-sensing receptor. *J Am Soc Nephrol* 13:1481-1489. 2002.
124. Sassen, M.C., Kim, S.W., Kwon, T.H., et al. Dysregulation of renal sodium transporters in gentamicin-treated rats. *Kidney Int* 70:1026-1037. 2006.
125. Lee, C.T., Chen, H.C., Ng, H.Y., et al. Renal adaptation to gentamicin-induced mineral loss. *Am J Nephrol* 35:279-286. 2012.
126. Nijenhuis, T., Renkema, K.Y., Hoenderop, J.G., et al. Acid-base status determines the renal expression of Ca2+ and Mg2+ transport proteins. *J Am Soc Nephrol* 17:617-626. 2006.
127. Faroqui, S., Sheriff, S., and Amlal, H. Metabolic acidosis has dual effects on sodium handling by rat kidney. *Am J Physiol Renal Physiol* 291:F322-331. 2006.
128. Fanestil, D.D., Hyde, R.H., Blakely, P., et al. Dietary magnesium, not calcium, regulates renal thiazide receptor. *J Am Soc Nephrol* 10:458-463. 1999.
129. Kiuchi-Saishin, Y., Gotoh, S., Furuse, M., et al. Differential expression patterns of claudins, tight junction membrane

proteins, in mouse nephron segments. *J Am Soc Nephrol* 13:875-886. 2002.
130. Simon, D.B., Lu, Y., Choate, K.A., et al. Paracellin-1, a renal tight junction protein required for paracellular Mg2+ resorption. *Science* 285:103-106. 1999.
131. Konrad, M., Schaller, A., Seelow, D., et al. Mutations in the tight-junction gene claudin 19 (CLDN19) are associated with renal magnesium wasting, renal failure, and severe ocular involvement. *Am J Hum Genet* 79:949-957. 2006.
132. Cao, Y., Liao, C., Tan, A., et al. Meta-analysis of incidence and risk of hypomagnesemia with cetuximab for advanced cancer. *Chemotherapy* 56:459-465. 2010.
133. Tejpar, S., Piessevaux, H., Claes, K., et al. Magnesium wasting associated with epidermal-growth-factor receptor-targeting antibodies in colorectal cancer: a prospective study. *Lancet Oncol* 8:387-394. 2007.
134. Vickers, M.M., Karapetis, C.S., Tu, D., et al. Association of hypomagnesemia with inferior survival in a phase III, randomized study of cetuximab plus best supportive care versus best supportive care alone: NCIC CTG/AGITG CO.17. *Ann Oncol* 24:953-960. 2013.
135. Thebault, S., Alexander, R.T., Tiel Groenestege, W.M., et al. EGF increases TRPM6 activity and surface expression. *J Am Soc Nephrol* 20:78-85. 2009.
136. Megías Vericat, J., Ruiz Ramos, J., Reig Aguado, J., et al. DGI-041 Hypomagnesemia as a Possible Marker of Effectiveness in Patients Treated with Panitumumab *Eur J Hosp Pharm* 20:A110. 2013.
137. Dempsey, P.J., Meise, K.S., Yoshitake, Y., et al. Apical enrichment of human EGF precursor in Madin-Darby canine kidney cells involves preferential basolateral ectodomain cleavage sensitive to a metalloprotease inhibitor. *J Cell Biol* 138:747-758. 1997.
138. Tong, Q., and Stockand, J.D. Receptor tyrosine kinases mediate epithelial Na(+) channel inhibition by epidermal growth factor. *Am J Physiol Renal Physiol* 288:F150-161. 2005.
139. Quigley, R., Kennerly, D.A., Sheu, J.N., et al. Stimulation of proximal convoluted tubule phosphate transport by epidermal growth factor: signal transduction. *Am J Physiol* 269:F339-344. 1995.
140. Humes, H.D., Cieslinski, D.A., Coimbra, T.M., et al. Epidermal growth factor enhances renal tubule cell regeneration and repair and accelerates the recovery of renal function in postischemic acute renal failure. *J Clin Invest* 84:1757-1761. 1989.
141. Journe, F., Wattiez, R., Piron, A., et al. Renal epidermal growth factor precursor: proteolytic processing in an in vitro cell-free system. *Biochim Biophys Acta* 1357:18-30. 1997.
142. Dong, J., Opresko, L.K., Chrisler, W., et al. The membrane-anchoring domain of epidermal growth factor receptor ligands dictates their ability to operate in juxtacrine mode. *Mol Biol Cell* 16:2984-2998. 2005.
143. Mroczkowski, B., Reich, M., Chen, K., et al. Recombinant human epidermal growth factor precursor is a glycosylated membrane protein with biological activity. *Mol Cell Biol* 9:2771-2778. 1989.
144. Dong, J., and Wiley, H.S. Trafficking and proteolytic release of epidermal growth factor receptor ligands are modulated by their membrane-anchoring domains. *J Biol Chem* 275:557-564. 2000.
145. Le Gall, S.M., Auger, R., Dreux, C., et al. Regulated cell surface pro-EGF ectodomain shedding is a zinc metalloprotease-dependent process. *J Biol Chem* 278:45255-45268. 2003.
146. Hobert, M.E., Friend, L.A., and Carlin, C.R. Regulation of EGF signaling by cell polarity in MDCK kidney epithelial cells. *J Cell Physiol* 181:330-341. 1999.
147. Pennacchio, L.A. Insights from human/mouse genome comparisons. *Mamm Genome* 14:429-436. 2003.
148. Peters, L.L., Robledo, R.F., Bult, C.J., et al. The mouse as a model for human biology: a resource guide for complex trait analysis. *Nat Rev Genet* 8:58-69. 2007.

149. Ito, R., Takahashi, T., Katano, I., et al. Current advances in humanized mouse models. *Cell Mol Immunol* 9:208-214. 2012.
150. Kurien, B.T., Everds, N.E., and Scofield, R.H. Experimental animal urine collection: a review. *Lab Anim* 38:333-361. 2004.
151. Belz, E.E., Kennell, J.S., Czambel, R.K., et al. Environmental enrichment lowers stress-responsive hormones in singly housed male and female rats. *Pharmacol Biochem Behav* 76:481-486. 2003.
152. Zucker, I., and Beery, A.K. Males still dominate animal studies. *Nature* 465:690. 2010.
153. Hughes, R.N. Sex does matter: comments on the prevalence of male-only investigations of drug effects on rodent behaviour. *Behav Pharmacol* 18:583-589. 2007.
154. Pezeshki, Z., Nematbakhsh, M., Mazaheri, S., et al. Estrogen Abolishes Protective Effect of Erythropoietin against Cisplatin-Induced Nephrotoxicity in Ovariectomized Rats. *ISRN Oncol* 2012:890310. 2012.
155. Huang, R.S., Kistner, E.O., Bleibel, W.K., et al. Effect of population and gender on chemotherapeutic agent-induced cytotoxicity. *Mol Cancer Ther* 6:31-36. 2007.
156. Stakisaitis, D., Dudeniene, G., Jankunas, R.J., et al. Cisplatin increases urinary sodium excretion in rats: gender-related differences. *Medicina (Kaunas)* 46:45-50. 2010.
157. Franson, K.L., Kuk, J.M., Lam, N.P., et al. Gender effect on diuretic response to hydrochlorothiazide and furosemide. *Int J Clin Pharmacol Ther* 34:101-105. 1996.
158. Brandoni, A., Villar, S.R., and Torres, A.M. Gender-related differences in the pharmacodynamics of furosemide in rats. *Pharmacology* 70:107-112. 2004.
159. McLean, A.J., and Le Couteur, D.G. Aging biology and geriatric clinical pharmacology. *Pharmacol Rev* 56:163-184. 2004.
160. Corsonello, A., Pedone, C., and Incalzi, R.A. Age-related pharmacokinetic and pharmacodynamic changes and related risk of adverse drug reactions. *Curr Med Chem* 17:571-584. 2010.
161. Kolzsch, M., Bolbrinker, J., Drager, D., et al. [Prescribing of antihypertensive drugs to elderly residents of nursing homes in Germany]. *Dtsch Med Wochenschr* 135:2400-2405. 2010.
162. van Kraaij, D.J., Jansen, R.W., de Gier, J.J., et al. Prescription patterns of diuretics in Dutch community-dwelling elderly patients. *Br J Clin Pharmacol* 46:403-407. 1998.
163. Kearney, P.M., Whelton, M., Reynolds, K., et al. Global burden of hypertension: analysis of worldwide data. *Lancet* 365:217-223. 2005.
164. Rosas-Carrasco, O., Garcia-Pena, C., Sanchez-Garcia, S., et al. The relationship between potential drug-drug interactions and mortality rate of elderly hospitalized patients. *Rev Invest Clin* 63:564-573. 2011.

Chapter 7

Nederlandse Samenvatting

Nederlandse Samenvatting

Hoofdstuk 1: Algemene Introductie

Magnesium (Mg^{2+}) is een belangrijke component van het menselijk lichaam. Het is het meest voorkomende intracellulaire tweewaardig positief geladen ion. Ongeveer 60% van het Mg^{2+} is opgeslagen in botweefsel, de rest bevindt zich met name in de skeletspieren en het bindweefsel. Mg^{2+} is betrokken bij verschillende enzymatische reacties, de synthese van DNA en eiwit en het heeft een sleutelfunctie in neuronen en spiercellen. De dagelijks aanbevolen inname aan Mg^{2+} voor volwassenen is 350 mg. Zaden, granen, groene bladgroenten, peulvruchten en noten zijn de rijkste Mg^{2+} bronnen, echter, enkel in onbewerkte vorm.

Regulatie van de Mg^{2+} balans, resulterend in een Mg^{2+} concentratie in het plasma tussen 0.7-1.1 mmol/L, is van levensbelang. Deze regulatie vindt plaats door Mg^{2+} opname door de darm (absorptie), uitwisseling met botweefsel en heropname door de nieren (resorptie). Met name dit laatste orgaan handhaaft de Mg^{2+} concentratie in het bloed door de mate van Mg^{2+} uitscheiding in de urine te bepalen. De menselijke nier bevat ongeveer 1 miljoen functionele eenheden, de nefronen. Elk nefron bestaat uit een glomerulus (nierlichaam) met daarop aansluitend de tubulus (nierbuis). Gemiddeld wordt 80% van de hoeveelheid Mg^{2+} in het bloed gefiltreerd door de glomerulus, de rest is gebonden aan eiwit. Het gefiltreerde bloed wordt de voorurine genoemd en komt terecht in de nierbuis. Bruikbare bestanddelen inclusief het meeste water worden geresorbeerd uit de voorurine naar het bloed, afvalproducten blijven achter en worden uitgescheiden via de urine. Het merendeel van het gefiltreerde Mg^{2+} wordt geresorbeerd in de nierbuis. Onder normale omstandigheden wordt slechts 3-5% van het Mg^{2+} filtraat via de urine uitgescheiden. De nier beschikt over een groot aanpassingsvermogen om te reageren op veranderingen in Mg^{2+} absorptie en verschuivingen van de hoeveelheid Mg^{2+} in het bot. In de proximale tubulus en het dikke opstijgende deel van de lis van Henle (TAL) gebeurt het grootste deel van de resorptie van het Mg^{2+} filtraat, door middel van passief paracellulair transport. De nauwkeurige afstemming vindt plaats in het distaal convoluut (DCT), waar Mg^{2+} actief en transcellulair wordt geresorbeerd. Het epitheliale Mg^{2+} kanaal TRPM6 dat specifiek tot expressie komt in het DCT is geïdentificeerd als poortwachter van dit transport. De afgelopen jaren is de moleculaire regulatie van TRPM6 duidelijker geworden door de ontdekking en karakterisering van verschillende bindingseiwitten. Daarnaast heeft DNA analyse van patiënten met geïsoleerde autosomale recessieve renale hypomagnesiëmie (IRH), epidermale groeifactor (EGF) onthuld als cruciaal magnesiotroop hormoon. Bovendien hebben andere erfelijkheidstudies van patiënten met Mg^{2+} verlies, aanvullende eiwitten ontdekt die essentieel zijn voor het Mg^{2+} transport in de nier. Voor de meeste van deze eiwitten is de functie inmiddels opgehelderd, maar voor sommige blijft deze (deels) onbekend.

In dit proefschrift ligt de focus op de bestudering van de (patho)fysiologische impact van externe factoren die aangrijpen op de Mg^{2+} balans. Zo werd het effect van de geneesmiddelen cisplatine en furosemide bestudeerd, alsmede de toediening van verschillende hoeveelheden Mg^{2+} in het dieet, dit alles in muisstudies. De functie en het belang van individuele 'magnesiotrope spelers' en de capaciteit van de nieren, in het

bijzonder van het DCT, om zich aan te passen aan deze uitdagende fysiologische omstandigheden, werd onderzocht.

Hoofdstuk 2: Cisplatine-geïnduceerde schade aan het distaal convoluut

Cisplatine is een effectief geneesmiddel in de strijd tegen solide tumoren die zich bevinden in bijvoorbeeld de eierstokken, baarmoeder, testis, hoofd-hals of longen. Het gebruik van dit geneesmiddel wordt echter beperkt door dosis-afhankelijke niertoxiciteit. Het merendeel van de cisplatine-behandelde patiënten ontwikkelt hypomagnesiëmie, vaak geassocieerd met een verminderde glomerulaire filtratiesnelheid (GFR), polyurie en andere elektrolytverstoringen.

Het doel van dit hoofdstuk is om het moleculaire mechanisme bloot te leggen dat ten grondslag ligt aan de bijwerking van het renale Mg^{2+} verlies. Twee groepen van elk 10 muizen werden 3-maal, eenmaal per vier dagen, geïnjecteerd met cisplatine of met controle vloeistof. De cisplatine-behandelde muizen ontwikkelden een significante polyurie, verlaagde creatinineklaring en een aanmerkelijk verlaagde plasma Mg^{2+} concentratie, terwijl plasma calcium (Ca^{2+}), natrium (Na^{+}) en kalium (K^{+}) waarden niet veranderd waren. Bepalingen van de 24-uurs urine toonden een aanzienlijk verhoogde Mg^{2+}, Ca^{2+}, Na^{+} en K^{+} excretie in de cisplatine-behandelde groep, terwijl de fosfaat (P_i) excretie niet was gewijzigd. De mRNA expressie van TRPM6, de NaCl cotransporteur (NCC) en parvalbumine (PV) in de nier, was significant verlaagd in de cisplatine groep. De expressie van genen die karakteristiek zijn voor andere delen van het nierbuisje waren onveranderd, behalve de expressie van claudine-16; deze was verhoogd door de cisplatine behandeling. De waargenomen afname van de hoeveelheid aan DCT-specifieke mRNA's werd bevestigd op eiwitniveau.

Deze studie heeft het DCT geïdentificeerd als renaal segment dat in belangrijke mate wordt beschadigd door cisplatine. Aangezien de functie van het DCT essentieel is voor regulatie van de Mg^{2+} balans, verklaart dit de hoge prevalentie van Mg^{2+} verlies in patiënten die met dit medicijn behandeld worden. Verder onderzoek zal moeten aantonen waarom juist het DCT verhoogde toxiciteit van cisplatine ondervindt; bijvoorbeeld door specifieke transporteurs die cisplatine in de cellen van het DCT brengen of doordat de relatief grote hoeveelheid mitochondria dit deel van de tubulus extra gevoelig maken.

Hoofdstuk 3: Het distaal convoluut compenseert voor furosemide-geïnduceerd Mg^{2+} verlies

Furosemide is een lisdiureticum dat de Na^{+}, K^{+}, $2Cl^{-}$ cotransporteur (NKCC2) in het TAL blokkeert. Hierdoor vermindert de resorptie van NaCl, verlaagt de lumen-positieve membraanpotentiaal en dit heeft weer tot gevolg dat het paracellulaire transport van Mg^{2+} en Ca^{2+} afneemt. Het directe effect van furosemide is dat het de Mg^{2+} excretie vergroot, maar het is niet duidelijk of chronische behandeling tot hypomagnesiëmie leidt.

De resultaten laten zien dat de muizen die een 7-daagse furosemide behandeling ondergingen een polyurie samen met verhoogd plasma Na^{+} ontwikkelen, terwijl de plasma K^{+}, Ca^{2+} en Mg^{2+} waarden onveranderd bleven. Bovendien werd de Na^{+}, K^{+}, Ca^{2+} en Mg^{2+} excretie via de urine niet beïnvloed door de chronische furosemide behandeling. Middels real-time PCR, immunohistochemie en immunoblotting werd vervolgens aangetoond dat de hoeveelheid TRPM6, NCC, het epitheliale Ca^{2+} kanaal TRPV5 en calbindine-D_{28K} was

toegenomen ten gevolge van de furosemide behandeling.

Uit deze resultaten kan de conclusie worden getrokken dat tijdens chronische behandeling met furosemide, verhoogde resorptie van Mg^{2+} via TRPM6 in DCT compenseert voor de verminderde resorptie van Mg^{2+} in TAL. Dat soms bij patiënten die behandeld worden met lisdiuretica desondanks hypomagnesiëmie wordt gediagnosticeerd, heeft waarschijnlijk te maken met comorbiditeit of onvoldoende Mg^{2+} inname. Het monitoren van de Mg^{2+} balans bij patiënten die furosemide of soortgelijke medicatie krijgen toegediend is daarom belangrijk.

Hoofdstuk 4: Het effect van Mg^{2+} restrictie op magnesiotrope en calciotrope genen

Voorgaande studies hebben laten zien dat een dieet met een minimale Mg^{2+} hoeveelheid resulteert in Mg^{2+} behoud door de nier, terwijl een verrijkt Mg^{2+} dieet de Mg^{2+} uitscheiding via de urine verhoogt. Ook is aangetoond dat de hoeveelheid Mg^{2+} in het dieet de expressie van TRPM6 in de nier beïnvloedt. Daarnaast kunnen veranderingen in de Mg^{2+} balans ook effect hebben op de Ca^{2+} huishouding. Het doel van deze studie was om te onderzoeken welke moleculaire consequenties restrictie van de hoeveelheid Mg^{2+} in het dieet heeft op andere Mg^{2+} transporteurs in de nier.

Een laag Mg^{2+} dieet resulteerde in een significante daling van de plasma Mg^{2+} en Ca^{2+} waarden. Ook was de excretie van deze ionen via de urine sterk verminderd. De expressie van de transcriptiefactoren HNF1B en TRPM6 was verhoogd in de nier als reactie op de Mg^{2+} restrictie, daar waar andere magnesiotrope spelers niet werden beïnvloed. HNF1B reguleert de transcriptie van FXYD2, die codeert voor de γ-subunit van de Na^+, K^+-ATPase. De regulatie van HNF1B wijst mogelijk op het belang van basolateraal Mg^{2+} transport in het DCT. Vervolgonderzoek naar HNF1B zou het mechanisme van Mg^{2+} uitscheiding over de plasmamembraan naar het bloedcompartiment kunnen ophelderen. Daarnaast was de expressie van PV verhoogd, terwijl NCC significant minder aanwezig was. PV staat bekend als een Ca^{2+}-bindend eiwit dat in de nier exclusief tot expressie komt in het DCT. Onze hypothese is dat hypomagnesiëmie resulteert in een verhoogd $[Ca^{2+}]_i$ in DCT cellen, wat tot een verminderde expressie van NCC leidt. Daarbij heeft de verhoogde hoeveelheid aan PV tot doel om het effect van $[Ca^{2+}]_i$ op NCC tegen te werken. Echter, een regulerende rol voor $[Mg^{2+}]_i$ zelf op PV en/of NCC kan niet uitgesloten worden. Deze data wijzen op een essentiële adaptieve rol voor het DCT gedurende hypomagnesiëmie, aangezien TRPM6, HNF1B, PV en NCC expressie niveaus waren aangepast.

In tegenstelling tot de Ca^{2+} excretie was de P_i excretie aanzienlijk toegenomen in de muizen op een laag Mg^{2+} dieet. Verder was de hoeveelheid FGF23 in het plasma verhoogd in deze muizen, vergeleken met muizen op een hoog Mg^{2+} dieet. Bovendien resulteerde het Mg^{2+} tekort in een substantiële verlaging van de renale expressie van de calciotrope eiwitten TRPV5 en calbindine-D_{28K}. De combinatie van al deze veranderingen suggereert verstoorde secretie en/of synthese van parathormoon (PTH) en weerstand tegen PTH, geïnduceerd door langdurige hypomagnesiëmie.

Hoofdstuk 5: Verwerking van pro-EGF in MDCK cellen

De identificatie van een homozygote mutatie (P1070L) in het EGF gen, dat codeert voor de voorloper van EGF (pro-EGF), in twee zussen met IRH, heeft dit hormoon gekoppeld aan de Mg^{2+} homeostase. Het gezonde pro-EGF (wild-type) wordt naar de plasmamembraan getransporteerd en aldaar uitgescheiden en gesplitst tot volwassen EGF. EGF activeert de

EGF receptor (EGFR) aan de basolaterale zijde van het DCT: dit is een essentiële stap voor activering van TRPM6. Het is aangetoond dat de P1070L mutatie in pro-EGF de uitscheiding van dit eiwit aan de basolaterale kant van gepolariseerde Madin-Darby canine kidney (MDCK) cellen belemmert. Dit heeft als consequentie dat de EGF receptor (EGFR) in de nier ontoereikend wordt geactiveerd, wat resulteert in verminderde stimulatie van TRPM6 en daarmee renaal Mg^{2+} verlies.

Om het onderliggende moleculaire defect te ontrafelen is de lokalisatie en uitscheiding van wild-type pro-EGF (pro-EGF-WT) en pro-EGF-P1070L geanalyseerd in MDCK cellijnen die deze eiwitten stabiel tot expressie brengen. Met behulp van het induceerbare Tetracycline-gereguleerde Expressie (T-REx) systeem werd het sorteren en splitsen van pro-EGF en de mutant bestudeerd in gepolariseerde MDCK cellen. Middels immunocytochemie kon worden aangetoond dat pro-EGF-WT en pro-EGF-P1070L beide voornamelijk aanwezig zijn op de apicale membraan. Verder zijn de zijde-specifieke kweekmedia, die de MDCK cellen op de filters omringen, onderzocht met immunoblotting en enzyme-linked immunosorbent assay methoden. Hieruit bleek dat (pro-)EGF vooral wordt uitgescheiden aan de apicale kant van de cel en aldaar gekliefd wordt tot het volwassen 6 kD EGF. Bovendien werd een verminderde uitscheiding van de mutant zichtbaar ten opzichte van wild-type, in zowel het apicale als het basolaterale compartiment. Tot slot, toevoeging van de metalloprotease remmer phenanthroline had geen invloed op de secretie van pro-EGF.

Onze conclusie is dan ook dat pro-EGF-WT en pro-EGF-P1070L voornamelijk worden gesorteerd naar de apicale zijde in MDCK cellen en aldaar uitgescheiden en verder gekliefd worden. De bevindingen suggereren verder dat de mutatie resulteert in verminderde splitsing van pro-EGF-P1070L aan zowel de apicale als de basolaterale zijde. De hypomagnesiëmie gediagnosticeerd in patiënten die aangedaan zijn door de mutatie wordt waarschijnlijk veroorzaakt door verminderde stimulatie van de EGFR aan de basolaterale zijde. Dit doordat de drempelwaarde voor uitgescheiden EGF niet wordt gehaald, welke nodig is voor stimulatie van de EGFR en vervolgens activering van Mg^{2+} resorptie via TRPM6.

Hoofdstuk 6: Conclusies

Transcellulaire Mg^{2+} resorptie in de nier is essentieel voor de Mg^{2+} homeostase, zoals benadrukt is door de bestudering van mutaties in verschillende genen die tot expressie komen in het DCT en resulteren in hypomagnesiëmie. In dit proefschrift is uiteengezet dat het DCT over een indrukwekkend aanpassingsvermogen beschikt in reactie op externe factoren die ingrijpen op de Mg^{2+} balans. Als het DCT zelf is aangedaan, bijvoorbeeld door behandeling met cisplatine, heeft dit onmiddellijk negatieve gevolgen voor de Mg^{2+} balans. Voorts wijst toediening van een laag Mg^{2+} dieet en de daarmee gepaard gaande verhoogde expressie van PV en HNF1B op een belangrijke rol van deze eiwitten bij renale Mg^{2+} resorptie.

Vervolgonderzoek moet de moleculaire identiteit van Mg^{2+} transport naar en over de basolaterale plasmamembraan van het DCT onthullen. Daarnaast is meer aandacht van artsen voor het herkennen en monitoren van patiënten met een verhoogd risico op ontwikkeling van hypomagnesiëmie zeer gewenst. Dit is met name belangrijk omdat hypomagnesiëmie kan leiden tot secundaire hypocalciëmie en hypokaliëmie, welke enkel gecorrigeerd kunnen worden middels Mg^{2+} suppletie.

Chapter 8

List of abbreviations
Curriculum Vitae
List of publications
Dankwoord

List of abbreviations

$1,25(OH)_2D_3$	active form of vitamin D
A	
ADAM	a disintegrin and metalloprotease
ANOVA	analysis of variance
AQP1	water channel aquaporin 1
AQP2	water channel aquaporin 2
ATP	adenosine 5'-triphosphate
C	
C57BL/6J	C57 black 6 mouse strain
$[Ca^{2+}]_i$	intracellular Ca^{2+} concentration
Ca^{2+}	calcium ion
CaSR	Ca^{2+}-sensing receptor
C_{Cr}	creatinine clearance rate
CD	collecting duct
cDNA	complementary DNA
cisplatin	cis-diamminedichloroplatinum(II)
CKD	chronic kidney disease
Cl^-	chloride ion
CLC-Kb	Cl^- channel, subunit b
CLDN7	claudin-7
CLDN8	claudin-8
CLDN16	claudin-16
CLDN19	claudin-19
CLSM	confocal laser scanning microscopy
CNNM2	cyclin M2
CNT	connecting tubule
CTR1	copper transporter 1
D	
DCT	distal convoluted tubule
DCT1	early DCT
DCT2	late DCT
DM2	diabetes mellitus type 2
DMEM	ulbecco's modified Eagle's medium
DNA	deoxyribonucleic acid
DTT	dithiothreitol
E	
EDTA	ethylenediaminetetraacetate
EGF	gene encoding pro-EGF
EGF	epidermal growth factor
EGFR	EGF receptor

ELISA	enzyme-linked immunosorbent assay
ENaC	epithelial Na^+ channel
ER	endoplasmic reticulum
F	
FCS	fetal calf serum
FHHNC	familial hypomagnesemia with hypercalciuria and nephrocalcinosis
FXYD2	gene encoding the Na^+, K^+-ATPase γ-subunit
G	
GAPDH	glyceraldehyde 3-phosphate dehydrogenase
GFP	green fluorescent protein
GFR	glomerular filtration rate
GS	Gitelman syndrome
H	
H_2O	water
H_2O_2	hydrogen peroxide
HEK293	human embryonic kidney 293
HNF1B	hepatocyte nuclear factor 1 homeobox B
HSH	hypomagnesemia with secondary hypocalcemia
I	
ICD	initial CD
IDH	isolated dominant hypomagnesemia
IHC	immunohistochemistry
IMCD	inner medullary collecting duct
IRH	isolated autosomal recessive renal hypomagnesemia
K	
K^+	potassium ion
kD	kilodalton
Kim-1	kidney injury molecule-1
Kir4.1	inward rectifier K^+-channel 4.1
Kir5.1	inward rectifier K^+-channel 5.1
Kv1.1	voltage-gated K^+ channel 1.1
M	
$[Mg^{2+}]_i$	intracellular Mg^{2+} concentration
MDCK	Madin-Darby canine kidney
Mg	magnesium
Mg^{2+}	magnesium ion
$MgSO_4$	magnesium sulfate
mRNA	messenger RNA
MsrB1	methionine sulfoxide reductase B1

N

n	number per group
Na^+	sodium ion
NCC	thiazide-sensitive Na^+, Cl^- cotransporter
NCX1	Na^+, Ca^{2+} exchanger
NHE3	Na^+, H^+ exchanger 3
NKCC2	Na^+, K^+, $2Cl^-$ cotransporter

O

OCT2	organic cation transporter 2

P

P	probability of events
P1070L	pro-EGF mutant
PAGE	polyacrylamide electrophoresis gel
PBS	phosphate buffered saline
pCB7	plasmid CB7
PCR	polymerase chain reaction
PCT	proximal convoluted tubule
PEI	polyethylenimine
P_i	inorganic phosphate
PIP_2	phosphatidylinositol 4,5-bisphosphate
PKA	protein kinase A
PKA	protein kinase C
PLP	periodate-lysine-paraformaldehyde
PMA	phorbol myristate acetate
PMCA1b	plasma membrane ATPase type 1b
PMSF	phenylmethylsulphonylfluoride
pro-EGF	precursor EGF
PST	proximal straight tubule
PT	proximal tubule
PTH	parathyroid hormone
PV	parvalbumin
PVDF	polyvinylidene difluoride

Q

qPCR	quantitative PCR

R

RAAS	renin-angiotensin-aldosterone system
RACK1	receptor for activated C-kinase
RDA	recommended dietary allowance
REA	repressor of estrogen receptor activity
RNA	ribonucleic acid
ROMK	renal outer medullary K^+ channel
RT	room temperature

S

SDS-PAGE	sodium dodecyl sulphate polyacrylamide gel electrophoresis
SEM	standard error of the mean
SGLT1	sodium-glucose cotransporter 1
SPAK	proline alanine-rich kinase
Src	sarcoma

T

T-REx	Tetracycline-Regulated Expression
TAL	thick ascending limb of Henle's loop
TetR	Tet repressor
TM	transmembrane
Tris	tris(hydroxy-methyl)aminomethane
TBS-T	Tris-buffered saline Tween-20
TRPM	transient receptor potential channel, subfamily melastatin
TRPM6	transient receptor potential channel subfamily M, member 6
TRPM7	ransient receptor potential channel subfamily M, member 7
TRPV5	transient receptor potential channel subfamily V, member 5

W

WNK	with-no-lysine kinase

Curriculum Vitae

Annelies van Angelen werd op 27 oktober 1981 geboren te Utrecht. In 2000 werd het atheneumdiploma behaald aan het St. Bonifatiuscollege, te Utrecht. Vervolgens studeerde zij Bio-medische wetenschappen aan de Universiteit van Amsterdam. Tijdens deze studie liep zij een korte stage bij het Interuniversitair Oogheelkundig Instituut (Dr. M. Kamermans) en langere stages bij de afdeling Celbiologie (Dr. A. Sonnenberg) van het Nederlands Kanker Instituut en bij de Provincie Zuid-Holland afdeling Milieubeleid en Luchtkwaliteit (Drs. C. van Dam). De Master Bio-medische wetenschappen werd in 2007 succesvol afgerond. Daarnaast behaalde zij in 2005 haar Propedeuse Geneeskunde aan dezelfde Universiteit. In januari 2008 startte zij als onderzoeker in opleiding bij de afdeling Fysiologie van het UMC St Radboud in het Nijmegen Centre for Molecular Life Sciences. Hier verrichtte zij onder leiding van Prof. Dr. R.J.M. Bindels en Prof. Dr. J.G.J. Hoenderop het onderzoek dat in dit proefschrift staat beschreven en wat gefinancierd werd door de Nederlandse organisatie voor wetenschappelijk onderzoek NWO en de European Science Foundation (EURYI 044.036.001). Tijdens deze periode heeft zij een Bachelor student begeleid. Daarnaast heeft zij in 2010 de cursus Proefdierkunde met goed gevolg doorlopen (Artikel-9 bevoegdheid).

List of publications

van Angelen AA, Hoenderop JG and Bindels RJ. Sorting and cleavage of pro-EGF in MDCK cells. *In preparation*

van Angelen AA, San-Cristobal P, Pulskens WP, Hoenderop JG and Bindels RJ. The impact of dietary magnesium restriction on magnesiotropic and calciotropic genes. *Nephrol Dial Transplant* 28: 2983-93, 2013

van Angelen AA*, Bob Glaudemans B*, van der Kemp AW, Hoenderop JG, and Bindels RJ. Cisplatin-induced injury of the renal distal convoluted tubule is associated with hypomagnesemia in mice. *Nephrol Dial Transplant* 28: 879–889, 2013
*authors contributed equally

van Angelen AA, van der Kemp AW, Hoenderop JG, and Bindels RJ. Increased expression of renal TRPM6 compensates for Mg^{2+} wasting during furosemide treatment. *Clin Kidney J* 5: 535-544, 2012

van den Bout I, van Rheenen J, **van Angelen AA,** de Rooij J, Wilhelmsen K, Jalink K, Divecha N, and Sonnenberg A. Investigation into the mechanism regulating MRP localization. *Exp Cell Res* 314: 330-341, 2008

Dankwoord

Voilá mijn proefschrift! Promoveren en het leveren van sportprestaties lijken veel op elkaar. Het begint allemaal met goede voorbereiding, training, oftewel studie en vaardigheden aanleren (stages) en een beetje talent is mooi meegenomen. Dan is het belangrijk om een mooi doel voor ogen te hebben waar je wilt 'vlammen'; een toernooi, wedstrijd of dus een uitdagende promotieplaats. Vervolgens is het belangrijk om met teleurstelling om te kunnen gaan en juist succes(jes) te vieren, door te zetten en wat geluk te hebben. Soms moet je even relativeren; er is altijd een nieuwe kans, wedstrijd, een nieuw experiment of project. En net zoals sportsuccessen was dit proefschrift er niet gekomen zonder goede begeleiding, teamwork, trainingsmaatjes of een 'clubgevoel'.

Ten eerste wil ik mijn promotoren, Prof. dr. René Bindels en Prof. dr. Joost Hoenderop bedanken. Beste René en Joost, ik heb veel bewondering voor de passie en inzet waarmee jullie leiding geven aan de afdeling. Het lab en alles daar omheen is tot in de puntjes georganiseerd, maar even bij jullie binnenlopen kon meestal ook en dat was voor mij heel plezierig werken. Bedankt dat jullie vertrouwen in mij bleven houden en mij de kans hebben gegeven om me te verdiepen in het proefdieronderzoek. En wat heb ik ook veel geleerd van jullie schrijf- en presentatievaardigheden.

Todd, thank you for familiarizing me with the lab, and teaching me how to make beautiful immunocytochemical stainings for confocal microscopy.

Titia, AnneMiete en Anke ik zou niet weten hoe ik zonder jullie tot geslaagde dierproeven zou zijn gekomen. Titia, veel dank voor alle hulp bij de DEC-aanvragen, de experimenten zelf of een opfriscursus statistiek. Ik ben ervan overtuigd dat ze een goede docent aan jou hebben daar in 't hoge noorden. Ook kijk ik met veel plezier terug op de etentjes, met onze mannen erbij. AnneMiete, enorm bedankt dat je altijd voor mij klaarstond om te helpen bij dierproeven, het doen van een kleuring of het testen van antilichamen. En gezellig dat je me ook regelmatig in Arnhem kwam opzoeken. Ik hoop dat je nog lang van je pensioen mag genieten. Anke wat ben jij creatief en praktisch ingesteld, heerlijk! Fijn dat ik bijvoorbeeld kon meeliften met jou poepjesbakkerij om de magnesium concentratie te bepalen in de muizenontlasting of dat je me er vriendelijk op wees dat ik toch echt niet de longen aan het prepareren was maar de lever ☺.

Femke, jij bent de perfecte research analist. Niet alleen kun je heel nauwkeurig werken, je bent ook enorm betrokken bij al het onderzoek op de afdeling en hebt vaak goede ideeën of oplossingen. In vond het altijd gezellig met jou tijdens de pauzes of op Koninginnedag/nacht waarbij we elkaar troffen in Arnhem. Fijn dat je mij wilt bijstaan als paranimf!

Bob, wat was het fijn om jou in de Unit te hebben; je peptalk heeft me door moeilijke momenten geholpen en ik heb veel gehad aan jouw kennis van genetica. Eline, in Arnhem wonen schept een band; samen in de trein naar het werk of met de auto naar een feestje. Dank voor je luisterend oor, belangstellende mailtjes en ik ben benieuwd naar jouw

boekje binnenkort. Liz, bedankt dat je tijdens mijn zwangerschap hielp bij het maken van de SDS-PAGE gels voor western blot.

Irene, wat is het een luxe (maar zeker geen overbodige) om jou op het lab te hebben. Altijd denk je mee dat materiaal op tijd besteld wordt en we zo optimaal mogelijk omgaan met 'het budget' zodat we zoveel mogelijk mooie experimenten kunnen doen, geweldig.

Gitte, ik vond het leerzaam en gezellig om jou als student te mogen begeleiden. Bedankt voor je inzet en enthousiasme.

En dan zijn er nog een aantal mensen die ik wil bedanken voor hun collegialiteit op het lab of hun gezelligheid tijdens de pauzes. Sandor, Joris, Theun, Jenny, Anne S, Sjoerd, Dennis, Melissa, Mark de G, Mark H, Sjoeli, Silvia, Joanna, Tim, Johan, Christiane, Leonie, Sergio, Wendy, Anne L, Monique, Jeroen, Anil, Ellen, Kukiat, en ik hoop dat ik niemand vergeten ben…..bedankt!

De proefdierstudies zijn uitgevoerd op het dierenlaboratorium (CDL). De collega's daar wil ik op deze plaats bedanken, in het bijzonder Henk, Janneke, Jeroen en Bianca. Zonder jullie uitstekende organisatorische en praktische vaardigheden was dit boekje er niet gekomen.

Daarnaast zijn er nog de mensen buiten het lab die ik wil bedanken voor hun plezierige of behulpzame aanwezigheid in mijn leven; waaronder vrienden, (schoon)familie, kennissen, (buren van) buren en een aantal mensen in het bijzonder.

Lisa, fijn om met jou lief en leed te kunnen delen. De skivakanties, weekendjes weg en andere afspraakjes, met Walter ook, waren heerlijke onderbrekingen van het onderzoek doen. Jammer dat we sinds onze studententijd steeds verder uitelkaar zijn gaan wonen, maar de komende tijd gaat het me vast lukken vaker jullie kant op te komen. Michiel fijn dat jij mij wegwijs wilde maken met de layout. Gezellig dat we ondanks onze drukke levens, samen met Karlijn ook, tijd hebben voor etentjes of speelafspraakjes met onze kinderen. Marlous, mijn 'grote zus', jammer dat we geen buurmeisjes meer zijn, maar wat mij betreft blijven we altijd 'buurten'. Rosanne dank voor je inspirerende Chi Neng lessen, ze gaven me steeds weer nieuwe inzichten, rust en daardoor energie.

Tot slot wil ik mijn naaste familie bedanken. Jan, wat is het fijn om als oudste in ons gezin toch niet alles als eerste te hoeven doen. Met je rijbewijs halen ging je me voor en ik ben trots je al aan te mogen spreken met Doctor. Fijn dat je mijn broer bent! Martine, leuk dat ik altijd een beetje mag meegenieten van je avonturen als je daarvan verslag doet in beeld & geluid. Wie weet waag jij je ook nog aan een promotieonderzoek, ik ben in ieder geval heel blij dat jij aan mijn andere zijde wilt staan als paranimf. Papa en mama, Albi en Cor enorm bedankt voor de kansen die jullie mij geboden hebben en jullie onvoorwaardelijke steun bij alles.

Lieve Hans, het is niet altijd makkelijk om onze carrières en de laatste jaren ook een gezin daarbij te combineren. Soms was het behoorlijke puzzelen over wie wanneer wat kon

doen, de tijd eerlijk te verdelen of juist nog tijd voor elkaar te vinden. Maar we kwamen er altijd uit en de momenten samen met jou en ons 4tjes compenseren ruimschoots voor alle hectiek. Ik ben blij mijn leven met jou te mogen delen. Myrthe en Sacha jullie zijn het mooiste 'resultaat' van de afgelopen jaren.